# Dynamic behaviour of floating wind turbines

## A comparison of open water and level ice conditions

C.P.M. Curfs

Master of Science Thesis

TU Delft Delft University of Technology

MSc Offshore and Dredging Engineering

# Dynamic behaviour of floating wind turbines

## A comparison of open water and level ice conditions

Master of Science Thesis

For the degree of Master of Science in Offshore and Dredging Engineering at Delft University of Technology

C.P.M. Curfs
1384155

January 4, 2015

**Thesis committee**

Prof. dr. A.V. Metrikine

Dr. Ir. A.C. Vire

Ir. P. van der Male

Ir. C. Keijdener

Faculty of Civil Engineering and Geosciences · Delft University of Technology

TU Delft Delft University of Technology



MSc Offshore and Dredging Engineering
Specialization Bottom Founded Structures, Arctic and Wind
Section Offshore Engineering, Department Hydraulic Engineering
Faculty of Civil Engineering and Geosciences

# Abstract

In the past couple of decades, the offshore wind industry has developed from applications in shallow water to ever deeper, more remote locations with harsher environments. In these progressively larger water depths, bottom founded support structures become no longer applicable and floating support structures could provide a viable alternative. Various studies have focused on floater designs for this application and multiple prototypes have been developed. However, no research has been done on the interaction of floating support structures with ice.

In this thesis, the effect of level ice conditions on the dynamics of floating offshore wind turbines is studied. The MIT-NREL TLP is used as reference floater design. Based on the structure's motions and mooring loads, a comparison is made between ice structure interaction and wave loading in harsh open water conditions.

The combined floater and turbine arrangement is modelled in a rigid body approach, with three degrees of freedom (surge, heave and pitch). The system's non-linear restoring stiffness is defined from contributions of its mooring system and hydrostatics. Hydrodynamic characteristics from fluid-structure interaction are derived with Ansys AQWA in frequency domain and transformed to time domain for the performed simulations. Wind and wave loading are covered, taking into account irregular wind velocity and wave height.

Ice structure interaction is simulated for both failure of ice in crushing and bending modes. Ice crushing failure is simulated by the application of a Matlock-Sodhi model and is applied for vertical walled geometry. Ice loads from bending failure are considered for a sloping geometry at the waterline and are modelled by application of elastic beam- and friction-theory.

Simulations of open water characteristics are performed for sea states with significant wave heights ranging from 2 to 14 meters. The results are compared to ice crushing for ice thickness ranging from 0.1 to 0.7 m and ice bending for ice thickness from 0.25 to 1.5 meters.

From the simulations it is found that motion and mooring load maxima from ice bending loads for ice thickness up to approximately 1 m are in line with those for very harsh open water conditions. In the case of ice crushing, structure response is found to be far larger and more volatile, even for limited ice thickness. Crushing action of level ice with 0.2 m thickness will already cause larger mooring loads than the most extreme open water condition considered (with a 14 m significant wave height). On top of that, dynamic amplification issues can arise as a result of ice loading near the structure's natural frequencies. This mainly poses issues for the high energy loading of crushing, where motions and force variations are considerable for loads near the structure's pitch natural frequency.

# Table of Contents

# List of Figures

# List of Tables

# List of Symbols

## Abbreviations

| | |
|---|---|
| $\alpha$ | Wind profile exponent |
| $\bar{u}$ | Mean wind velocity |
| $\ddot{X}$ | Acceleration vector |
| $\Delta f$ | Frequency step size |
| $\Delta p$ | Pressure drop along the rotor of the wind turbine |
| $\delta(t)$ | Tooth deflection ice crushing model |
| $\delta^s$ | Platform set-down |
| $\delta_f$ | Failure deflection ice teeth in ice crushing model |
| $\dot{X}$ | Velocity vector |
| $\eta$ | Wave elevation |
| $\eta_a$ | Wave elevation amplitude |
| $\gamma$ | Wave spectrum peak factor |
| $\kappa$ | Relative position of ice sheet w.r.t. the platform's position |
| $\nabla$ | Platform submerged volume |
| $\nabla_0$ | Undisplaced submerged volume of the floater |
| $\omega$ | Angular wave frequency |
| $\phi_n$ | Phase angle of wave force vector from Ansys AQWA |
| $\phi_n$ | Random phase angle at each defined frequency |
| $\rho_a$ | Air mass density |
| $\sigma_b$ | Brittle crushing failure strength of ice |
| $\sigma_d$ | Ductile crushing failure strength of ice |
| $\sigma_f$ | Failure strength ice in crushing |
| $\sigma_w$ | Standard deviation of wind velocity variations |
| $\sigma_{bend}$ | Maximum bending stress along the ice sheet |
| $\theta$ | Angle of tendons with vertical as a result of horizontal displacement |
| $\varepsilon$ | Tether strain |
| $\varphi$ | Angle between the floater's slope and the waterline |
| $a$ | Turbine axial induction factor |
| $A_n$ | Cross-sectional area per tether |
| $a_n$ | Frequency dependent wave amplitude from spectral density |
| $A_{ij}$ | Hydrodynamic added mass |
| $A_{prj}$ | Projected area of interaction between fluid particle flow and floater |
| $A_{rotor}$ | Rotor swept area |
| $A_{WL}$ | The platform's water plane area |
| $B_{ij}$ | Hydrodynamic added damping |
| $C$ | 3x3 Damping matrix |
| $C_{D,h}$ | Hydrodynamic drag coefficient for flow around the floater |

$C_{D,w}$ Drag coefficient wind loads
$D$ Platform diameter
$D(z)$ Varying turbine tower diameter along height
$E$ Young's modulus
$E_{ice}$ Ice bending elasticity
$f$ Frequency
$F_e$ Ice crushing residual force
$F_f$ Ice crushing failure force
$F_i^{Hydr}$ Hydrostatic restoring force in $i^{th}$ DOF
$F_i^{Waves}$ Incident wave force acting in $i^{th}$ DOF
$F_{bend,3}$ Platform overturning moment induced by load of ice in bending failure
$F_{drag,1}$ Drag force in surge direction
$F_{drag,2}$ Drag force in heave direction
$F_{drag,3}$ Drag overturning moment in pitch direction
$F_i^{Rad}$ Hydrodynamic radiation loads resulting from platform oscillations
$F_{mem}$ Force resulting from memory effect in wave radiation loads
$h_ice$ Ice sheet thickness
$H_s$ Significant wave height
$h_w$ Water depth
$I$ Wind turbulence intensity
$I_{WL}$ Platform moment of inertia of water line
$K$ 3x3 Stiffness matrix
$k$ Wave number
$k(t)$ Retardation kernel function
$k_{11}$ Surge-surge stiffness contribution
$k_{22}$ Heave-heave stiffness contribution
$k_{33}$ Pitch-pitch stiffness contribution
$k_{ice}$ Ice crushing stiffness
$K_{ij}^{Hydr}$ Hydrostatic restoring stiffness matrix
$L$ Length of tethers (mooring lines)
$L_u$ Kaimal spectrum length scale
$L_z$ Vertical distance of platform bottom to seabed when platform is deflected in surge direction
$M$ 3x3 Mass matrix
$M_A$ Inertial part of added mass in time domain
$M_{bending}$ Bending moment along ice sheet in bending failure mode
$N_t$ Total number of tethers
$N_{ice}$ Horizontal interaction force between platform and ice in bending failure mode
$n_{ice}$ Number of teeth that have passed the structure in ice crushing model
$p$ Ice tooth separation ice crushing model

$P_{ice}$ Vertical interaction force between platform and ice in bending failure mode
$Q$ Platform gravity force
$q_{aero}$ Aerodynamic distributed drag loading along the turbine tower
$Re$ Reynolds number
$S(f)$ Spectral density Kaimal turbulence spectrum
$S_\eta$ Jonswap wave spectral density
$T$ Total tendon force
$T_h$ Horizontal component of tendon force
$T_n$ Tendon force in individual tether
$T_p$ Spectrum peak wave period
$T_{wind}$ Wind turbine thrust
$U$ Platform buoyancy force
$u(t)$ Wind velocity
$u(z,t)$ Wind velocity in time along tower height
$U_tip$ Vertical ride-up deflection of the tip of the ice sheet in bending failure mode
$u_{current}$ Constant ocean current velocity
$u_{ice}$ Vertical deflection of the ice sheet
$u_{platform,h}$ Horizontal platform motion induced water particle velocity
$u_{platform,h}$ Vertical platform motion induced water particle velocity
$u_{platform}$ Velocity along the depth of the fluid resulting from platform motions
$u_{res,v}$ Residual vertical water particle velocity
$u_{res}$ Residual fluid particle velocity around the floater
$u_{w,rel}$ Relative wind velocity taking into account platform motions
$u_{waves,h}$ Horizontal wave induced water particle velocity
$u_{waves,v}$ Vertical wave induced water particle velocity
$u_{waves}$ Wave induced fluid particle velocity
$V_0$ Upstream wind velocity
$v_r$ Residual velocity of platform-ice interaction
$v_t$ Ice transitional velocity
$v_{ice}$ Ice travelling velocity
$X$ Displacement vector
$x$ Horizontal axis definition
$X_1$ Surge displacement
$X_1(0)$ Initial platform surge displacement
$X_2$ Heave displacement
$X_3$ Pitch displacement
$X_{br}$ Counter for total length of broken ice pieces
$X_{i,n}$ Wave force vector from Ansys AQWA, for $i^{th}$ DOF
$X_{T,n}$ Horizontal offset of connection point of individual tethers
$z$ Vertical axis definition

| | |
|---|---|
| $z_0$ | Surface roughnes |
| $z_B$ | z-coordinate of the platform's centre of buoyancy |
| $z_G$ | z-coordinate of the platform's centre of gravity |
| $z_T$ | z-coordinate tendon connection point |
| $z_{ref}$ | Reference height for wind velocity determination |

# Chapter 1

# Introduction

## 1-1 Wind energy

Decreasing global reserves of fossil fuels cause an increasing demand for alternative energy sources. The limited varieties of proven alternative energy sources, combined with limited applicability of these alternatives, makes wind energy a very promising source in considerable parts of the world for example in: Western and Northern Europe, as well as parts of Northern America and coastal China. Placement of turbines to source wind energy started onshore, but has faced multiple difficulties throughout its development:

- Relatively low wind velocities over land, influenced by vegetation, rural development and overall landscaping.
- Limited unused land area in areas where demand for energy is highest, a good example is the densely populated western part of the Netherlands.
- Negative public opinion, formed by landscape pollution and noise, introduces great difficulties for licensing of wind farms, decelerating the development of onshore wind.

Driven by the limitations of onshore wind power, the continuously growing demand and the availability of subsidies, wind farms have been installed offshore Europe since 1991 [7]. In first developments with monopiles (large single piles) were used as the support structure, providing a simple and cost efficient structure. However, although relatively cheap, the applicability of a monopile support structure is limited to water depths of roughly $20m$ [8]. To gain access to areas with larger water depths, alternative bottom-founded structures have been developed. With this innovation the commercial applicability has been widened to water depths of 40 to $50m$ [9]. These structures, however, typically require larger amounts of material, and still are not capable of covering most areas. With an increasing demand for wind energy, a solution for the application of wind energy in ever deeper waters is required, this could potentially be solves by the application of floating wind turbines.

Based on the experiences in the oil and gas industry, various types of floating support structures for wind turbines are being studied and developed.

These developments are often categorized in three main categories [10], also see figure1-1:

- Spar hull
- TLP
- Barge-type

Hybrid floaters containing characteristics of several of these types are also investigated, an example of such a hybrid structure is found a semi-submersible support structure. More info on the working principle of the distinct types can be found in section 1-2 below.

Up to this moment, no commercial application of floating support structures for wind turbines has been realised. Along the past couple of years however, considerable work has been done in this field both scientifically and practically, resulting in the development of several prototypes worldwide. Two of these projects have reached the stage of development with full scale turbines. First, in 2009 the spar buoy of Statoil's Hywind project has been installed off the west coast of Norway[11]. In 2011 in the WindFloat project, Principle Power installed a floating wind turbine with a semi-submersible type floater off the coast of Portugal[12]. The TLP type floater has not been applied in a full scale prototype yet, deployment of the Pelastar prototype is however considered [10] and in Europe the Blue H concept is undergoing scaled testing [9]. Other deviating designs that are currently in the pilot stage of development are the SWAY and Poseidon 37 concepts [9].

The industry of floating wind turbines is still in its infancy, and therefore it forms an interesting field of research. Compared to onshore turbines and offshore turbines with a bottom founded foundation, floating support structures introduce additional forces and motions to the wind turbine system. Therewith challenges have to be overcome in understanding and modelling the combined system of floating platform and mooring system [13].

Various studies have already been performed focussing on the dynamic structural behaviour of floating wind turbines resulting from hydrodynamic and wind loading, for the various floater type designs available. In this research, the aim is to extend the knowledge in this field to the effects of ice loading on the dynamic behaviour of the turbines. With the application of floating wind turbines off the coasts of for example Denmark, Sweden or any other country near the Baltic, ice loads might be incurred. An understanding of the effects of ice loading is essential for the understanding of the potential application of wind turbines in such regions.

## 1-2 Floater types

As already briefly introduced above, there are several fundamentally different floater types. They have emerged from the decades of offshore experience in the oil and gas industry and are studied nowadays to help support wind turbines. The main categories of floater types currently considered in literature on floating wind turbines are: TLP, Spar Buoy and Barges [10] [13], as seen in Figure 1-1. This categorization of floaters is based on their different stabilization mechanisms [14] [15], typified by:

- A spar type floater can be categorized as a ballast stabalized floater. This type achieves rotational stability by the application of ballast to lower the centre-of-gravity (COG)

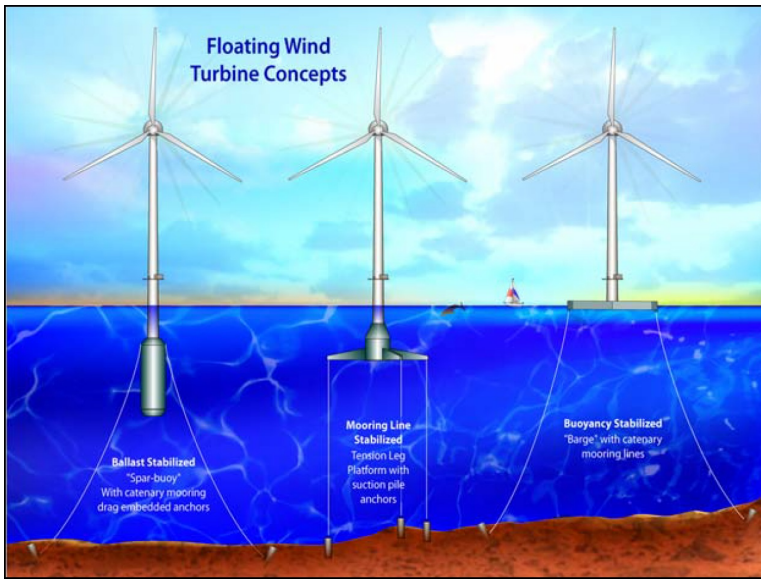


**Figure 1-1:** Working principle of the three floater type categories

below the centre-of-buoyancy (COB). Translational stability is achieved by either a catenary or a taut-wire mooring arrangement.

- TLP floaters are categorized as mooring line stabilized structures. This type of floater typically possesses excess buoyancy, which is compensated by tension forces in pre-tensioned tethers that connect the floater to the seabed. These tensile forces have a stabilizing effect on both rotational movements and translational deflections.
- A barge type floater is typically buoyancy stabilized and depends on a large water plane area for stabilization of rotational motions and on a catenary type mooring for the in plane translational motions.

Besides this strict categorization there also are designs that contain properties of multiple classes, for example a semi-submersible floater type. This floater type consists stabilization characteristics of both the spar and barge types.

For this research, only one of the floater types mentioned above is studied. This is done to provide focus and to fit in the scope of a MSc Thesis research. The selection of floater type is based on several considerations that are linked both to the practicability of the study at hand and the practical applicability of the studied design. First, since in this study ice loading will be introduced to the support structure, it is important to study a floater that could be suitable for resisting ice-loads. For this requirement the water plane area of the floater is of importance, since this will form the impact area of the ice [16]. In this respect both the semi-submersible and the barge type floaters are not suitable, which favours the spar and TLP type of floaters. The impact of platform motions on the turbine and the overall economic feasibility of a proposed design are of importance as well [16].

Compared to onshore or bottom-founded offshore turbines, floating support structures will introduce additional (cyclic) loading to the wind turbine as a result of platform movements. In order to withstand these additional load cycles, turbine designs are required to be adjusted. These adjustment require both design efforts and reinforcements of the turbine, both accom-

panied with additional costs. In this respect a TLP support is thought to perform better than the other types [14] [16].

The economic feasibility of offshore wind projects is typically determined by the so called cost of energy, which is formed by the project life-cycle costs combined with its energy production. Myhr et al (2014) [12] provides an interesting comparison of these levelised cost of energy for several types of floating wind turbines. The main outcomes of this study show that tension leg systems (in various designs) prove to be beneficial over catenary moored systems from a cost-efficiency perspective.

Finally, looking at the practicability of the study, the ease of modelling a certain floater type is most relevant. For example, the application of certain simplifications and linearisation of hydrodynamic loading are thought to be valid for a TLP structure, whereas for a barge-type floater they may not be applied [16]. For a spar-type structure, additional non-linear wave forces might be required to be taken into account as well, which would significantly complicate modelling as well.

Considering the above, a TLP floater type is thought to be most suitable for this study and therefore will be the focus for the remainder of this report.

## 1-3 Research aim

Whereas plentiful research is done in the field of coupled wind and wave forcing on and the dynamic behaviour of floating wind turbines, the interaction of such an arrangement with sea ice has not been studied yet. Therefore, the aim of this research is to provide a first insight in the effects of loading from sea-ice on structural dynamics. By comparing these findings with the dynamics in open water conditions, it is aimed to enhance understanding of the implications this loading type can have for the applicability and design of floating wind turbines in environments with presence of level ice.

As a tool in this study, a numerical model is developed for simulating the motions and mooring loads of a TLP floating wind turbine. The fundamentals for this model are formed by the formulation of structural properties, forces and restraints that fit the fundamental equation of motion: $m\ddot{x} + c\dot{x} + kx = f(t)$. In the simulations performed with this model, the structure is subjected to aerodynamic, hydrodynamic and ice loading both in order to compare open water and ice covered loading conditions and to study the interaction between load types. Given the interdependence of loads and the movements of the floater and turbine system, they are coupled to capture effects of dynamic interaction.

Where possible, the modelling approach and structure lay-out are based on the outcomes of existing studies. This is done in order to benchmark some of the findings with the outcomes of preceding studies and to enhance progress, given the limited scope of a MSc project.

# Chapter 2

# Model definition

There are multiple approaches to develop a model for the representation of a floating wind turbine and multiple design tools are available, capable of simulating (semi) coupled dynamics of such a structure. These tools vary in the extend to which they include complexity of loading phenomena (both aerodynamic and hydrodynamic loads) and in the approach of modelling structural behaviour of the system.

Both hydrodynamic and aerodynamic loads on a floating wind turbine system are complex natural phenomena that require simplified representations that allow for mathematical modelling. The applied methods for load determination and the accompanied simplifications are discussed in Chapter 3.

The two fundamental approaches in modelling structural behaviour of both the floater and the turbine are: 1. a rigid body approach in which structural deflections are neglected by assuming infinite structural stiffness, or 2. a finite element (FEM), in which the structural flexibility is taken into account. The application of a FEM approach in this field would be considerably more demanding compared to the rigid body approach and therefore, in this research the latter is applied. In this simplified rigid body representation, the combined floater-turbine arrangement is represented by a rigid body, which is subjected to environmental loading. A simplified graphical representation of this model is presented in Figure **??**.

Since this study is limited to a 2D representation of the structure, the number of degrees of freedom (DOF from this point onwards) is limited from 6 (in 3D representation) to 3. As indicated in Figure **??**, the remaining DOF of the system are: Surge($X_1$) , Heave($X_2$) and Pitch($X_3$) . [*]

Concerning the orientation of axes and motions of the system the following configurations have been applied. The x-axis is defined from the centreline of the structure in wave propagation direction at mean sea level (MSL from this point onwards). The z-axis is defined from the intersection of MSL and the centerline of the platform upwards. Positive $X_1$ is along positive x, positive $X_2$ is along positive z and positive $X_3$ is from positive z to positive x .

In this report the main aim will be to find a formulation of structural properties, forces and restraints in a form that fits the fundamental equation of motions (2-1).

[*]It should be noted that this notation is different from the notation typically used for 3D ship-motions (Surge($X_1$), Sway($X_2$), Heave($X_3$), Roll($X_4$), Pitch($X_5$) and Yaw($X_6$)).

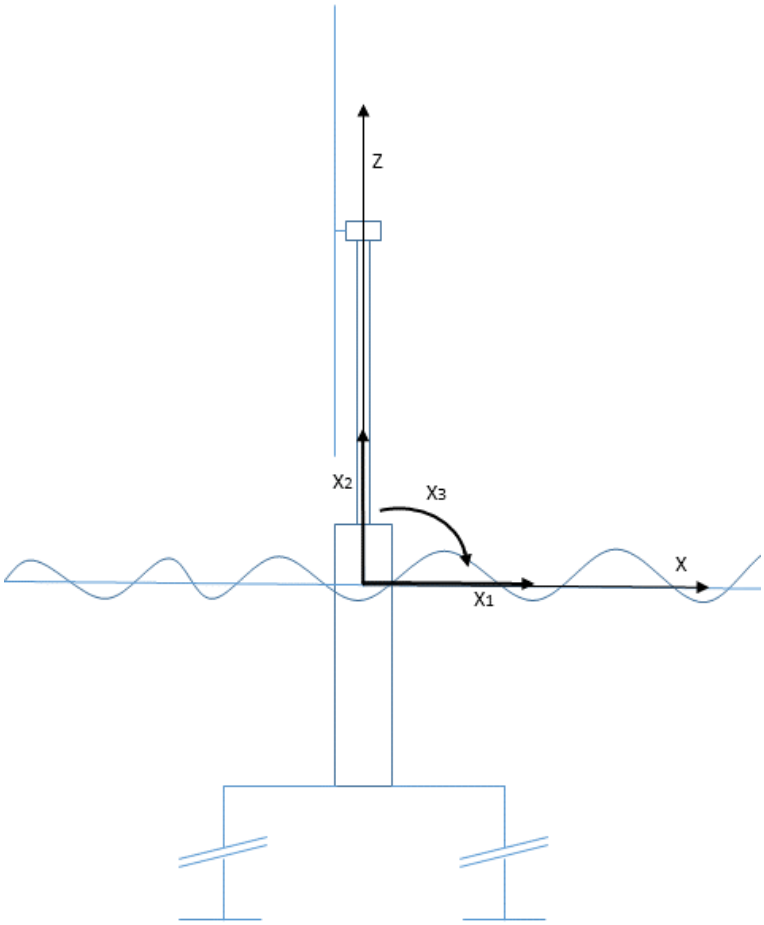


**Figure 2-1:** Rigid body system

$$M\ddot{X} + C\dot{X} + KX = F(t) \tag{2-1}$$

Here $M$, $C$ and $K$ are $3 \times 3$ mass, damping and stiffness matrices corresponding with mass, damping and stiffness characteristics of the system for each direction of motion and the correlations between them. From Chapter 3 it will become clear that not only structural properties, but also loads can influence these characteristics. $X$ represents a $1 \times 3$ motion vector which consists of motions in the three DOFs. $\dot{X}$ and $\ddot{X}$ form the first and second time derivatives of $X$ respectively and therewith represent velocities and accelerations in the 3 DOFs. $F(t)$ represents the force acting on the system at time instant $t$, represented by a $1 \times 3$ vector consisting of force contributions in all 3 DOFs. By solving the system of equations for consecutive time steps insights in the dynamic behaviour of the system can be derived.

The system described above in essence consists of three main parts: the turbine, the floater and the mooring system. The main characteristics of all parts will be discussed in the remaining sections of this chapter.

## 2-1 Turbine

Based on the common practice in existing literature [17] [2] [18] [19], the NREL 5MW Reference Wind Turbine, as defined in [1], is used as an input for the turbine characteristics required in this study. Here a rigid body approach for the combined floater-turbine arrangement is taken, thereby neglecting body deflections of the turbine structure and rotational motions of the turbine. As a result the input from the reference turbine is limited to its gross properties, these are presented in Table 2-1.

| Turbine properties | |
|---|---|
| Rating | 5 MW |
| Configuration | 3 Blades |
| Rotor diameter | 126 m |
| Hub diameter | 3 m |
| Hub height | 90 m |
| Rotor Mass | 110,000 kg |
| Nacelle Mass | 240,000 kg |
| Tower Mass | 347,460 kg |
| Tower Diameter Bottom | 6 m |
| Tower Diameter Top | 3.87 m |
| Coordinates overall CM | (-0.2, 0.0, 64.0) m |

**Table 2-1:** Gross properties NREL 5MW Reference Wind Turbine

Another important input of this reference turbine is the availability of thrust characteristics over a wide range of wind speeds. These characteristics are used to determine the mean aerodynamic loads onto the turbine. In figure 2-2 the thrust on the turbine is represented by the purple (lowest) line in the graph.

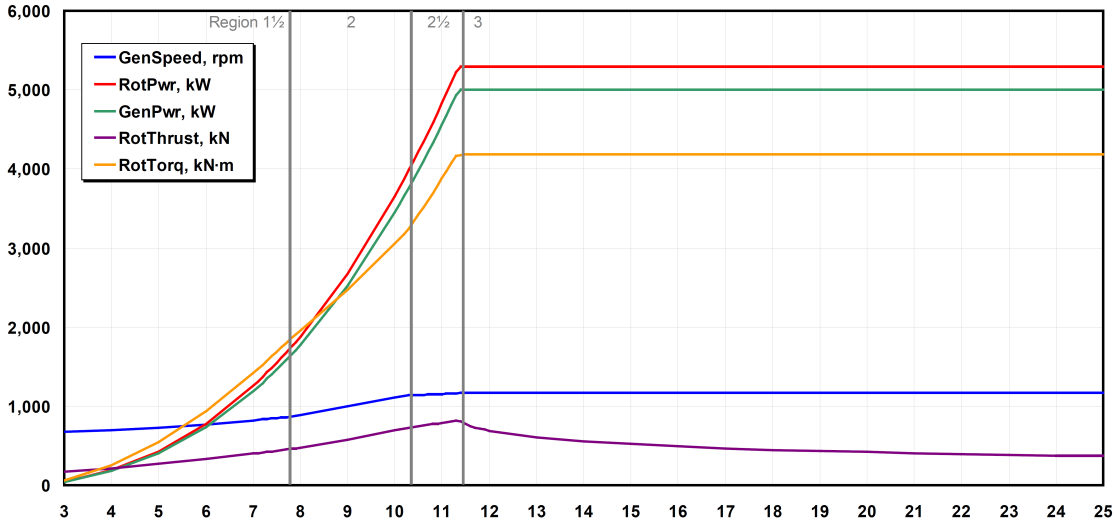


**Figure 2-2:** Thrust characteristics of the NREL 5MW Reference Turbine [1] for range of wind velocities on horizontal axis

## 2-2 Support structure

As discussed in section 1-2, this study focuses on the application of a floating wind turbine supported by a TLP support structure. In this section a brief introduction to the design of this TLP structure is provided.

Based on the availability and detail of existing research, the MIT TLP floater design, introduced by MIT [20] and adjusted by NREL [2], has been found most suitable as a basic design for this study. This design provides a basis for comparison of our model outcomes with the existing study for open water characteristics, before extending the model to capture ice loading characteristics.

The floater design consists of a cylindrical vertical steel hull, with a concrete mass extending several meters from the bottom of the floater. At the bottom of the hull 4 horizontal arms are attached perpendicular to the floater, which connect the platform to the tethers that keep the TLP station. A graphical representation of this structure is presented in figure 2-3 [2].

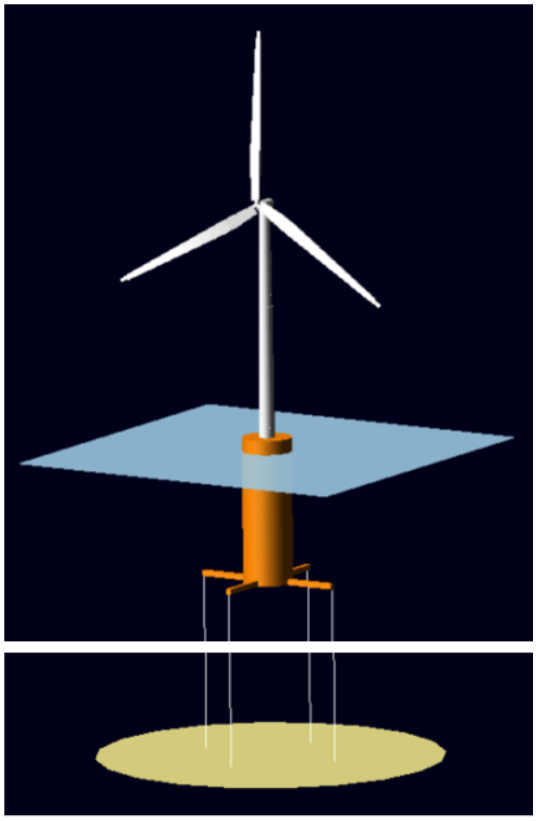

**Figure 2-3:** 3D illustration of MIT TLP floater design [2]

The horizontal arms act as lever arms distributing to the restoring loads between floater and tethers. However, for the hydrodynamical properties of the floater the arms themselves are considered to be slender compared to the main hull and therefore are not included in the hydrodynamic analysis of the platform*.

*Research has been done on the effect of neglecting this, and it was concluded that effects were mostly

The main characteristics of the platform that are required as an input are presented in table 2-2 below. More detailed structural properties can be found in Appendix A, which shows the prints of an Excel file that was used to determine the required structural characteristics based on the general lay-out of the system.

| Floater properties | |
|---|---|
| Platform diameter | 18 m |
| Platform draft | 47.89 m |
| Platform freeboard | 5 m |
| Water depth | 200 m |
| Concrete ballast mass | 8,216,000 kg |
| Concerete ballast height | 12.6 m |
| Total displacement | 12,187,000 kg |
| Z-coordinate centre of mass | -40.76 m |

**Table 2-2:** Gross properties MIT TLP floater design

An additional note should be made towards the floater's centre of mass. Compared to more traditional tension leg platform designs, the structure at hand has a centre of mass that is located rather deep. This is a result of the design requirement of stable hydrostatic characteristics for the combined floater-turbine arrangement, without being connected to its tethers.

## 2-3 Mooring system

The mooring system applied is known as a tensioned leg mooring system. This system consists of tensioned (and in this case) vertically aligned tethers that connect to arms that horizontally extend from the floater's hull. The main properties of this mooring system are presented in table 2-3 below.

| Mooring system properties | |
|---|---|
| Number of mooring lines | 8 |
| Fairlead distance from center | 27 m |
| Line diameter | 0,127 |
| Line mass per unit length | 116.03 kg/m |
| Mean tension per tendon | 3931 kN |
| Line extensional stiffness | 1,500,000,000 N |

**Table 2-3:** Gross properties MIT TLP mooring system

Modelling the characteristics of the mooring system is done based on Senjanovic et al (2012) [21], which provides an elaborate method of modelling TLP mooring systems, prescribing its overall stiffness characteristics. The tensioned tendons in the system provide station keeping

limited to the yaw motion of the platform [17], which is not in the scope of this research. Therefore this approximation of negligible influence of the arms on the hydrodynamics seems acceptable.

of the floater in all DOFs. The stiffness characteristics will be discussed below for the all DOFs.

### 2-3-1 Surge tendon stiffness

In surge direction the stiffness is defined by the tension force acting along a tendon. A displacement in $X_1$ direction is counteracted by a force $F$, resulting from the obliquity of the tether with the vertical ($\theta$) . This contribution is visualised in figure 2-4 below.

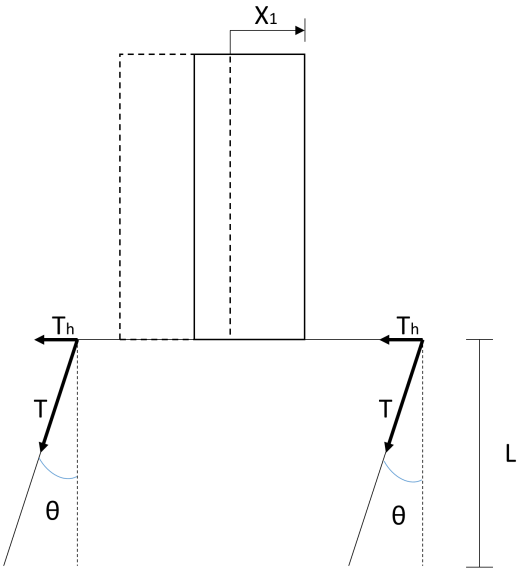


**Figure 2-4:** Representation of tendon restoring force in surge direction

Here we can derive that $T_h = sin(\theta)T$ with $sin(\theta) = X_1/L$ . Therefore the surge restoring stiffness resulting from tendon tension is defined to be:

$$k11 = \sum_{n=1}^{N_t} \frac{T_n}{L} \tag{2-2}$$

Where $N_t$ is the total number of tethers connected to the platform and $T_n$ is the tension per individual tether.

### 2-3-2 Heave tendon stiffness

For the heave direction, the stiffness is directly linked to the axial extensional resistance of the tendons, see figure 2-5.

A displacement in heave direction will result in a tendon extension $\varepsilon = X_2/L$. This extension is counteracted by a force $F = EA\varepsilon$, therefore the restoring stiffness is defined to be:

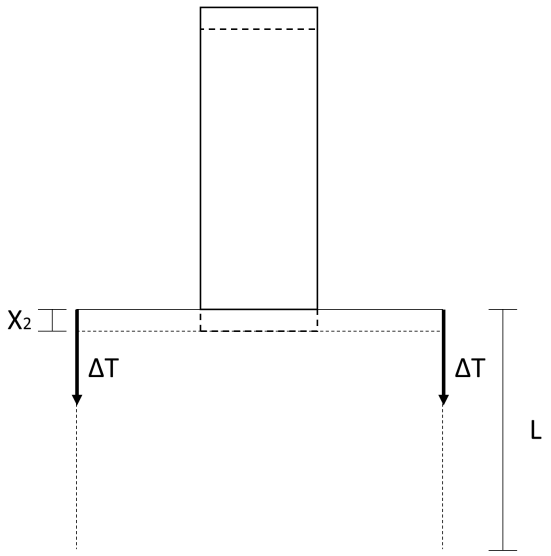


**Figure 2-5:** Representation of tendon restoring force in heave direction

$$k22 = \sum_{n=1}^{N} \frac{EA_n}{L}^{*} \tag{2-3}$$

### 2-3-3 Pitch tendon stiffness

In pitch direction the tendon stiffness resisting rotational motions is formed by the extensional resistance, offset by the horizontal arms from the connection point with the platform's hull, schematically presented in figure 2-6.

The restoring moment counteracting pitch motions can be defined by the force resulting from the extension of the tendons times the offset from the platform center $M = \varepsilon EAX_T$, with $\varepsilon = \frac{X_3 X_T}{L}$. Combining both, the tendon restoring stiffness in pitch direction is defined by:

$$k33 = \sum_{n=1}^{N} \frac{EA_n {X_{T,n}}^2}{L}^{*} \tag{2-4}$$

For both heave and pitch direction $E$ is the extensional stiffness of steel, $A_n$ is the cross-sectional area of a single tether, $L$ is the length of the tether.

In pitch direction, $X_{T,n}$ is the horizontal offset of the connection point of the tether to the reference point of the system. This offset takes into account the effect that some tethers do not contribute to the pitch restoring stiffness, since they are aligned with the reference system in x-direction. This effect is visualised in a topview presented in figure 2-7.

*Note: these stiffness contributions are only resulting from the mooring lines themselves, additional stiffness terms are to be included in the hydrodynamics part of the report, see section 3-3.

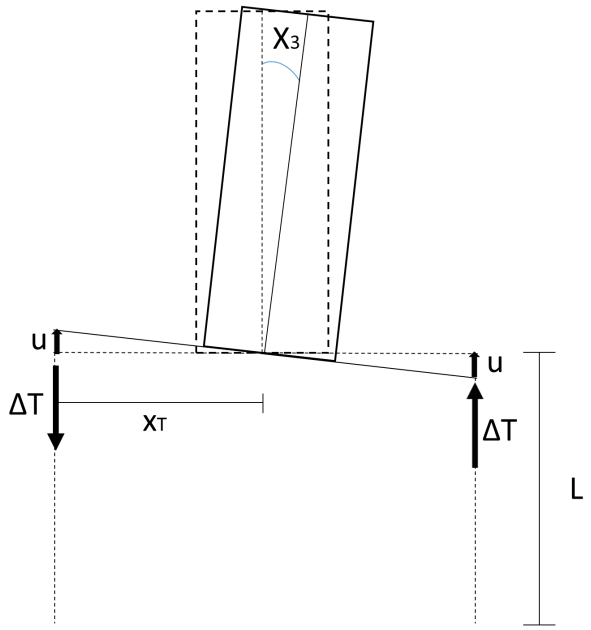


**Figure 2-6:** Representation of pitch tendon restoring force

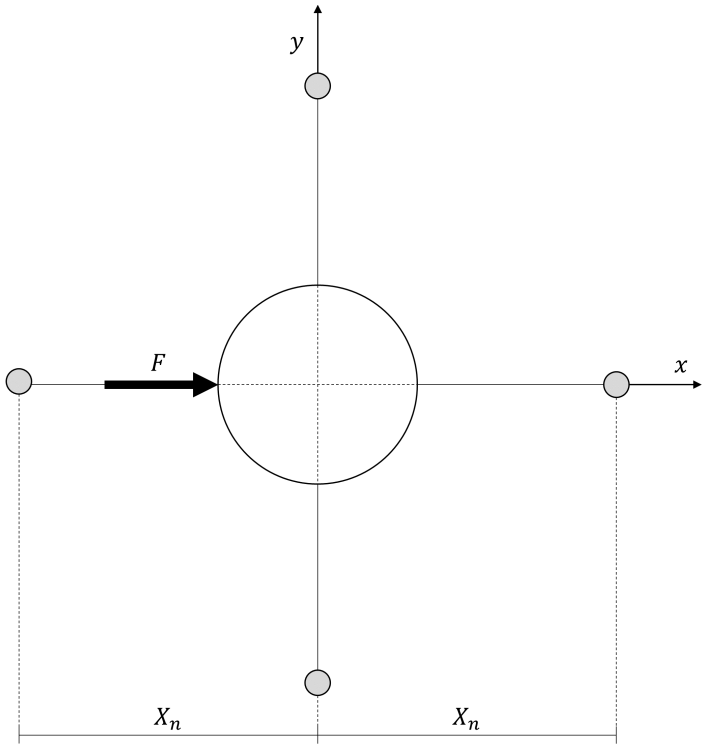


**Figure 2-7:** Topview illustration of Xn

# Chapter 3

# Load identification

In order to get an understanding of a structure in its environment it is key to know how this environment acts on that structure. In the case of a floating wind turbine this environment mainly consists of wind and water acting on the structure. On top of that, this study aims to extend the environment with the presence of level ice to investigate ice loading.

Therefore, in this chapter, the influence of aerodynamics, hydrodynamics and ice loads is introduced, as well as the formulation that is applied to take these loads into account. Finally, the chapter concludes with the load cases that are investigated, these include combinations and magnitudes of the different load contributions. Here a main distinction is made between an open water season and an ice covered sea.

## 3-1 Aerodynamic loading

Aerodynamic (or wind) loading on wind turbines is a complex phenomenon that is influenced by many factors, such as: wind speeds, rotor flexibility and turbulence effects. Placing a wind turbine on a floating foundation adds to the complexity of this loading type: the aerodynamic loads and the dynamic structural behaviour of the system influence one another [22]. Since a full-detail approach in determining aerodynamic loading, including platform motions, would place the emphasis of this study on the aerodynamic part of the problem definition, a more simplified approach of aerodynamic loading is considered. In the sections below, the behaviour and modelling of wind velocities is briefly discussed, after which the resulting loads on the structure are touched upon as well.

### 3-1-1 Wind regime

As a first foundation of determining the aerodynamic loading on the structure, it is key to formulate a representation of the wind velocities that will be present. These wind velocities are typically not constant, but vary over time. These variations can be annual and seasonal variations, synoptic and diurnal variations or changes over seconds and minutes (called turbulence). For the scope of this research (in which the aim is to model the system in a seconds or minutes range), the latter is of most influence and will therefore be taken into account. The former fluctuations are outside the scope of this research.

In order to capture the effect of turbulence, the wind velocity is described as a superposition of a steady (mean) wind speed $\bar{u}$ and a varying turbulent wind speed $u_0(t)$. These wind speed variations can be described by a turbulence intensity and a power spectral density (PSD) [23]. The intensity is a characterisation of the overall level of turbulence and is defined as. [4].

$$I = \frac{\sigma_w}{\bar{u}} \tag{3-1}$$

Here $\sigma$ is the standard deviation of the variation of wind speed about $\bar{u}$, the mean wind speed (taken as a 10 minute average). This intensity only captures non temporal information (height, roughness at surface, etc.) and could be interpreted to form the boundary conditions for the temporal fluctuations.

The temporal information of the turbulence (e.g. the frequency of wind speed fluctuations) is captured in the turbulence power spectral density function (PSD) [23], from which a wind time series can be constructed.

In literature several turbulence spectra are recurring, for simplicity however only the Kaimal type PSD function is used in this study. Whereas the Kaimal PSD type function provides a certain standard relation, various formulations of this type are available. Here the Kaimal PSD as defined in [24] is used. This formulation is described by equation 3-2 below and visualised in figure 3-1.

$$S(f) = \sigma^2 \frac{4L_u/\bar{u}}{(1 + 6fL_u/\bar{u})^{5/3}} \tag{3-2}$$

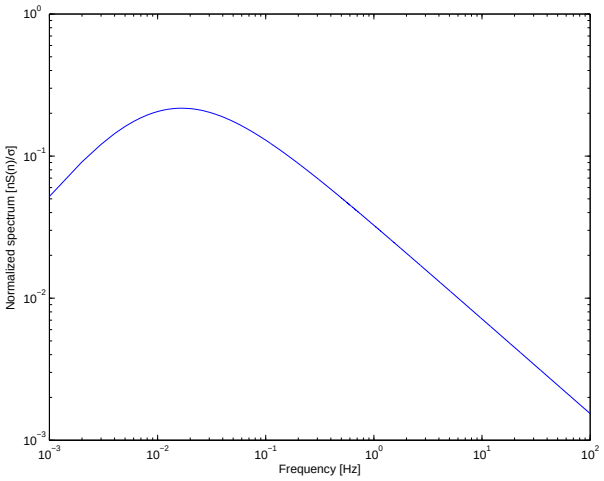


**Figure 3-1:** Kaimal spectrum

In which $f$ is frequency [Hz], $\sigma = \bar{u}/ln\frac{z_{ref}}{z_0}$, $\bar{u}$ is the 10 minute average wind speed and $L_u$ is a predefined length scale. $L_u = 5z$ for $z < 30m$ and $L_u = 150m$ for $z > 30m$, in which $z$ represents the height above ground or, in the case of offshore application, the sea level. $z_0$ is a measure for surface roughness, which is set to 0.001 for locations offshore.

The Kaimal PSD is typically valid for time scales from roughly 0.02 sec to 600 sec [25].

From this spectrum a wind velocity time series is constructed to come to aerodynamic loading over time. One of the mathematical procedures to come to this time series is found in the harmonic series method [26]. This method involves the summation of a series of cosine waves at various frequencies ($\omega_n$) with weighted amplitudes in line with the spectrum definition, covered in equation 3-3. By doing so, a time series as presented in figure 3-2 is developed.

$$u(t) = \bar{u} + \sum_{n=1}^{N} \sqrt{2S(f)\Delta f}\ \ cos(\omega_n t - \phi_n) \tag{3-3}$$

Here $\omega_n$ is the radial frequency corresponding to frequency $f$, $\phi_n$ is the radial phase angle at frequency $f$, modelled as a random number between 0 and $2\pi$ and $S(f)$ is the power spectral density.

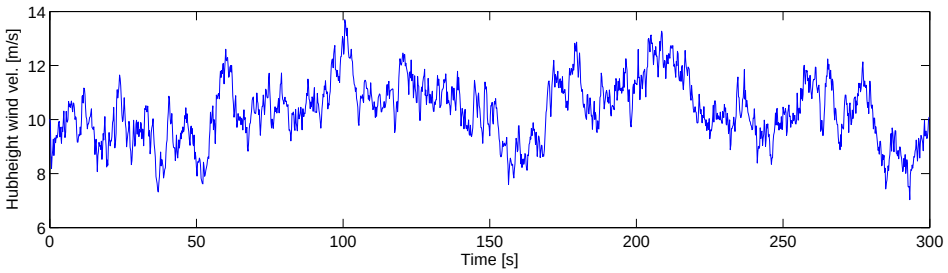


**Figure 3-2:** Wind speed time series

In Hansen (2008) [4] a note is made towards the application of a power density spectrum, a PSD function typically assumes the presence of all frequencies from 0 to $\infty$, in practice however, not all frequencies are present in a time series of finite length. Therefore, for the application of the Kaimal spectrum, the considered frequencies are defined by the duration and the time step size of the simulation. $f_{min}$ is defined by $1/T_{sim}$, with a minimum of 0.002 $Hz$ (corresponding to a sample duration of 500 seconds), and $f_{max}$ is defined by $1/(2\Delta t)$. Therewith the higher end of applied frequencies (approximately $5Hz$ for $\Delta t = 0.1s$) is within the applicable range of the Kaimal spectrum and the minimum frequency applied is the cut-off frequency of $0.002Hz$, neglecting additional low-frequency effects in longer simulations.

### 3-1-2 Aerodynamic loads

From this wind speed time record, the actual loads acting on the structure can be determined. There are various approaches available to describe these loads, ranging from approximate simple methods to very detailed and more exact methods. In this study a simplified method is applied. First a separation is made between the loads acting on the turbine(blades) and the loads acting on the tower supporting the turbine, as seen in the schematic representation in figure 3-3. This enables us to determine both contributions separately before adding them up through the principle of superposition to come to the overall aerodynamic loading.

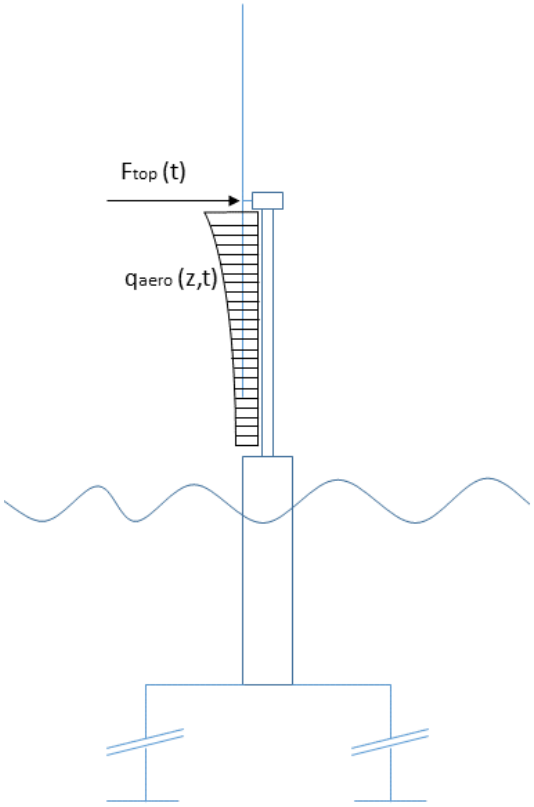


**Figure 3-3:** Aerodynamic loads

### Loads on the tower

The aerodynamic load along the turbine tower can be expressed by an approach based on Morison's equation [3], presented in equation 3-4 below.

$$q_{aero}(z,t) = C_{D,w}\frac{1}{2}\rho_a \left[u(z,t)|u(z,t)|\right] D(z) \tag{3-4}$$

Here $u(z,t)$ is the wind velocity along the tower height and in time, based on the representation presented in the previous section. $C_D$ is the dimensionless drag coefficient, which depends on tower dimensions and wind flow regime. $\rho_a$ is the air density and $D(z)$ is the tower diameter at elevation z. $D(z)$ follows from the definition of the turbine system used, as described in section 2-1.

The variation of wind velocities over height and time $u(z,t)$ is defined based on the reference wind speed at hub height as presented in the previous section, using equation 3-5 below.

$$u(z,t) = u(z_{ref})\left(\frac{z}{z_{ref}}\right)^{\alpha} \tag{3-5}$$

$u(z_{ref})$ is the wind speed at reference heigh ($z_{ref}$), which is set to the hubheight of the turbine. The vertical coordinate $z$ varies along the height of the tower and the windprofile exponent

$\alpha = 0.14$ is based on the GL offshore rules for wind turbines [27]. This results in a wind profile along the height of the tower, an example for a wind velocity of 11 m/s at hub height (at $z = 90m$) is presented in figure 3-4.

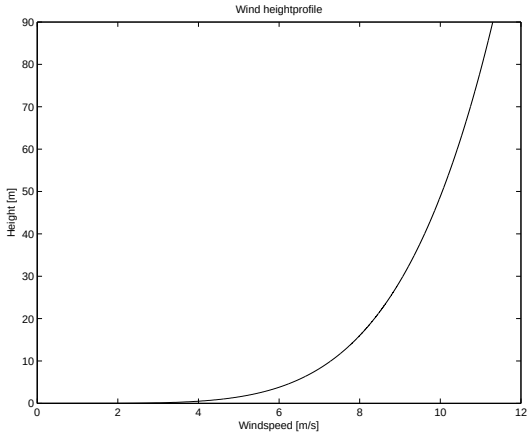


**Figure 3-4:** Wind profile along turbine tower, for $11m/s$ wind velocity at hub height

$C_D$ in equation 3-4 is approximated using the graph displayed in figure 3-5. In this figure the drag coefficient is displayed as a function of the Reynolds number.

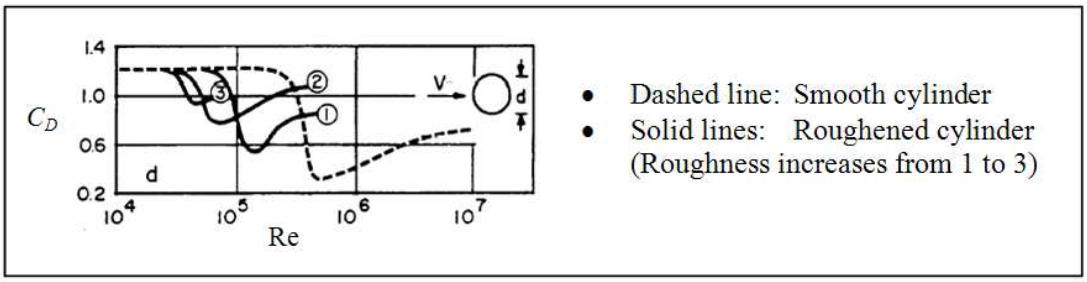


**Figure 3-5:** $C_D$ values for a range of Reynolds numbers [3]

The Reynolds number seen in figure 3-5 can be determined using equation 3-6 below.

$$Re = \frac{u(z,t)D}{\nu} \tag{3-6}$$

In which $u(z,t)$ is in the order of 10 $m/s$, the tower diameter ($D$) is around 6 $m$ and kinematic viscosity of air ($\nu_{air}$) is $15 * 10^{-6}$ $m^2/s$. This combines to a Reynolds number of $4 * 10^6$. This gives an approximate $C_D$ value of 0.6 along the height of the tower.

### Loads on the turbine

Naturally the loads acting on (the blades of) the wind turbine depend on the incoming wind velocity and the shape and size of the turbine. They also depend on for example the blade rotational movements and their orientation (or pitch angle). Since the focus of this study

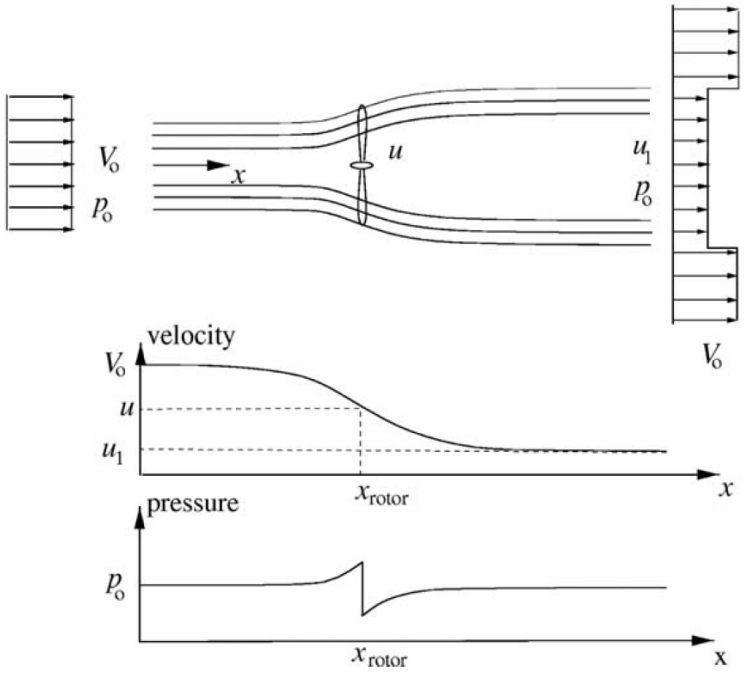


**Figure 3-6:** Streamlines and axial velocity and pressure drop over turbine rotor [4]

is not on the details of the aerodynamic loading principle of wind turbines, it is chosen to apply a simplified approach that includes these effects to some extend, without adding to the complexity of the model. Two main possible methods have been assessed here: the actuator disk theory and the application of the predefined thrust curve fo the reference turbine (as presented in chapter 2).

In the actuator disk theory the turbine is represented by an ideal cylindrical disk perpendicular to the wind flow direction [4]. From the fundamentals of momentum theory, the basic principle of the thrust (force acting in horizontal direction) on the rotor results from the pressure drop over the rotor. This principle is represented in equation 3-7 and figure 3-6 below.

$$T_{wind} = \Delta p A_{rotor} \tag{3-7}$$

Here $A_{rotor}$ is the swept area of the turbine, corresponding to the area of a circle with diameter equal to turbine diameter. $\Delta p$ is the pressure drop, which can be expressed according to equation 3-8, where $\rho_a$ is air density, $V_0$ is the velocity far upstream and $u_1$ is the velocity far downstream.

$$\Delta p = \frac{1}{2}\rho_a({V_0}^2 - {u_1}^2) \tag{3-8}$$

$u$ (the velocity in the rotor plane) is the mean of $V_0$ and $u_1$. The introduction of the axial induction factor 'a' defined in equation 3-9 (with a maximum of 1/3) provides the expression of thrust force as a function of the upstream wind velocity (equation 3-10).

$$u = (1 - a)V_0 \tag{3-9}$$

$$T_{wind} = 2\rho_a V_0 |V_0| a(1-a) A_{rotor} \tag{3-10}$$

The application of this theory, however, does not accurately describe thrust loads over the workable range of wind velocities of the turbine. This effect is visualised in figure 3-7 in a comparison with the reference thrust curve defined by NREL [1].

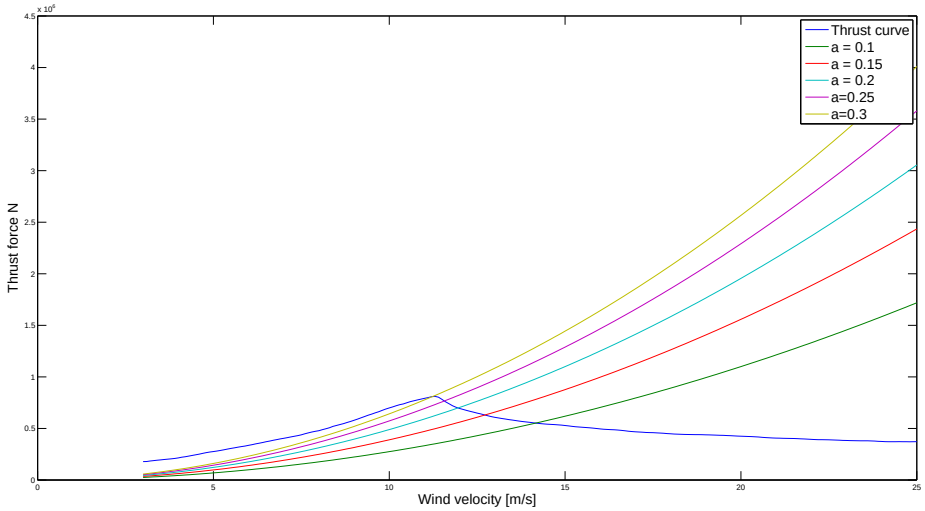


**Figure 3-7:** Thrust force from actuator disk theory for a range of 'a' values, compared to reference curve [1]

The direct application of the reference thrust curve on the other hand is unable to correctly capture effects of turbulence and platform motions, since for certain wind velocities it yields that an increase of wind velocity will result in a decrease in thrust force. This might be true for steady wind conditions in which the control system has adjusted its blade pitch, but for turbulence effects or platform motions this is not thought to be the case.

Although both methods are fundamentally based on steady wind velocities and therefore not directly applicable for turbulent wind conditions. The application of the combination of both can help to overcome some of the shortcomings of the application of either one of them separately. The thrust curve is applied to tune the induction factor of the actuator disk approach such that the thrust force matches that of the reference thrust curve. Then, any fluctuations in wind velocity are covered by the actuator disk approach, which overcomes the main shortcoming of the thrust curve approach. In appendix D the choice for this combined approach is more elaborately explained.

### The effect of platform motions

Although the concepts used for determining the aerodynamic loading are relatively simple, it is opted to couple these to the platform motions. In order to come to such a coupling, the load definitions are adjusted to accommodate the influence of platform motions.

The load definitions are a direct product of the incoming wind velocities and therefore the effect of platform motions on these velocities is captured in a relative wind speed as 'seen' by the turbine. Looking at the schematic representation in figure 3-8, the DOFs of interest here are the surge ($X_1$) and pitch ($X_3$) motions, since they both have contributions to the horizontal movements along the height of the tower.

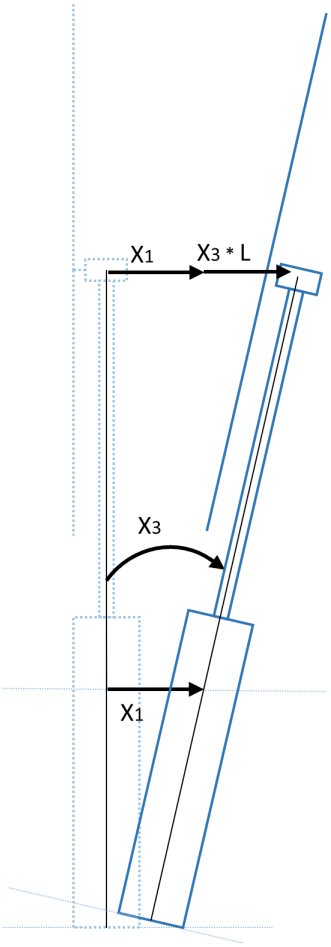


**Figure 3-8:** The effect of platform motions at hub height on relative wind velocity

The resulting velocity for which the aerodynamic loads are determined is defined to be:

$$u_{w,rel} = u(z,t) - (\dot{X}_1 + \dot{X}_3 z) \tag{3-11}$$

This relative velocity is fed into the load determinations as introduced in the previous sections.

## 3-2 Hydrostatic loads

The first effects of water surrounding the platform are in the form of hydrostatics. Hydrostatic loading on the submerged structure is independent of both incoming waves and radiating waves resulting of platform motions; instead these loads are influenced by submergence of a volume and the effects of platform motions on this submergence. The linear hydrostatic force on the floating platform consists of two parts, as presented in equation 3-12.

$$F_i^{Hydr} = \rho g \nabla_0 \delta_{i2} - K_{ij}^{Hydr} X_j \tag{3-12}$$

The first part of the equation is a formulation for the buoyancy force, defined by Archimedes' principle, which is a vertical (upward) force with a magnitude equal to the weight of the displaced fluid resulting from the submerged volume of the platform in undisplaced position. In this part of the equation, $\rho$ is the water density, $g$ is the gravitational acceleration, $\nabla_0$ is the undisplaced volume of the floating platform under water and $\delta_{i2}$ represents the (i,2) component of the Kronecker Delta function, used to indicate that this force is limited to the heave direction.

The second part of the equation captures the influence of platform motions on the hydrostatic loads acting on the floater. $K_{ij}^{Hydr}$ forms the (i,j) component of the hydrostatic restoring matrix formed by effects of water plane area and centre of buoyancy, $X_j$ is the $j^{th}$ platform DOF. Both $i$ and $j$ in equation 3-12 range from 1 to the number of DOFs.

These restoring forces can be expressed as a restoring stiffness for motions in the DOF they act. In surge direction there is no hydrostatic restoring present, the only restoring forces present in that direction source from the mooring system, as introduced in section 2-3. For the heave direction, given the vertical walled characteristics of the floater, the stiffness definition in equation 3-13 holds.

$$K_{22}^{Hydr} = \rho g A_{WL} \tag{3-13}$$

In which $\rho$ is the water density and $A_{WL}$ is the water plane area of the floater. For the pitch direction, the hydrostatic restoring stiffness of a body in water includes the water plane area's moment of inertia and the position of both the center of buoyancy and gravity [28], as indicated in equation 3-14 below.

$$K_{33}^{Hydr} = \rho g \left[ I_{WLY} + \nabla (z_B - z_G) \right] \tag{3-14}$$

The application of this equation in the case of a TLP would be incorrect, since the tensioned mooring arrangement provides an imbalance of buoyancy and gravity, which should be accounted for. This is done by the introduction of the tension forces as lumped masses at connection point of the tendons.[21]

$$K_{33}^{Hydr} = \rho g I_{WLY} + U z_B - Q z_G - \sum_{n=1}^{N} T_n z_T \tag{3-15}$$

In which U and Q represent the buoyancy and weight respectively and $z_B$ and $z_G$ are the vertical locations of both. $\sum_{n=1}^{N} T_n = U - Q$ is the total tension force acting on the platform, equalling the difference between buoyancy and weight, $Z_T$ is the vertical coordinate of the connection point of the tendons. A more detailed description of this formulation of pitch hydrostatics can be found in [21].

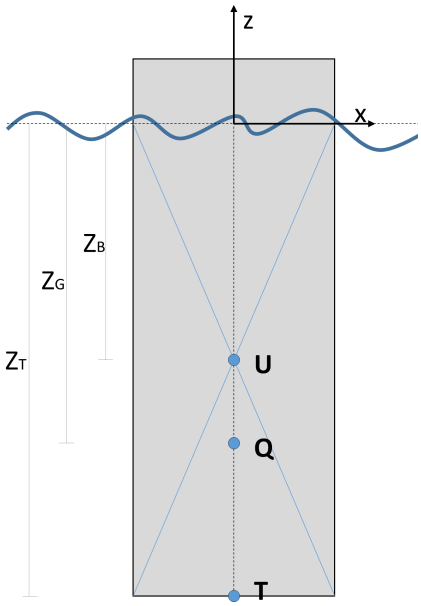


**Figure 3-9:** Vertical position of centres of buoyancy, gravity and tendons on the platform floater

## 3-3 Hydrodynamics

When placing a body in water at an offshore location, the loads of the water on the structure are not only influenced by the static interaction with water, but also by motions of the surrounding water mass. Therefore in this section, the effects of waves and current are introduced.

Wave loading on the floating platform can be divided in: 1. loads resulting from incoming waves and 2. loads that result from radiating outgoing waves (oscillation loads). Common practice in offshore engineering is to separate both load types and determine their magnitude separately before combining both in their combined action on the floater. Current loads are dominated by drag forces, resulting from the flow of water particles past its surface.

In the sections below all three contributions are discussed in detail.

### 3-3-1 Oscillation loads

Oscillation wave loads on a floating structure are formed by waves that propagate radially from the structure outwards, as a result of platform oscillating motions. Wave radiation loads on the floating support structure are typically defined by contributions in the from of

hydrodynamic added mass, damping and restoring terms to the system's equation of motion. These characteristics are independent of incident waves, since the radiation problem has been separated from the diffraction problem.

The added mass and damping terms are steady state hydrodynamic forces and moments due to forced harmonic rigid body motions. In the determination of these forces, the forced motions generate outgoing waves resulting in fluctuating fluid pressures along the body. Integrating these fluid pressure forces over the surface gives the forces on the body, as defined in equation 3-16.

$$F_i^{Rad} = -A_{ij}\frac{d^2\eta_j}{dt^2} - B_{ij}\frac{d\eta_j}{dt} \tag{3-16}$$

This representation defines that a motion in direction $j$ will have a contribution to a force acting in direction $i$. The motions considered in this study are visualised in figure 3-10. From this definition it becomes clear that there are a total of $DOF^2$ added mass and damping coefficients, which in this 2D approximation (with $X_1, X_2$ and $X_3$ as DOFs) leaves us with 9 coefficients each. These coefficients can be bundled in matrix notation in the following manner, equation 3-17.

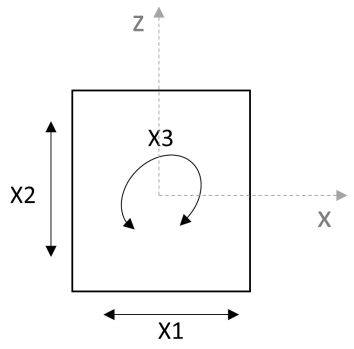


**Figure 3-10:** Motion definitions for oscillation loads

$$A_{i,j} = \begin{bmatrix} A_{1,1} & A_{1,3} & A_{1,5} \\ A_{3,1} & A_{3,3} & A_{3,5} \\ A_{5,1} & A_{5,3} & A_{5,5} \end{bmatrix}, \quad B_{i,j} = \begin{bmatrix} B_{1,1} & B_{1,3} & B_{1,5} \\ B_{3,1} & B_{3,3} & B_{3,5} \\ B_{5,1} & B_{5,3} & B_{5,5} \end{bmatrix} \tag{3-17}$$

The values of these added mass and damping coefficients mainly depend on oscillating frequency and the geometric shape of the support platform. For this thesis research Ansys AQWA software has been made available and is used to come to the added mass and damping characteristics.

For the combined floater and turbine system the added mass and damping coefficients (in frequency domain) have been determined for the frequency range of interest. A graphical representation of these added mass and damping characteristics can be found in Appendix C.

Since the analysis performed in Ansys AQWA is in frequency domain, the added mass and damping characteristics are output in frequency domain as well. This representation provides insight in the system's behaviour at various oscillating frequencies, but is not directly applicable in the time domain analysis we want to perform.

In order to make use of these coefficients in the time domain analysis, a transformation from frequency to time domain is required. The relation between frequency domain coefficient and the required time domain coefficient can be derived by applying Ogilvie's method (1964) [29]. Here Cummins equation (1962) [30] (equation 3-18 below) is related to the frequency domain equation of motion to come to the relation of frequency and time domain coefficients in equation 3-19 below [31].

$$(M + M_A)\ddot{x} + \int_0^\infty k(\tau)\dot{x}(t-\tau)d\tau + Cx(t) = F(t) \tag{3-18}$$

$$F^{Rad}(t) = -A(\omega_k)\ddot{\zeta}(t) - B(\omega_k)\dot{\zeta}(t) = -M_A\ddot{\zeta}(t) - \int_0^t k(t-\tau)\dot{\zeta}(\tau)d\tau \tag{3-19}$$

Where $A(\omega)$ and $B(\omega)$ are added mass and damping matrices in frequency domain, $M_A$ is the inertial part of added mass in time domain and $k(t)$ is the wave radiation kernel defined by either of both Fourier transforms presented in equations 3-20 and 3-21 below [31] [18].

$$k(t) = \frac{2}{\pi}\int_0^\infty B(\omega)\cos(\omega t)d\omega \tag{3-20}$$

$$k(t) = \frac{2}{\pi}\int_0^\infty \omega(A(\omega) - M_A)\sin(\omega t)d\omega \tag{3-21}$$

In this study, the definition in equation 3-20 is implemented, since it requires the least computational steps and therefore is most beneficial in view of simulation time. The inertial part of oscillation loads in time domain is defined to be the value of added mass in frequency domain for infinite frequency [31]. Since infinite frequency is not a physical outcome of Ansys AQWA the value for the highest considered frequency is implemented.

$$M_{A_{ij}} = A_{ij}(\infty) \tag{3-22}$$

In the system's equation of motion, $M_A$ is added to the mass matrix.

The wave radiation kernel is combined with the system's velocity in a convolution integral to come to the radiation loads acting on the platform. This convolution integral is implemented to include the so-called memory effect of the water surface, see equation 3-23.

$$F_{memory} = \int_0^t k_{ij}(t-\tau)\dot{X}_j(\tau)d\tau \tag{3-23}$$

More detail on Ogilvie's method is presented in appendix E and additionally, full derivations of the relation of frequency and time-domain coefficients can be found in [31] and [32].

### 3-3-2 Wave excitation loads

In contrast with the oscillating loads, the wave excitation loads consist of forces and moments that act on the structure as if it were restrained. These loads are typically composed of Froude-Kriloff and diffraction forces and moments [33], which are related to the wave elevation. Therefore it is important to define a realistic description of the wave climate before actual load determination can take place.

#### Regular wave theory

In this study, airy wave theory is applied as a basic description of waves. This is a fundamental theory that defines waves as an orbital motion that can be described as a sinusoidal function.

The application of this theory is valid for waves with limited steepness (defined as the ratio of wave height $H$ and length $\lambda$, $\left(\frac{H}{\lambda}\right)$), which seems valid since the application of floating support structures for wind turbines will be applied only in deep waters. One major disadvantage of this approach is its inability to model breaking waves, slam and slap forces. However, in view of modelling simplicity, these effects are kept out of the scope of this work.

Airy wave theory describes the motion of water particles dependent of vertical and horizontal position and time. These wave particles are described to move in a circular orbital motion in which the wave period and length are related through the dispersion relation, see equation 3-24 below.

$$\omega^2 = gk \tanh(kh_w) \tag{3-24}$$

Here $\omega$ is the angular wave frequency ($\frac{2\pi}{T}$), $g$ is the gravitational acceleration, $k$ is the wave number and $h_w$ is water depth. From this relation, the wave number can be derived for a wave with a prescribed period-water depth relation.

The surface elevation ($\eta$) is described by equation 3-25, in which $\eta_a$ is the wave amplitude ($\eta_a = \frac{H}{2}$) and $x$ is the horizontal position relative to the neutral position.

$$\eta = \eta_a cos(\omega t - kx) \tag{3-25}$$

Figure 3-11 is a graphical representation of a regular wave prescribed by airy wave theory, with an amplitude $\eta_a$ of 3 meters and a period T of 10 seconds.

#### Irregular waves

When looking at the wave representation in figure 3-11, it is clear that the regular wave theory described previously does not provide a realistic representation of a real life ocean or sea surface. The actual wave climate can be more realistically described by a superposition

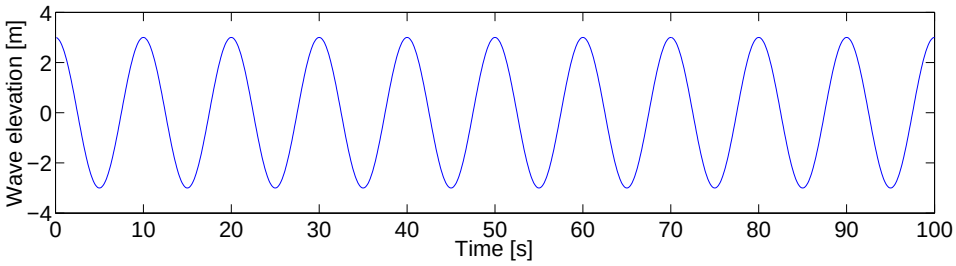


**Figure 3-11:** 2D regular wave, with $\eta_a = 3m$ and $T = 10s$

of many regular waves with various amplitudes and frequencies [28] [5]. This principle of superposition is visualised in figure 3-12 below, obtained from Holthuijsen 2007 [5].

The relation between frequency and amplitude in this superposition of regular waves can be characterised by a wave-spectrum, which defines the distribution of wave energy over frequency which is representative for a certain sea-state. For this research a Jonswap spectrum is considered, defined by the power spectral density, formed by equations 3-26 through 3-28 [18]. A graphical representation of the Jonswap spectrum is presented in figure 3-13, defined for $Hs = 5m$ and $T_p = 10s$ and a frequency range of 0.04 to 0.35 Hz.

$$S_\eta(\omega) = \frac{1}{2\pi}\frac{5}{16}H_s^2 T_p \left(\frac{\omega T_p}{2\pi}\right)^{-5} exp\left[-\frac{5}{4}\left(\frac{\omega T_p}{2\pi}\right)^{-4}\right][1 - 0.287ln(\gamma)]\gamma^{exp\left\{-0.5\left[\frac{\frac{\omega T_p}{2\pi}-1}{\sigma(\omega)}\right]^2\right\}} \tag{3-26}$$

$$\gamma = \begin{cases} 5 & \text{for} \quad \frac{T_p}{\sqrt{H_s}} \leq 3.6 \\ exp\left(5.75 - 1.15\frac{T_p}{\sqrt{H_s}}\right) & \text{for} \quad 3.6 < \frac{T_p}{\sqrt{H_s}} \leq 5 \\ 1 & \text{for} \quad \frac{T_p}{\sqrt{(H_s)}} > 5 \end{cases} \tag{3-27}$$

$$\sigma = \begin{cases} 0.07 & \text{for} \quad \omega \leq \frac{2\pi}{T_p} \\ 0.09 & \text{for} \quad \omega > \frac{2\pi}{T_p} \end{cases} \tag{3-28}$$

This spectrum representation can be used in the development of a wave elevation time series. This time series consists of the sum of many regular waves of different frequency ($\omega_n$) and amplitude ($a_n$), which is formed by the inverse Fourier transformation of the wave spectrum. This transformation is performed in equation 3-29, by application of the harmonic series method [5]. In equation 3-29, $k_n$ is the wave number and $\theta_n$ forms a random phase angle between 0 and 2 $\pi$. The wave number is determined from the dispersion relation using the Newton-Raphson method for each frequency along the defined Jonswap spectrum (equation 3-24).

$$\eta(x,t) = \sum_n a_n cos(\omega_n t - k_n x + \theta_n) \tag{3-29}$$

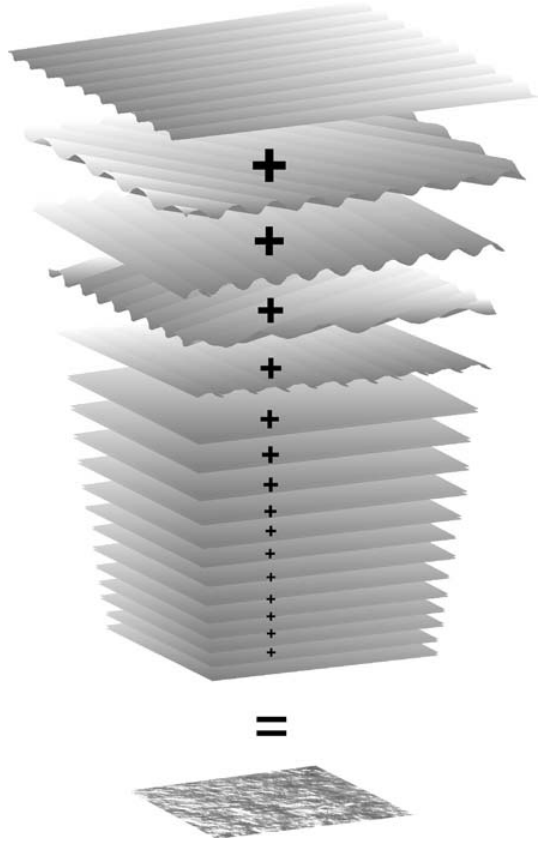

**Figure 3-12:** Irregular sea, as a summation of many harmonic waves, retrieved from [5]

Equation 3-30 defines the frequency dependent wave amplitude, in which $\Delta\omega$ is the radial frequency step size and $S_\eta$ is the spectral density of the Jonswap spectrum [34].

$$a_n = \sqrt{2S_\eta(\omega)\Delta\omega} \tag{3-30}$$

By applying equation 3-29 to the Jonswap spectrum, defined in equation 3-26, a time series of surface elevation is constructed, as visualised in figure 3-14.

This surface elevation in its turn is used to determine the hydrodynamic wave forces at a given time instant, as will be discussed in the next section.

### Incident wave forces

Any body, submerged in a sea or ocean will be subject to hydrodynamic forces that result from fluctuations in water plane elevation over time. For the determination of the magnitude of these forces, two distinguishable methods were considered.

1. Application of the Morison equation
2. Making use of a diffraction software package

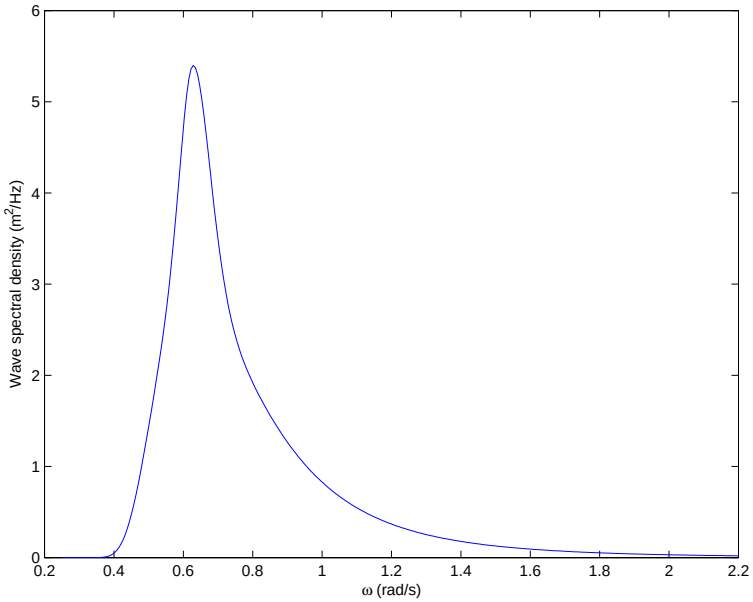


**Figure 3-13:** Graphical representation of a Jonswap spectrum, for $H_s = 5m$, $T_p = 10s$

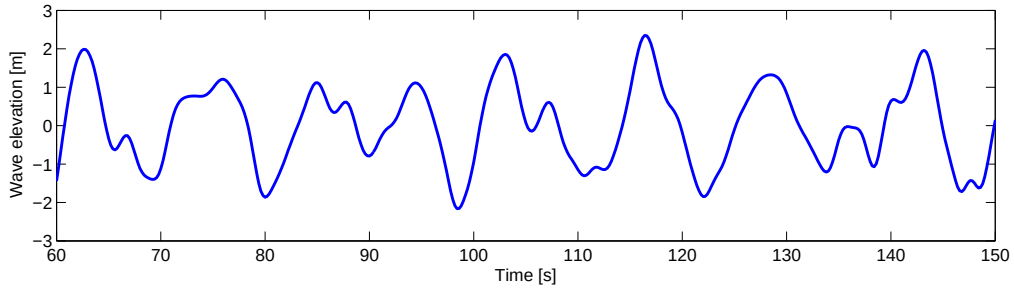


**Figure 3-14:** Surface elevation time series (Jonswap: Hs=4.4m, Tp=11s)

Whereas some platform geometries do not allow for the application of the Morison equation, the straightforward geometry of the platform in this study should not pose any issues. When looking at the complexity of the method, the Morison equation is quite straightforwardly determined from fluid velocity and acceleration along the surface of the submerged body, whilst a diffraction analysis requires a software package to perform an analysis based on 3D panel method. The choice for a method for the cylindrical structure at hand should be based on the ratio between the diameter of the structure (at the waterline) and the wave length. In case this ratio remains below 0.2, it can be considered that diffraction can be neglected and for values above 0.2 diffraction can no longer be neglected. Therefore, for $\frac{D}{\lambda} < 0.2$ the Morison equation can be applied [28] and for $\frac{D}{\lambda} > 0.2$ a diffraction analysis should be done.

This requirement can be used to formulate a range of wave frequencies for which the Morison equation can be applied. This would only hold for waves with a frequency below approximately 0.83 rad/s, which clearly does not cover the full sea-state at hand (visible in the example Jonswap spectrum in figure 3-13). Therefore a diffraction software package (Ansys AQWA) is used for determination of both Diffraction and Froude-Krylov forces acting on the platform. The outcomes of this analysis can be found in Appendix C.

The resulting wave exciting force vector from this analysis provides the combined Froude-Krylov and Diffraction force acting on the structure per direction as a function of wave frequency and per meter wave elevation. By expanding equation 3-29 with the introduction of the wave force vector ($X_i$) in frequency domain, an expression for wave forces over time can be found, resulting in equation 3-31 [18].

$$F_i^{Waves}(t) = \sum_N \sqrt{2\Delta\omega S(\omega)} cos(\omega_n t - k_n x + \theta_n + \phi_n) X_{i,n} \tag{3-31}$$

This expression provides the time signal for wave forces on the floater by performing an inverse Fourier transform on the Jonswap spectrum and wave excitation force. Here $\omega_n$ is the frequency of the incoming harmonic wave $n$, $k_n$ is the wave number, $\theta$ is a random phase angle (with uniform distribution between 0 and 2 $\pi$) and $\phi_n$ is the phase shift between wave elevation and the force acting on the body (derived from Ansys AQWA, figure C-5 in Appendix C).

In figure C-7 in Appendix C, an example time series of wave forces for all three directions is plotted against wave elevation, for a sea state of $H_s = 4m$, $T_p = 10s$.

### 3-3-3 Viscous drag loads

The final hydrodynamic effect that is included in the model of this study is the phenomenon of viscous drag. The hydrodynamic effects described in the previous sections only include non-viscous fluid forces onto the structure, based on fluid pressures acting on the hull. As a result of ocean currents, platform motions and water particle velocity resulting from the passing of incident waves, viscous effects are to be included as well.

The viscous drag effects act in both horizontal and vertical direction and can be described as a function of the fluid velocity along the hull's surface, as defined in equation 3-32.

$$dF_{drag} = \frac{1}{2}\rho C_{D,h} u_{res} |u_{res}| A_{prj} \tag{3-32}$$

Here $C_{D,h}$ is the hydrodynamic drag coefficient for flow around the floater, $A_{prj}$ is the projected area of interaction and $u_{res}$ is the residual fluid velocity acting on the floater.

For the horizontal and vertical interaction, several parts of equation 3-32 are defined differently. First off, the projected area for drag loads in both directions is quite different; in horizontal direction the projected area is a rectangle with dimensions: '$D \cdot Draft$'. In the vertical direction the area of interaction is formed by the bottom of the floater with area $\frac{\pi}{4}D^2$.

$C_D$ typically is a function of the shape of the area of interaction, and is defined to be 1 in case of horizontal flow (which is the flow around a cylinder) and 2 for vertical flow.

The residual fluid velocity is influenced by the effects of ocean current, platform motions and water particle velocities resulting from travelling incident waves. Since the environmental loads acting on the platform in this study are assumed to be aligned and unidirectional, the velocity effects can be directly summed up:

$$u_{res}(z,t) = u_{current} + u_{waves}(z,t) + u_{platform}(z,t) \tag{3-33}$$

The ocean current velocity in this study is assumed to be constant along the depth of the floater, which seems reasonable for the relatively small depth range.

The effect of platform motions on the residual horizontal velocity sources from both surge and pitch motions, whereas the contribution to the vertical component is formed by heave motions. All three DOF are visualised in figure 3-15 below, the velocity contributions are defined by equation 3-34 and 3-35.

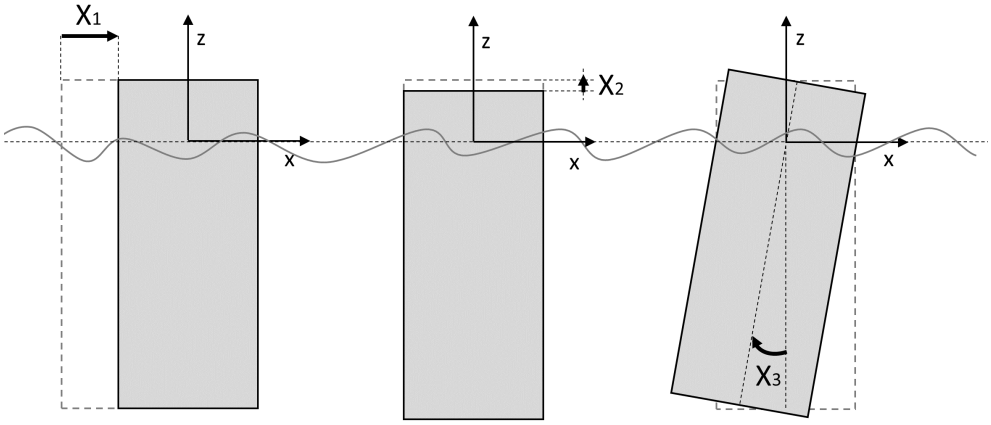


**Figure 3-15:** Effect of platform motions in all DOFs on residual fluid velocity

In line with the reference system, a positive surge velocity will reduce the residual incoming velocity and positive pitch velocities will increase the incoming velocity. In vertical direction, with positive heave defined upward, positive heave reduces residual velocity.

$$u_{platform,h}(z,t) = \dot{X}_3(t)|z| - \dot{X}_1(t) \tag{3-34}$$

$$u_{platform,v}(t) = -\dot{X}_2(t) \tag{3-35}$$

The final contribution to the residual fluid velocity results from travelling waves past the platform. This contribution can be incorporated by application of linear wave theory to come to the accompanied wave kinetics. From this theory, both the horizontal and vertical velocity component can be defined as a function of time and depth (as well as platform displacement).

$$u_{waves,h}(z,t) = \sum_{n=1}^{N} a_n \omega_n \frac{cosh(k_n)(z+h_w)}{sinh(k_n h_w)} cos(\omega_n t - k_n x \theta_n) \tag{3-36}$$

$$u_{waves,v}(z,t) = \sum_{n=1}^{N} -a_n \omega_n \frac{sinh(k_n)(z+h_w)}{sinh(k_n h_w)} sin(\omega_n t - k_n x \theta_n) \tag{3-37}$$

Here $n$ is the number of the regular wave in frequency range, $N$ is the total number of frequencies taken into account, $k_n$ is the wave number (as presented in equation 3-24), $z$ is the vertical coordinate, $h_w$ is the water depth, $\omega_n$ is the angular frequency, $t$ is time and $\theta$

is the random phase angle (ranging from 0 to $2\pi$) incorporated to come to a random wave signal. More detailed background information on the depth profile of horizontal wave kinetics can be found in appendix G.

Finally both horizontal and vertical resulting forces can be determined. In horizontal direction, drag acting on the structure will not only act as a force onto the structure, but will also introduce an overturning moment (in pitch direction). Both contributions depend on the horizontal residual flow along the height of the floater. In order to capture velocity variations along the height of the floater, several height segments of $\Delta z$ are considered. The force contributions along the height of the floater, as introduced in equation 3-32, are summed to come to an overall force contribution caused by viscous drag onto the floater.

$$F_{drag,1} = \sum_{-draft}^{0} \frac{1}{2} C_D \rho \, D \, u_{res,h}(z,t) |u_{res,h}(z,t)| \, \Delta z \tag{3-38}$$

$$F_{drag,3} = \sum_{-draft}^{0} \frac{1}{2} C_D \rho \, D \, u_{res,h}(z,t) |u_{res,h}(z,t)| \, z \, \Delta z \tag{3-39}$$

In vertical direction the residual velocity of interest is taken at the platform bottom (at $z = -47.89m$), resulting in the velocity contribution of equation 3-40, which is applied in equation 3-41 to come to the drag force acting in heave direction.

$$u_{res,v}(t) = u_{waves,v}(-47.89, t) - \dot{X}_2(t) \tag{3-40}$$

$$F_{drag,2} = \frac{\pi}{8} C_D \rho \, D^2 \, u_{res,v}(t) |u_{res,v}(t)| \tag{3-41}$$

## 3-4 Ice loading

Ice loading is added as part of the environmental loading, which is considered a novelty in research concerned with floating wind turbines. The presence of ice is assumed to be in the form of level ice, a sheet of ice covering the water surface in the vicinity of the turbine. The driving force of ice motions is assumed to be unlimited and constant, such that failure of the ice will occur as a result of constant stress and strain building (caused by a constant ice velocity). It is assumed that the ice can fail by either of two mechanisms:

- Failure through crushing
- Failure through bending

Failure through crushing is most likely to occur against vertical walled structures, whereas bending failure occurs against sloping structures. Through which type of failure the ice sheet will eventually fail is governed by ice mechanical behaviour which extends beyond the scope of this research, therefore both mechanisms are considered separately as distinct loading types.

### 3-4-1 Ice crushing

The crushing failure of ice has been investigated for bottom founded structures on many occasions, for floating structures however, limited research is readily available. For this study it is chosen to apply a model that has been developed for the determination of ice crushing loads on bottom founded structures. Even though this model was not intended for floating structures, its application seems reasonable based on the analogy of a bottom founded structure and a floating structure at larger deflections. It is thought that mooring stiffness will increase with larger deflections and the floater will show behaviour comparable to a bottom founded structure. On top of that, while the direct application of this model on a floating structure might not be fundamentally correct, it enable us to use a tested model and potentially compare outcomes for fixed and floating structures.

The model used here is presented by Huang and Liu (2009) [6] and is a modification of the Matlock-Sodhi model, which includes modelling the structure consisting of a Mass, Dashpot and a Damping coefficient (as is the case in the main modelling approach of this study). The ice cover is modelled as a series of ice teeth, in order to simulate discrete failure mode in ductile and transitional regions. In Figure 3-16 a graphical representation of this modelling approach can be found [6].

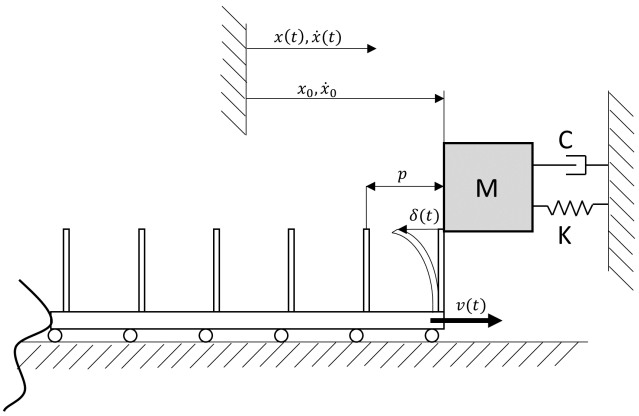


**Figure 3-16:** Ice crushing model, based on Huang (2009) [6]

As can be seen from Figure 3-16, the discrete teeth come into contact with the structure as a result of the movement of the ice. Depending on the relative velocity between the ice sheet ($v$) and the displacement of the structure ($x(t)$) the tooth is deflected ($\delta(t)$) until it reaches its breaking strength. When the breaking strength is reached the ice fails, after which it progresses to move along the structure until it reaches the next tooth, placed at a distance $p$ from the previous one, forming the constant failure zone.

The tooth deflection in this model is defined by

$$\delta(t) = X_1(0) + v_{ice}t - X_1(t) - pn_{ice} \tag{3-42}$$

Here $t$ is time and $n_{ice}$ is the number of teeth that have already passed the structure, which can be defined by rounding down $\frac{v_{ice}t}{p}$.

The ice force resulting from the contact between the structure and the 'tooth', is built up linearly from the moment of contact until the force reaches the failure force $F_f$. After this failure force is reached, the structure is subjected to a residual force, $F_e$ until the next tooth comes into contact. The time it takes for this force to build up is governed by the stiffness of the ice ($k_{ice}$), since the velocity of the ice is the driving mechanism which is assumed to be constant. Residual force, failure force, stiffness and deflection are related by:

$$\delta_f = \frac{(F_f - F_e)}{k_{ice}} \tag{3-43}$$

Where $\delta_f$ is the deflection at which the tooth fails, representing the maximum deflection. The residual force is assumed to be equal to 5% of the failure force. For the determination of $F_f$ two approaches have been studied (Korzhavin's formula [36] and the ISO 19906 [37]), a detailed description of both and the parametrization can be found in appendix H.

Both approaches make use of a predefined crushing strength of ice. This strength typically depends on the strain velocity of the loading at hand. Based on a variation in strain velocity three regions of failure types can be distinguished: the ductile, transitional and brittle regions [6].

The strength can be related to the strain velocity by:

$$\bar{\sigma}_f = \begin{Bmatrix} (1 - \bar{\sigma}_{fd})(v_r/v_t)^{\alpha} + \bar{\sigma}_{fd} & v_r/v_t \leq 1 \\ (1 - \bar{\sigma}_{fb})(v_r/v_t)^{\beta} + \bar{\sigma}_{fb} & v_r/v_t > 1 \end{Bmatrix} \tag{3-44}$$

where $\bar{\sigma_f} = \sigma_f/\sigma_{fmax}$, $\bar{\sigma}_{fd} = \sigma_{fd}/\sigma_{fmax}$ and $\bar{\sigma}_{fb} = \sigma_{fb}/\sigma_{fmax}$ with $\alpha > 0$ and $\beta < 0$ and $\sigma_{fd}$ and $\sigma_{fb}$ are minimum ice crushing strengths in the ductile and brittle regions respectively.

No in depth approach on the ice characteristics is applied, ice parameters are derived from existing literature. The main characteristics for ice in crushing failure can be found in table 3-1.

In the resulting force model for ice crushing action, three regions of loading can be distinguished:

- Loading phase ($0 \leq \delta < \delta_f$ and $\dot{X_1} \leq v_{ice}$)

  This phase is represented by the contact of ice 'tooth' before the failure force ($F_f$) is reached and its force is described by $F = k[X_1(0) + v_{ice}t - X_1 - p(n_{ice} - 1)] + F_e$

- Residual phase ($\delta_f \leq \delta < p$ and $\dot{X_1} \leq v_{ice}$)

  During this phase the ice has 'failed' and only the residual force ($F_e$) acts on the structure until the next ice 'tooth' comes into contact with the structure

- Lost of contact ($\dot{X_1} > v_{ice}$)

  Here the ice sheet and the structure are not in contact, since the velocity of the structure is greater than the ice sheet.

| Crushing ice parameters | |
|---|---|
| Max crushing strength ($\sigma_{fmax}$) | 1.8e6 $N/m^2$ |
| Ductile crushing strength ($\sigma_{fd}$) | 1.8e5 $N/m^2$ |
| Brittle crushing strength ($\sigma_{fb}$) | 1.8e5 $N/m^2$ |
| Ductile coefficient ($\alpha$) | 0.5 |
| Brittle coefficient ($\beta$) | $-2$ |
| Crushing stiffness ($k_{ice}$) | 2e7 $N/m$ |

**Table 3-1:** General ice crushing characteristics

The stiffness coefficient of the ice is chosen as $k_{ice} = 2.0e7N/m$. Furthermore, the distance between two ice teeth (p) has been set to $\delta_{fmax}$ which is the failure deflection at transitional ice velocity.

Since this model is defined for rigid structures, the structure's deflection x(t) is relatively small compared to the distance between two ice 'teeth' (p). In the current study however, motions are typically large, since it deals with a floating structure. Therefore, the application of the tooth deflection as introduced in equation 3-42 can not be directly applied. To account for the larger platform deflections, an adjustment is made to the correction term $n$ for deflections which are larger than p. Whereas in the original adjustment term $n$ only the travelled distance of the ice ($v_{ice}t$) was taken into account, in our application the effect of the platform motion $x(t)$ is included as well. So the definition of $n$ is adjusted to: $n =$ round down$(\frac{vt-x(t)}{p})$. A more in depth explanation of the adjustment is presented in Appendix H.

### 3-4-2 Ice bending

The second failure mechanism of level ice that is considered is the failure through bending. This mechanism is modelled by the application of an approach introduced by Aksnes (2010) [38]. This model describes the loading onto the structure governed by the failure of the incoming ice sheet resulting from bending loads caused by ride-up of the ice sheet against the structure.

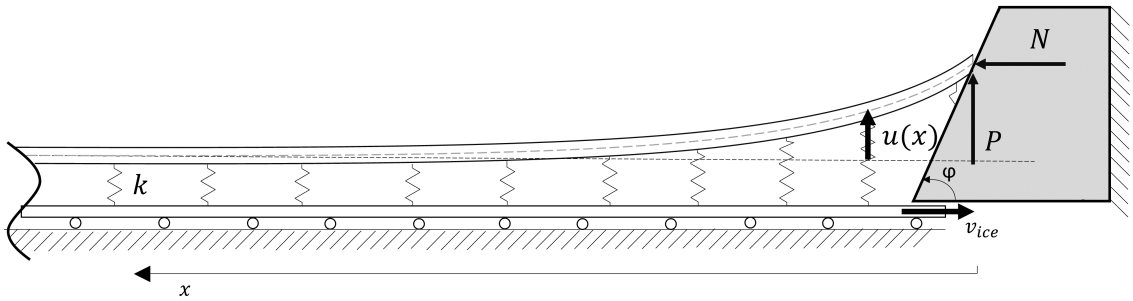


**Figure 3-17:** Visualisation of the applied model for ice bending load

In figure 3-17, $N_{ice}$ and $P_{ice}$ are the horizontal and vertical contact forces between the structure and the ice sheet and $k$ is the vertical stiffness characteristic of the ice on water, which is

equal to $\rho_w g B$. The mechanical properties of the ice sheet are described by the application of an Euler Bernoulli beam with properties that are in line with what can be expected of the ice sheet at hand. The differential equation applied in describing the deflection of the beam $u(x)$ is given in equation 3-45, with boundary conditions as shown in equation 3-46 below.

$$E_{ice} I \frac{d^4 u}{dx^4} + N_{ice} \frac{d^2 u}{dx^2} + \rho_w g D u = 0, \quad x > 0 \tag{3-45}$$

Here $E_{ice}$ is the ice bending elasticity, $I$ is the moment of inertia defined by: $I = \frac{1}{12} D h_{ice}^3$, $g$ is the gravitational acceleration and $B$ is the width of the floater.

$$\lim_{x \to \infty} u_{ice}(x) = 0, \quad \lim_{x \to \infty} \frac{du_{ice}}{dx} = 0, \quad \frac{d^2 u_{ice}(0)}{dx^2} = 0, \quad -EI \frac{d^3 u_{ice}}{dx^3} = -P_{ice} \tag{3-46}$$

These boundary conditions imply that:

- The beam is perfectly horizontal with zero deflection at a great distance from the structure.
- There is no bending moment present at the interaction point between the ice sheet and the structure ($x = 0$)
- The shear force in the beam at the interaction point between the ice sheet and the structure equals the vertical force acting on the structure.

Solving $u(x)$ from the boundary problem above, gives the solution

$$u_{ice}(x) = e^{-\beta x}(C_1 cos(\alpha x) + C_2 sin(\alpha x) \tag{3-47}$$

In which $C_1$ and $C_2$ are

$$C_1 = \frac{2 P_{ice}}{E_{ice} I} \frac{\alpha \beta}{2\alpha^3 \beta^2 + \alpha \beta^4 + \alpha^5} \tag{3-48}$$

$$C_2 = \frac{P_{ice}}{E_{ice} I} \frac{\beta^2 - \alpha^2}{2\alpha^3 \beta^2 + \alpha \beta^4 + \alpha^5} \tag{3-49}$$

With

$$\alpha = \sqrt{\lambda^2 + \frac{N_{ice}}{4 E_{ice} I}}, \quad \beta = \sqrt{\lambda^2 - \frac{N_{ice}}{4 E_{ice} I}}, \quad \lambda = \sqrt[4]{\frac{\rho_w g B}{4 E_{ice} I}} \tag{3-50}$$

In figure 3-18, an example of the bending shape of the ice beam is plotted against the distance 'x' with respect to the platform. In these definitions $N_{ice}$ is the horizontal and $P_{ice}$ is the vertical force resulting from interaction between the structure and the ice sheet. These forces are related by $N_{ice} = P_{ice} \xi$, where $\xi$ is derived from the angle of the structure ($\varphi$) and the kinematic surface roughness ('$\mu$') through:

$$\xi = \frac{sin(\varphi) + \mu cos(\varphi)}{cos(\varphi) - \mu sin(\varphi)} \tag{3-51}$$

From the solution of beam deflections along the length of the beam (equation 3-47) two important characteristics can be derived:

- The forces that act on the platform as a result of the ice-platform interaction
- The bending moment along the beam that will result into failure of the ice sheet

### Force determination

The forces can be derived by setting the difference between the beam deflection at the tip (x=0) equal to tip displacement resulting from the ride-up mechanism of the beam at the structure. The deflection of the beam at the tip derived from its differential equation(3-45) is known to be.

$$u_{ice}(0) = \frac{2P_{ice}}{E_{ice}I} \frac{\alpha\beta}{2\alpha^3\beta^2 + \alpha\beta^4 + \alpha^5} \tag{3-52}$$

The ride-up mechanism is defined by the combination of the structure's geometry and the velocity of the ice. By definition (as a result of the sloping structure), a movement of the ice at the structure in horizontal direction is accompanied by a vertical deflection. This vertical deflection is defined by:

$$U_{tip} = (v_{ice}t - X_1(t))tan(\varphi) \tag{3-53}$$

Where $\varphi$ is the angle of the slope of the structure, as indicated in figure 3-17, $v_{ice}$ is the ice velocity and $X_1(t)$ is the horizontal offset of the structure at time instant $t$ with respect to its neutral position. Setting the difference of the definition of $u(0)$ and $U_{tip}$ to zero and solving for $P_{ice}$, the vertical force ($P_{ice}$) acting on the structure can be found for time instant $t$. From the relation between the horizontal and the vertical force (equation 3-51) the horizontal interaction force can be derived as well and both can be used as an input in the system's equation of motion.

### Breaking limit

The force determination as defined in the model above would continually built up in time. In reality however, the ice sheet will break at a certain point. The breaking (stress) limit will be reached as a result of the bending moments in the beam, which source from the beam deflections. The bending moments along the beam can be determined by application of the following formula:

$$M_{bending}(x) = -E_{ice}I\frac{d^2u_{ice}}{dx^2} \tag{3-54}$$

Where $\frac{d^2u_{ice}}{dx^2}$ can be found by differentiating the $u_{ice}(x)$ definition from equation 3-47 twice, resulting in:

$$\frac{d^2u_{ice}}{dx^2} = e^{-\beta x}[(C_1\beta^2 - 2C_2\alpha\beta - C_1\alpha^2)cos(\alpha x) + (C_2\beta^2 + 2C_1\alpha\beta - C_2\alpha^2)sin(\alpha x)] \quad (3\text{-}55)$$

Figure 3-18 below presents both the beam deflection and the bending moment along the beam. From the bending moment along the x-axis the maximum bending stress can be determined, see equation 3-56.

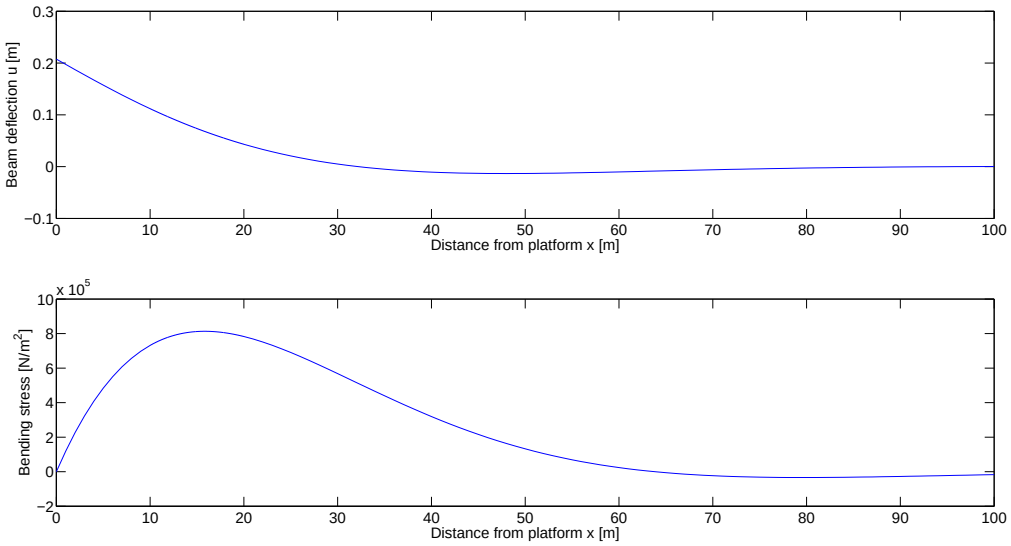


**Figure 3-18:** Typical deflection and stress profiles along the ice beam length

$$\sigma_{bend}(x) = \frac{6M_{bending}(x)}{Dh_{ice}^2} \quad (3\text{-}56)$$

A condition is added to compare this stress to the failure stress of the ice. If this failure stress is exceeded, the ice sheet breaks at location $x$ along the beam. As a result, the load acting on the structure drops to zero until the ice sheet beyond this breaking point comes into contact with the structure. The influence of this breaking length of the ice is implemented by adjusting the relative position of ice sheet with respect to the platform:

$$\kappa(t) = v_{ice}t - X_{br} \quad (3\text{-}57)$$

Here $X_{br}$ can be seen as a counter for the total length of all broken pieces of ice together. This counter is adjusted at the time instant at which the ice sheet breaks, then the breaking length is added to $X_{br}$. This effect is fed into the determination of the tip deflection and is used to determine whether the ice sheet and the structure are in contact or not.

The parameters used in the determination of bending loads are based on ranges of ice bending characteristics presented in [38], [37] and [39]. Overall, a conservative approach is applied in selecting the parameters. The applied characteristics can be found in table 3-2 below.

| Bending ice parameters | |
|---|---|
| Bending strength ($\sigma_f$) | $7e5\ N/m^2$ |
| Modulus of elasticity ($E$) | $2e9$ N/m |
| Kinetic friction ($\mu$) | 0.1 |
| Structure slope ($\varphi$) | 45 deg |
| Width of the ice sheet ($B$) | 18 m |

**Table 3-2:** General ice bending characteristics

From the ice failure mechanism described above, the breaking force contributions acting on the structure are determined to be $N_{ice}$, acting in horizontal direction and $P_{ice}$, acting in vertical direction. Both loads will however also contribute to the overturning moment acting on the floater.

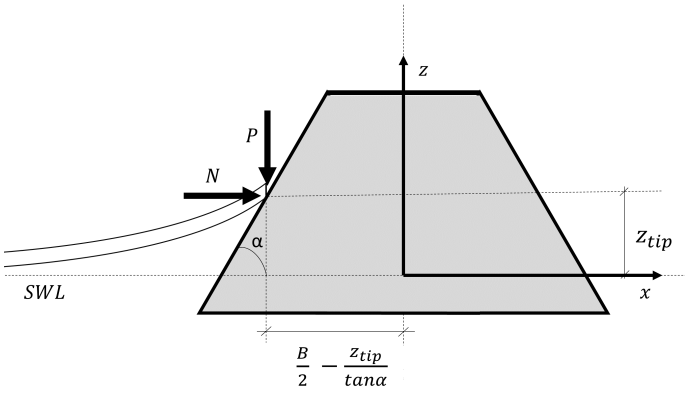


**Figure 3-19:** Overturning moment contribution ice bending loads

As can be seen from the schematic representation of the interaction between the ice sheet and the structure in figure 3-19, the ride up of the sheet and the horizontal offset of the point of interaction with respect to the reference system result in contributions to the overturning moment.

This is defined to be:

$$F_{bend,3} = U_{tip} N_{ice} - P_{ice} \left( \frac{D}{2} - \frac{U_{tip}}{tan\varphi} \right) \tag{3-58}$$

Where $U_{tip}$ is the ice beam's ride up against the structure, D is the width of the floater and $\varphi$ is the angle of the slope of the conical structure corrected for platform pitch.

### Rotation and friction forces

After failure of the ice sheet, a piece of ice with a certain length will break off from the front of the ice sheet. This piece of ice in reality will not suddenly disappear and will most likely

further interact with the structure. In the proposed model by Aksnes (2010) [38], which is aimed for interaction of level ice with moored vessels, rotation and friction force contributions are proposed to take into account further interaction between the ice and the structure. Since the structure in this research has a considerably deviating shape from that of a vessel hull, application of the proposed methods is not possible.

Instead, a highly simplified approach is applied in which the interaction of the ice sheet and the structure is imposed as a residual force, which is linked to the breaking force of the ice sheet. Based on the loading outcomes of Aksnes (2010), with the absence of friction force of the ice underneath the vessel's hull, the residual force is set to be 4 times the breaking force of the ice in bending.

Since this approach is very approximate, no definite conclusions can be drawn from this residual force contribution. Therefore, in the findings presented in chapter 5 a distinction is made between the outcomes resulting from bending loads with and without residual load contributions.

## 3-5 Load cases

In this research two main load case categorizations are considered: an open water load case and an ice covered load case. In the former, the system is subjected to a combination of waves, wind and current. The latter load case consists of loads resulting from interaction with ice, wind and current. In order to get insights in the dynamic behaviour of the floater-turbine arrangement under varying conditions, a range of load cases is considered both for open water and ice covered conditions.

### 3-5-1 Open water load case

In the case of open water conditions, variations in significant wave height, wind velocity and currents define different load cases. For the comparison of the model outcomes with existing literature, two load cases will be predefined to compare the model outcomes with the limited time series data available. These load cases consist of: 1. $Hs = 4.4\ m$, $Tp = 11.3\ s$ and a constant wind velocity of 20 $m/s$. 2. $Hs = 15\ m$, $Tp = 19.2\ s$ and mean wind velocity of 8 $m/s$.

Besides these predefined load cases a wider range of sea states is considered. First, the incoming wind can range anywhere between cut-in and cut-out wind velocity. Here, however, three distinct wind velocities are taken into account: 8 $m/s$, 11 $m/s$ and 20 $m/s$. First, ocean currents are set to 0 $m/s$, after which its effect is studied by application of a 0.5 $m/s$ current for the 11 $m/s$ wind velocity load cases.

The variations in sea-state are defined by combinations of significant wave height ($H_s$) and peak period ($T_p$). These are defined by a range of significant wave heights that are linked to peak period by the Bretschneider relation of wave period and significant wave height [28].

$$T_p = 5\sqrt{H_s} \tag{3-59}$$

From this relation, the following $H_s$ - $T_p$ combinations were derived for the sea state definition applied in the open water load cases.

| | Sea state load cases | | | | | | |
|---|---|---|---|---|---|---|---|
| | 1 | 2 | 3 | 4 | 5 | 6 | 7 |
| $H_s$ $(m)$ | 2 | 4 | 6 | 8 | 10 | 12 | 14 |
| $T_p$ $(s)$ | 7 | 10 | 12.5 | 14 | 15.75 | 17.25 | 18.75 |

**Table 3-3:** Wave height and period definition sea states

### 3-5-2 Ice covered load cases

The ice covered load case is governed by ice, current and wind loads. The main interest lies with both the thickness and the travelling velocity of the ice sheet. For an indication of ice thickness and velocity ranges, the ISO19906 standard [37] was used. For the placement of the turbine arrangement in for example the Baltic Sea, this standard shows that a range of velocities up to 0.35 $m/s$ would provide a reasonable estimation. Concerning the ice thickness, magnitudes with a maximum of 0.7 $m$ could be expected.

So for ice crushing load cases a velocity range from 0.1 to 0.4 $m/s$ and a thickness range from 0.1 to 0.7 $m$ is considered, with all possible combinations of both. For the ice bending load cases, ice velocities of 0.1, 0.2 and 0.3 $m/s$ are considered with an ice thickness of 0.25 to 1.5 $m$ is considered, since bending loads typically become significant at larger thickness.

It is chosen to apply wind velocity with a mean of 11 $m/s$ in all load cases across the ice load combinations. The effect of current velocity is studied by including 0.5 $m/s$ to the ice load cases of $v_{ice} = 0.2$ $m/s$ for both crushing and bending loads as a separate set of load cases. An overview of the load case definitions can be found in Appendix L.

# Chapter 4

# Dynamic modelling

In this chapter the system definitions from the previous chapters are extended to include effects of system dynamics. Additionally the set-up of the model for the main load cases is explained.

## 4-1 System definitions

As already indicated in chapter 2, the general equation applied in the model approach of this research is in the form of equation 4-1 below.

$$M\ddot{X} + C\dot{X} + KX = F(t) \tag{4-1}$$

Here $X$ is defined to be a vector covering motions in the prescribed 3 DOFs of the system (1. Surge, 2. Heave, 3. Pitch). $\ddot{X}$ and $\dot{X}$ are the second and first derivative of $X$ in time, which are the system's acceleration and velocity respectively. $M$, $C$ and $K$ are the system's mass, damping and stiffness matrices and include contributions of these three characteristics in all three DOFs and their correlations. All these system characteristics are defined in the coordinate system located at the centre of the floating support structure, at the cross section with the water line. Separate contributions of $M$, $C$, $K$ and $F(t)$ have already been introduced in chapters 2 and 3. In the next sections of this chapter, all contributions are combined and non-linearities are introduced.

### 4-1-1 Mass characteristics

The system's mass matrix consists of all inertial mass terms of the combined floater-turbine arrangement. It is build up from its structural characteristics and the inertial component of the floater's hydrodynamic added mass (as introduced in Chapter 3).

The structural mass characteristics have been derived from contributions of the various parts of the wind turbine arrangement as graphically represented by figure 4-1 below. The combined mass characteristics have been defined with reference to the centre of the floater at waterline. For the determination of the system's pitch mass moment of inertia Miner's rule is applied for the each component's mass and coordinate definitions.

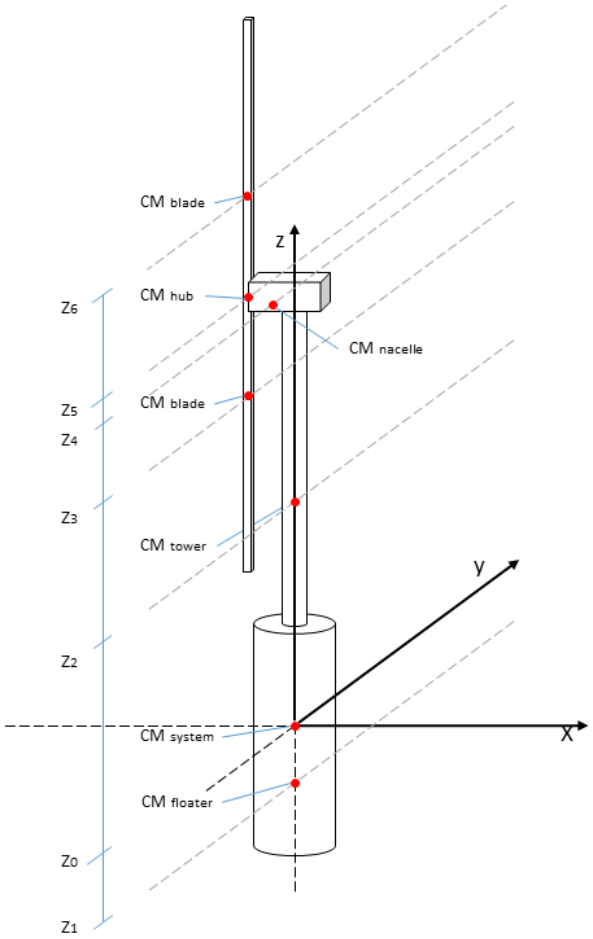


**Figure 4-1:** Component mass contributions w.r.t. combined centre of mass

Although in this formulation with the system's centre of mass (COM) as reference point, the structural mass of the system comprises to a diagonal mass matrix, the transformation from the COM to the waterline reference point results in the following mass matrix.

$$M_{Structural} = \begin{bmatrix} m & 0 & mz_G \\ 0 & m & -mx_G \\ mz_G & -mx_G & I_{yy} \end{bmatrix} \tag{4-2}$$

Where $m$ is the overall system's mass, $I_{yy}$ is the system's moment of inertia for rotations over the global $y$-axis with reference to the waterline reference point. $X_G$ and $Z_G$ are the $x$ and $z$ coordinates of the COM with respect to the reference coordinate system.

The inertial part of the system's hydrodynamic added mass has been determined in section 3-3. The eventual mass matrix of the system is the summation of the system's added mass matrix and the structural mass as presented above.

$$M = \begin{bmatrix} m + M_{A_{11}} & M_{A_{12}} & mz_G + M_{A_{13}} \\ M_{A_{21}} & m + M_{A_{22}} & -mx_G + M_{A_{23}} \\ mz_G + M_{A_{31}} & -mx_G M_{A_{32}} & I_{yy} + M_{A_{33}} \end{bmatrix} \tag{4-3}$$

The $M_{A_{ij}}$ terms are the inertial mass part of the system's hydrodynamic added mass, as introduced in section 3-3-1.

### 4-1-2 Damping characteristics

The damping characteristics of the system are formed by hydrodynamic damping of the floater resulting from motions in the surrounding fluid, as described in section 3-3-1. The time-domain formulation of the damping characteristics was found as indicated in equation 4-4 below.

$$k_{ij}(t) = \frac{2}{\pi} \int_0^\infty B_{ij}(\omega) cos(\omega t) d\omega \tag{4-4}$$

This wave radiation kernel represents the load contribution from added damping and an additional contribution of the added mass that has not been covered by the inertial part of the added mass ($M_{A_{ij}}$), as described in the previous section. This kernel function is convoluted with the velocity time trace of the system to come to the radiation force acting on the structure.

$$\int_0^t k_{ij}(t-\tau) \;\; \dot{X}_j \;\; d\tau \tag{4-5}$$

Since the relation of the load and the system's velocities is captured in the convolution integral, it is chosen to cover the system's damping in the $F(t)$ contribution of equation 4-1 instead of $C$. This has some consequences for the order of calculations, which will be touched upon in section 4-2.

### 4-1-3 Stiffness characteristics

The stiffness characteristics of the turbine-floater arrangement source from the submergence of (part of) the floater and its mooring system. Contributions are typically split into three categories:

- Hydrostatic restoring stiffness
- Conventional tendon stiffness
- Geometric stiffness

The separate contributions to the system's stiffness characteristics have already been introduced in Chapter 2 and 3 separately. Put together, they form the combined overall stiffness characteristic per DOF, defined in equations 4-6 through 4-8 below. These stiffness definitions are defined in line with Senjanovic (2013) [21], and with respect to the centre of the platform's bottom (the pole).

$$k11 = \sum_{n=1}^{N} \frac{T_n}{L} \tag{4-6}$$

$$k22 = \rho g A_{WL} + \sum_{n=1}^{N} \frac{EA_n}{L} \tag{4-7}$$

$$k33 = \rho g I_{WL} + U z_B + Q z_G - \sum_{n=1}^{N} \frac{EA_n {X_n}^2}{L} \tag{4-8}$$

The formulas provided above represent linear mooring stiffness definitions, which are valid only in the case of limited platform motions. From initial model outcomes however, it became clear that this assumption is not truly valid. Therefore the definitions are expanded to include non-linear effects resulting from platform movements.

For both the surge and heave motions, the non-linear effects evolve around the phenomenon of platform set-down. This phenomenon is typical for a TLP support structure and is best explained as the vertical motion that results from horizontal platform motions in combination with a (simplified) sketch presented in figure 4-2.

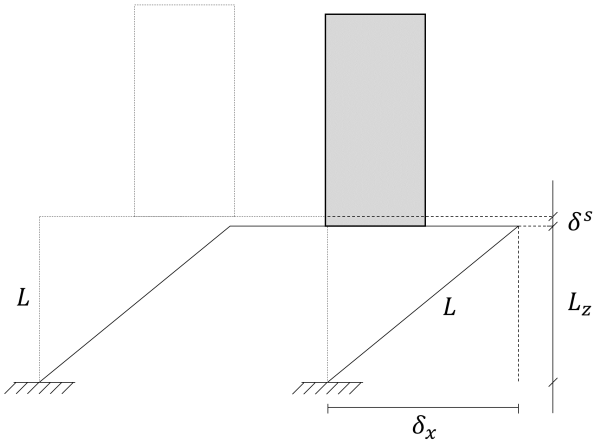


**Figure 4-2:** Visualisation of the TLP's set-down effect

From this graphical representation, it becomes clear that the definition of set-down can be described with:

$$\delta^s = L - L_z = L - \sqrt{L^2 - {X_1}^2} \tag{4-9}$$

In which $X_1$ equals the platform's surge motion and $L$ is the un-stretched mooring line length. This set-down definition is included in the surge motions stiffness [40]:

$$\tilde{k}11 = \sum_{n=1}^{N} \frac{T_n}{L_z} + \rho g A_{wl} \frac{\delta^s}{L_z} \tag{4-10}$$

From [40] [41] it is found that for the formulation of equations of motion at hand, the most convenient way to cover the set-down effect on heave is by coupling of surge and heave motions through the introduction of an additional stiffness term (k21), as defined in equation 4-11.

$$\tilde{k}21 = k22 \frac{X_1}{2L} \tag{4-11}$$

This stiffness contribution accounts for the vertical component of the non-linear heave stiffness resulting from set-down. Since set-down is considered to be very small in comparison with surge offsets, the horizontal component of the set-down effect is neglected. As a result, the stiffness matrix in equation 4-14 has an a-symmetric contribution $\tilde{k_{21}}$, neglecting coupling of surge by heave. This is in line with the reasoning in [40] that vertical motions strongly depend on horizontal displacements, whereas this is not the case vice versa.

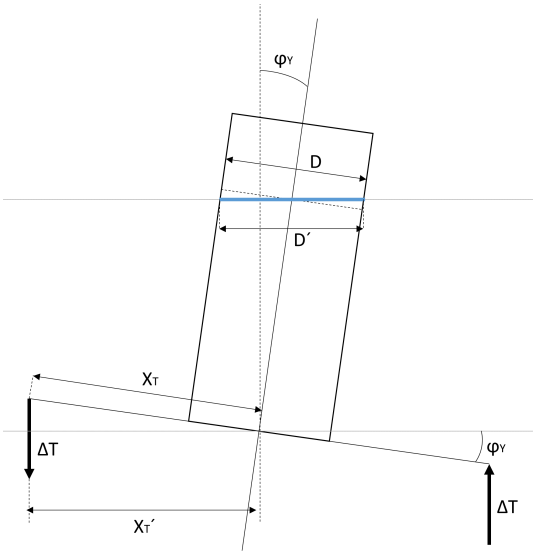


**Figure 4-3:** Non-linear pitch schematisation

In the pitch stiffness characteristics the non-linear effects, besides the set-down effect, include two additional contributions. First, the water-plane-area of the structure is altered from a cylindrical into an ellipsoidal shape due to the elongation of its longitudinal dimension from $D$ to $D'$, with $D' = D/cos\varphi_y$. This effect is taken into account by the introduction of the $cos^3\varphi_y$ term in the moment of inertia of the water plane ($I'_{WLY} = \frac{\pi}{64} D D'^3 = \frac{I_{WLY}}{cos\varphi_y}$). Secondly, the distance of the tether connection to the centre of the floater is decreased from $X_T$ to $X'_T$ as a result of pitch motion (see figure 4-3). This effect is covered by the introduction of $cos^2\varphi_y$ to adjust the $I_y$ term accordingly. Adding this to the definition of equation 4-8 gives equation 4-12.

$$k\tilde{3}3 = \frac{\rho g I_{WLY}}{cos^3\varphi_y} + U(Z_B - Z_T) - Q(Z_G - Z_T) + \tilde{k} + \frac{EI_y}{L}cos^2\varphi_y \tag{4-12}$$

Here $\tilde{k}$ includes the effect of set-down on the pitch motion, as presented in equation 4-13. This term reflects the effect of additional buoyancy from set-down on the pitch restoring overturning moment.

$$\tilde{k} = \rho g A_{WL}(Z_B - Z_T)\delta^s \tag{4-13}$$

A matrix representation of equations 4-10 through 4-13 gives the system's non-linear stiffness matrix with respect to the pole of the floater $K^P$ as presented in equation 4-14 below.

$$K^P = \begin{bmatrix} \tilde{k}_{11} & 0 & 0 \\ \tilde{k}_{21} & k_{22} & 0 \\ 0 & 0 & \tilde{k}_{33} \end{bmatrix} \tag{4-14}$$

For the implementation of this stiffness matrix in the equation of motion, it needs to be transformed to fit the coordinate system with the centre of the floater at SWL as the origin. This transformation introduces some additional off-diagonal terms to the one presented above. The resulting non-linear stiffness matrix with respect to SWL is defined in equation 4-15 below, in which changes to the matrix with the platform's pole as reference are indicated with $^*$.

$$K^{WL} = \begin{bmatrix} \tilde{k}_{11} & 0 & \tilde{k}^*_{13} \\ \tilde{k}_{21} & k_{22} & \tilde{k}^*_{23} \\ \tilde{k}^*_{31} & 0 & \tilde{k}^*_{33} \end{bmatrix} \tag{4-15}$$

The adjusted elements are defined as follows:

$$\tilde{k}^*_{13} = \tilde{k}^*_{31} = -z_{WLT}\tilde{k}_{11} \tag{4-16}$$

$$\tilde{k}^*_{23} = -z_{WLT}\tilde{k}_{21} \tag{4-17}$$

$$\tilde{k}^*_{33} = \tilde{k}_{33} + {z_{WLT}}^2\tilde{k}_{11} \tag{4-18}$$

## 4-2 Model set-up

The system's characteristics and load specifications from the previous sections and chapters are brought together in an overall equation of motion, which is implemented in Matlab. In this section, the overall model structure is briefly discussed an the model flow sheets are presented for the main distinctive load cases.

### 4-2-1 Main model structure

The model is developed based on a main Matlab function in which a time-loop is constructed that includes the Ordinary Differential Equation solver (in this case ODE45). For all load and system characteristic determinations, various separate function files have been defined (including: wind, wave and ice loading as well as radiation and stiffness characteristics). All functions, except for the radiation function, have been directly implemented in the system's solver to achieve high outcome accuracy. For the radiation characteristics this was not possible since the determination of radiation forces includes the evaluation of a convolution integral. This convolution integral does not work well with the variable step-size approach that Matlab solvers apply. Therefore it is chosen to determine the radiation forces on the structure separately in the main time-loop. This is thought not to introduce large errors, especially when the time step size in the time-loop is small, since in that case very limited velocity fluctuations are to be expected between two time instants.

### 4-2-2 Model flow sheets

In this section, the order of calculations as applied in the model is explained in figures 4-4 through 4-6. Three distinctive flow sheets are included, covering the open water, ice crushing and ice bending load cases respectively, since for the different load cases different modules are used.

In the open water load case, the model includes environmental loading from wind, waves and current simultaneously. These are combined with the standard modules that cover the structural characteristics, the mooring stiffness and radiation forces, as well as the general E.M. module in which the ODE45 solver is applied.

In the ice crushing load case wave loading is no longer taken into account, as well as the wave spectrum definitions. The ice crushing module is implemented in the ODE solver instead of the wave loading module.

For the ice bending load case, the main difference compared to ice crushing is the location of the ice bending model outside the solver. This implies that ice loads are calculated for each time step in the time loop, but are kept at a constant value in the solver. This replacement is applied in order to reduce the calculation time, which otherwise will become very large. The error made by this replacement is thought to be small as long as the time-step in the time loop is small.

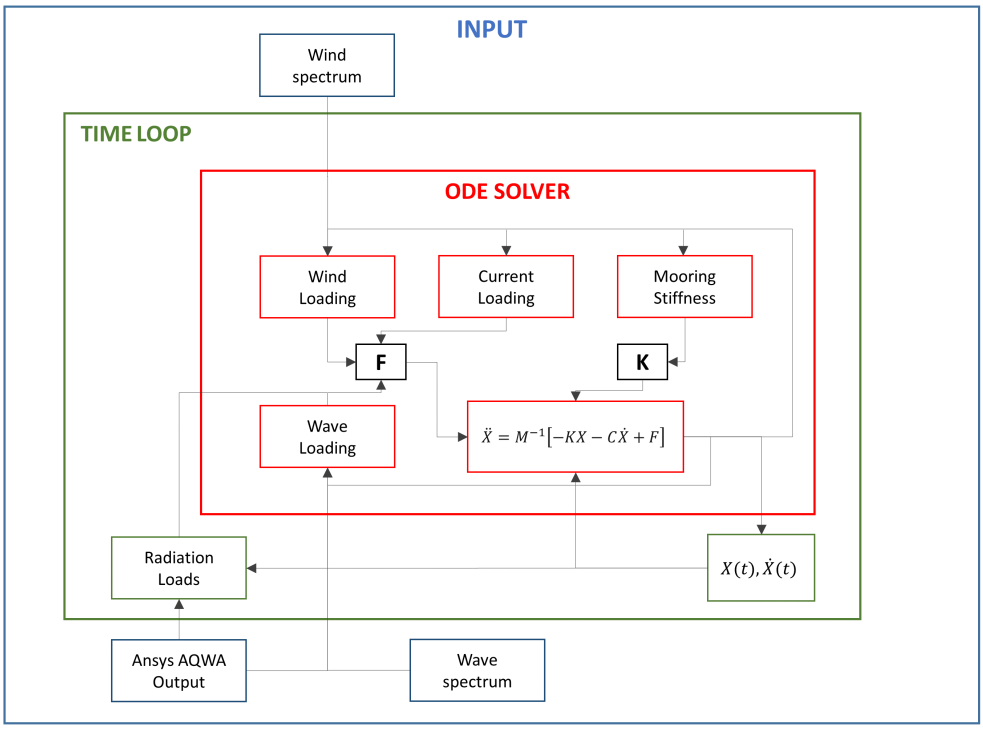


**Figure 4-4:** Order of calculations in Matlab mode for the open water load case

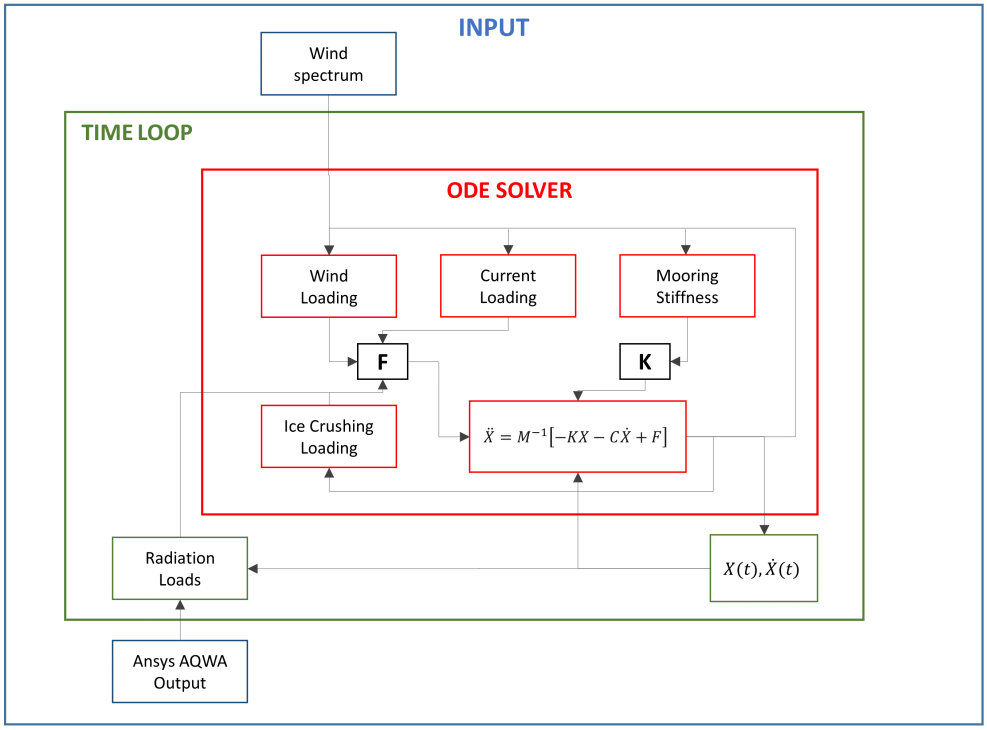


**Figure 4-5:** Order of calculations in Matlab mode for the ice crushing load case

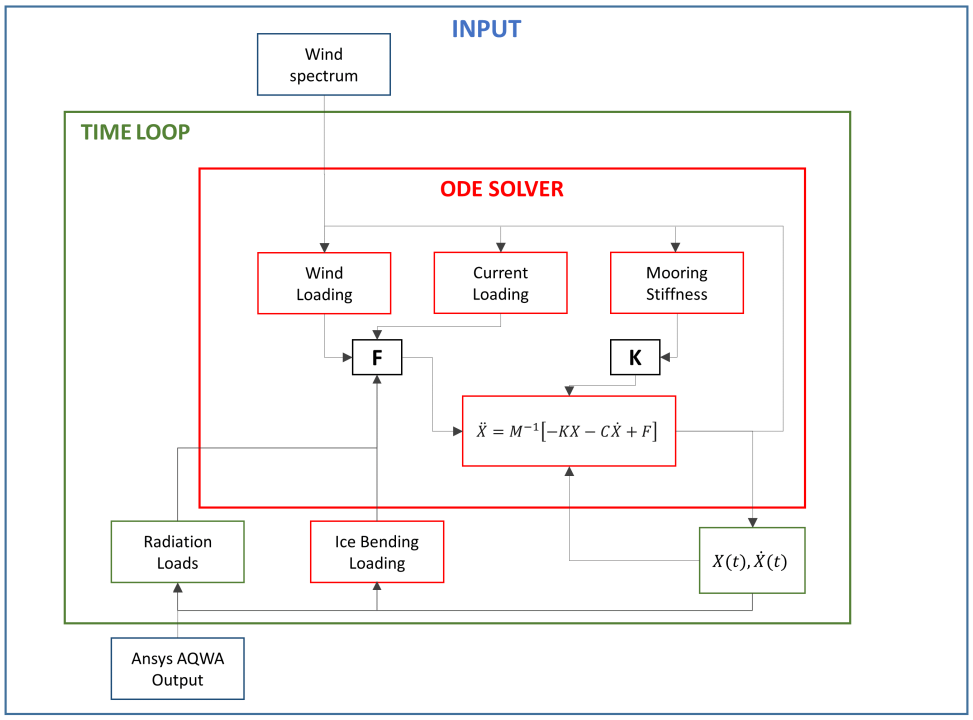


**Figure 4-6:** Order of calculations in Matlab mode for the ice bending load case

## 4-3 Motion characteristics

### 4-3-1 Natural frequencies

As a key characteristic of the dynamic behaviour of the platform-turbine arrangement, the natural frequencies of the system's motions are determined. This is done by solving equation 4-19 for $\omega$, for the stiffness and mass characteristics as defined in sections 4-1-1 and 4-1-3. Finally dividing the results by $2\pi$ to come to frequency in Hz.

$$det(-\omega^2 M + K) = 0 \tag{4-19}$$

The system and mass * are defined in table 4-1 and 4-2 below.

| System's mass characteristics | | |
|---|---|---|
| m11 = 1.80e7 | m12 = 0 | m13 = -2.39e8 |
| m21 = 0 | m22 = 1.07e7 | m23 = 1.94e5 |
| m31 = -2.99e8 | m32 = 1.39e5 | m33 = 1.87e10 |

**Table 4-1:** Mass characteristics in $kg$, $kgm$ and $kgm^2$

*The mass characteristics presented include both structure mass and added mass

| System's stiffness characteristics | | |
|---|---|---|
| k11 = 2.01e5 | k12 = 0 | k13 = -1.00e7 |
| k21 = 0 | k22 = 8.14e7 | k23 = 0 |
| k31 = -1.00e7 | k32 = 0 | k33 = 3.08e10 |

**Table 4-2:** Stiffness characteristics for zero offsets in $N/m$, $N$ and $Nm/rad$

From these characteristics, the fundamental system's natural frequencies can be derived. In table 4-3 below, the outcomes can be found.

| Natural frequencies | |
|---|---|
| Surge $f_{nat}$ | 0.017 $Hz$ |
| Heave $f_{nat}$ | 0.438 $Hz$ |
| Pitch $f_{nat}$ | 0.229 $Hz$ |

**Table 4-3:** System's natural frequencies for zero offsets

Besides these natural frequencies in un-displaced position, the alterations of these frequencies for deflections within the range of applications in this thesis has also been derived. From this brief analysis it became clear that frequency deviations are very limited, even for considerable deflections from the platforms initial position. For example, in the case of a surge deflection of $40m$ and a pitch deflection of $3deg$ pitch and surge natural frequency increased with approximately $0.003Hz$. The influence of platform deflections (in either of the three DOFs) on heave natural frequency is even less significant. For the application of natural frequencies in the analysis in this research, these variations are considered not to be of influence. Therefore, in the remainder of this thesis, the natural frequencies as presented in table 4-3 are referred to as natural frequencies irrespective of platform deflections.

### 4-3-2 Free decay test

A free decay test is performed for all three distinct degrees of freedom. The results can be observed in figures 4-7 through 4-9, in which both the time-trace of the free decay test as well as the power spectral density are plotted. The time trace plot shows the direct oscillation profile and the decay of the DOF, in the spectral analysis plot the oscillation frequency is distinguished from the time-trace by application of a Fourier Transform.

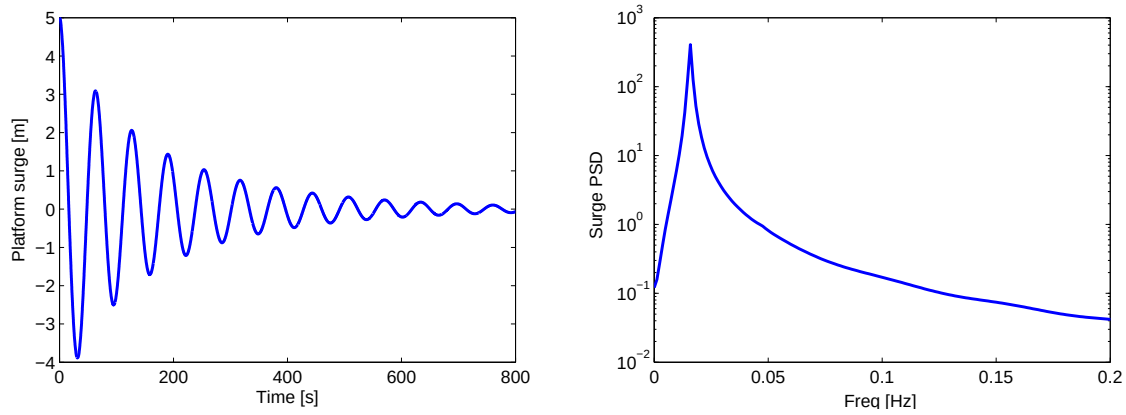


**Figure 4-7:** Time trace and spectral analysis plot for free decay test surge

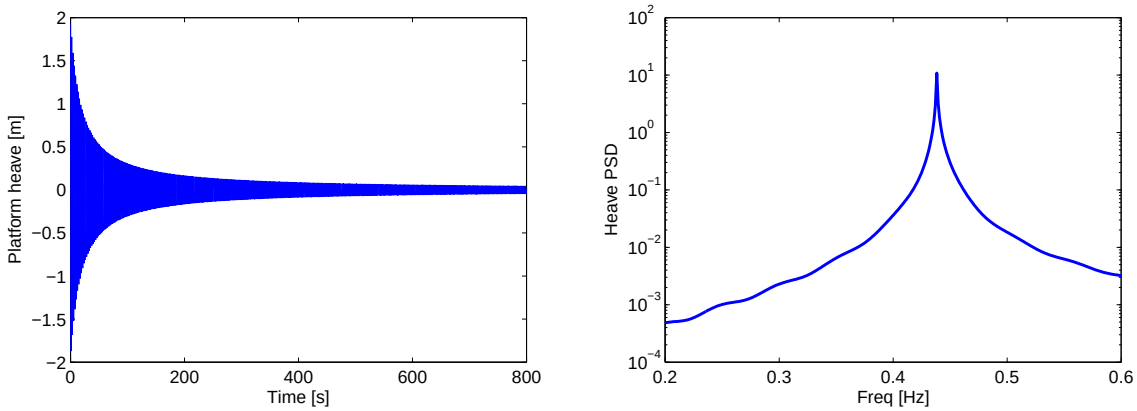


**Figure 4-8:** Time trace and spectral analysis plot for free decay test heave

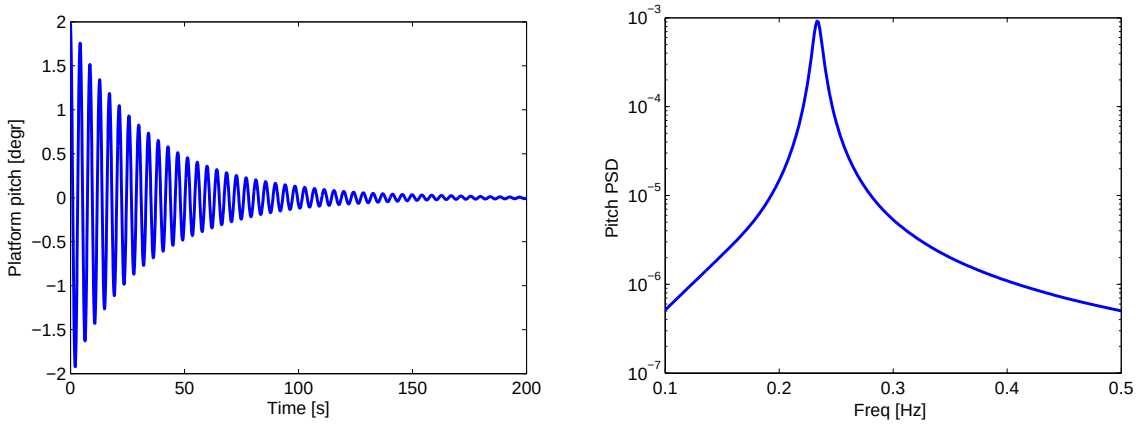


**Figure 4-9:** Time trace and spectral analysis plot for free decay test pitch

### 4-3-3 Motion coupling

From the definition of the mass and stiffness matrices presented in section 4-1-3, motions are coupled by the presence of off-diagonal terms in both matrices. Below, the PSD outcomes of the decay test with initial heave offset are presented for motions in surge and pitch. The coupling effects resulting from decay tests of other initial offsets can be found in Appendix J.

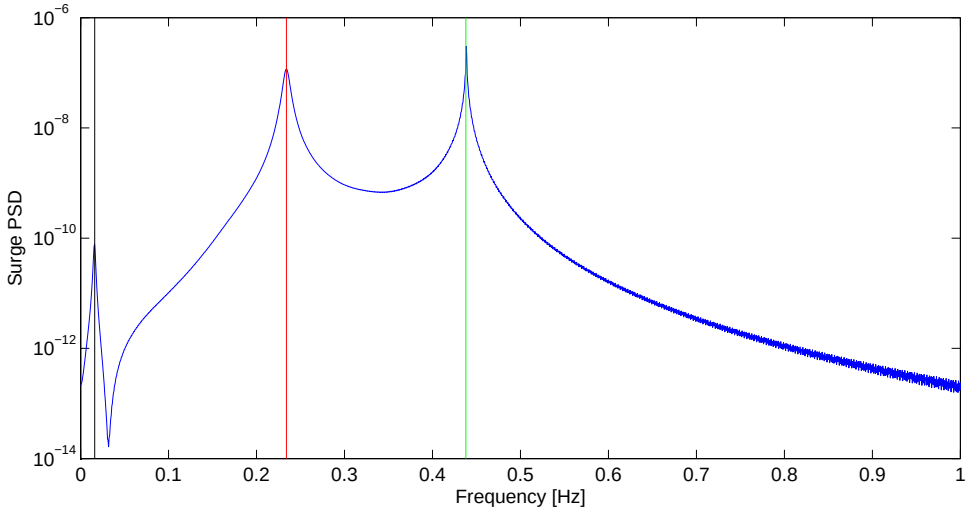


**Figure 4-10:** PSD coupled motions surge, from initial heave offset

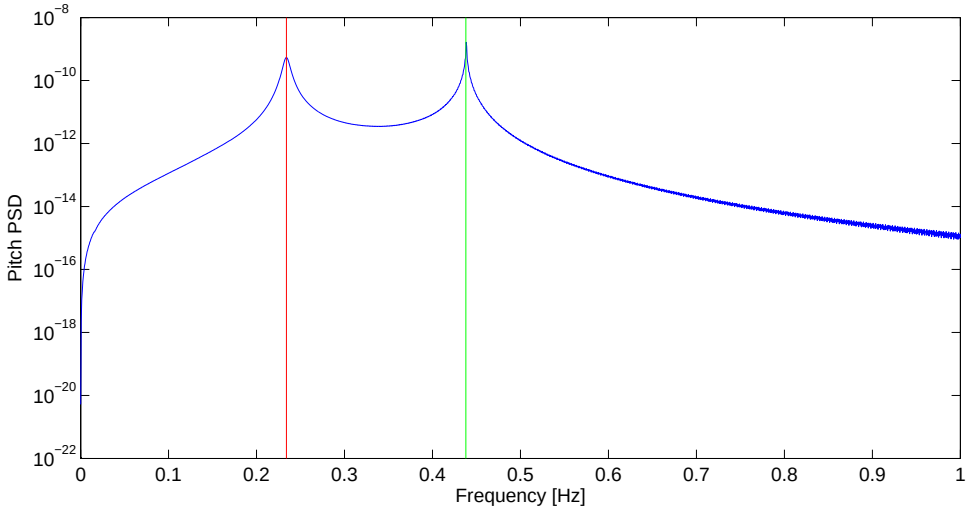


**Figure 4-11:** PSD coupled motions pitch, from initial heave offset

# Chapter 5

# Results and discussion

In this chapter, the outcomes of the simulations for the various load cases are presented [*]. First the simulation outcomes for the open water load cases are discussed. After that the findings of the level ice load cases are presented for both distinct failure modes. In the last section of this chapter a comparison is made between the outcomes of the two distinct ice failure modes and the open water conditions to form an understanding on how these relate.

## 5-1 Open water load cases

For the open water conditions, in addition to the load cases presented in section 3-5, a comparison is made with existing literature.

### 5-1-1 Comparison with existing literature

As already indicated in chapter 1 the model outcomes of the open water season can be compared to the outcomes of Matha (2009) [2]. In this reference study, the same floater geometry has been applied and therefore it forms an opportunity for comparison.

In the reference report, two time records of extreme motion outcomes were included. These cover different sea states and wind velocities.

1. Hs = 4.4, Tp = 11.3, with a constant wind velocity of 20 m/s
2. Hs = 15, Tp = 19.2, with mean wind velocity of 8 m/s

In figure 5-1 below, the outcomes for the first load case as presented in Matha (2009) [2] are shown. Here, the maximum and minimum pitch angle are 0.68 deg and $-0.48$ deg respectively and the leeward anchor tension has a minimum of $646kN$.

In figure 5-2 below, the outcomes of the developed model are presented for a part of a 3600 seconds simulation, for the same load case as covered in the reference study. It becomes clear that platform (pitch) motions from the current model are less volatile than is the case in the

[*] In the presented outcomes on multiple occasions time series of loading and motions are plotted, these often do not cover the full extend of the simulation, but only present a limited range of interest

reference results. The maximum and minimum pitch angles here are 0.46 deg and -0.23 deg respectively.

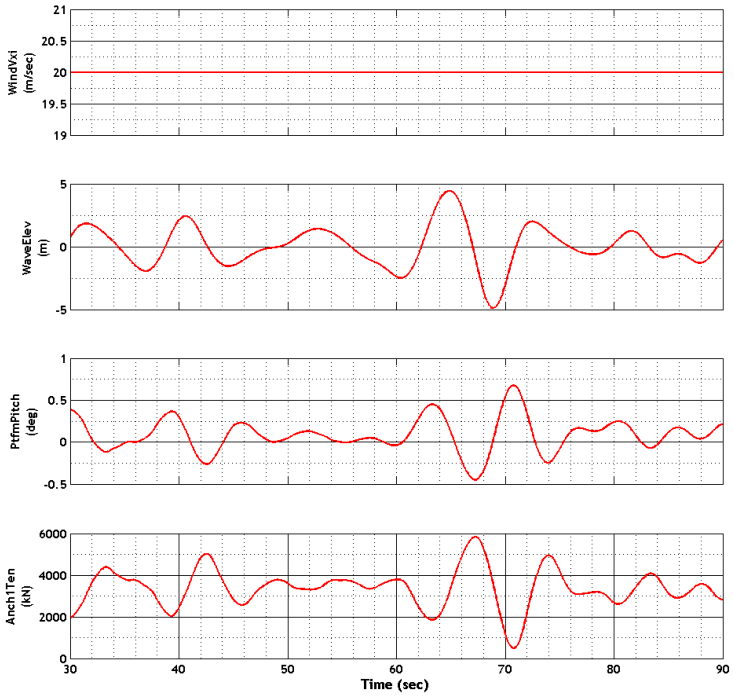


**Figure 5-1:** Reference data Load Case 1 Matha (2009)

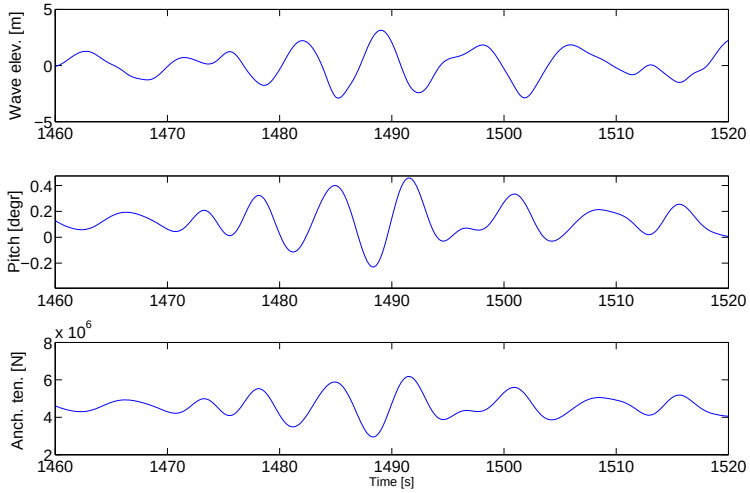


**Figure 5-2:** Model outcomes for reference Load Case 1

A comparison for the second load case is made as well. In figure 5-3, first the reference outcomes are presented and in figure 5-4 the outcomes of the developed model are shown.

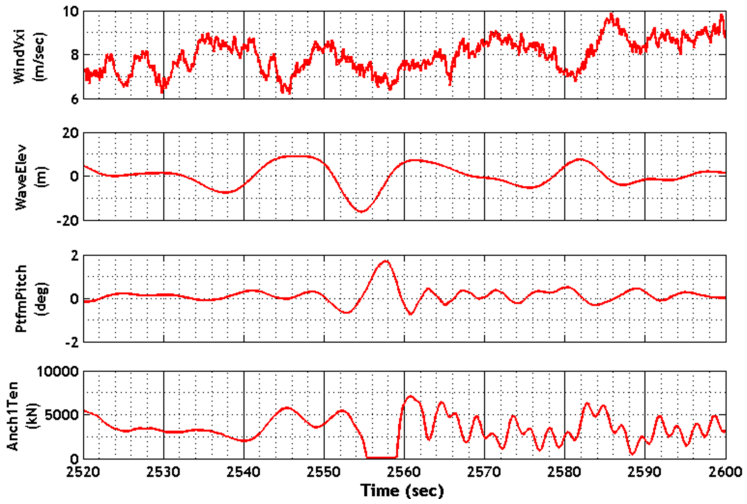


**Figure 5-3:** Reference data Load Case 2 Matha (2009)

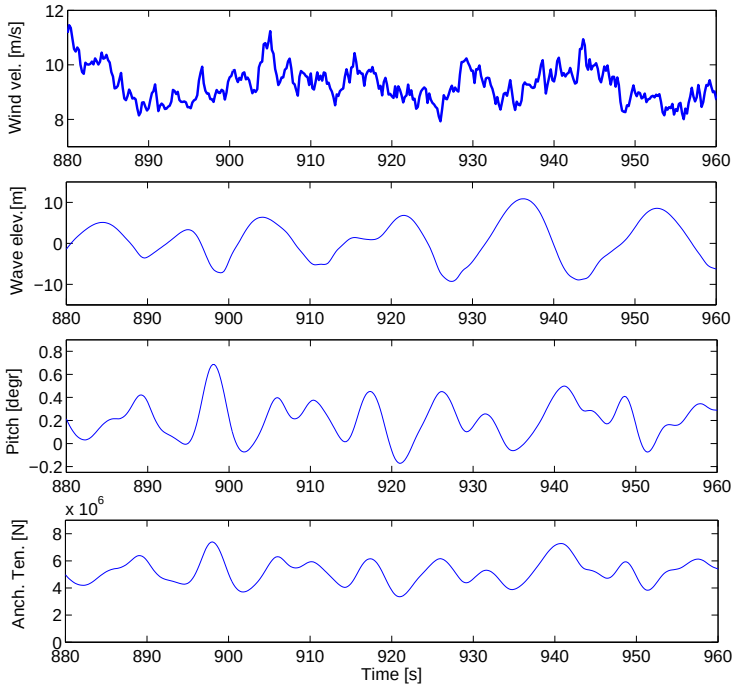


**Figure 5-4:** Model outcomes for reference Load Case 2

From the comparison with regards to the second reference load case, it is seen that the maximum pitch deflection in the reference study is 1.68 deg, the outcomes of the simulation with the current model show a maximum of 0.69 deg. It should however also be noted that the wave height for which the reference value was reached (25m) is significantly higher than the highest wave simulated with the current model(20m). This deference in maximum simulated wave elevation is also observed in the former load case.

From both comparisons of extreme pitch offset and tendon loads, it should be concluded that

the developed model is not capable of reproducing the extreme pitch responses as presented by [2]. Since the model in the reference study has not been thoroughly studied it is difficult to assess what could be the source of these differences. However, there are two main potential sources that could cause differences in outcomes. First the modelling approach for the mooring system is different, whereas in the current study TLP mooring loads are directly characterised in a stiffness matrix, in the reference study generalised software applicable for any mooring type is applied. Secondly the applied method to capture wind loads in this study is considerably more simplified compared to the method applied in NREL's software, applied by [2], which also accounts for, for example,turbine blade pitch. As indicated by [35], this type of control driven parameters can have considerable influence on platform motions. It is thought that this might especially hold for extreme load cases, in which the coincidence of multiple influencing factors can lead to extreme motions. Further attempts to mimic the extreme events of the reference study are thought to be ineffective since different modelling approaches are applied. Therefore no further effort is made in this respect.

Based on the difficulties in comparing the outcomes of extreme load cases for the model at hand with existing literature, the absolute results of this study cannot be directly compared with the reference research. For the relative comparison between open water and level ice conditions, however, this is not thought to be a limiting factor.

### 5-1-2 Open water load case outcomes

In this section some findings of the simulations done for the open water load cases, as introduced earlier on in section 3-5-1, are presented. First, in order to introduce an understanding of how wind and wave loads acting on the structure typically compare in order of magnitude, in figure 5-5 both loading types are presented for both horizontal force and overturning moment contribution.

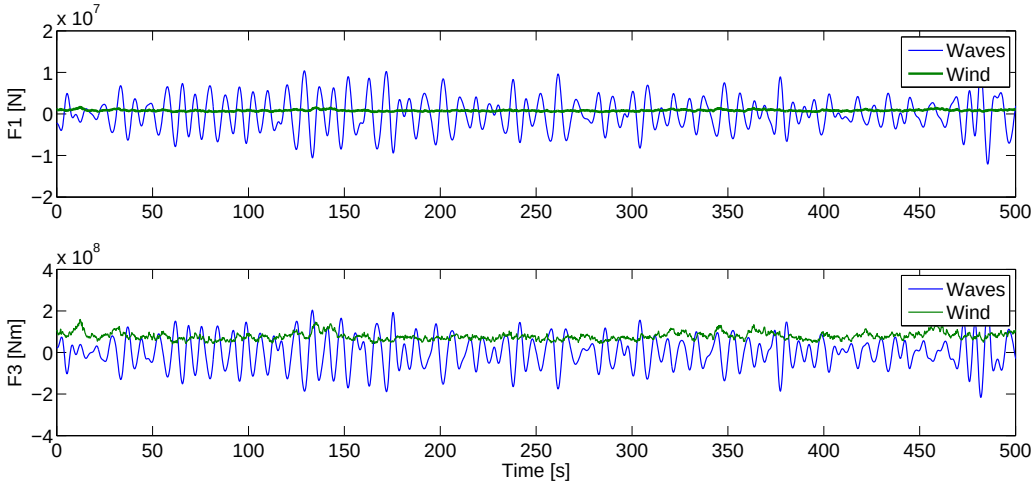


**Figure 5-5:** Wind and wave loads $H_s = 4m$, $T_p = 10s$ and $U_{wind} = 11m/s$

It is observed that whereas in horizontal direction the force contribution of waves outweigh that of wind, for the overall overturning moment in pitch direction, both are in the same

order of magnitude. Besides that, whereas fluctuations of wave loads pass through zero, the fluctuations of wind force are smaller, causing the force to act only in positive direction.

Based on this relation between both loads, the system is thought to reach a positive mean offset in both surge and pitch direction as a result of wind contribution. The wave loads will cause oscillation about this mean, which will become larger for more severe sea states. This effect can be observed in figure 5-6, which presents the resulting motions of the platform in a sea state of $H_s = 4m$ and $T_p = 10s$ and a mean wind velocity at hub height of $11m/s$. The mean, maximum and minimum motions for the remaining sea states in combination with $11m/s$ mean wind velocity can be found in table 5-1.

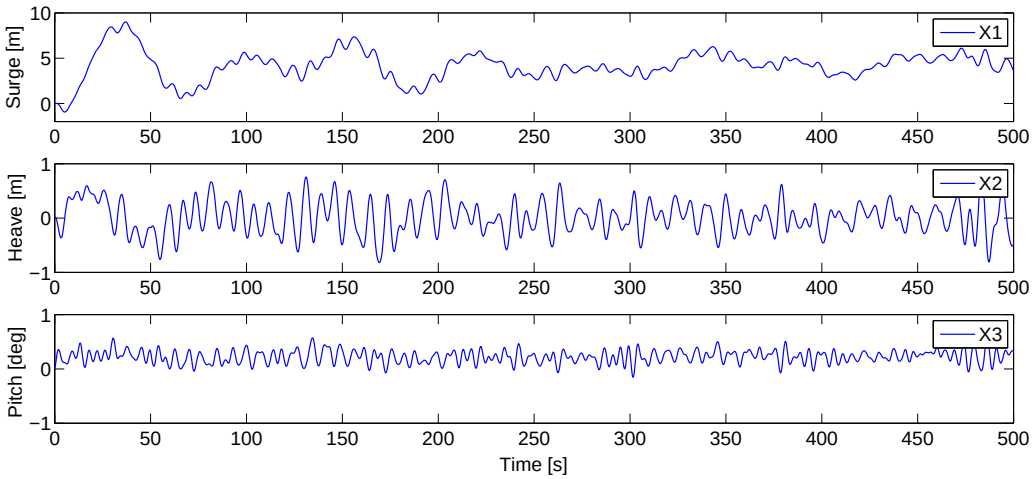


**Figure 5-6:** Platform motions for $H_s = 4m$, $T_p = 10s$ and $U_{wind} = 11m/s$

**Table 5-1:** Resulting motions for the open water load cases with $11m/s$ wind velocities

| | Surge [m] | | | Heave [m] | | | Pitch [deg] | | |
|---|---|---|---|---|---|---|---|---|---|
| | Mean | Min | Max | Mean | Min | Max | Mean | Min | Max |
| 1 | 4,11 | 0,23 | 7,37 | 1,8E-06 | -1,6E-03 | 1,7E-03 | 0,22 | -0,14 | 0,56 |
| 2 | 4,17 | -0,35 | 8,15 | 5,1E-05 | -1,3E-02 | 1,3E-02 | 0,22 | -0,31 | 0,60 |
| 3 | 4,30 | -0,14 | 9,64 | 1,9E-04 | -3,4E-02 | 3,5E-02 | 0,23 | -0,24 | 0,65 |
| 4 | 4,44 | -1,63 | 10,64 | 4,2E-04 | -5,4E-02 | 5,3E-02 | 0,23 | -0,25 | 0,65 |
| 5 | 4,24 | -2,18 | 15,65 | 8,1E-04 | -9,1E-02 | 1,0E-01 | 0,22 | -0,27 | 0,70 |
| 6 | 4,35 | -3,88 | 15,63 | 1,3E-03 | -1,2E-01 | 1,3E-01 | 0,22 | -0,29 | 0,74 |
| 7 | 4,57 | -7,01 | 23,54 | 2,0E-03 | -1,9E-01 | 2,0E-01 | 0,23 | -0,31 | 0,67 |

The allowable tension in the platform's tendons connection the platform to the seabed is an important design criteria for TLP floaters. The actual tension acting on the tendons will be heavily dependent of platform motions and therefore influenced by the sea state and wind velocity present.

For the sea states considered, the maximum tension in the windward tendons and the minimum tension in the leeward tendons is determined and presented in figure 5-7 and 5-8.

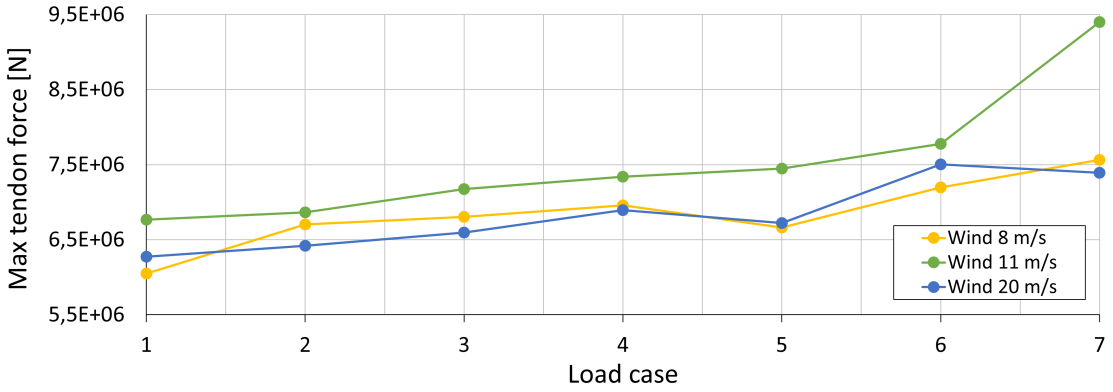


**Figure 5-7:** Maximum tendon force for open water load cases

As can be expected from the turbine thrust curve in figure 2-2, the $11m/s$ mean wind velocity load cases result in higher maximum tension than the $8m/s$ and $20m/s$ cases. Besides that, caused by larger motions, both in surge and pitch direction, sea states with increasing wave height result in higher maximum tendon forces.

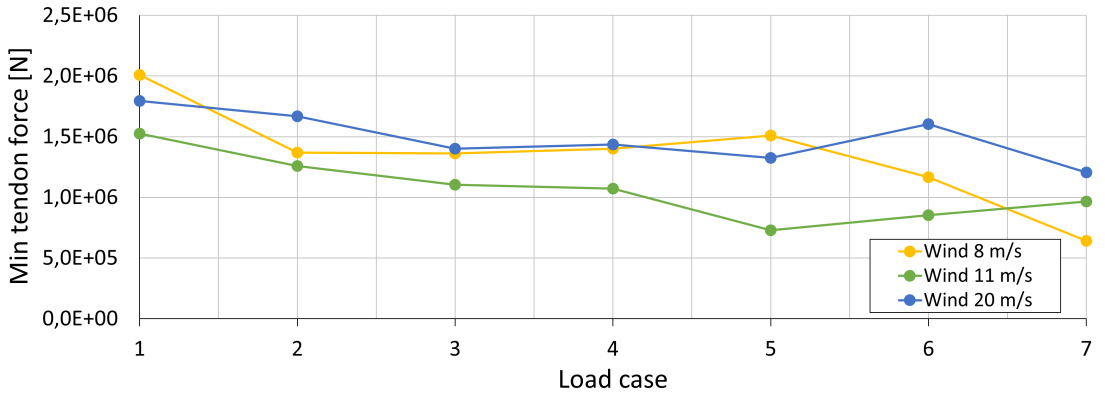


**Figure 5-8:** Minimum tendon force for open water load cases

As was the case for the maximum tension restrictions, the minimum leeward tension is also governed by the $11m/s$ wind load cases. For the minimum leeward tension outcome, the pitch motions is the main driving factor in lowering tension, whereas higher surge will only increase tension.

## 5-2 Ice loading

As already introduced in chapter 3, the ice loading considered in this research describes the failure of level ice against the structure in two distinct failure modes: either by crushing or bending of the ice. In the sections below, the loading pattern of both failure types is described and the outcomes of simulations of the predefined load cases are presented.

### 5-2-1 Crushing ice loads

#### Ice loading only

From the simulation results of the ice crushing loads the implementation of the load model on the structure at hand is compared to the application of the same load model on a rigid non-moving wall. Based on this reference, the load time-trace is expected to be comparable to what is observed from figure 5-9.

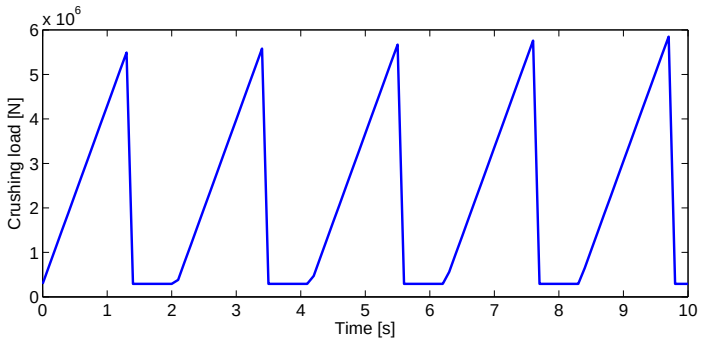


**Figure 5-9:** Ice crushing loads against a solid structure $v_{ice} = 0.2$, $h_{ice} = 0.2$

For the application of the ice crushing model to the floater, it is expected that the system requires some time to come to a steady state. In this steady state the structure reaches a steady deflection in surge motion, after which the ice loading pattern will be more or less in line with what we have observed in figure 5-9. The structure will eventually perform (small) oscillations around this steady state offset as a result of cyclic crushing loads [*].

Resulting platform motions and loading pattern are presented in figure 5-10 and 5-11 below, for the example load case with an ice velocity of $0.3m/s$ and an ice thickness of $0.2m$.

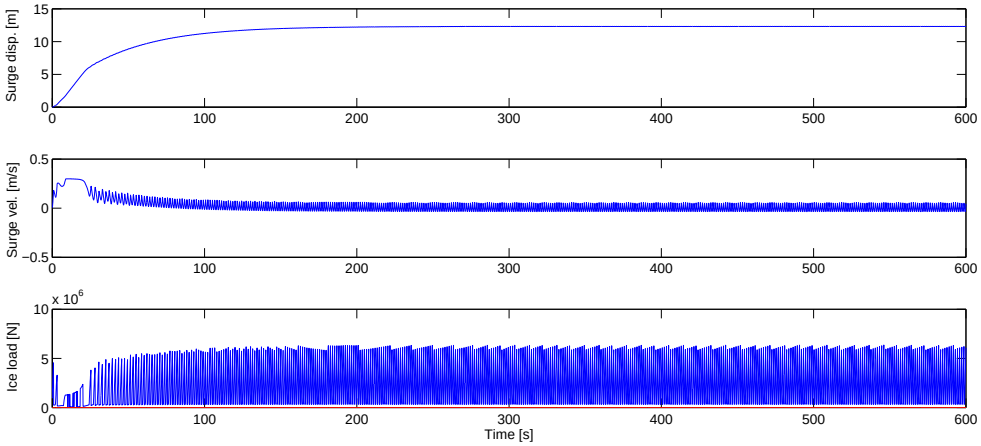


**Figure 5-10:** Surge motions and crushing action for $v_{ice} = 0.3m/s$ and $h_{ice} = 0.2m$

[*]This behaviour corresponds to crushing action of ice in ductile failure, in Appendix K a comparison is drawn to results from brittle ice crushing as well. The results of this comparison are left out of the scope for in the comparison and conclusion in the main text of this report.

From the results of the load case presented in figure 5-10, it is observed that the system indeed follows the expected surge offset until enough restoring force is reached to resist the crushing loads. After this, the platform indeed will continue to oscillate around its stable position.

In figure 5-11 a more detailed representation of the results can be seen, here it becomes clear that the loading pattern is very much in line with what could be expected from the rigid structure reference case.

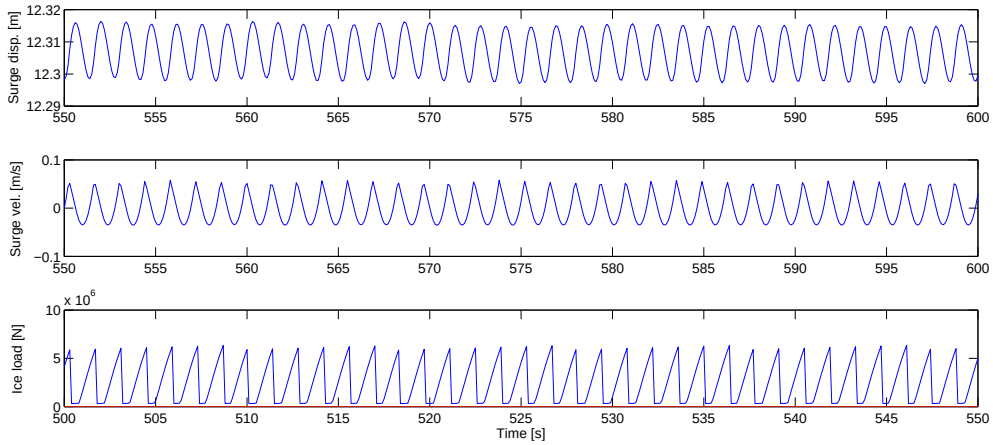


**Figure 5-11:** Zoomed-in: Surge motions and crushing action for $v_{ice} = 0.3m/s$ and $h_{ice} = 0.2m$

For several of the considered load cases more irregular platform motions and loading patterns resulted. As an example of this type of results, the outcomes for the $v_{ice} = 0.2m/s$, $h_{ice} = 0.4m$ load case are presented in figure 5-12. Here the platform does not come to a stable surge offset, instead a more or less linear increase of surge offset is observed until the structure suddenly accelerates back, after which the same cycle is observed. Besides this irregularity, larger offsets are observed compared to load cases with a more regular motion pattern, even when compared to load cases with large ice thickness.

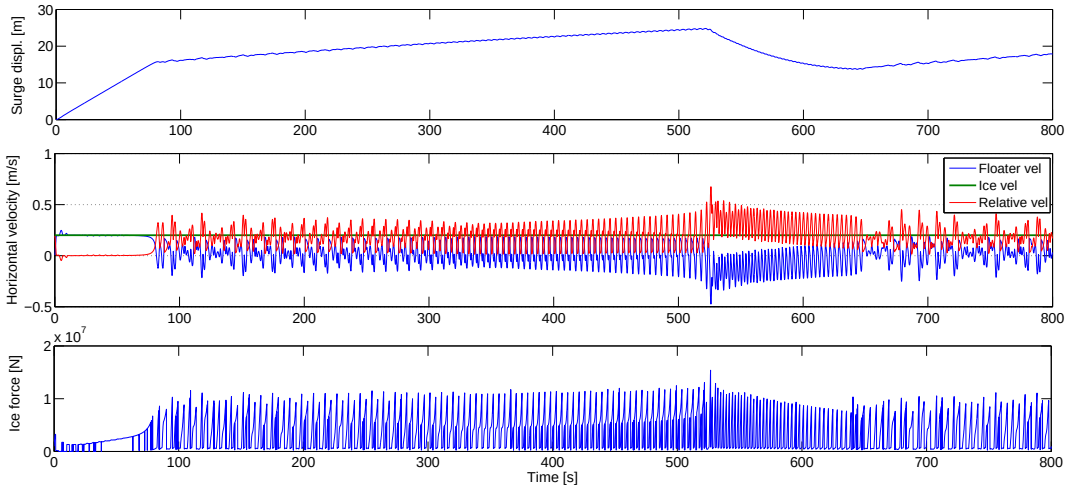


**Figure 5-12:** Surge motions and crushing action for $v_{ice} = 0.2m/s$ and $h_{ice} = 0.4m$

From the more detailed representation in figure 5-13 below, it becomes clear that the loading pattern also does not resemble what was expected from the rigid structure reference. This irregularity in crushing load is caused by the large platform motions that result in a non-linear load built up and in some cases the lost of contact because the structure's surge position is larger than that of the ice front. The latter is an explanation for the dip in ice load pattern in figure 5-13.

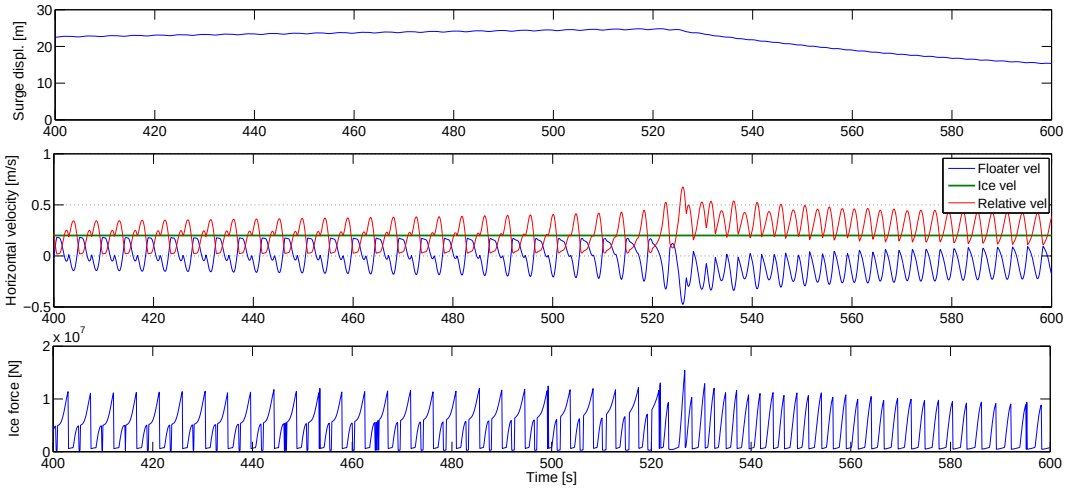


**Figure 5-13:** Zoomed-in: Surge motions and crushing action for $v_{ice} = 0.2m/s$ and $h_{ice} = 0.4m$

The cause of the change of loading regime at $t = 520s$ is thought to be related to the relative velocity between the ice sheet and the structure. From a closer inspection of this relative velocity in figure 5-13, it can be seen that the platform motions (and therewith the relative velocity) gradually increase until the relative velocity of ice sheet and structure reaches the transitional ice velocity of $0.5m/s$. Once the relative velocity exceeds the transitional velocity, the ice force suddenly decreases (instead of an increase) for higher relative velocities. As a result of the lower ice force the structure accelerates back in negative surge direction. This results in a different loading pattern, until the structure's motions are stopped by the incoming ice loads and the cycles is started over again.

The observed amplifications of platform motion and irregular ice loading, before the $t = 520s$ point, can be linked to the loading frequency of crushing loads. In figure 5-14 the approximate frequencies for the crushing of ice against a rigid structure are presented for the case without platform motions. In this simplified approach the frequency is determined by: $f = \frac{v_{ice}}{p}$, where $v_{ice}$ is the constant velocity of the ice sheet and p is the distance between two distinct ice teeth, as defined in the applied model (figure 3-16).

From figure 5-14 it can be seen that the crushing frequency varies for varying combinations of ice thickness and travelling velocity. For some of the considered load cases this frequency is expected to coincide with the structure's heave of pitch natural frequency.

To verify this potential cause for the unexpected dynamic behaviour, the $v_{ice} = 0.2m/s$, $h_{ice} = 0.4m$ load case is considered again. In figure 5-15 the pitch and heave motions as well as the ice force are plotted for the region of interest near $t = 520s$.

It is observed that the crushing load return period before $t = 520s$ is approximately 4.9 seconds. In line with the expectations from the frequency plot in figure 5-14, this coincides

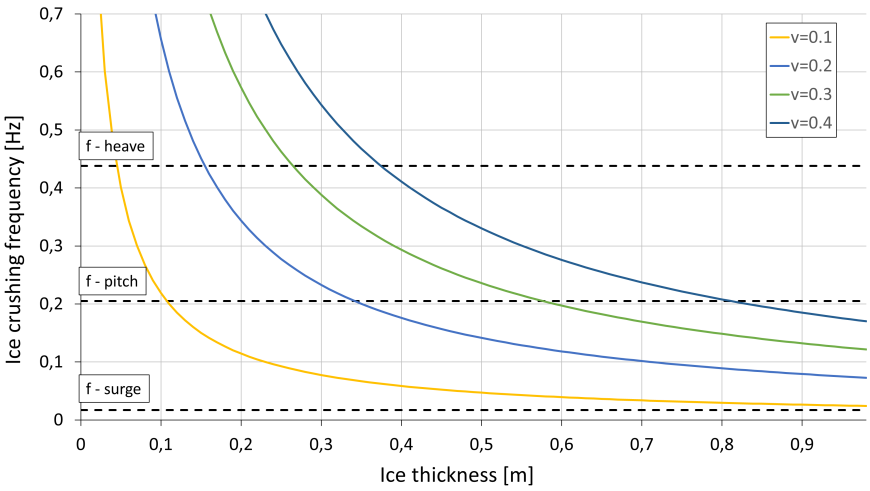


**Figure 5-14:** Crushing frequency for varying ice thickness and velocity

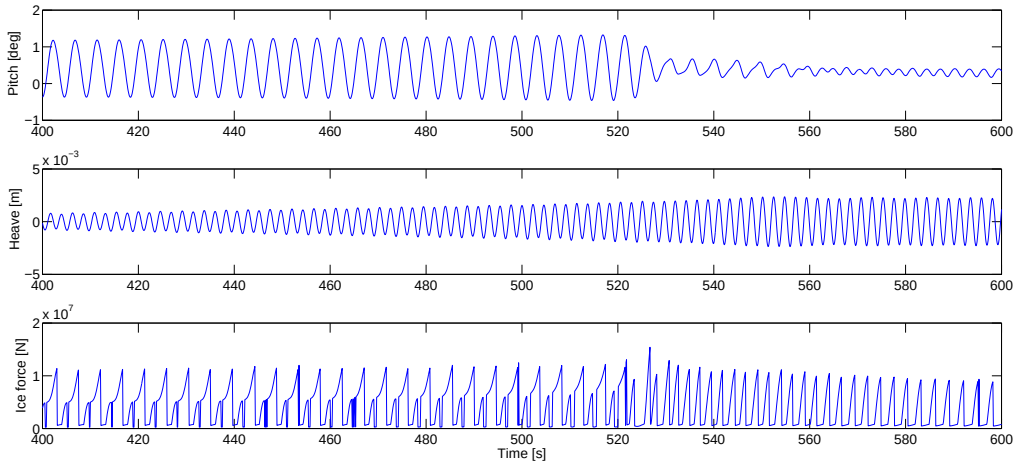


**Figure 5-15:** Pitch & heave motions and crushing action for $v_{ice} = 0.2m/s$ and $h_{ice} = 0.4m$

with the systems pitch natural frequency. As a result, large pitch amplitudes of oscillation are observed. As already mentioned, after the relative velocity has exceeded transitional velocity, the loading pattern suddenly changes. Here the return period is approximately 2.2 seconds, after which it slowly increases again until the same cycle is repeated. In the region just after the $t = 520s$ mark, pitch oscillations suddenly decrease dramatically. Heave oscillations, on the other hand, increase. This is caused by the ice loading that coincides with the natural frequency in that DOF. Once the ice loading frequency drops again, the heave amplitude of oscillation slowly decreases as a result of the system's (hydrodynamic) damping [*]. From this it can be concluded that the irregular loading and motion pattern before the $t = 520s$ point are caused by dynamic amplification of pitch motions as a result of crushing loads near its natural frequency. The same loading frequency and motion pattern is observed in the results of several other load cases considered.

[*]The latter is difficult to visualise since damping contributions in heave direction are rather small.

Transferring the frequency related information back to the simulation outcomes of the other load cases, it is interesting to visualise the dynamic amplifications in a comparison between the considered load cases. The windward tendon force is chosen as a base for comparison here. In figure 5-16, the relative deviation ($\sigma_F/F_{mean}$) is plotted for the load cases with ice velocities of $0.1, 0.2$ & $0.3m/s$. The $v_{ice} = 0.4m/s$ load cases are left out here, since the dynamic amplification is limited to the $h_{ice} = 0.7m$ and therefore might extend beyond the ice thickness range considered.

The outcomes in figure 5-16 clearly show peaks for relative force deviations for ice thickness 0.2, 0.4 and $0.6m$, for velocities of 0.1, 0.2 and $0.3m/s$ respectively. Except for the $v_{ice} = 0.1$ load case, this closely matches what was expected from the frequency plot in figure 5-14. From this zero motion reference one would expect dynamic amplification for the $v_{ice} = 0.1m/s$ case at an ice thickness of $0.1m$ instead of $0.2m$. As a check of the loading frequency, for the $v_{ice} = 0.1$, $h_{ice} = 0.1$ and $v_{ice} = 0.1$, $h_{ice} = 0.2$ load cases the ice load return period is derived and found to be 2.2 and 4.7 seconds respectively. From this it becomes clear that the dynamic amplification in the $v_{ice} = 0.1m/s$,$h_{ice} = 0.2m$ case also sources from loading at pitch natural frequency. Besides that it should be noted that, crushing frequency of ice against a floating structure can deviate from the rigid structure reference as a result platform motions.

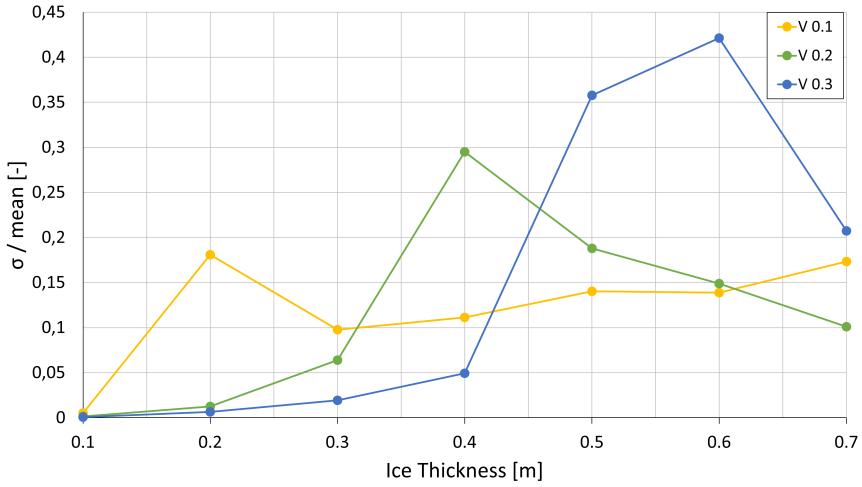


**Figure 5-16:** Relative deviations of tendon force for ice crushing only

From these outcomes it can be drawn that for the ice crushing load cases considered in these simulations, dynamic effects can have a considerable influence (or magnifying effect) on structure response and tendon forces.

### Combined wind and ice loads

Adding to the complexity of the load cases, combined wind and ice loads are considered as well for all crushing load cases presented in the previous section. Here, the considered mean wind velocity is $11m/s$ at hub height. To give an understanding of how the orders of magnitude of both types of loading relate, in figure 5-17 both load contributions are plotted for the $v_{ice} = 0.3m/s$ and $h_{ice} = 0.2m$ load case. It is clearly noticeable that the contributions of

ice crushing action outweigh those of wind Note that this figure only includes horizontal load contributions, for the wind load, however, an overturning moment contribution is present as well.

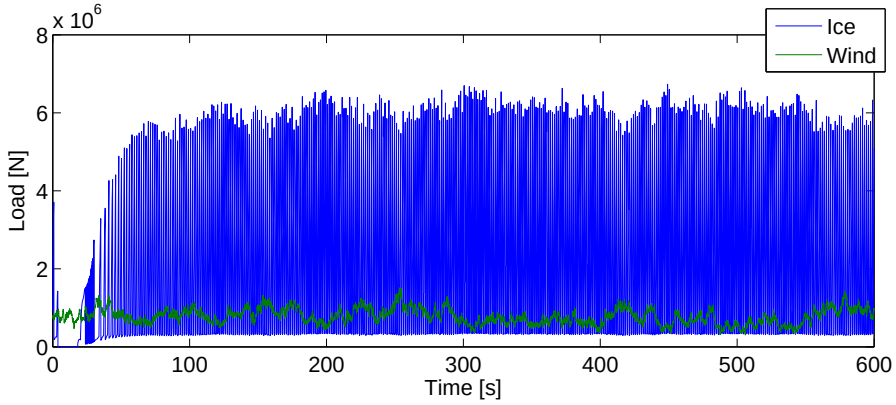


**Figure 5-17:** Order of magnitude comparison of wind and ice loading in surge direction

The influence of the introduction of wind loads to the ice crushing load case can best be visualised by figure 5-18. Here, the platform surge motion and ice loading pattern is plotted for the load case with ice contributions equal to those in figure 5-10, with the addition of wind velocity. It is observed that the surge offset is increased compared to the load case without wind. Besides that, as a result of the turbulence effect in the simulated wind velocity, variations about the steady state offset are larger.

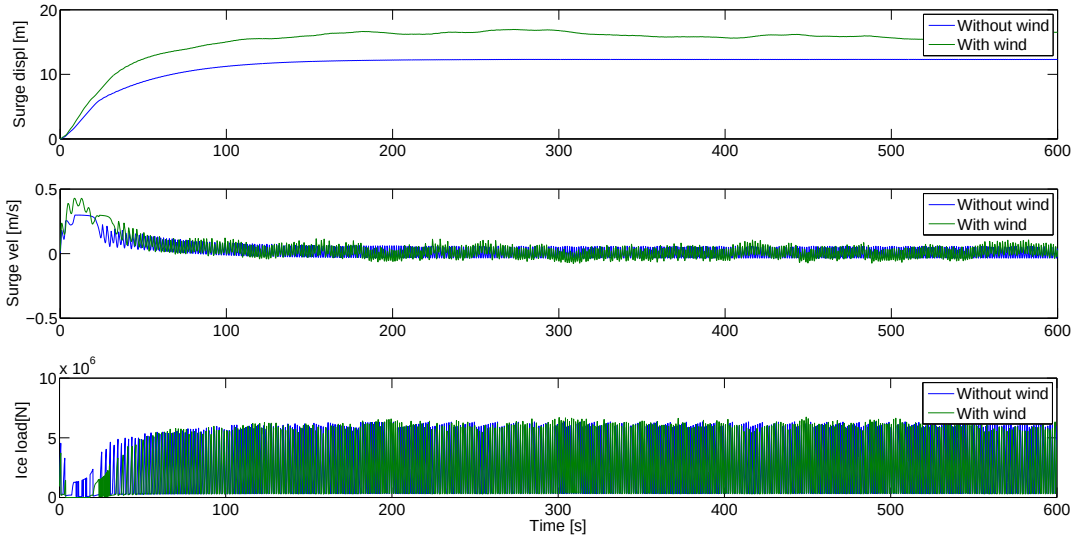


**Figure 5-18:** Surge motions and crushing action for $v_{ice} = 0.3m/s$ and $h_{ice} = 0.2m$

In the detailed representation in figure 5-19, it can be seen that the ice loading pattern is not heavily affected by the addition of wind loads. This is the result of the relatively large periods of oscillation of the large deflection contributions (caused by wind loading).

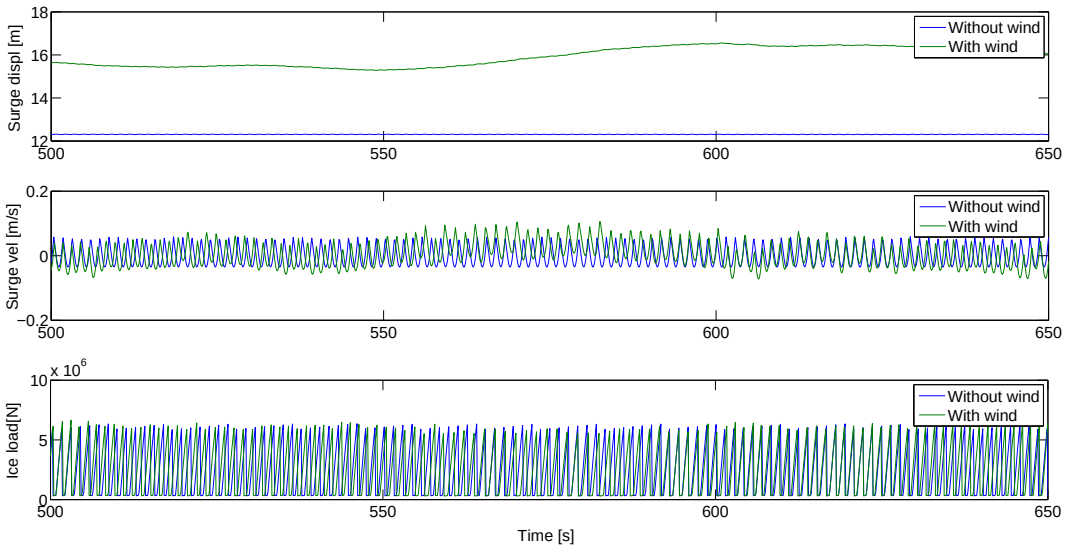


**Figure 5-19:** Zoomed-in: Surge motions and crushing action for $v_{ice} = 0.3m/s$ and $h_{ice} = 0.2m$

When looking at the dynamic effect for various load cases a comparison can be drawn to the case of load cases without a contribution of wind loads. Comparing the outcomes presented in figure 5-16 with the results in figure 5-20 below, it can be observed that the dynamic effects for excitation near the system's pitch natural frequency are reduced. This in part results from an increase of the mean tendon forces (due to increased mean surge and pitch offset), and on the other hand, aerodynamic damping as an effect of motion coupled wind loads is thought to have a reducing effect.

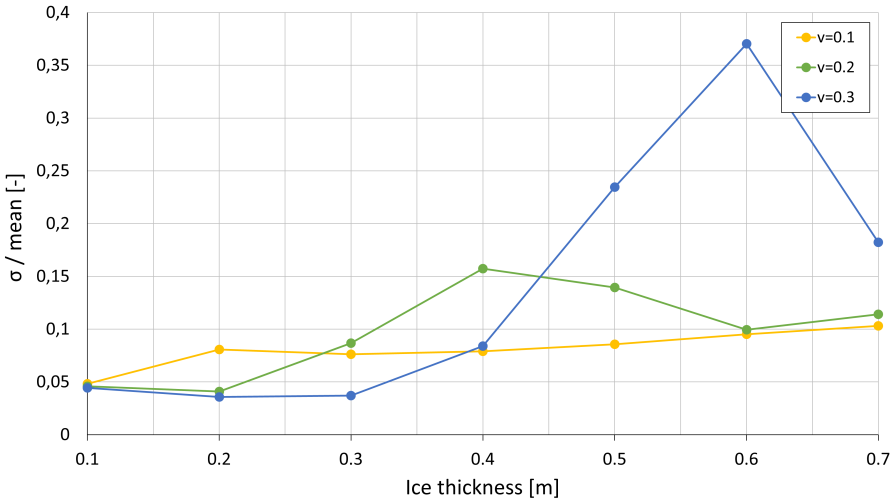


**Figure 5-20:** Crushing frequency for varying ice thickness and velocity

For a direct absolute comparison between load cases with and without wind contributions, in figures 5-21 and 5-22 below the maximum tendon force at the windward side of the platform is plotted for the considered range of load cases*. Figure 5-21 represents the outcomes for the $v_{ice} = 0.1$ and $v_{ice} = 0.2$ load cases and figure 5-22 those of $v_{ice} = 0.3$ and $v_{ice} = 0.4$. It is observed that the addition of wind loads increases tendon forces, it is however also notable that the dynamic effects are smaller, especially for the $v_{ice} = 0.2$ and $h_{ice} = 0.4$ simulation this is significantly apparent.

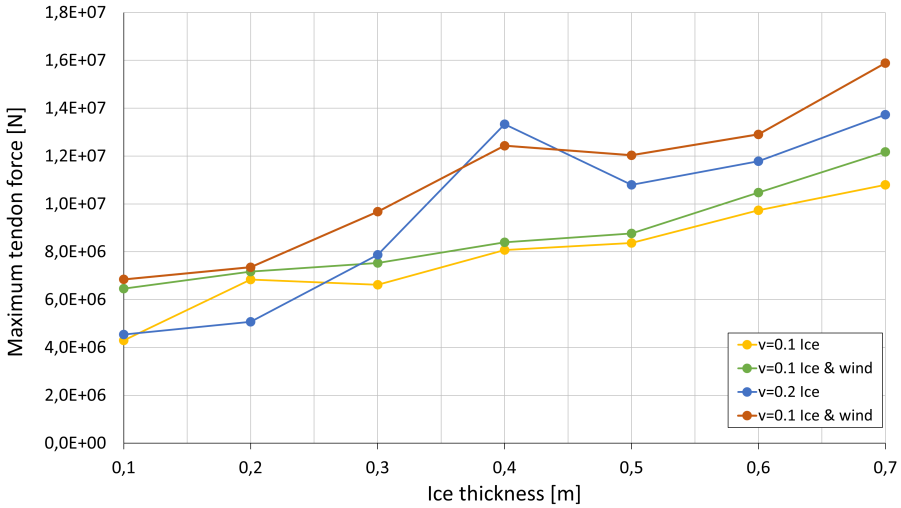


**Figure 5-21:** Max tendon force, ice crushing $v_{ice} = 0.1$ & $v_{ice} = 0.2$ load cases - Comparison with and without wind

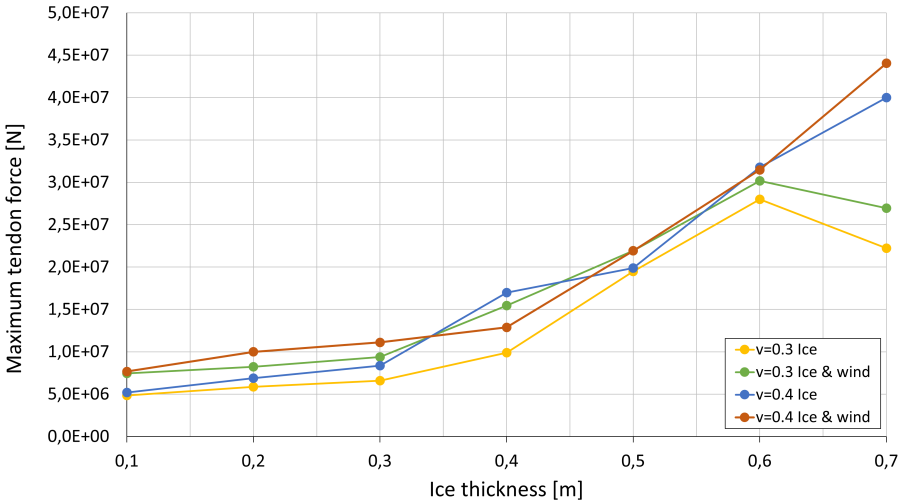


**Figure 5-22:** Max tendon force, ice crushing $v_{ice} = 0.3$ & $v_{ice} = 0.4$ load cases - Comparison with and without wind

*Whereas in the open water load cases the minimum tendon force at leeward side of the platform was of interest as well to check for tendon slacking, here this is not the case as a result of large steady state surge offset and therefore not considered.

### Effect of current

The final environmental load contribution that is taken into account in combination with ice crushing is the presence of ocean currents. Here a constant and uniform $0.5m/s$ current in positive surge direction is considered, combined with the ice load cases for ice velocity of $0.2m/s$ and a mean hub height wind velocity of $11m/s$.

In figure 5-23 below, the current force contribution in horizontal direction is plotted against the wind and ice contributions. It becomes clear that the force contribution of current is limited compared to especially that of ice.

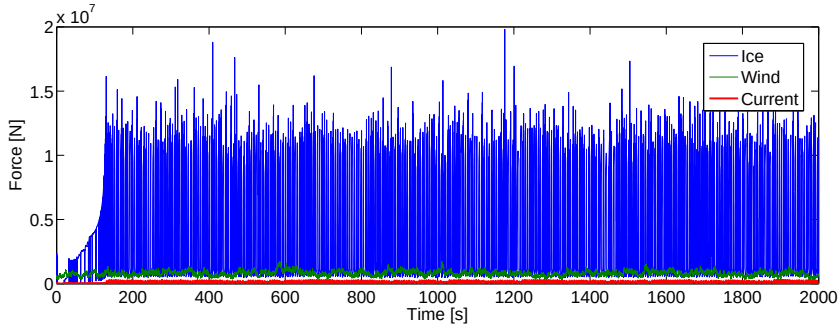


**Figure 5-23:** Order of magnitude comparison of wind ice and current loading in surge direction

In figures 5-24 through 5-26 the results from the addition of current loading are plotted against the outcomes of the load combinations of ice crushing and wind loads. The maximum tendon forces in figure 5-37 show some slight deviations from the combined ice and wind load cases, however these are limited and not consistently higher or lower.

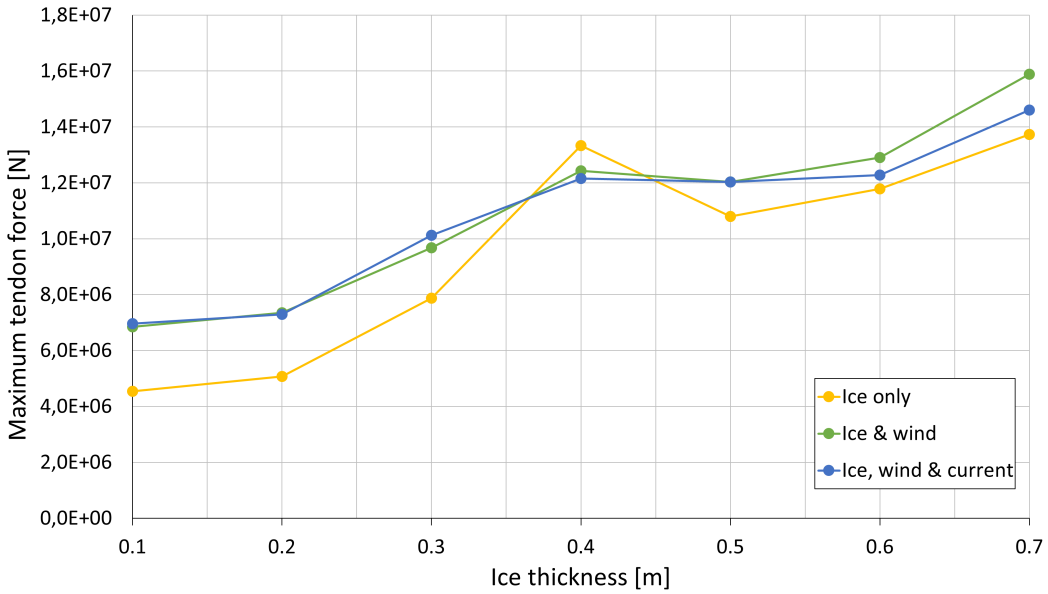


**Figure 5-24:** Comparison of max tendon forces for ice ($v_{ice} = 0.2$), wind ($11m/s$) and current($0.5m/s$) loads

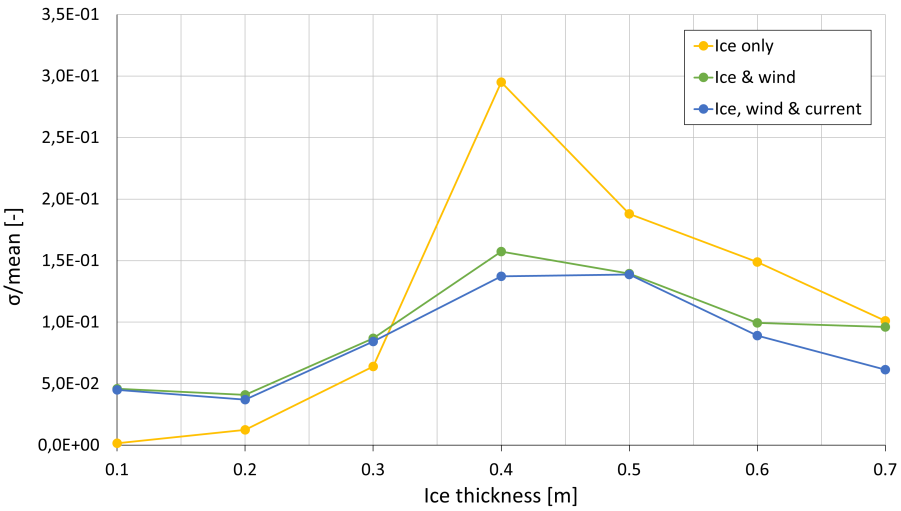


**Figure 5-25:** Comparison of relative tendon force deviations for ice, wind and current combinations

The relative force deviations also seem only very limitedly affect by the introduction of the constant current velocity, although they present a slight but consistent reduction.

The mean tendon force is slightly increased by the addition of current, which can be intuitively explained by an increased mean force in surge direction as a result of current drag loads.

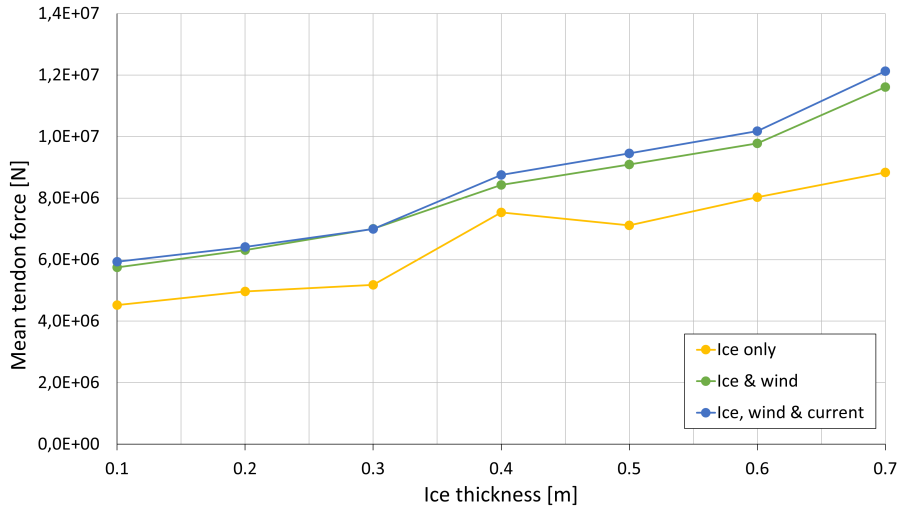


**Figure 5-26:** Comparison of mean windward tendon force for ice, wind and current combinations

Overall the effect of the 0.5 m/s current velocity is very limited in the simulation outcomes for the load cases considered.

### 5-2-2 Bending ice loads

In the presentation of the results for the ice bending load cases in this section, a distinction is made between the contributions of ice breaking loads only and the inclusion of a residual term to take into account secondary ice actions, as discussed in section 3-4. Finally the concurrence of ice, wind and current loading is studied as well to form an understanding of how these terms are related and to look at their combined influence on platform motions.

#### Breaking loads

As a first consideration, the residual forces that should account for load effects after breaking of the ice sheet are excluded from the load case. Focus is solely on the ice breaking force in bending failure.

In figure 5-27 the resulting platform surge motions and horizontal ice force is presented for the load case of $v_{ice} = 0.1m/s$ and $h_{ice} = 0.95m$. When compared with the typical loading pattern of ice in crushing failure, shown in figure 5-10, it stands out that the ice loads resulting from bending failure have a loading frequency that is considerably lower. Secondly the breaking load is a lot smaller, approximately a factor 10. Furthermore, given the low loading frequency, the structure does not reach a steady state surge offset as is the case in ice crushing. Instead, it will oscillate around its neutral position with limited amplitude.

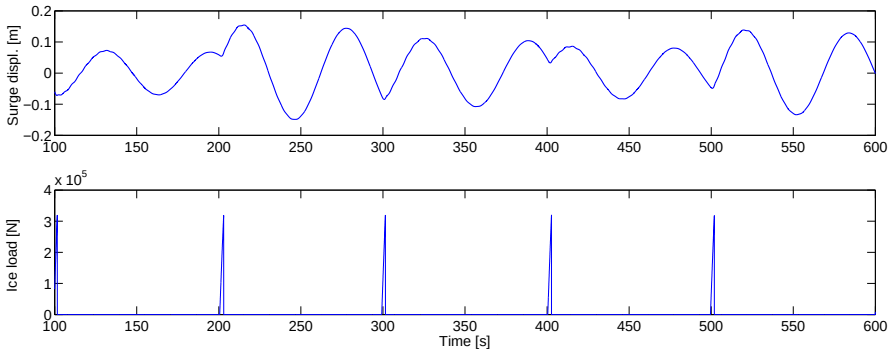


**Figure 5-27:** Platform surge and horizontal force from breaking loads of ice bending failure ($v_{ice} = 0.1$,$h_{ice} = 0.95$)

The maximum tendon loads that resulted from simulations for all considered load cases are presented in figure 5-28. As was the case in ice crushing loading, here quite an irregular relation between ice thickness and maximum tendon force is found as well. From these outcomes it can be observed that for the load combinations of $v_{ice} = 0.1m/s$ and $h_{ice} = 0.95m$, $v_{ice} = 0.1m/s$ and $h_{ice} = 1.5m$ and $v_{ice} = 0.3m/s$ and $h_{ice} = 1.5m$, unexpected large tendon forces are present.

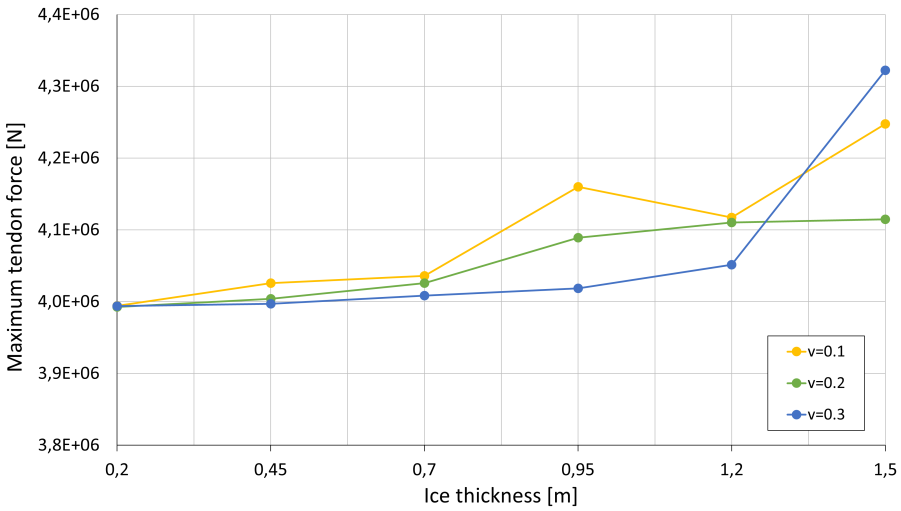


**Figure 5-28:** Maximum tendon force resulting from breaking loads due to ice bending

The source of these irregular outcomes can be found in two effects. In both the $v_{ice} = 0.1m/s$ cases a loading effect also seen in the results of Aksnes (2010) [38] causes larger deviations than expected. Along the simulation at several instances, the floater moves in the same direction as the ice sheet, but at a higher velocity. This causes the structure to lose contact with the ice sheet, after which loading will start again once the ice sheet gained distance on the structure again. This effect results in higher surge offset due to longer overall ice-structure interaction before the ice sheet breaks.

For the $v_{ice} = 0.3m/s$ and $h_{ice} = 1.5m$ load case the dynamic effects can be linked to the excitation of the system near its surge natural frequency, as was the case in crushing for the pitch natural frequency. In figure 5-29 the loading frequency in bending failure is plotted against ice breaking length for the ice velocities considered.

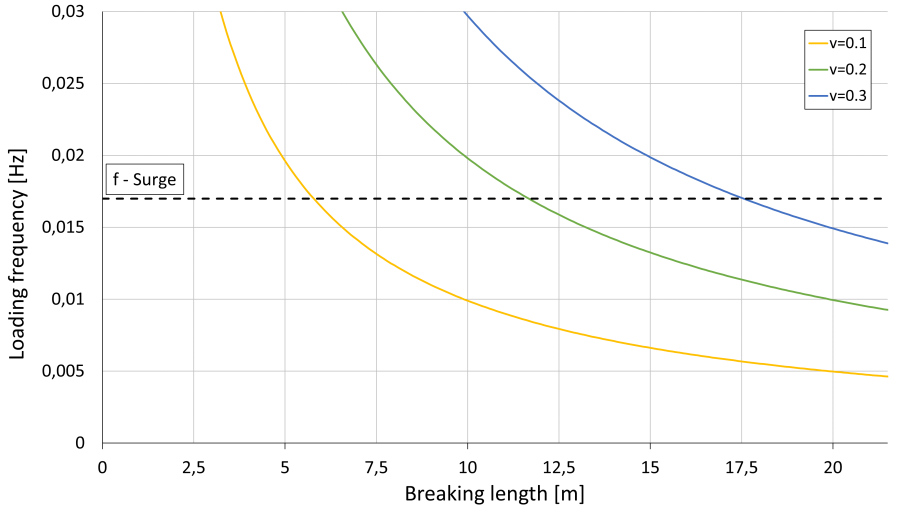


**Figure 5-29:** Ice bending loading frequency

Here the relation between ice loading frequency and breaking length is defined by:

$$f_{breaking} = \frac{v_{ice}}{L_{br}} \tag{5-1}$$

From the information presented in figure 5-29, the critical breaking length for $v_{ice} = 0.3$ can be determined to be approximately $17.5m$. From the breaking length record for the $v_{ice} = 0.3$, $h_{ice} = 1.5m$ load case, the breaking length in this simulation is found to be $17.1m$. This is considered to be an explanation for the larger than expected tendon forces and also indicates that ice bending loads can impose dynamic load amplification.

### Combined residual and breaking ice loads

The effects of the introduction of residual forces, to cover secondary effects of ice structure interaction as introduced in section 3-4-2, will be discussed here. In figure 5-30 below, the typical loading pattern and floater motions that result from ice bending loads including residual load effects are presented for the $v_{ice} = 0.2$ and $h_{ice} = 0.75$ load case.

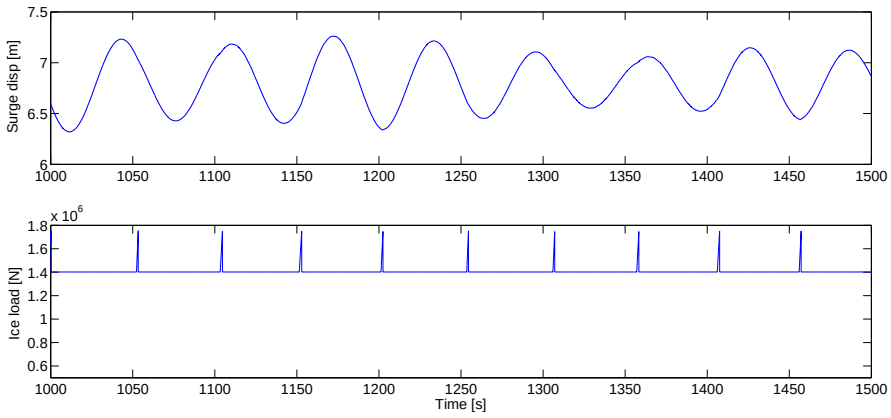


**Figure 5-30:** Platform surge and horizontal force from loads of ice bending failure including residual load effects ($v_{ice} = 0.2$,$h_{ice} = 0.75$)

The resulting motion clearly show a steady state surge offset, as a result of the constant residual load onto the platform, besides that, the low frequency breaking loads are superimposed to this constant residual force.

In figure 5-31 the resulting maximum tendon forces for all considered load cases are presented. A clear positive relation between ice thickness and tendon force is observed as expected. Three slightly deviating load cases can be distinguished: $v_{ice} = 0.1$ & $h_{ice} = 1.25$, $v_{ice} = 0.2$ & $h_{ice} = 1$ and $v_{ice} = 0.3$ & $h_{ice} = 1.5$. In order to better visualise these outliers, their relative deviations are presented in figure 5-32 as well.

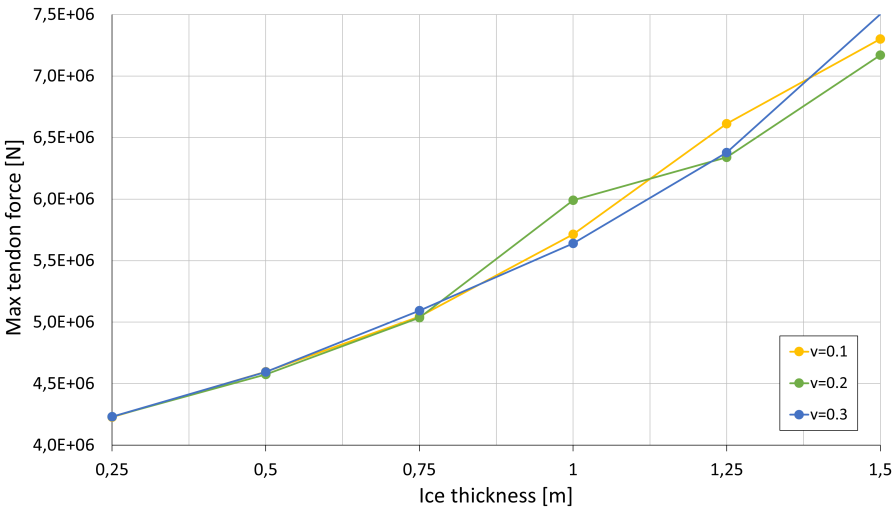


**Figure 5-31:** Maximum tendon force resulting from total loads due to ice bending

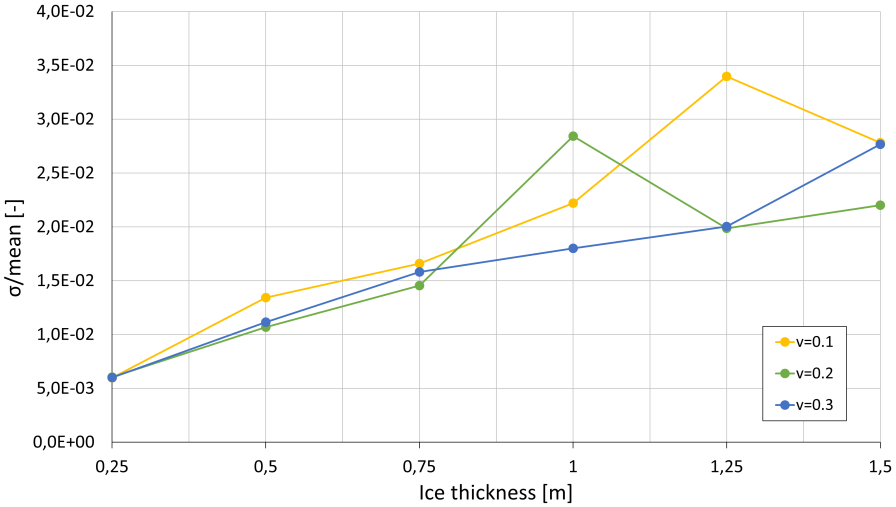


**Figure 5-32:** Relative deflection of tendon force for ice bending load cases

As was the case in the situation without residual force contributions, the deviating outcomes of the $v_{ice}$ load case are found to source from the consecutive loss and resuming of contact between ice sheet and structure. For the other two deviating load cases, the breaking length is found to (nearly) match the critical breaking length, as indicated in figure 5-29: $12.6m$ for the $v_{ice} = 0.2$ case and $17.1m$ for the $v_{ice} = 0.3$ case.

### Influence of wind

To get an understanding of the interaction of ice bending and wind loads acting on the structure simultaneously, in this section, a $11m/s$ wind velocity is added to the $v_{ice} = 0.2m/s$ load case from previous section.

In figure 5-33, the horizontal ice and wind loads are presented.

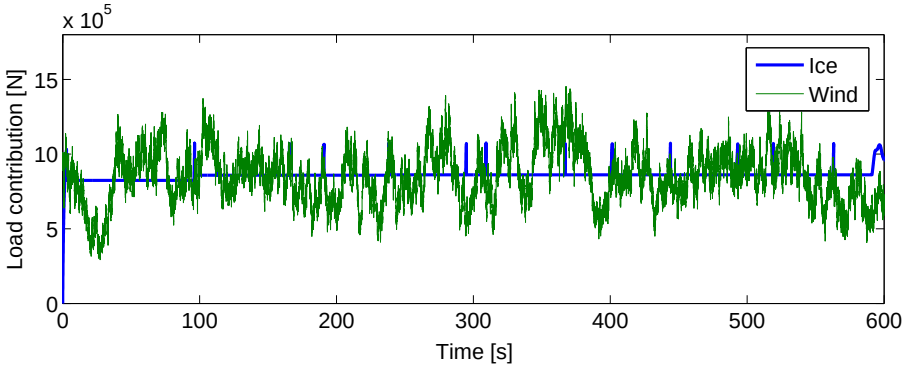


**Figure 5-33:** Horizontal contributions of ice bending and wind load, $u_{mean} = 11m/s$, $v_{ice} = 0.2m/s$, $h_{ice} = 0.5m$

For this load combination, both ice and wind loads have comparable contributions to the overall horizontal force, for other load cases however contributions of ice tend to be smaller or larger.

In figure 5-34 the resulting platform motions, ice loads and wind loads are plotted against time. When comparing the platform motions with the loading time traces it can be clearly observed that wind load contributions dominate surge fluctuations around the mean offset. The ice loading contribution mainly increases this mean offset but does not have a (large) influence on the dynamic surge offset of the structure.

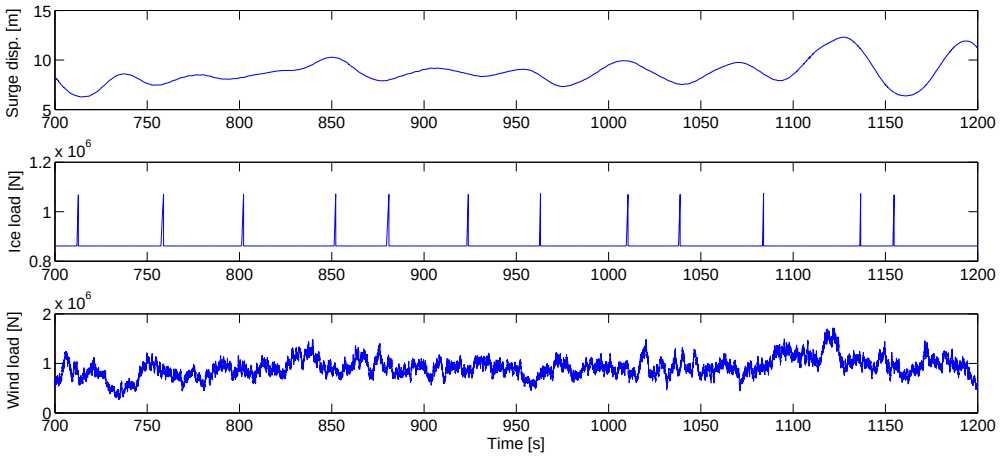


**Figure 5-34:** Horizontal contributions of ice bending and wind load, $u_{mean} = 11m/s$, $v_{ice} = 0.2m/s$, $h_{ice} = 0.5m$

In figure 5-35 the maximum tendon force results of wind and ice loads are plotted for the range of ice thickness considered with an ice velocity of $v_{ice} = 0.2m/s$.

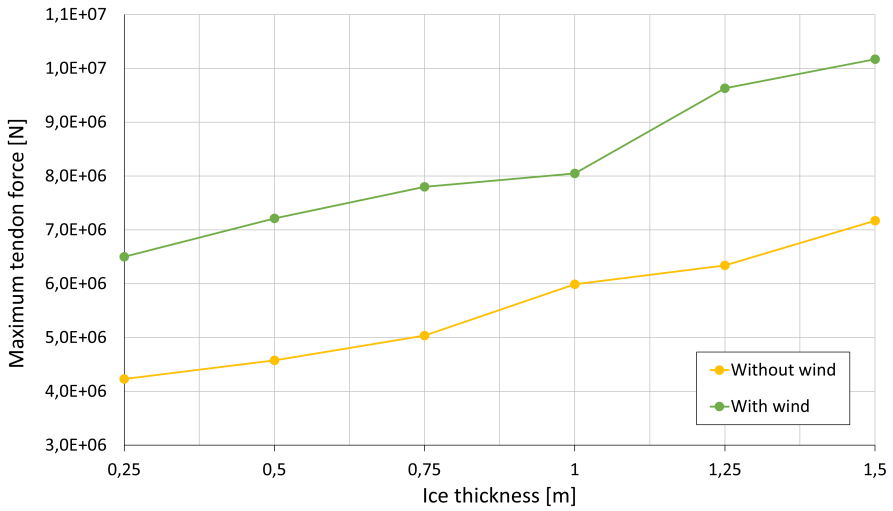


**Figure 5-35:** Maximum tendon force ice bending with and without wind

From these outcomes, it can be concluded that the addition of wind to the ice bending load case significantly increases maximum tendon forces and on top of that it nullifies the dynamic loading effect of the ice loads as discussed in the previous section. This latter effect is further represented in the relative deviation plot of tendon forces in figure 5-36, which clearly shows that the thickness of the ice sheet has no significant influence on the fluctuations of motions around their steady-state mean.

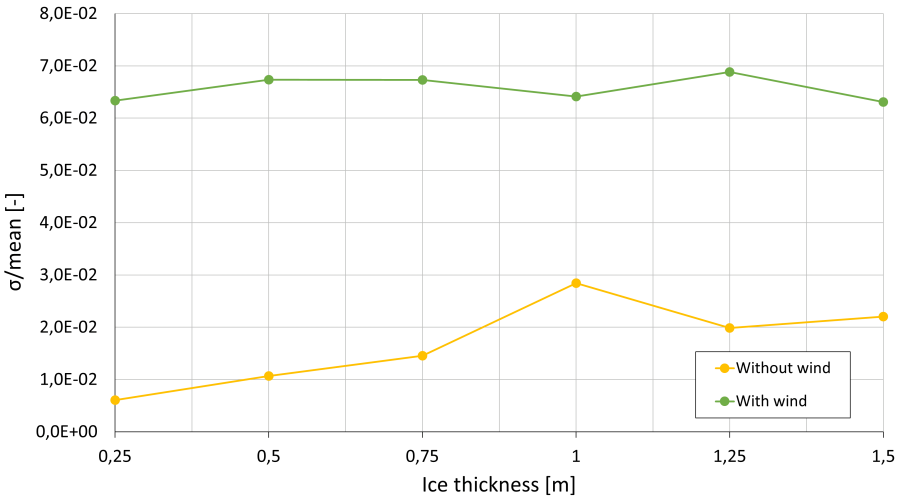


**Figure 5-36:** Relative deflection of tendon force ice bending with and without wind

### Effect of current

The effect of the introduction of a $0.5m/s$ constant current is considered as well. In figure 5-37 the outcomes of the simulations is presented and compared with the outcomes for the combined ice and wind load case that was introduced in the previous section.

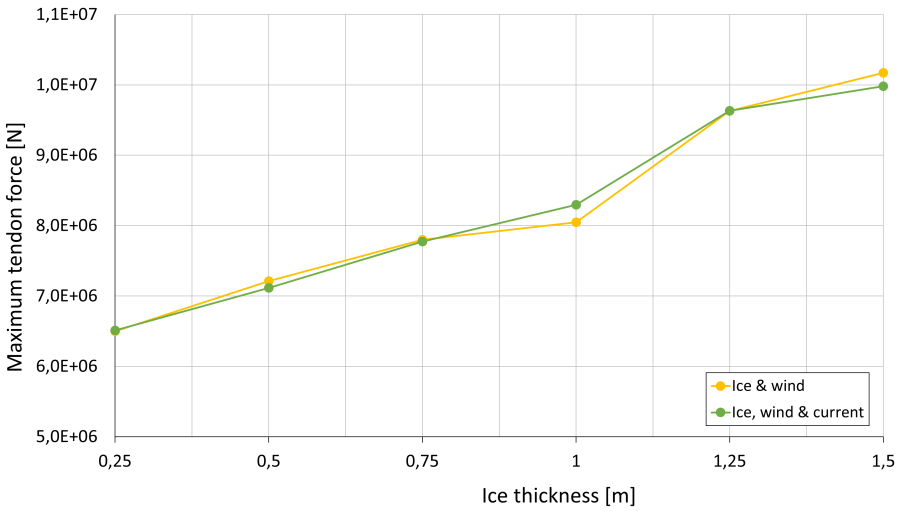


**Figure 5-37:** Comparison of maximum tendon force for ice bending with and without current

It can be seen that the effect on the maximum expected tendon force is negligible, despite the introduction of an additional constant horizontal force acting on the structure. From figure 5-38 it is observed that the addition of current loads slightly reduces the relative tendon force deviation. This effect is thought to be the combined result of an increase of mean tendon force and a dampening effect of motions resulting from wind turbulence due to increased drag loads.

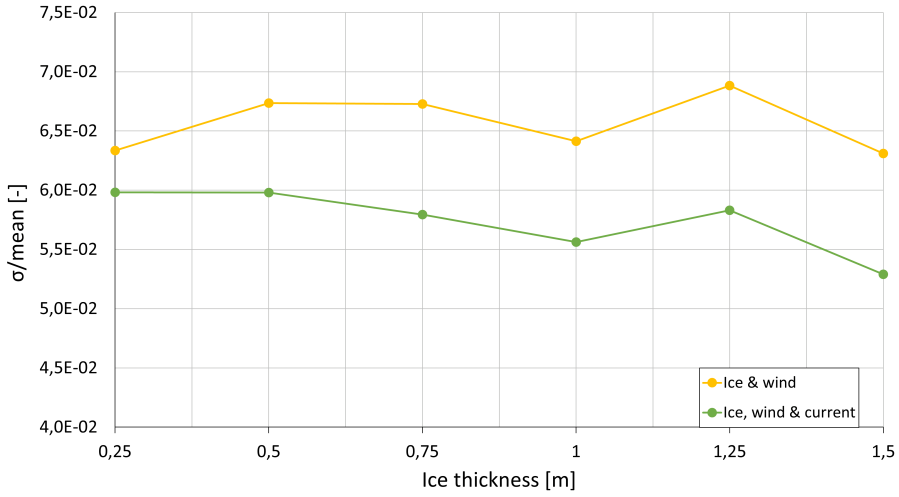


**Figure 5-38:** Relative variations of tendon force for ice bending with and without current

## 5-3 Comparison of open water and level ice conditions

From the results in the previous sections it can be seen that the different types of loading (open water and ice crushing & bending) all result in very different platform dynamics. For the comparison of these results in this section, the windward tendon force is used as a common indicator of platform dynamics. By doing so, the outcomes can be related to each other directly.

Since a comparison of all the results from the previous sections would result in chaos rather than insights, only a very limited selection of the results is used in this comparison. All of the studied cases below take into account a 11 $m/s$ mean wind velocity at hub height. The presented ice load cases of both crushing and bending failure, have an ice velocity of $v_{ice} = 0.2$ $m/s$. The full thickness ranges as considered in the previous sections is covered: 0.1 to 0.7 $m$ for crushing and 0.25 to 1.5 $m$ for bending. For the open water load cases, all seven sea states are included. For all three loading types, the load cases do not include current.

In figure 5-39, the maximum windward tendon force is plotted for the reference cases of the three distinct loading types. The open water load outcomes are plotted against their load case number on the secondary horizontal axis. This number represents the $H_s$-$T_p$ combinations presented in section 3-5-1. The ice load cases are plotted against their ice thickness on the primary horizontal axis.

The outcomes show that ice crushing action poses significantly higher loads than the other loading types, even for relatively limited ice thickness. This difference rapidly increases for larger ice thickness. The ice bending maximum tendon force is found to be in the same order of magnitude as the outcomes for the considered open water load cases. This might seem an unexpected finding, it should however be noted that these open water load cases represent (very) harsh open water conditions.

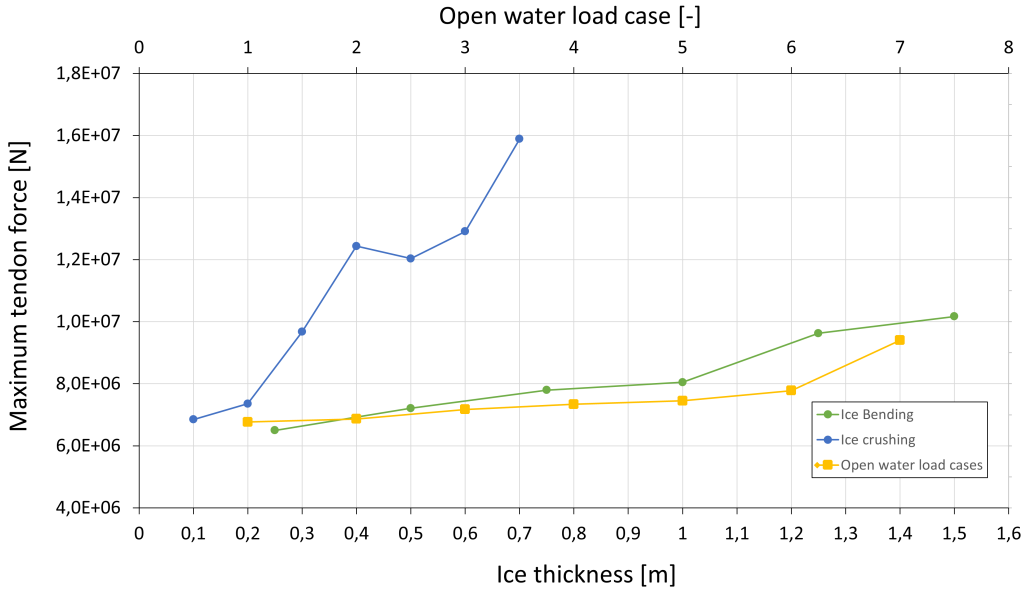


**Figure 5-39:** Load type comparison of maximum tendon forces, $v_{ice} = 0.2$ $m/s$, $u_{wind} = 11$ $m/s$

In figure 5-40, the relative force deviations are plotted for the same load cases as in figure 5-39. These relative deviations provide a basic view on the force (and stress) deviations that act on the tendons for the various load cases. From these results it can be clearly observed that in the ice bending load case the relative force variations are quite limited compared to the other two types of loading. For the ice crushing load cases, the force variations heavily depend on ice thickness. On top of that the $v_{ice} = 0.2\ m/s$, $h_{ice} = 0.4\ m$ dynamic effect, already mentioned in section 5-2-1, clearly poses serious fluctuations when compared to the other load types. These force variations can have serious implications for the structure's fatigue life.

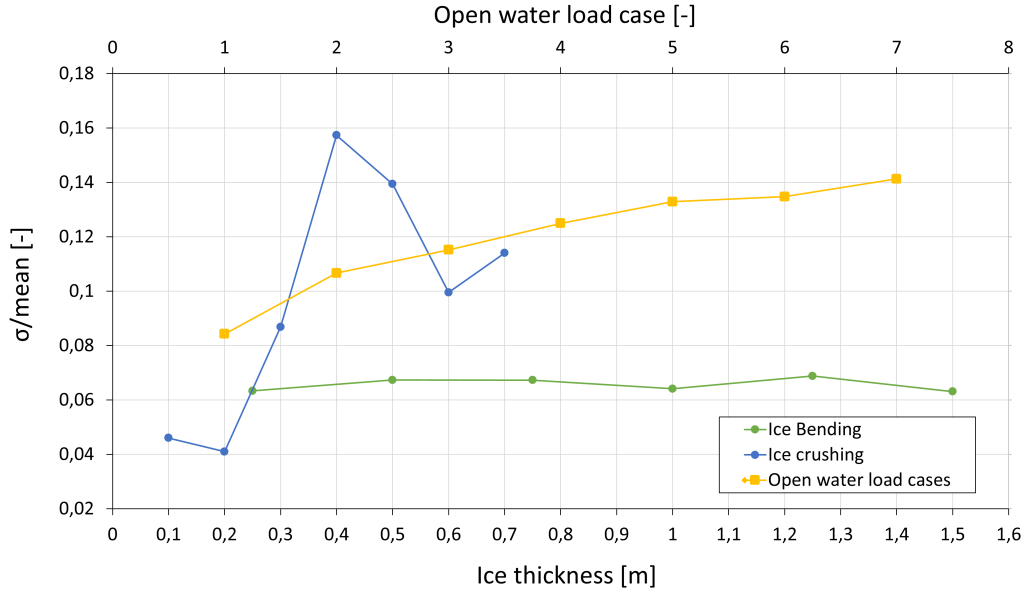


**Figure 5-40:** Load type comparison of relative force variations, $v_{ice} = 0.2\ m/s$, $u_{wind} = 11\ m/s$

The relative force fluctuations in the open water load cases are overall significantly higher than those of both the other loading types. This can be explained by the oscillating character of incoming wave loads, which typically have force contributions in both positive and negative surge direction and a zero mean. Besides that, the mean tendon force is of influence on the relative deviation in figure 5-40. Therefore in figure 5-41 and 5-42, the mean and the standard deviation of windward tendon force are plotted as well. From figure 5-41 it is noted that the mean tendon force in open water conditions is not related to the severity of the sea state. Instead, the mean tendon force (and therewith the mean platform motions) is a function of wind loads acting on the turbine.

The mean tendon force in the ice crushing load cases is considerably larger than for the other two load types, which also holds for the tendon force standard deviation. Therefore it can be concluded that ice crushing loads post most severe loading to the structure.

For the loads from ice bending failure against the structure, results are found to be far less extreme. Although mean tendon forces are larger than those in the case of open water conditions, the force fluctuations are less severe. Therewith this loading type is thought to pose less problems to structural integrity and (for limited ice thickness) might not require a mooring system with higher capacity compared to open water conditions.

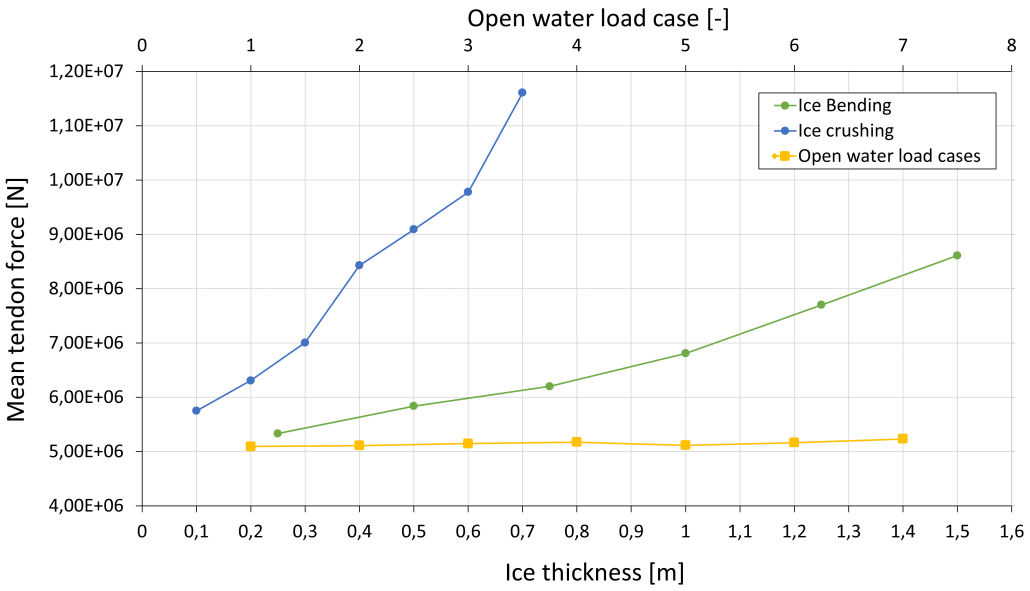


**Figure 5-41:** Load type comparison of mean tendon forces, $v_{ice} = 0.2\ m/s$, $u_{wind} = 11\ m/s$

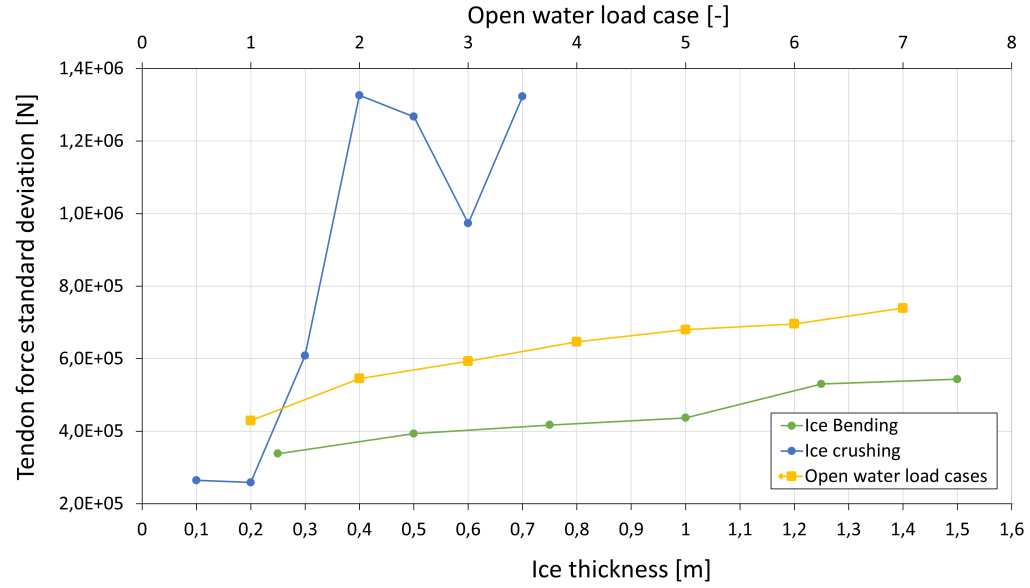


**Figure 5-42:** Load type comparison of tendon force standard variations, $v_{ice} = 0.2\ m/s$, $u_{wind} = 11\ m/s$

# Chapter 6

# Conclusions & recommendations

## 6-1 Conclusions

The main aim of this research is to gain insight in the dynamic behaviour of offshore floating wind turbines in level ice conditions, in comparison with open water conditions.

For this purpose, a Matlab model is developed to simulate structural response and mooring forces of the NREL-MIT TLP floater design. In this model three degrees of freedom are considered (surge, heave and pitch). The structure is modelled in a rigid body approximation, assuming no structural deformations. Non-linear restoring characteristics from hydrostatics and the system's mooring system are derived and applied in the system's stiffness definitions. The hydrodynamic characteristics from fluid-structure interaction are derived in frequency domain with Ansys AQWA and transformed to time-domain by application of an inverse Fourier transform and a convolution integral.

Wind velocity turbulence and irregular wave patterns are covered in the wind and wave load definitions by application of sea state and turbulence spectrum definitions (Kaimal and Jonswap spectrum respectively). Level ice loads are applied in two distinct failure modes: failure through crushing or bending. The crushing loads are simulated by the application of a Matlock-Sodhi model and bending loads are modelled by a combination of elastic beam and friction theory.

With the resulting model, simulations are performed for a range of load cases for the three main loading types: open water conditions, ice crushing and ice bending.

In the open water conditions the structure's motions are dominated by waves and wind acting on the system. Wind loading will mainly contribute to a steady state offset in surge and pitch, as well as in tendon force. Wave action has a dominant contribution to the large variation of motions and mooring forces, which can range up to approximately 75% of its mean value. Mean offsets and tendon force are independent of sea state, but result from wind load contributions.

In level ice conditions, the effects of loading on the structure's motions and mooring forces are heavily dependent on the mode in which the ice sheet will fail. Both failure modes have very different loading patterns and the relative effect of other environmental loads (wind and current) differ as well.

In the case of ice crushing loading, large mean tensile forces occur once the structure reaches its steady state. On top of this mean force, fluctuations are observed as a result of structure oscillations around this steady state. These fluctuations typically have a high frequency, and especially for large ice thickness can become very large. The effects of wind and current mainly have a contribution to the mean offset, their effect on force and displacement variations is limited. When compared to the other load types, mooring forces resulting from ice crushing action are very large. For an ice thickness of only 0.2 $m$ the maximum tendon forces are in the same order of magnitude as for the most extreme sea state considered ($H_s = 14m$, $T_p = 18.75$). For ice sheets of larger thickness, both motions and tendon forces become that large that they might compromise the platform's survivability.

When considering the load cases including residual forces for ice bending, a mean steady state offset and tendon force is observed as well. Fluctuations in tendon forces are dominated by turbulence effects in wind velocity, whereas the effect of ice bending action on platform motions is limited. This is a result of the low loading frequency, as well as relatively low force fluctuations in ice action when compared to wind force variations. Ice loads resulting from the failure of the ice sheet in bending pose far less severe loading to the platform than those resulting from crushing failure. Both the order of magnitude and the frequency of loading are found to be less severe. In ice bending failure a sheet thickness of 1 to 1.25 $m$ will yield tendon forces of the same order of magnitude as the most extreme open water load case. Force fluctuations are limited, especially when compared to ice crushing loading.

Loads resulting from both crushing and bending failure of ice impose a cyclic loading pattern to the structure. For a loading frequency at, or near one of the structure's natural frequencies, this can cause dynamic amplification of structure oscillations and mooring forces. In the ice bending load cases these effects are limited and will be overpowered by fluctuations in wind force. When ice crushing occurs with a frequency near one of the structure's natural frequencies however, these effects can become significant. In this failure mode, loading frequency is defined by the combination of ice velocity and thickness. For several of the considered load cases, loading frequency is found to be near the structure's pitch natural frequency of 0.2 Hz. Most severe dynamic effects are found to occur at $v_{ice}$, $h_{ice}$ combinations of $0.2m/s$, $0.4m$ and $0.3m/s$, $0.6m$. Here, large motion and tendon force variations are observed, as well as irregular loading patterns. Presence of wind loading has a limiting effect on this dynamic amplification due to aerodynamic damping resulting from the applied load-motion coupling. Tendon force fluctuations however, still are considerably large and potentially could pose issues to the structure's fatigue life time.

From the above it is shown that in open water conditions the main dynamic load contributions source from waves and rotor movements, whilst in level ice conditions crushing loads can also introduce high energy loading at a wide range of frequencies. Therefore the dynamic effects of ice crushing loads form a serious additional design challenge for floating wind turbines placed in the presence of level ice. To overcome this design difficulty, it seems key to force the level ice travelling against the structure in its bending failure mode. As a result, less severe loads will occur and dynamic amplification as a result of ice loading can be mitigated.

## 6-2 Recommendations

For the successful design of a floating wind turbine arrangement for application in the presence of level ice, below several recommendations are made.

In view of the dynamic ice-structure interaction, it could also be interesting to not only focus on rigid body approach applied in this study. The application of an approach that includes non-rigid tower and turbine characteristics, as has been done in existing literature for open water conditions, could provide more insights. Additional dynamic effects might for example arise from the cyclic ice loading in interaction with the system's tower or blade flexural vibrations.

The successful application of floating wind turbines in ice will, even more than in open water conditions, depend on load minimization by design in order to come to an economic solution. From this research it can be drawn that the application of a sloping design at the waterline is key to avoid ice crushing failure and thereby to minimize the magnitude of ice loading. However, major challenges lie in the correct prediction of loads in ice bending failure.

To better understand effectiveness of design considerations when dealing with ice bending loads, additional work should be done in understanding secondary effects of this type of loading. Especially the interaction of the structure and ice piece after failure of the ice sheet is a major unknown. By scenario development of ice-structure interaction and a corresponding physical force description a more enhanced loading pattern can be derived for this phenomenon. Additional effects that could be considered are the potential of rubble accumulation and the transition to crushing failure mode.

For a more exhaustive view on the ice mechanics considered, it is recommended to employ a sensitivity analysis on ice characteristics. Besides that, to come to a more realistic approach of ice loading, stochastic ice properties could be applied. By doing so a more realistic approximation of the heterogeneity of ice characteristics can be achieved.

Finally, in this thesis only two ice loading models have been applied. Since there currently is no common standard in modelling of ice loading, it might be very interesting to also apply other modelling approaches and compare outcomes. This could help to gain insights from a different perspective and provide an additional benchmark in the comparison of level ice with open water conditions.

# Bibliography


[1] J. Jonkman, S. Butterfield, W. Musial, and G. Scott, "Definition of a 5-mw reference wind turbine for offshore system development," tech. rep., NREL, 2009.

[2] D. Matha, *Model Development and Loads Analysis of an Offshore Wind Turbine on a Tension Leg Platform, with a Comparison to Other Floating Turbine Concepts.* PhD thesis, University of Colorado, April 2009.

[3] D. C. Salzmann, "Aerodynamic loading." Lecture slides on Aerodynamic Loading for the course Offshore Wind Support Structures TU Delft., 2011.

[4] M. O. Hansen, *Aerodynamics of Wind Turbines.* Earthscan, 2nd ed., 2008.

[5] L. Holthuijsen, *Waves is Oceanic and Coastal Waters.* Cambridge university press, 2007.

[6] G. Huang and P. Liu, "A dynamic model for ice-induced vibrations of structures," *Journal of Offshore Mechanics and Arctic Engineering*, vol. 131, 2009.

[7] Environmental and E. S. Institute, "Offshore wind energy - fact sheet," 2010.

[8] P. Schaumann and C. Böker, "Can jackets and tripods compete with monopiles," in *Contribution to Copenhagen Offshore Wind 26-28 October 2005*, 2005.

[9] A. Arapogianni and A. Genachte, "Deep water, the next step for offshore wind energy," tech. rep., European Wind Energy Association, 2013.

[10] A. L. H. Hopstad, K. O. Ronold, and J. Slätte, "Design standard for floating wind turbine structures," in *Deep Sea Offshore Wind R&D Conference 2013*, 2013.

[11] Statoil, "Hywind - factsheet," http://www.statoil.com/en/TechnologyInnovation/NewEnergy/RenewablePowerProduction/Offshore/Hywind/Downloads/Hywind

[12] A. Myhr, C. Bjerkseter, A. Agotnes, and T. A. Nygaard, "Levelised cost of energy for offshore floating wind turbines in a life cycle perspective," *Renewable Energy*, vol. 66, pp. 714–728, 2014.

[13] M. Hall, B. Buckham, and C. Crawford, "Evaluating the importance of mooring line model fidelity in floating wind turbine simulations," *Wind energy*, 2013.

[14] J. Jonkman and D. Matha, "Dynamics of offshore floating wind turbines - analysis of three concepts," *Wind energy*, vol. 14, pp. 557–569, 2011.

[15] J. Jonkman and P. Sclavounos, "Development of fully coupled aeroelastic and hydrodynamic models for offshore wind turbines," in *ASME Wind Energy Symposium Reno, Nevada*, 2006.

[16] S. Butterfield, W. Musial, J. Jonkman, and P. Sclavounos, "Engineering challenges for floating offshore wind turbines," in *Copenhagen Offshore Wind Conference*, NREL, MIT, 2005.

[17] H. feng Wang, Y. hua Fan, and Y. Liu, "Dynamic analysis of a tension leg platform for offshore wind turbines," *Journal of Power Technologies*, vol. 94, pp. 42–49, 2014.

[18] J. Jonkman, "Dynamics modeling and loads analysis of an offshore floating wind turbine (nrel/tp-500-41958)," tech. rep., National Renewable Energy Laboratory (NREL), 2007.

[19] A. Henderson, K. Argyriadis, J. Nichols, and D. Langston, "Offshore wind turbines on tlps - assessment of floating support structures for offshore wind farms in german waters," in *10th German Wind Energy conference*, GL Garrand Hassan, November 2010.

[20] T. Christopher, "Parametric design of floating wind turbines," Master's thesis, MIT, 2007.

[21] I. Senjanovic, N.Hadzic, and M. Tomic, *Sustainable Maritime Transportation and Exploitation of Sea Resources - Rizzuto & Guedes Soares*. Taylor & Francis Group, Chapter 127. On the linear stiffness of tension leg platforms 2012.

[22] M. Karimirad, *Stochastic Dynamic Response Analysis of Spar-Type Wind Turbines with Catenary or Taut Mooring Systems*. PhD thesis, NTNU, 8 2011.

[23] S. Schreck, "Integrated wind energy / desalination system," Tech. Rep. NREL/SR-500-39485, NREL, October 2004.

[24] T. Burton, D. Sharpe, N. Jenkins, and E. Bossanyi, *Wind Energy Handbook*. John Wiley & Sons Ltd, 2001.

[25] P. Sorensen, P. Pinson, N. A. Cutululis, H. Madsen, L. E. Jensen, J. Hjerrild, M. H. Donovan, J. R. Kristoffersen, and A. Vigueras-Rodriguez, "Power fluctuations from large wind farms," tech. rep., DTU, 2009.

[26] S. M. Vernardos, *Aerodynamic calculation of loads and dynamic behavior of wind turbine towers*. PhD thesis, National Technical University of Athens, February 2013.

[27] "Guideline for the certification of offshore wind turbines," 2005.

[28] J. Journée and W. Massie, *Offshore Hydromechanics*. Delft University of Technology, 2001.

[29] T. Ogilvie, "Recent progress toward the understanding and prediction of ship motions.," in *The Fifth Symposium on Naval Hydrodynamics*, 1964.

[30] W. Cummins, "The impulse response function and ship motions," *Institut für Shiffbau der Universität Hamburg*, 1962.

[31] K. Unneland, *Identification and order reduction of radiation force models of marine structures*. PhD thesis, NTNU, 2007.

[32] E. Kristiansen and O. Egeland, "Frequency-dependent added mass in models for controller design for wave motion damping," *NTNU - IFAC*, 2003.

[33] O. Faltinsen, *Sea loads on ships and offshore structures*. Cambridge university press, 1990.

[34] E. Branlard, "Wind energy: Generation of time series from a spectrum," *National Laboratory for Sustainable Energy, DTU*, 2010.

[35] G. Ramachandran, *A numerical model for a floating TLP wind turbine*. PhD thesis, Technical University of Denmark (DTU), 2012.

[36] K. Korzhavin, "Action of ice on engineering structures," *Cold regions research and engineering lab Hanover NH*, 1971.

[37] "Iso19906 - arctic offshore structures," 2010.

[38] V. Aksnes, "A simplified interaction model for moored ships in level ice," *Cold Regions Science and Technology*, vol. 63, pp. 29–39, 2010.

[39] G. Timco and W. Weeks, "A review of the engineering properties of sea ice," *Cold Regions Science and Technology*, vol. 60, pp. 107–129, 2010.

[40] I. Senjanovic, M. Tomic, and N. Hadzic, "Formulation of consistent nonlinear restoring stiffness for dynamic analysis of tension leg platform and its influence on response," *Marine Structures*, vol. 30, pp. 1–32, 2013.

[41] I. Senjanovic, M. Tomic, and S. Rudan, "Investigation of nonlinear restoring stiffness in dynamic analysis of tension leg platforms," *Engineering Structures*, vol. 56, pp. 117–125, 2013.

[42] P. Burton, *Kinematics and Dynamics of Planar Machinery*. Prentice Hall, 1979.

[43] V. Authors, *Mechanics of Geomaterial Interfaces*. Elsevier, 1995.

[44] K. Cheung, "Hydrodynamic interaction between ice masses and large offshore structures," Master's thesis, University of British Columbia, 1987.

[45] M. Tomlinson and J. Woodward, *Pile design and construction practice*. Taylor & Francis, 5th edition ed., 2008.

[46] B. Yu, *Offshore Wind Turbine Interaction with Floating Freshwater Ice on the Great Lakes*. PhD thesis, University of Michigan, 2014.

[47] B. Michel and N. Toussaint, "Mechanisms and theory of indentation of ice plates," *Journal of Glaciology*, vol. 19, pp. 285–300, 1977.

# Appendix A

# Excel files platform properties

Using the (limited) input properties available from existing literature, in the excel files presented below the structural properties of the structure (e.g. CoM and Moments of inertia) were derived. The figures below present (part of) the excel sheets used to come to overall structural properties of the system.

The main approach applied in determination of the system's mass moment of inertia in pitch direction is discussed in appendix B. The remainder of the calculations is based on structure dimensions and masses only and therefore will not be elaborately discussed.

Main dimensions floater structure

| | | | |
|---|---|---|---|
| Dimensions | Water depth | 200 | m |
| | Platform draft | 47,89 | m |
| | Freeboard | 5 | m |
| | Platform diameter | 18 | m |
| | wall thickness | 0,015 | m |
| | Concrete ballast height | 12,6 | m |
| Mass | Concrete ballast mass | 8216000 | kg |
| | Steel mass | 351880 | kg |
| | Platform mass | 8567880 | kg |
| CoM Positions | CoM Steel | -21 | m |
| | CoM Concrete | -41,59 | m |
| | CoM Platform (Z) | -40,76 | m |

Mass moment of inertia calculations

| | | |
|---|---|---|
| Hollow Cylinder | | |
| Mass | 268051,6581 | kg |
| R_inner | 8,985 | m |
| R_outer | 9 | m |
| Ixx=Iyy | 47098346,63 | kg m2 |
| Izz | 21676027,49 | kg m2 |
| z CoG | -15,145 | m |
| Δz CoG platform | 25,62 | m |
| Solid Cylinder | | |
| Mass | 8272632,109 | kg |
| Ixx=Iyy | 276967723 | kg m2 |
| Izz | 335041600,4 | kg m2 |
| z CoG | -41,59 | m |
| Δz CoG platform | -0,83 | m |
| Platform total | | |
| Mass | 8540683,767 | kg |
| Ixx=Iyy | 5,06E+08 | kg m2 |
| Izz | 3,57E+08 | kg m2 |

**Figure A-1:** Excel file - Structural properties floater

Tower calculations over height

| z [m] | D(z) | wt(z) | m(z) | Iy | d | Iy_steiner |
|---|---|---|---|---|---|---|
| 0 | 6 | 0,0351 | 55,909 | 248,6631 | 0 | 2,49E+02 |
| 0,01 | 5,999756849 | 0,035098813 | 55,905 | 248,6244 | -0,01 | 248,6299857 |
| 0,02 | 5,999513699 | 0,035097626 | 55,9 | 248,5857 | -0,02 | 248,6080908 |
| 0,03 | 5,999270548 | 0,035096438 | 55,896 | 248,5471 | -0,03 | 248,5973772 |
| 0,04 | 5,999027397 | 0,035095251 | 55,892 | 248,5084 | -0,04 | 248,5978424 |
| 0,05 | 5,998784247 | 0,035094064 | 55,888 | 248,4698 | -0,05 | 248,6094838 |
| 0,06 | 5,998541096 | 0,035092877 | 55,884 | 248,4311 | -0,06 | 248,6322989 |
| 0,07 | 5,998297945 | 0,035091689 | 55,88 | 248,3925 | -0,07 | 248,6662853 |
| 0,08 | 5,998054795 | 0,035090502 | 55,875 | 248,3538 | -0,08 | 248,7114405 |
| 0,09 | 5,997811644 | 0,035089315 | 55,871 | 248,3152 | -0,09 | 248,767762 |
| 0,1 | 5,997568493 | 0,035088128 | 55,867 | 248,2766 | -0,1 | 248,8352472 |
| 0,11 | 5,997325342 | 0,035086941 | 55,863 | 248,238 | -0,11 | 248,9138938 |
| 0,12 | 5,997082192 | 0,035085753 | 55,859 | 248,1993 | -0,12 | 249,0036991 |
| 0,13 | 5,996839041 | 0,035084566 | 55,855 | 248,1607 | -0,13 | 249,1046607 |
| 0,14 | 5,99659589 | 0,035083379 | 55,85 | 248,1221 | -0,14 | 249,2167761 |
| 0,15 | 5,99635274 | 0,035082192 | 55,846 | 248,0835 | -0,15 | 249,3400429 |
| 0,16 | 5,996109589 | 0,035081005 | 55,842 | 248,0449 | -0,16 | 249,4744584 |
| 0,17 | 5,995866438 | 0,035079817 | 55,838 | 248,0063 | -0,17 | 249,6200203 |
| 0,18 | 5,995623288 | 0,03507863 | 55,834 | 247,9677 | -0,18 | 249,776726 |
| 0,19 | 5,995380137 | 0,035077443 | 55,83 | 247,9291 | -0,19 | 249,9445731 |
| 0,2 | 5,995136986 | 0,035076256 | 55,826 | 247,8905 | -0,2 | 250,123559 |
| 0,21 | 5,994893836 | 0,035075068 | 55,821 | 247,852 | -0,21 | 250,3136812 |
| 0,22 | 5,994650685 | 0,035073881 | 55,817 | 247,8134 | -0,22 | 250,5149373 |
| 0,23 | 5,994407534 | 0,035072694 | 55,813 | 247,7748 | -0,23 | 250,7273248 |
| 0,24 | 5,994164384 | 0,035071507 | 55,809 | 247,7362 | -0,24 | 250,9508412 |
| 0,25 | 5,993921233 | 0,03507032 | 55,805 | 247,6977 | -0,25 | 251,185484 |
| 0,26 | 5,993678082 | 0,035069132 | 55,801 | 247,6591 | -0,26 | 251,4312507 |
| 0,27 | 5,993434932 | 0,035067945 | 55,796 | 247,6206 | -0,27 | 251,6881387 |
| 0,28 | 5,993191781 | 0,035066758 | 55,792 | 247,582 | -0,28 | 251,9561457 |
| 0,29 | 5,99294863 | 0,035065571 | 55,788 | 247,5435 | -0,29 | 252,2352691 |
| 0,3 | 5,992705479 | 0,035064384 | 55,784 | 247,505 | -0,3 | 252,5255065 |
| 0,31 | 5,992462329 | 0,035063196 | 55,78 | 247,4664 | -0,31 | 252,8268553 |
| 0,32 | 5,992219178 | 0,035062009 | 55,776 | 247,4279 | -0,32 | 253,139313 |
| 0,33 | 5,991976027 | 0,035060822 | 55,771 | 247,3894 | -0,33 | 253,4628773 |
| 0,34 | 5,991732877 | 0,035059635 | 55,767 | 247,3508 | -0,34 | 253,7975455 |
| 0,35 | 5,991489726 | 0,035058447 | 55,763 | 247,3123 | -0,35 | 254,1433151 |
| 0,36 | 5,991246575 | 0,03505726 | 55,759 | 247,2738 | -0,36 | 254,5001838 |
| 0,37 | 5,991003425 | 0,035056073 | 55,755 | 247,2353 | -0,37 | 254,868149 |
| 0,38 | 5,990760274 | 0,035054886 | 55,751 | 247,1968 | -0,38 | 255,2472082 |

Input parameters

| | | Mass [kg] | Z [m] |
|---|---|---|---|
| Mass properties | Rotor mass | 110000 | 90 |
| | Nacelle mass | 240000 | 89,4 |
| | tower mass | 347460 | 38,2 |
| | Total mass | 6,97E+05 | 64,0 |
| Turbine Dimensions | Rotor diameter | 126 | m |
| | Hub diameter | 3 | m |
| | Tower height | 87,6 | m |
| | Hub height | 90 | m |
| | blade length | 61,5 | m |
| Tower properties input | Δz | 0,01 | m |
| | Density steel | 8500 | kg/m3 |
| | Original bottom wt | 0,027 | |
| | Bottom wall thickness | 0,0351 | m |
| | Original top wt | 0,019 | |
| | Top wall thickness | 0,0247 | m |
| | Tower diameter base | 6 | m |
| | Tower top diameter | 3,87 | m |

**Figure A-2:** Excel file - Structural properties turbine tower

Blade calculations over length

| Input | | Interpolation of masses | | | Mass moment of inertia |
|---|---|---|---|---|---|
| z [m] | mass kg/m] | z [m] | Mass | 1st interpolation step | 2nd interpolation step | Iyy w.r.t. hub |
| 1,7 | 678,935 | 1,7 | 678,935 | 678,935 | 678,935 | 981,06108 |
| 2,7 | 773,363 | 2,2 | #N/A | 726,149 | 726,149 | 1757,2806 |
| 3,7 | 740,55 | 2,7 | 773,363 | 773,363 | 773,363 | 2818,9081 |
| 4,7 | 740,042 | 3,2 | #N/A | 756,9565 | 756,9565 | 3875,6173 |
| 5,7 | 592,496 | 3,7 | 740,55 | 740,55 | 740,55 | 5069,0648 |
| 6,7 | 450,275 | 4,2 | #N/A | 740,296 | 740,296 | 6329,4107 |
| 7,7 | 424,054 | 4,7 | 740,042 | 740,042 | 740,042 | 8173,7639 |
| 8,7 | 400,638 | 5,2 | #N/A | 666,269 | 666,269 | 9007,9569 |
| 9,7 | 382,062 | 5,7 | 592,496 | 592,496 | 592,496 | 9625,0975 |
| 10,7 | 399,655 | 6,2 | #N/A | 521,3855 | 521,3855 | 10021,029 |
| 11,7 | 426,321 | 6,7 | 450,275 | 450,275 | 450,275 | 10106,422 |
| 12,7 | 416,82 | 7,2 | #N/A | 437,1645 | 437,1645 | 11331,304 |
| 13,7 | 406,186 | 7,7 | 424,054 | 424,054 | 424,054 | 12571,081 |
| 14,7 | 381,42 | 8,2 | #N/A | 412,346 | 412,346 | 13863,073 |
| 15,7 | 352,822 | 8,7 | 400,638 | 400,638 | 400,638 | 15162,145 |
| 16,7 | 349,477 | 9,2 | #N/A | 391,35 | 391,35 | 16561,932 |
| 17,7 | 346,538 | 9,7 | 382,062 | 382,062 | 382,062 | 17974,107 |
| 19,7 | 339,333 | 10,2 | #N/A | 390,8585 | 390,8585 | 20332,459 |
| 21,7 | 330,004 | 10,7 | 399,655 | 399,655 | 399,655 | 22878,25 |
| 23,7 | 321,99 | 11,2 | #N/A | 412,988 | 412,988 | 25902,607 |
| 25,7 | 313,82 | 11,7 | 426,321 | 426,321 | 426,321 | 29179,541 |
| 27,7 | 294,734 | 12,2 | #N/A | 421,5705 | 421,5705 | 31373,277 |
| 29,7 | 287,12 | 12,7 | 416,82 | 416,82 | 416,82 | 33614,449 |
| 31,7 | 263,343 | 13,2 | #N/A | 411,503 | 411,503 | 35850,141 |
| 33,7 | 253,207 | 13,7 | 406,186 | 406,186 | 406,186 | 38118,525 |
| 35,7 | 241,666 | 14,2 | #N/A | 393,803 | 393,803 | 39703,218 |
| 37,7 | 220,638 | 14,7 | 381,42 | 381,42 | 381,42 | 41210,524 |
| 39,7 | 200,293 | 15,2 | #N/A | 367,121 | 367,121 | 42409,818 |
| 41,7 | 179,404 | 15,7 | 352,822 | 352,822 | 352,822 | 43483,347 |
| 43,7 | 165,094 | 16,2 | #N/A | 351,1485 | 351,1485 | 46077,837 |
| 45,7 | 154,411 | 16,7 | 349,477 | 349,477 | 349,477 | 48732,82 |
| 47,7 | 138,935 | 17,2 | #N/A | 348,0075 | 348,0075 | 51477,269 |
| 49,7 | 129,555 | 17,7 | 346,538 | 346,538 | 346,538 | 54283,445 |
| 51,7 | 107,264 | 18,2 | #N/A | #N/A | 344,73675 | 57095,301 |
| 53,7 | 98,776 | 18,7 | #N/A | #N/A | 342,3350833 | 59855,578 |
| 55,7 | 90,248 | 19,2 | #N/A | #N/A | 340,5338333 | 62767,196 |
| 56,7 | 83,001 | 19,7 | 339,333 | 339,333 | 339,333 | 65845,872 |
| 57,7 | 72,906 | 20,2 | #N/A | #N/A | 337,00075 | 68754,893 |
| 58,7 | 68,772 | 20,7 | #N/A | #N/A | 333,8910833 | 71534,495 |

Blade calculations w.r.t. blade orientation (θ)

| θ | Iyy blade1 | Iyy blade2 | Iyy blade3 | Iyy combined |
|---|---|---|---|---|
| 0 | 0,00E+00 | 1,06E+07 | 10607808 | 2,12E+07 |
| 5 | 1,07E+06 | 1,11E+07 | 10033664 | 2,22E+07 |
| 10 | 2,13E+06 | 1,15E+07 | 9383157 | 2,30E+07 |
| 15 | 3,17E+06 | 1,18E+07 | 8661239 | 2,37E+07 |
| 20 | 4,19E+06 | 1,21E+07 | 7873404 | 2,41E+07 |
| 25 | 5,18E+06 | 1,22E+07 | 7025647 | 2,44E+07 |
| 30 | 6,12E+06 | 1,22E+07 | 6124421 | 2,45E+07 |
| 35 | 7,03E+06 | 1,22E+07 | 5176584 | 2,44E+07 |
| 40 | 7,87E+06 | 1,21E+07 | 4189351 | 2,41E+07 |
| 45 | 8,66E+06 | 1,18E+07 | 3170234 | 2,37E+07 |
| 50 | 9,38E+06 | 1,15E+07 | 2126989 | 2,30E+07 |
| 55 | 1,00E+07 | 1,11E+07 | 1067557 | 2,22E+07 |
| 60 | 1,06E+07 | 1,06E+07 | 1,5E-09 | 2,12E+07 |
| 65 | 1,11E+07 | 1,00E+07 | 1067557 | 2,22E+07 |
| 70 | 1,15E+07 | 9,38E+06 | 2126989 | 2,30E+07 |
| 75 | 1,18E+07 | 8,66E+06 | 3170234 | 2,37E+07 |
| 80 | 1,21E+07 | 7,87E+06 | 4189351 | 2,41E+07 |
| 85 | 1,22E+07 | 7,03E+06 | 5176584 | 2,44E+07 |
| 90 | 1,22E+07 | 6,12E+06 | 6124421 | 2,45E+07 |
| 95 | 1,22E+07 | 5,18E+06 | 7025647 | 2,44E+07 |
| 100 | 1,21E+07 | 4,19E+06 | 7873404 | 2,41E+07 |
| 105 | 1,18E+07 | 3,17E+06 | 8661239 | 2,37E+07 |
| 110 | 1,15E+07 | 2,13E+06 | 9383157 | 2,30E+07 |
| 115 | 1,11E+07 | 1,07E+06 | 10033664 | 2,22E+07 |
| 120 | 1,06E+07 | 3,00E-09 | 10607808 | 2,12E+07 |
| 125 | 1,00E+07 | 1,07E+06 | 11101221 | 2,22E+07 |
| 130 | 9,38E+06 | 2,13E+06 | 11510146 | 2,30E+07 |
| 135 | 8,66E+06 | 3,17E+06 | 11831473 | 2,37E+07 |
| 140 | 7,87E+06 | 4,19E+06 | 12062754 | 2,41E+07 |
| 145 | 7,03E+06 | 5,18E+06 | 12202231 | 2,44E+07 |
| 150 | 6,12E+06 | 6,12E+06 | 12248842 | 2,45E+07 |
| 155 | 5,18E+06 | 7,03E+06 | 12202231 | 2,44E+07 |
| 160 | 4,19E+06 | 7,87E+06 | 12062754 | 2,41E+07 |
| 165 | 3,17E+06 | 8,66E+06 | 11831473 | 2,37E+07 |
| 170 | 2,13E+06 | 9,38E+06 | 11510146 | 2,30E+07 |

**Figure A-3:** Excel file - Structural properties turbine blades

| | | CM | | | WRT CM | WRT SWL |
|---|---|---|---|---|---|---|
| | Mass [kg] | Z [m] | X [m] | Iyy [kgm^2] | Iyy _ sys [kgm^2] | Iyy _ sys [kgm^2] |
| Rotor | 110000 | 95.0 | -5.4 | 1.84E+07 | 1.81E+09 | 1.01E+09 |
| Nacelle | 240000 | 94.4 | 1.9 | 0.00E+00 | 3.86E+09 | 2.14E+09 |
| Tower | 347460 | 43.2 | 0.0 | 2.15E+08 | 2.20E+09 | 8.62E+08 |
| Floater | 8540684 | -40.76 | 0.0 | 4.30E+08 | 1.02E+09 | 1.46E+10 |
| **System** | 9.24E+06 | -32.48 | -0.015 | | 8.89E+09 | 1.86E+10 |

**Figure A-4:** Excel file - Output system structural properties

# Appendix B

# Determination of system mass moment of inertia

To come to the overall system's mass moment of inertia in pitch direction to be used in the system's equation of motion, the system is divided in several parts with masses as indicated in figure B-1 below.

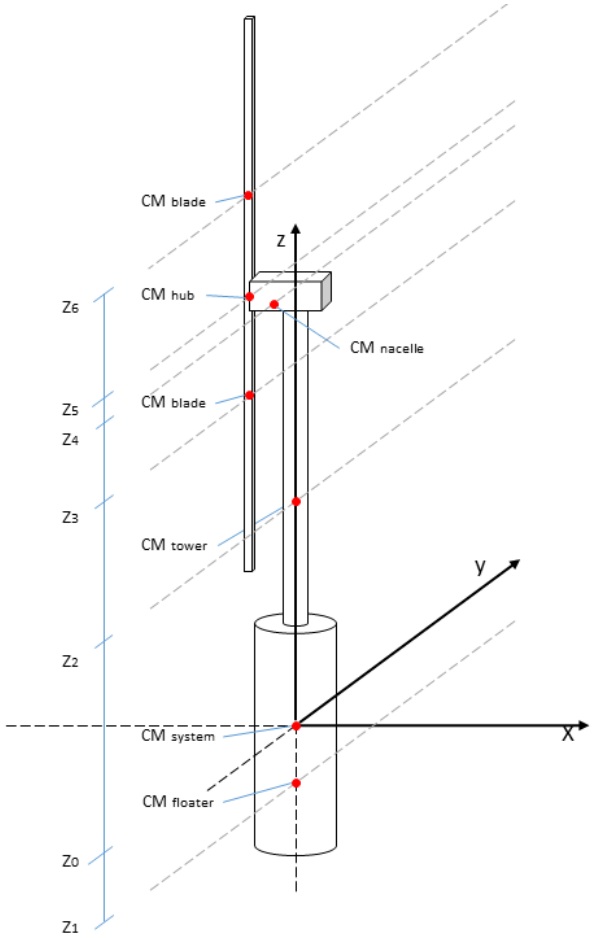


**Figure B-1:** Mass definitions of the various system parts

Following the available input, the mass moment of inertia of the various parts is defined using different methods. For the platform, detailed dimensioning was available and therefore mass moment of inertia could be determined applying dimension dependent formulae, as indicated in figures B-2 and B-3 and equations B-1 and B-2 below. The solid approximation of the mass moment of inertia is applied to the solid cylindrical part at the bottom of the floater, consisting of concrete ballast. The hollow cylinder approach is applied to the remainder of the floater.

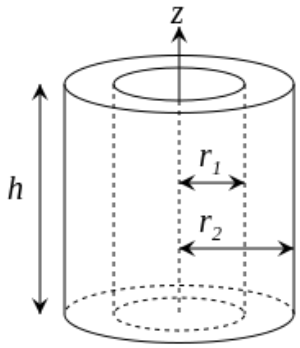


**Figure B-2:** Mass moment of inertia of a hollow tubular

$$I_y = \frac{1}{12} m \left[ 3(r_2^2 + r_1^2) + h^2 \right] \tag{B-1}$$

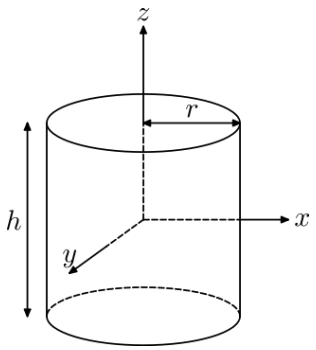


**Figure B-3:** Mass moment of inertia of a solid cylinder

$$I_y = \frac{1}{12} m(3r^2 + h^2) \tag{B-2}$$

Both parts of the floater are integrated to form an overall platform mass moment of inertia w.r.t. the platform's centre of mass using Steiner's Rule. The tower used in the turbine arrangement has both a varying diameter and a varying wall thickness along its height. In the determination of the mass moment of inertia, therefore, the tower divided into n number of sections of height $\Delta z$, with constant wall thickness and diameter. Equation B-1 is applied, in combination with Steiner's Rule, to come to the overall tower's mass moment of inertia.

Both the hub and nacelle applied in the turbine arrangement [1] are defined to be point masses at a predefined location. The contribution of the nacelle mass has been directly added to the overall system's mass moment of inertia, whereas the hub weight has been integrated with the contributions of the blades, to form the rotor specifications, before adding it to the overall system.

In the case of the blades, the dimensions are thought to be more complex, therefore the distribution of mass along the blade length could be interpolated from the data made available in [1]. Applying Steiner's Rule: $I_{y'} = \sum_{n=1}^{N} I_{y_n} + m_n {d_n}^2$ [42], the blade's mass moment of inertia w.r.t. the blade root can be determined. In order to obtain a realistic value for this mass moment of inertia, however, the orientation of the blades w.r.t. the hub center should be taken into account. This orientation is thought to be best captured by referencing to the angle of rotation $\theta$ of 1 blade with an axis parallel to the global x-y plane. As a result of the rotor geometry, it holds that the other blades have an angle of 120 and 240 degrees respectively, as seen in figure B-4.

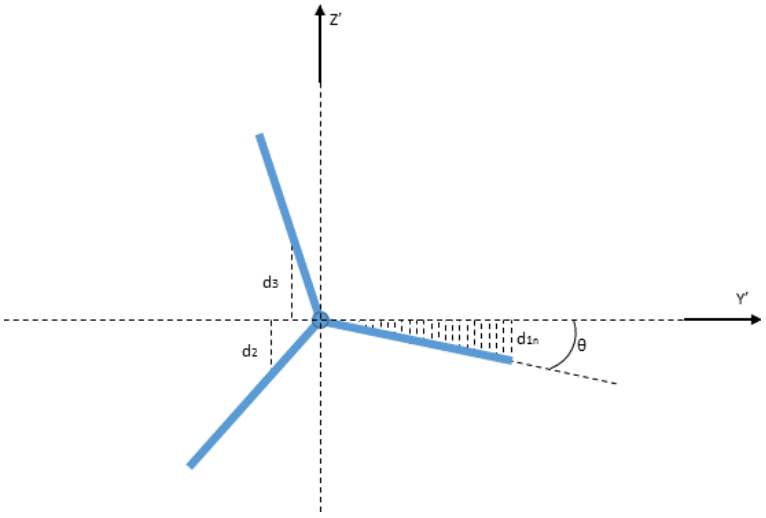


**Figure B-4:** Definitions of influence of rotation on contributions to global mass moment of inertia

From this definition of rotation, the distance in global z-direction of each element along the blade can be determined and integrated in Steiner's Rule presented above. This results in the definitions of pitch mass moment of inertia for all three blades as presented in equations B-3 through B-5 below.

$$I_{y_{blade1}} = \left| \sum_{n=1}^{N} m_n (d_n sin(\theta))^2 \right| = \left| sin(\theta)^2 \right| \sum_{n=1}^{N} m_n d_n^2 \tag{B-3}$$

$$I_{y_{blade2}} = \left| \sum_{n=1}^{N} m_n (d_n sin(\theta + 120))^2 \right| = \left| sin(\theta + 120)^2 \right| \sum_{n=1}^{N} m_n d_n^2 \tag{B-4}$$

$$I_{y_{blade3}} = \left| \sum_{n=1}^{N} m_n (d_n sin(\theta + 240))^2 \right| = \left| sin(\theta + 240)^2 \right| \sum_{n=1}^{N} m_n d_n^2 \tag{B-5}$$

As visualised in figure B-5, the combined mass moment of inertia of the three blades w.r.t. the turbine's hub is independent on the rotation of the blades in the rotor plane, whereas the contribution of each blade does change with rotor orientation. The combined mass and mass moment of inertia of the blades is added to the hub, to form the rotor.

After determination of these mass moments of inertia of all parts w.r.t. to a local point of interest, the contribution of each part to the overall system's mass moment of inertia is determined w.r.t. the overall center of mass applying Steiner's Rule [42]. This results in an overall mass moment of inertia for rotations in pitch direction of $9.47 * 10^9$. This system characteristic is used in the M(3,3) element in the system's mass matrix to form the equation of motion.

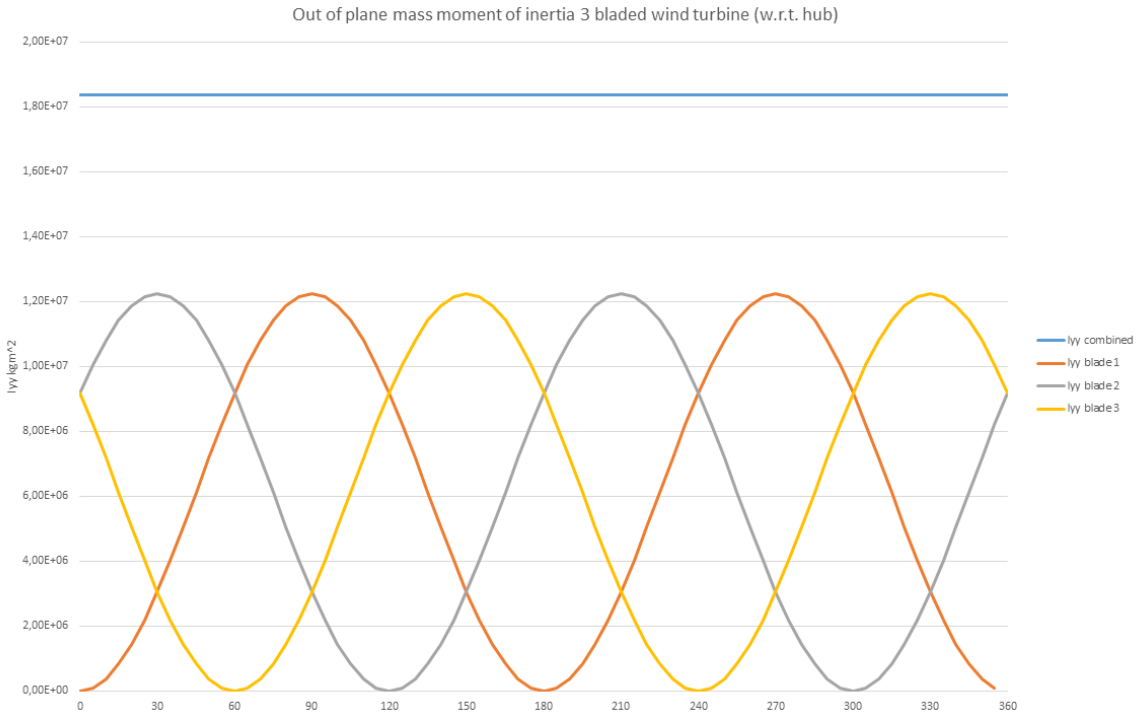


**Figure B-5:** Dependency of rotor mass moment of inertia on blade orientation

# Appendix C

# Ansys AQWA output

In this Appendix the output of the diffraction analysis performed with Ansys AQWA is presented. The output of Ansys AQWA used for further calculations in this study are the Added Mass, Added Damping and Wave Exciting Forces characteristics of the platform. All these characteristics are frequency dependent and are evaluated for the frequency range based on the Jonswap spectrum in figure 3-13.

## C-1 AQWA data plots

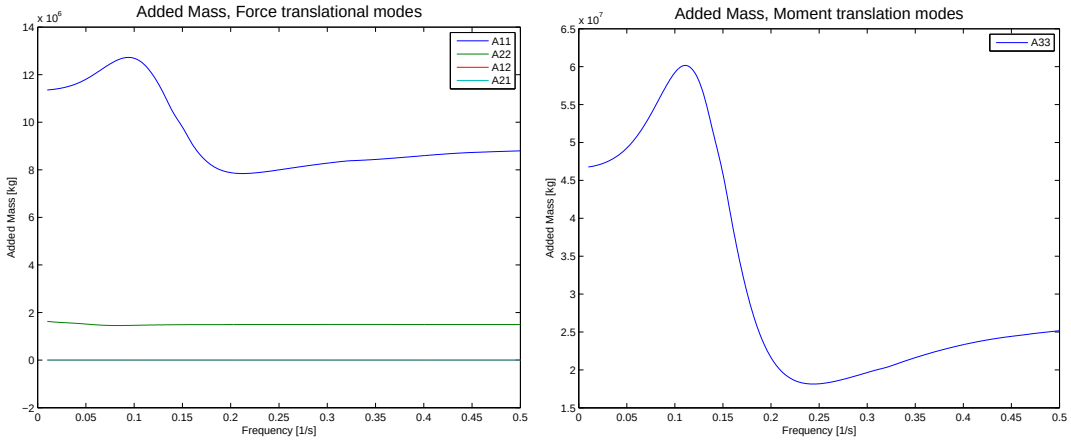


**Figure C-1:** Ansys AQWA output - Added mass Translational modes

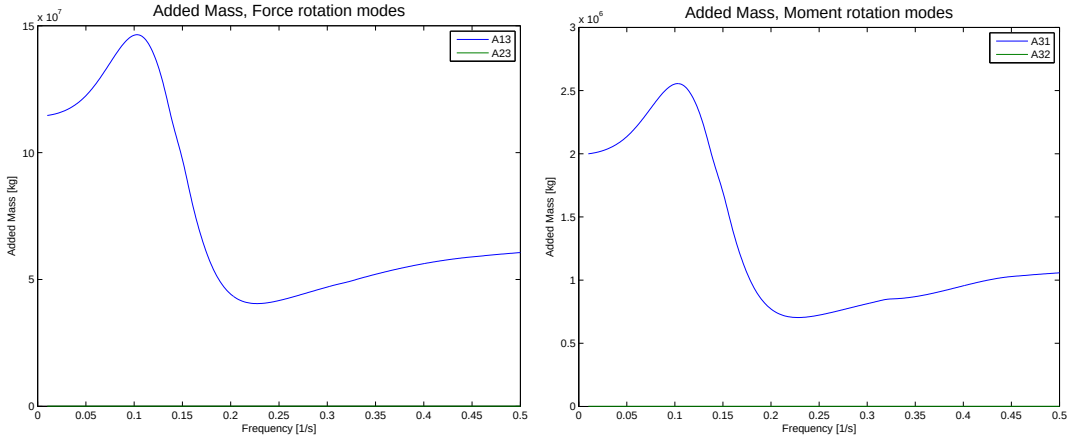


**Figure C-2:** Ansys AQWA output - Added mass Rotational modes

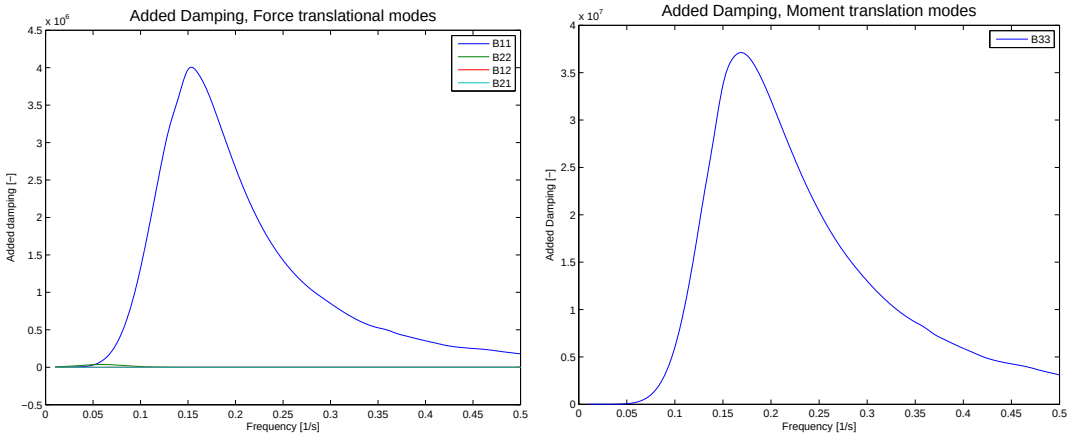


**Figure C-3:** Ansys AQWA output - Added damping Translational modes

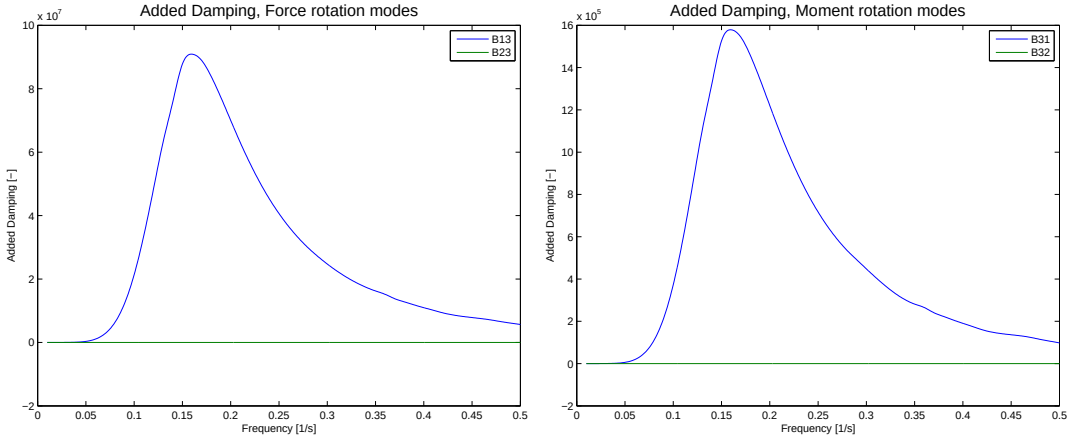


**Figure C-4:** Ansys AQWA output - Added damping Rotational modes

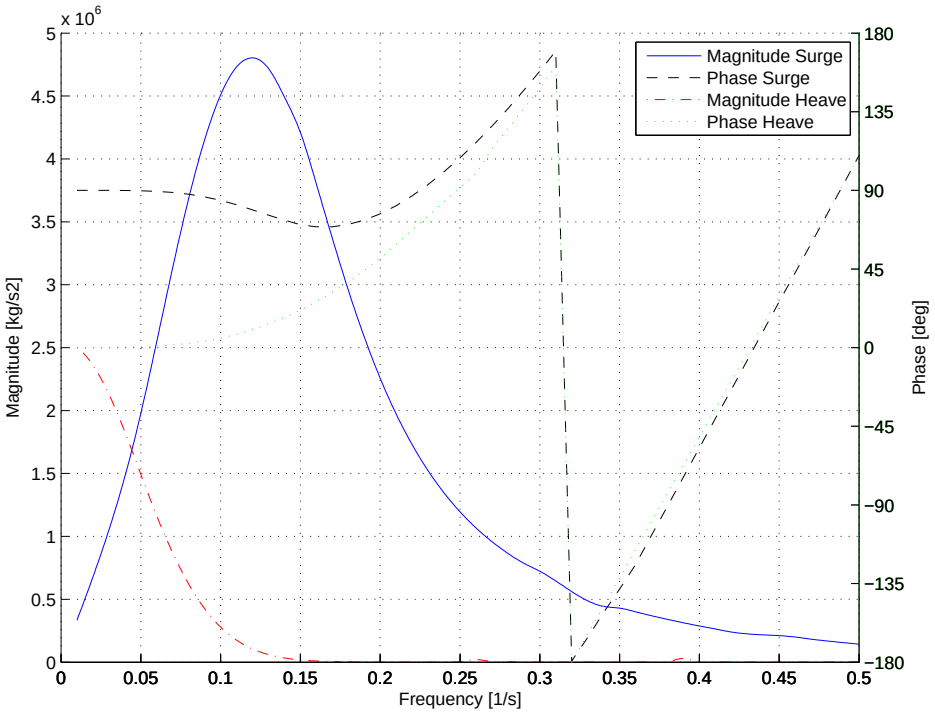


**Figure C-5:** Ansys AQWA output Surge & heave force and phase

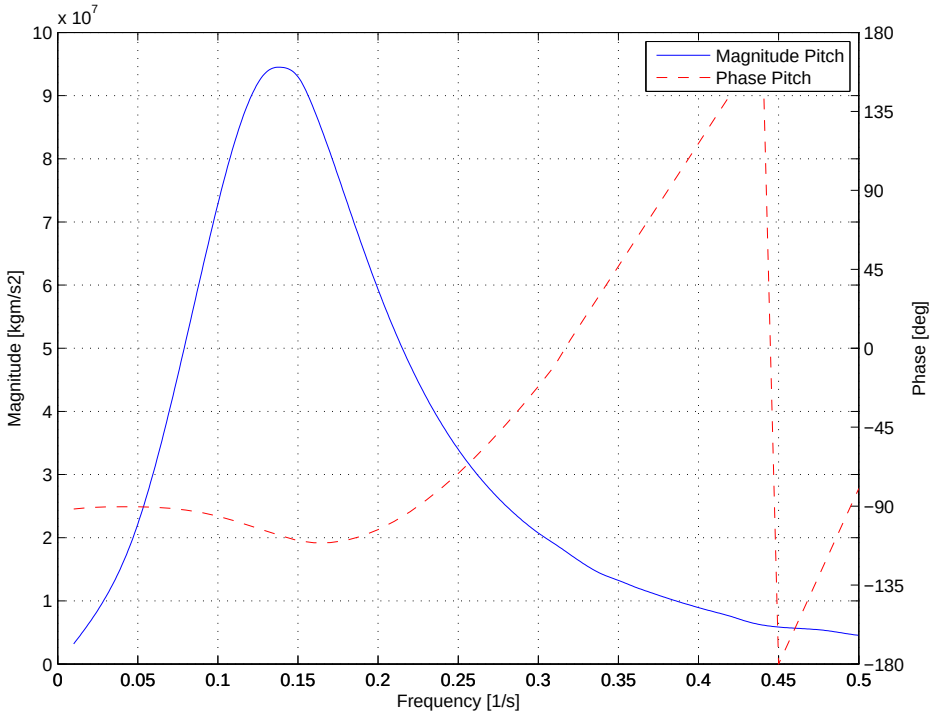


**Figure C-6:** Ansys AQWA output - Pitch force and phase

## C-2 Wave forces plots

From the data presented in figures C-5 and C-6 a wave loading time trace can be defined by the application of equation 3-31. In figure C-7 below, the resulting time trace is presented for a sea state of Hs=4.4 s and Tp=11 m.

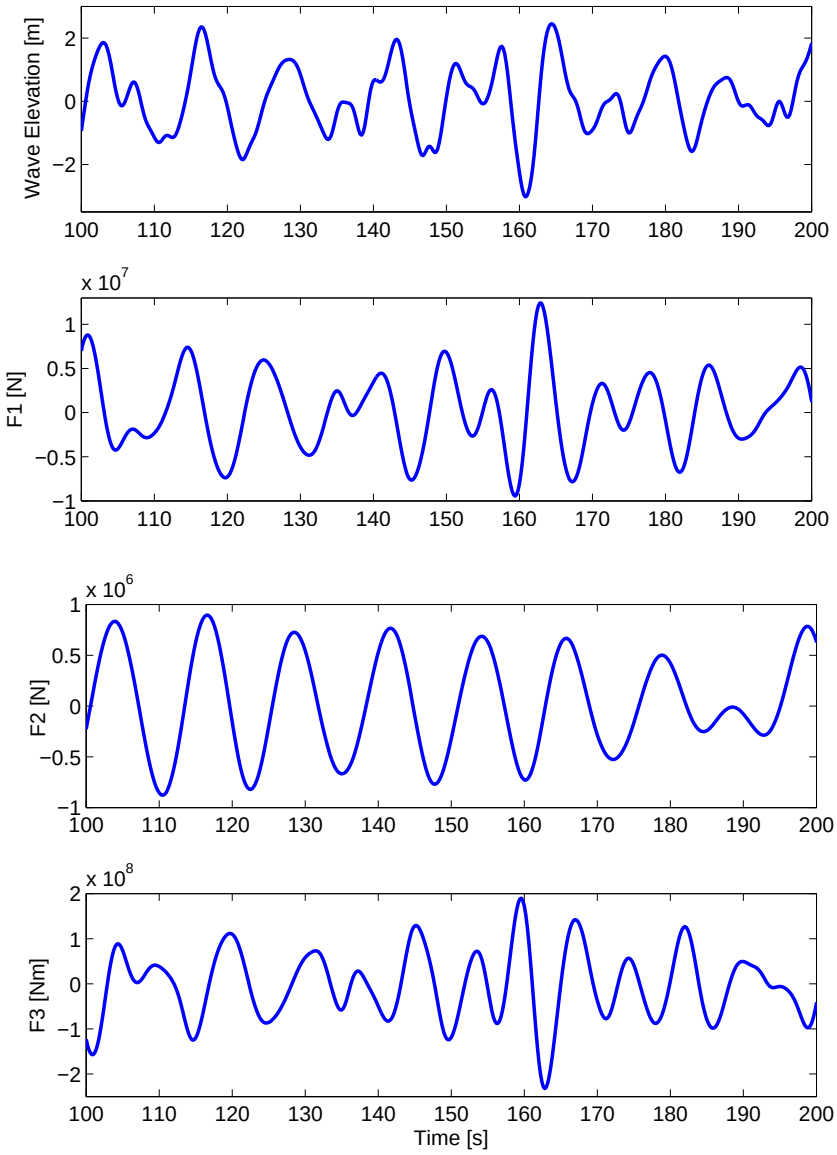


**Figure C-7:** Wave loading applying Ansys AQWA output for Hs=4 m, Tp=10 s

Here the upper plot is the wave elevation time record and the other plots (F1,F2 and F3) represent the loads in surge, heave and pitch direction respectively.

# Appendix D

# Turbine load determination

As indicated in chapter 3, two methods are considered to take into account wind loading onto the turbine: actuator disk theory and the use of a reference thrust curve. Both methods are defined for covering steady wind velocities and therefore are not strictly applicable in case of turbulence and platform motions. In an attempt to minimize modelling complexity, however, both methods are combined in a formulation that to some extent covers these effects.

Below, the reasoning behind combining both methods is briefly put forward.

First, when considering only the actuator disk theory, the main difficulty lies in the determination of an induction factor that is appropriate for a given mean wind speed. The induction has a dominant effect on the load definitions from the actuator disk theory, as can be seen in figure D-1.

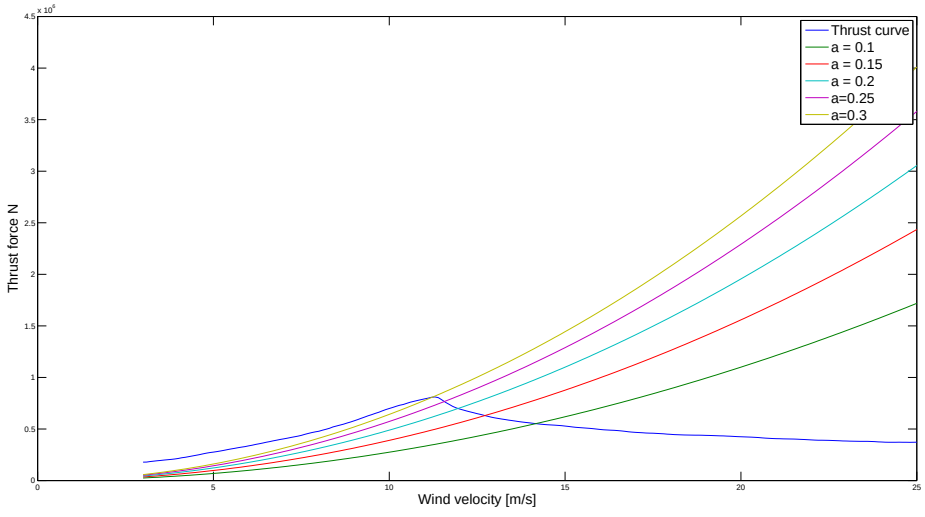


**Figure D-1:** Actuator disk theory for a range of 'a' values

To overcome this shortcoming of the actuator disk theory, the induction factor in this theory can be derived from the reference thrust curve. This approach helps to capture the optimal turbine set-up for the mean wind velocity and is visualised in figure D-2.

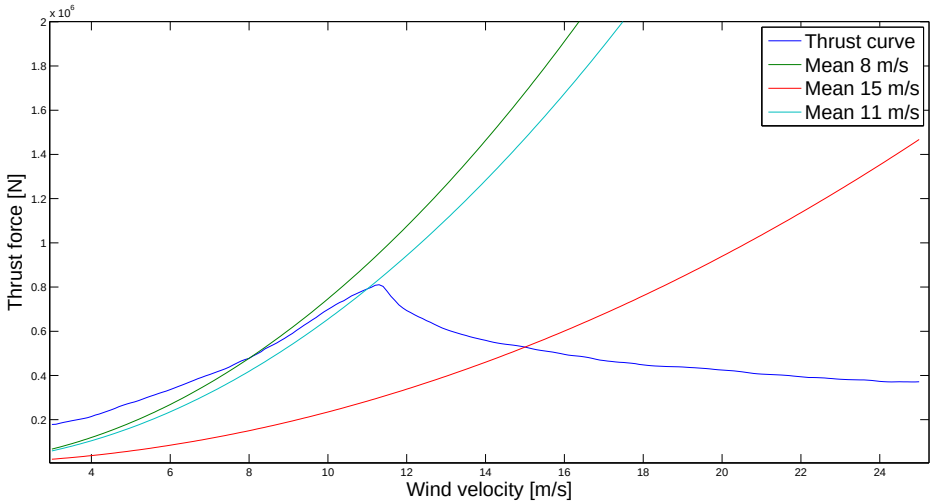


**Figure D-2:** Determination of 'a' values by matching thrust for mean wind velocity

For these mean wind velocities, the difference between the direct application of the thrust-curve is compared with the combination with actuator disk theory. This comparison is done for a fluctuating wind velocity, which for simplicity is set to

$$u(t) = \bar{u} + 1.5cos(\omega t) \tag{D-1}$$

With $\omega = \frac{2\pi}{T}$, T is set to 10 s.

In figures D-3 through D-5 the comparison is presented over time. It can be observed that whereas for the case of 8 m/s wind velocity both approaches yield reasonably comparable results, for the other two mean wind velocities this is not the case.

For the 11 m/s mean velocity case, it is observed that in the application of the reference thrust curve a strange effect occurs for fluctuations above the rated wind speed, which is reflected in a more frequent and less gradual thrust force variation. Here the thrust force drops for increasing wind velocities, whereas in the application of the actuator disk theory, this effect is mitigated. When coupling this back to figure D-2, it becomes clear that the difference sources from the difference in slope of the tangent of both. Where the tangent thrust curve switches sign above rated wind speed the actuator does not.

For the 15 m/s the slope of the tangent of both is opposite of sign and constant within the range of fluctuations. This is results in an out of phase loading pattern for the direct application of the reference thrust curve. This is due to the lowering of thrust force for increasing wind velocities.

From this it can be concluded that combining both methods provides a more accurate load determination than either of both separately. Although both are not intended for application on turbulent conditions, it does provide a reasonable indication of turbine loads.

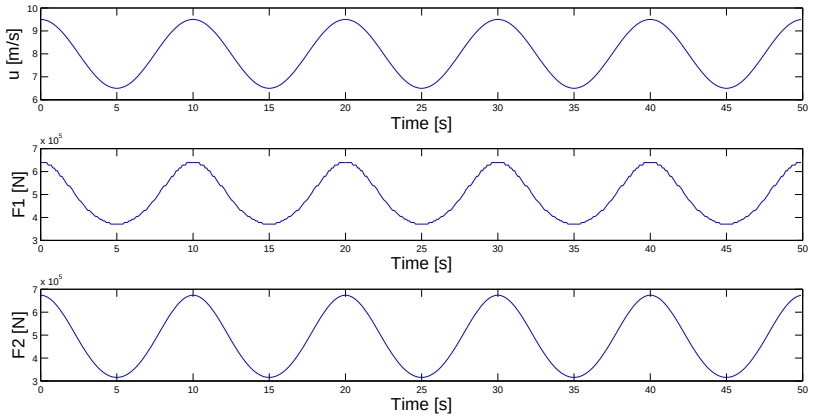


**Figure D-3:** Reference thrust curve (F1) and actuator disk approach (F2) for 8 m/s mean wind velocity

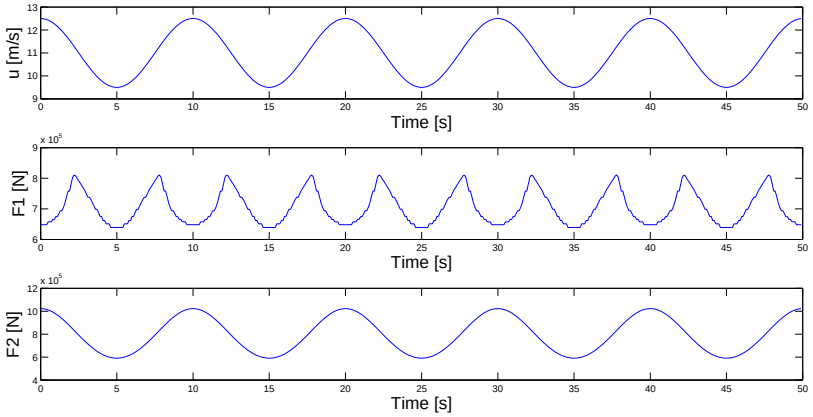


**Figure D-4:** Reference thrust curve (F1) and actuator disk approach (F2) for 11 m/s mean wind velocity

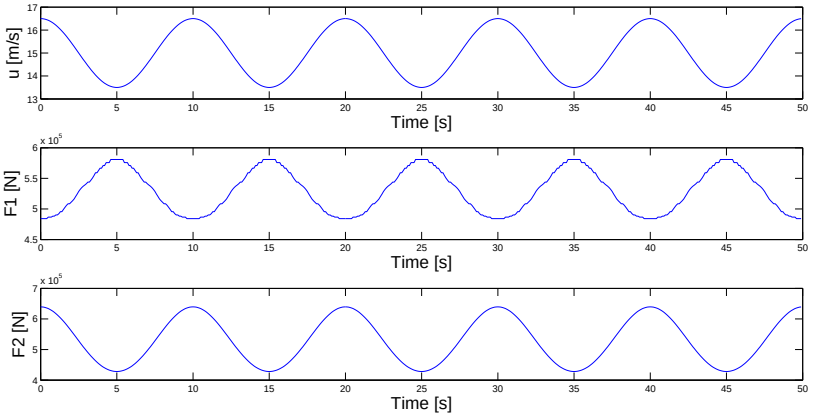


**Figure D-5:** Reference thrust curve (F1) and actuator disk approach (F2) for 15 m/s mean wind velocity

# Appendix E

# Radiation characteristics

In the fundamental equation of motion (equation 2-1) the, besides mass and stiffness the system does also contain certain damping characteristics. As discussed in chapter 3, for the structure at hand, these damping characteristics source mainly from waves radiating from the structure outward as a result of vertical oscillations in water. From the frequency domain analysis performed in Ansys AQWA the stiffness characteristics are obtained in frequency domain, which can be conveniently applied for further frequency domain analysis.

For the time-domain analysis performed in this thesis, however, these characteristics are not directly applicable. In order to make use of these characteristics, the frequency domain data is transformed to time domain, by application of a method discussed by K. Unneland (2007) [31].

The basis for this transformation is Cummins equation (1962) [30], in which potential flow theory is combined with the Bernoulli equation and integrated over the submerged body's area. In Cummins equation a separation is made between force components related to the structure's accelerations (or instantaneous contributions) and components related to the structure's velocity history, to capture the water surface's memory effect.

For displacement definition of $\xi(t) = Re\hat{\xi} \exp j\omega t$, Cummins equation is defined by:

$$\tau_R(t) = -M_A\ddot{\xi}(t) - \int_0^t k(t-\tau)\dot{\xi}(\tau)d\tau \tag{E-1}$$

$$= \omega^2 cos(\omega t)M_A\hat{\xi} - \omega cos(\omega t)\int_0^t k(\tau)\hat{\xi}sin(\omega\tau)d\tau + \omega sin(\omega t)\int_0^t k(\tau)\hat{\xi}cos(\omega\tau)d\tau \tag{E-2}$$

Relating this equation to the frequency domain equation of motions with substitution of $\xi(t) = Re\hat{\xi} \exp j\omega t$.

$$\tau_R(t) = \omega^2 cos(\omega t)A(\omega)\hat{\xi} + \omega sin(\omega t)B(\omega)\hat{\xi} \tag{E-3}$$

From this Ogilvie method (1962) [29], frequency and time-domain characteristics are related by

$$A(\omega) = M_A - \frac{1}{\omega}\int_0^t k(\tau)sin(\omega\tau)d\tau \tag{E-4}$$

$$B(\omega) = \int_0^t k(\tau)cos(\omega\tau)d\tau \tag{E-5}$$

By performing an inverse Fourier transform, the inverse relation is defined by:

$$k(t) = \frac{2}{\pi}\int_0^\infty B(\omega)cos(\omega t)d\omega \tag{E-6}$$

$$k(t =) - \frac{2}{\pi}\int_0^\infty \omega(A(\omega) - M_A)sin(\omega t)d\omega \tag{E-7}$$

From these relations, the retardation kernel function $k(t)$ can be defined for each element of the added mass and damping matrices in frequency domain. As an example, in figure E-1 the kernel for surge-surge damping is plotted against time. By the relation in equation E-4 it is defined that $M_A = \lim_{\omega\to\infty} A(\omega)$. This inertial part of radiation loads is directly added to the structure's mass matrix.

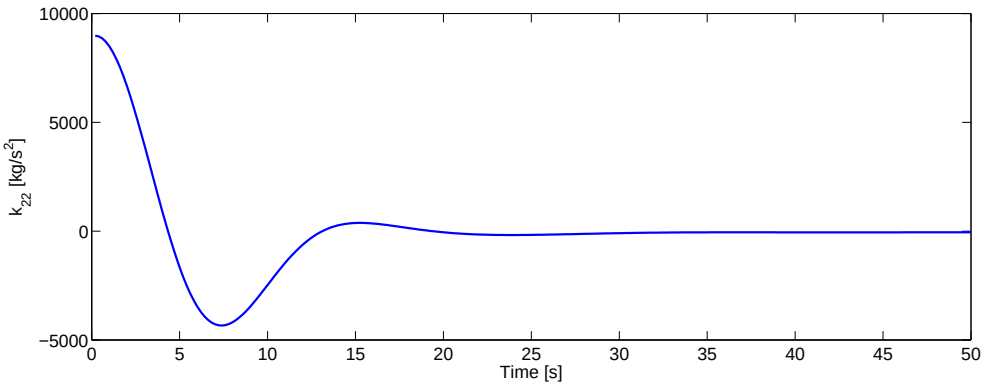


**Figure E-1:** Radiation Impulse Response heave

By convolution of the kernel function with the structure's velocity history in the DOF of interest the force contribution can be found.

$$F_{radiation_{ij}} = \int_0^t k_{ij}(t-\tau)\dot{X}_j(\tau)d\tau \tag{E-8}$$

By summing the contributions of the velocities in all DOFs to the DOF at interest, the total radiation force is determined and added to the E.M. as an external force.

# Appendix F

# Verification of spectrum usage

In chapter 3 for both wind and wave loading onto the structure a spectrum definition is used to apply irregular wind speed and wave elevation along the simulated time series. In this Appendix, the correct usage of these spectra is verified by applying an inverse Fourier analysis on both the time series of wind speed and wave elevation. Performing this check is thought to help verify whether any errors are made in the implementation of the spectrum definitions.

First, the irregular wave elevation has been simulated by the application of a Jonswap spectrum, as can be seen in figure 3-13 in chapter 3. The correctness of the time series formulation from this spectrum can be checked both by the application of a Fourier transfer of the wave elevation data from the time series, and by determination of the standard deviation of the elevation time series.

From [28] it is known that the significant wave height of a data series can be approximated by: $H_s = 4\sigma$. This check is performed for a significant wave height of 4.4 m and a peak period of 11.3 s. The standard deviation of the wave elevation for a time series of 500 s, was found to be 1.1021, only 0.0021 from the expected value of 1.1.

Secondly, a Fourier transform of the wave elevation data was performed and plotted against the applied Jonswap spectrum. Here it is observed that the spectrum definition as introduced in chapter 3, matches the Fourier transfer outcomes from the created time series, confirming the initial indication of correctness from the $\sigma$ rule of thumb.

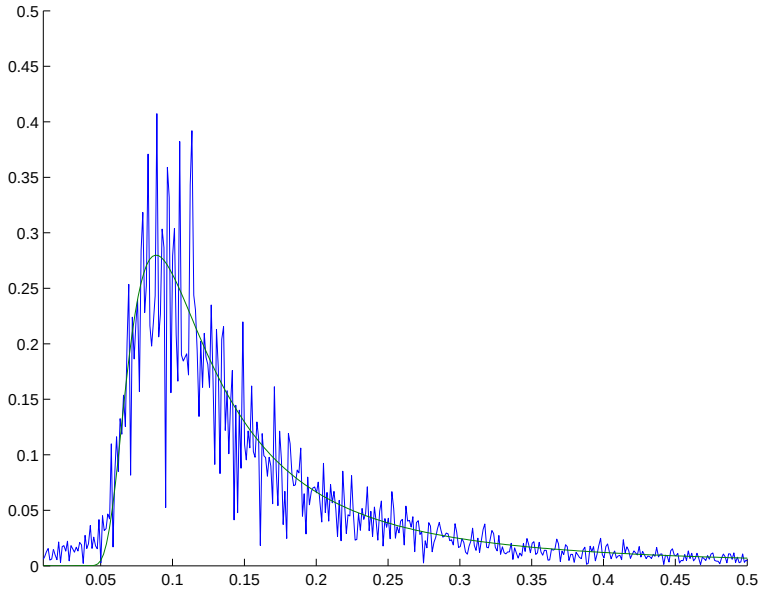


**Figure F-1:** Verification of Jonswap spectrum usage

For the development of the wind time series, no rule of thumb is known to the author, by which the statistics of the dataset can be checked. Therefore, here only the Fourier transfer is performed and plotted against the wind spectrum data. From visual inspection these also seem to be in reasonable agreement.

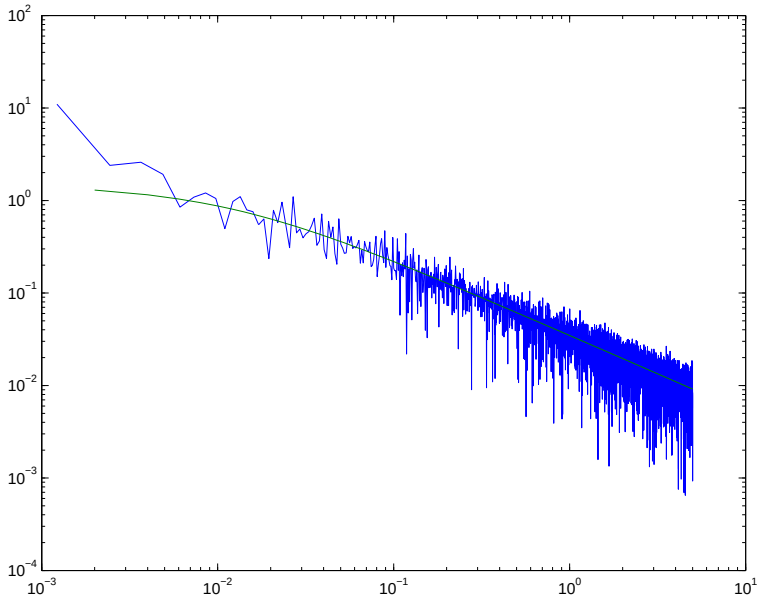


**Figure F-2:** Verification of Kaimal spectrum usage

# Appendix G

# Wave kinetics

Travelling waves not only cause loading onto the platform as a result of pressure differences near the structure, but also cause a flow of water along the structure, which causes viscous drag. In the application of Airy wave theory and linear superposition of regular waves to come to an irregular sea state (as is applied in this study), the temporal and spatial variation of fluid velocity is described by.

$$u_{waves}(z,t) = \sum_{n=1}^{N} a_n \omega_n \frac{cosh(k_n)(z+h_w)}{sinh(k_n h_w)} cos(\omega_n t - k_n x \theta_n) \tag{G-1}$$

Here $n$ is the number of the regular wave in frequency range, $N$ is the total number of frequencies taken into account, $k_n$ is the wave number (as presented in equation 3-24), $z$ is the vertical coordinate, $h_w$ is water depth, $\omega_n$ is angular frequency, $t$ is time and $\theta$ is the random angle (ranging from 0 to $2\pi$) incorporated to come to a random wave signal.

This description results in a velocity profile along water depth for each time instant t. Combining both time and spatial variations, the results are shown for several depths in figure G-1.

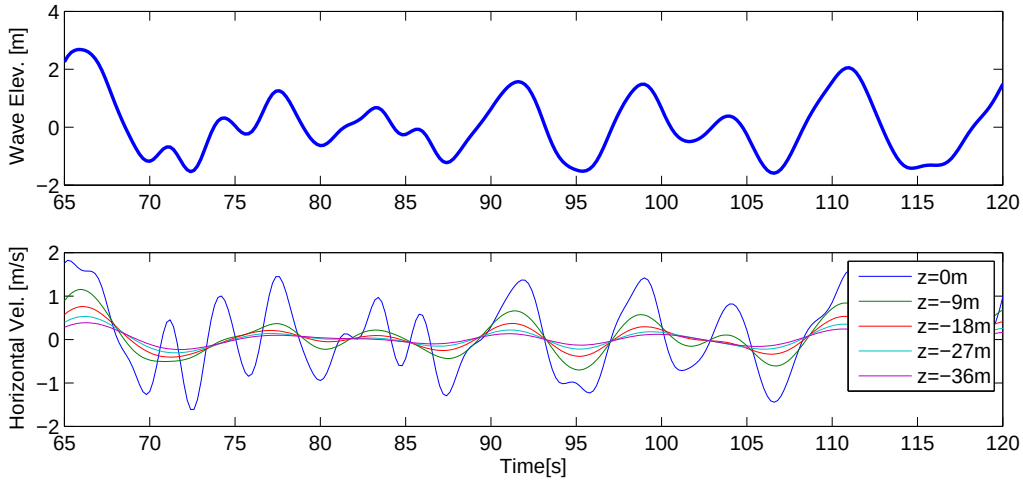


**Figure G-1:** Horizontal wave kinetics over depth and in time

It can be observed that in general horizontal fluid velocities follow wave elevation profile with highest velocities at water level and decreasing velocity amplitudes for increasing depth. The velocities are more or less damped with increasing depth. To highlight this phenomenon is further highlighted in figure G-2 below, where the velocity depth profile is plotted for time instants ranging from $t = 205$ to $t = 210$ from the data series in the previous figure.

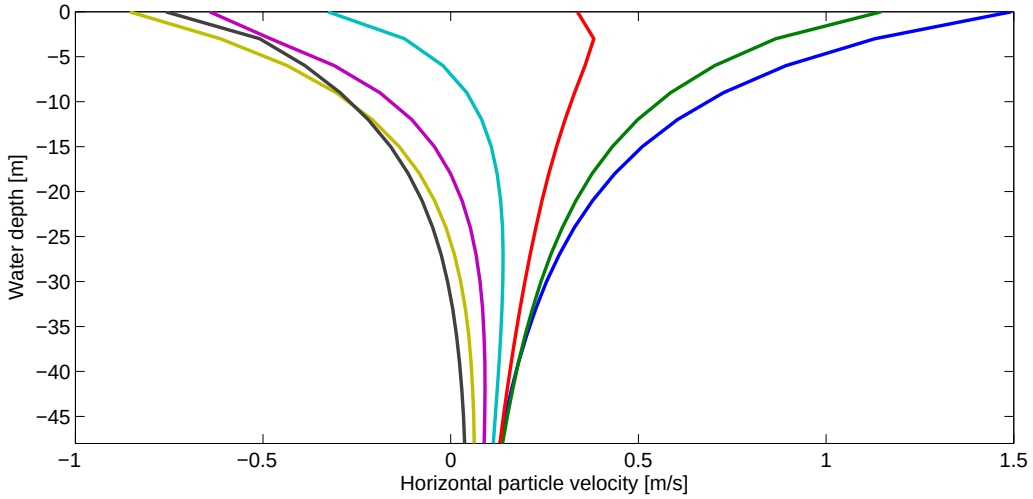


**Figure G-2:** Horizontal wave kinetics depth-profile

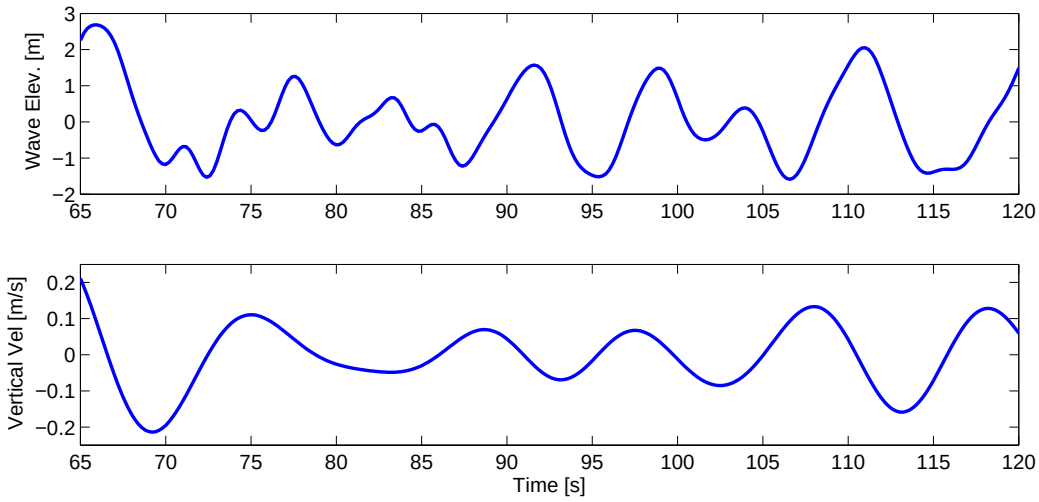


**Figure G-3:** Vertical wave kinetics at platform bottom in time

# Appendix H

# Ice crushing coefficients & model adjustments

An important part of the ice crushing load model applied is the determination of the coefficients used. Here two approaches to come to the ice failure force are applied. The first approach is based on Korzhavin's formula [36], additionally the approach as introduced in the ISO 19906 standard [37] is used.

## H-1 Korzhavin's formula

Along the past decades plentiful research is done containing definitions for coefficients used in Korzhavin's formula, for ice crushing strength determination. In this Appendix an overview is provided of the available benchmark studies and the resulting ranges in which the coefficients may vary.

Korzhavin's formula:

$$F_f = Im\kappa hD\sigma_f \tag{H-1}$$

Is used to determine the failure force of a given ice sheet in crushing failure against a structure. In order to come to this force determination the multiple influencing coefficients need to be determined.

### H-1-1 Indentation factor (I)

From tests, it was found that the indentation factor mainly depends on the aspect ratio (D/h) of the platform - ice-sheet combination. For the determination of the magnitude of the indentation factor various definitions could be identified:

- In a general materials book [43], an empirical formula provided by Afanasev was introduced.

$$I = \sqrt{5 + \frac{h}{D} + 1} \quad for \geq \frac{D}{h} \tag{H-2}$$

- In [44], a reference made is to a theoretical formulation of the indentation factor by Croteau (1983). Here a distinction is made for the indentation factor for ductile and brittle failure respectively.

$$I = 3.0 + \frac{0.8}{D/h} \leq 4.5 \tag{H-3}$$

$$I = 1.2 + \frac{0.32}{D/h} \leq 3.0 \tag{H-4}$$

- A more simple approach is found in [45]. Here a distinction is made between a wide structure and a narrow structure (with h/D=1). In case of a narrow structure the indentation factor is set to 2.5 whereas for a wide structure it is defined as 1.

In the case of this study, looking at ductile failure and a cylindrical structure of 18 m diameter, the indentation factor according to these definition ranges anywhere from 1 to approximately 3.

### H-1-2 Contact factor

The contact factor accounts for uneven contact and non-uniform crushing of the ice against the structure. This factor typically ranges from 0.3 (for non simultaneous failur) to 1.0 (for simultaneous failure) [46]. More specifically Michel and Toussaint distinguished between brittle failur and ductile and transitional failure [47]:

- $\kappa = 0.3 - 0.35$ in case of brittle failure
- $\kappa = 0.6$ in case of ductile and transitional failure

### H-1-3 Shape factor

The shape factor is widely acknowledged to be 0.9 for cylindrical objects and 1.0 for objects with a flat surface. Therefore in this study, a shape factor of 0.9 is used.

## H-2 ISO 19906

The ISO 19906:2010 standard prescribes a method for the determination of the global action as a result of crushing.

$$F_G = p_G h w \tag{H-5}$$

Where $p_G$ is the average pressure, h is the ice thickness and w is the projected width of the contact area of the ice on the surface of the structure, which is defined to be the structure's diameter (D) in this study.

The average (or global) ice pressure can be determined in the following approach.

$$p_G = C_R(\frac{h}{h_1})^n(\frac{w}{h})^m \tag{H-6}$$

where

$w$ is the projected width of the structure (in meters)

$h$ is the thickness of the ice sheet (in meters)

$h_1$ is the reference thickness, which is set to 1 m

$m$ is an emperical coefficient set to -0.16

$n$ is an emperical coefficient set to -0.5+h/5 for h<1.0 m and to -0.30 for h $\geq$ 1.0m

$C_R$ is the ice strength coefficient, expressed in MPa

The ISO code indicates that the applicability of this approach is limited to rigid structures for which it holds that w/h is greater than 2 and for which the waterplane area displacement is typically less than 10 mm. The latter is not the case in the study at hand, in absence of replacement theories, however, it is chosen to apply this approach. It should be kept in mind, however, that this might influence the validity of the outcomes.

Finally, the ISO code also includes a value for the ice strength, depending on its location. For temperate areas (which are of interest), this strength is defined to be 1.8 MPa.

## H-3 Comparison of approaches

In order to apply one failure force in the ice crushing model (as described in section 3-4-1), both the Korzhavin ans the ISO standard are compared here for the application in the study at hand.

First, the Korzhavin's coefficients contact factor and shape factor are specified, 0.6 and 0.9 respectively. Given the large variation in indentation factor a range of values is plotted (with I ranging from 1 to 3 in steps of 0.5).

The application of the ISO code is more straightforward and is applied in direct accordance with the approach presented in the previous section.

In figure H-1 the comparison of both approaches is provided for the structure at hand (with a diameter of 18 m) for ice thickness ranging from 0.1 to 1 m. It can be observed that the range of indentation factors in existing literature results in a very wide range of failure forces, especially for the somewhat thicker ice.

For the implementation of the Korzhavin formula in the ice crushing model, an indentation factor of 1.5 gives results most similar to the ISO code over a wide range of ice thickness.

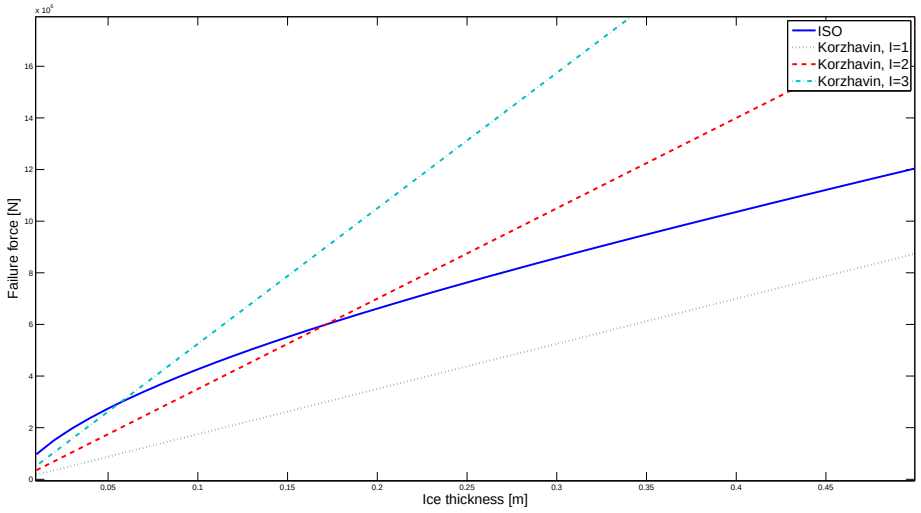


**Figure H-1:** Comparison of Ice Crushing failure forces ISO and Korzhavin

## H-4 New adjustment factor

For the ice crushing model to be applicable for a structure with displacements that exceed the distance between two teeth (p), the adjustment factor n is modified to accommodate larger structure displacements as well. The adjustment factor n is altered to include not only $v_{ice}t$, but $x(t)$ as well: $n =$ round down $(\frac{v_{ice}t - x(t)}{p})$ This adjustment overcomes the tooth deflection to become negative for larger structure deflections, as can be seen in figure H-2 below.

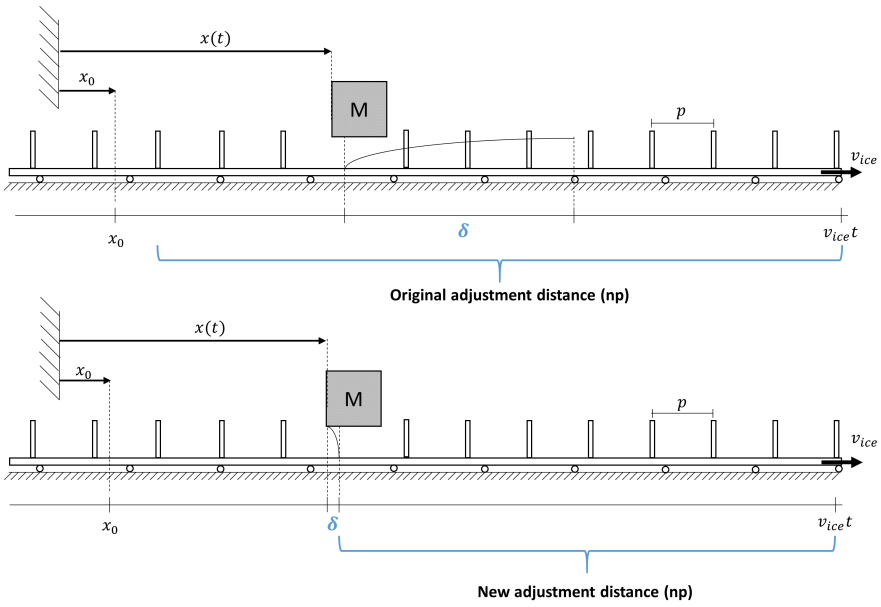


**Figure H-2:** Ice crushing: adjustment to the travelled distance correction factor

# Appendix I

# Stiffness non linearity

The stiffness definitions as introduced in chapter 4 consist of non-linear contributions in several directions. The main stiffness components in the overall system definition are surge and pitch stiffness the non-linearity of both contributions is highlighted in figures I-1 and I-2 below.

First, the surge restoring stiffness definition is increased for larger offsets in surge as a result of platform set-down, a phenomenon already discussed in section 4-1-3. The non-linear effect of the surge-surge stiffness contribution (K11) is presented in figure I-1 below.

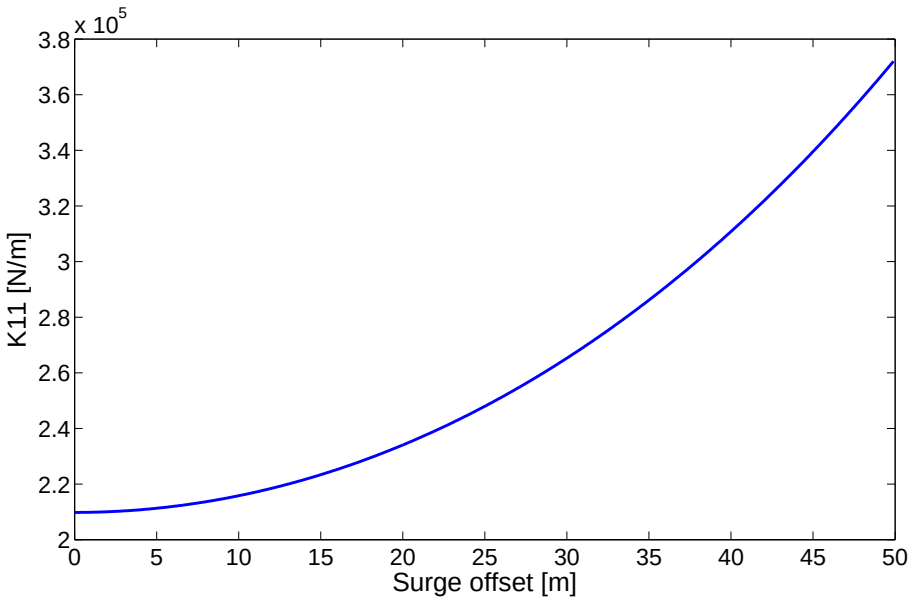


**Figure I-1:** Non-linearity of surge stiffness

It can be observed that for a surge offset of for example 10 meters the surge stiffness is increased with approximately 3 % compared to the platform's stiffness in neutral position. This effect of non-linearity will increase for increasing surge-offset and is only of influence for the most extreme offsets seen in this research.

For motions in pitch direction, the restoring stiffness has a negative non-linear relation to increasing pitch. The effect of this non-linearity, however, is very limited (approximately 0.2 % for 2.5 degrees pitch offset). These non-linearity effects are almost negligibly small compared to its initial value.

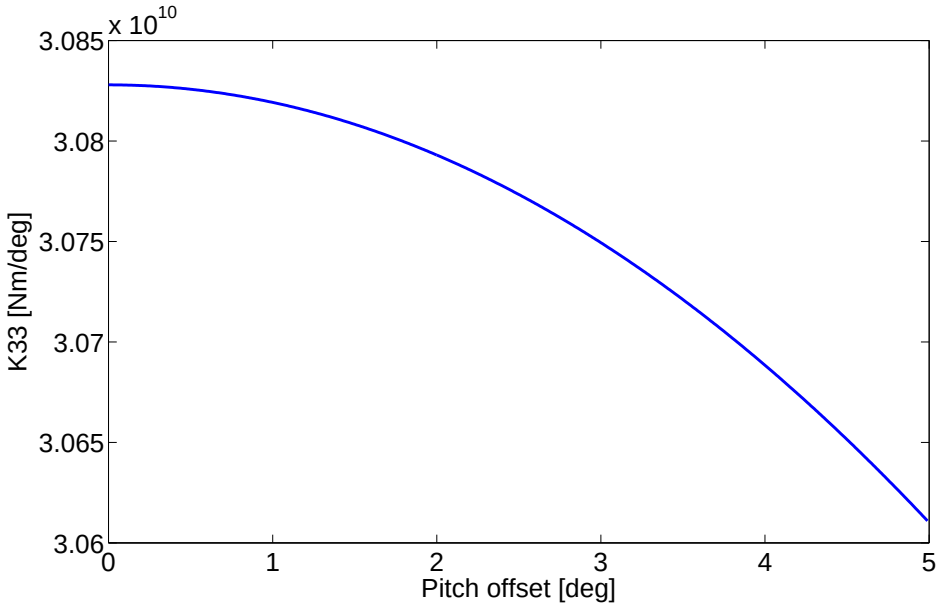


**Figure I-2:** Non-linearity of pitch stiffness

In heave non-linearity in heave direction is not directly present. The effects of set-down on heave direct stiffness, however, is taken into account, as discussed in section 4-1-3.

# Appendix J

# PSD plots coupled motions

As an addition to the results from the coupled motions from heave free decay test as presented in section 4-3-2, below the results of both the surge and pitch decay test are presented.

From the figure presented below, it can be observed that a coupling is present between all motions. The coupling between surge and pitch are very similar back and forth, which can be backed by the presence of equal off-diagonal stiffness and mass terms linking pitch and surge motion. Besides that, heave motions are coupled to both DOF as well.

Referring back to the figure presented in section 4-3, it could be noted that both pitch and surge are also coupled to an initial offset in heave direction as well. Surge motions resulting from heave offset not only include oscillations with surge and heave frequencies, but also consist of a considerable contribution from oscillations of pitch frequency, indicating the strong coupling between both pitch and surge. In figures J-1 through J-4 below, the resulting motions from initial surge and pitch offsets are presented to add to what is presented in section 4-3.

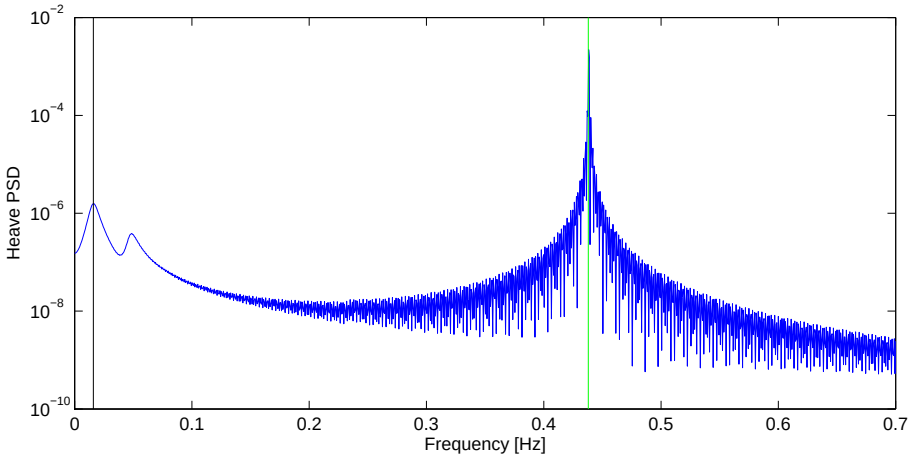


**Figure J-1:** PSD coupled motions heave, from initial surge offset

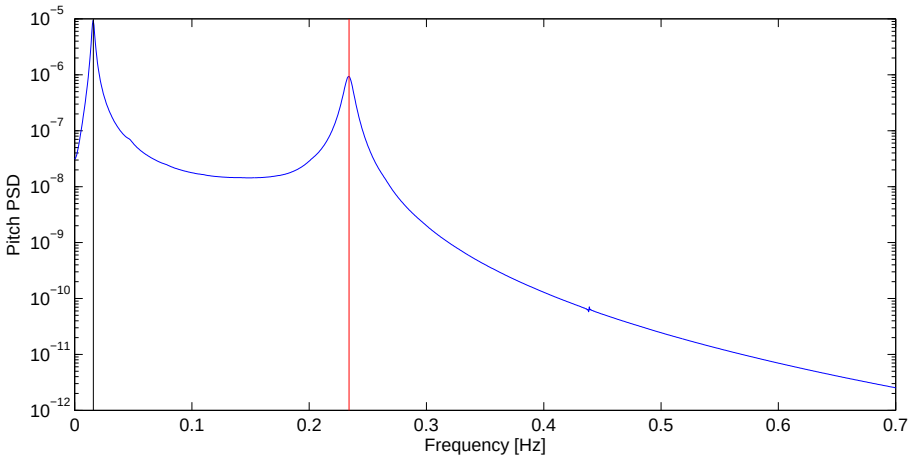


**Figure J-2:** PSD coupled motions pitch, from initial surge offset

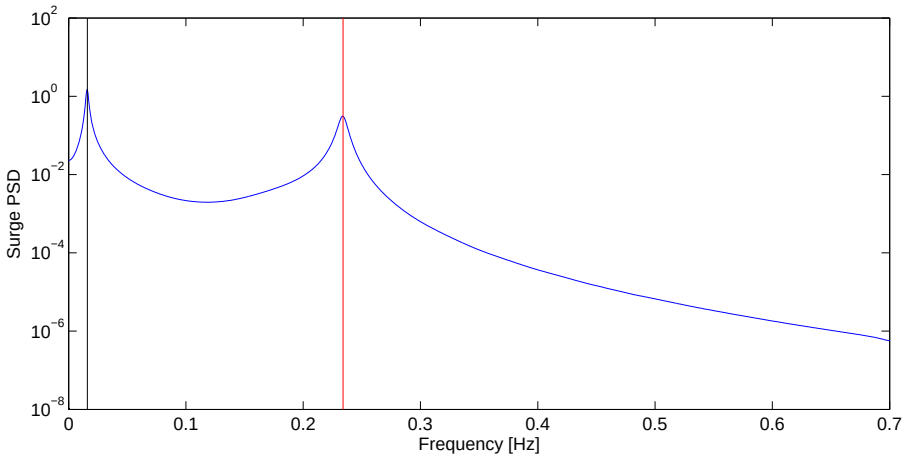


**Figure J-3:** PSD coupled motions surge, from initial pitch offset

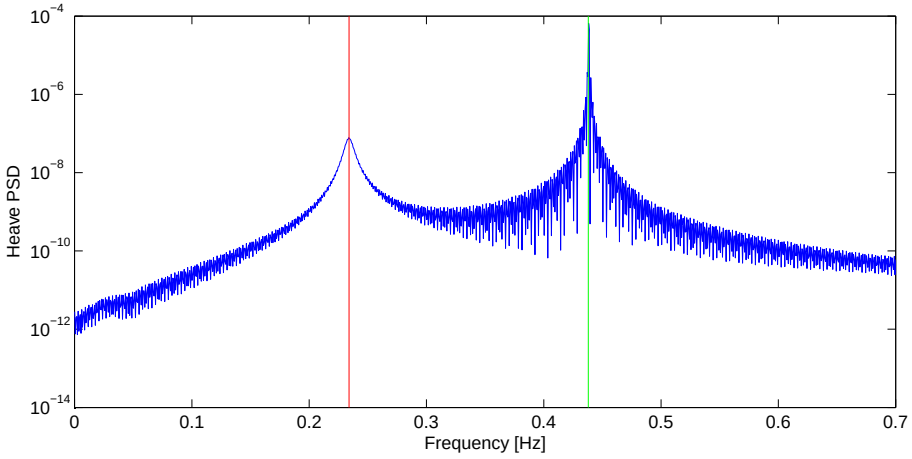


**Figure J-4:** PSD coupled motions heave, from initial pitch offset

# Appendix K

# Brittle ice crushing results

The outcomes of the ice crushing model presented in the results section of this report are based on a transitional crushing velocity of $0.5m/s$, which means that the results presented predominantly cover ductile ice crushing action. Although the ductile and transitional ice crushing regions form the main area of application of the applied model [6], in this Appendix the model is applied to generate results for brittle crushing as well. In order to force the ice into brittle failure, the transitional ice velocity is altered to $0.1m/s$ and simulations are performed for the same load cases as considered in chapter 5.

In figure K-1 below results of brittle crushing action for the $v_{ice} = 0.3m/s$, $h_{ice} = 0.2m$ load case is presented.

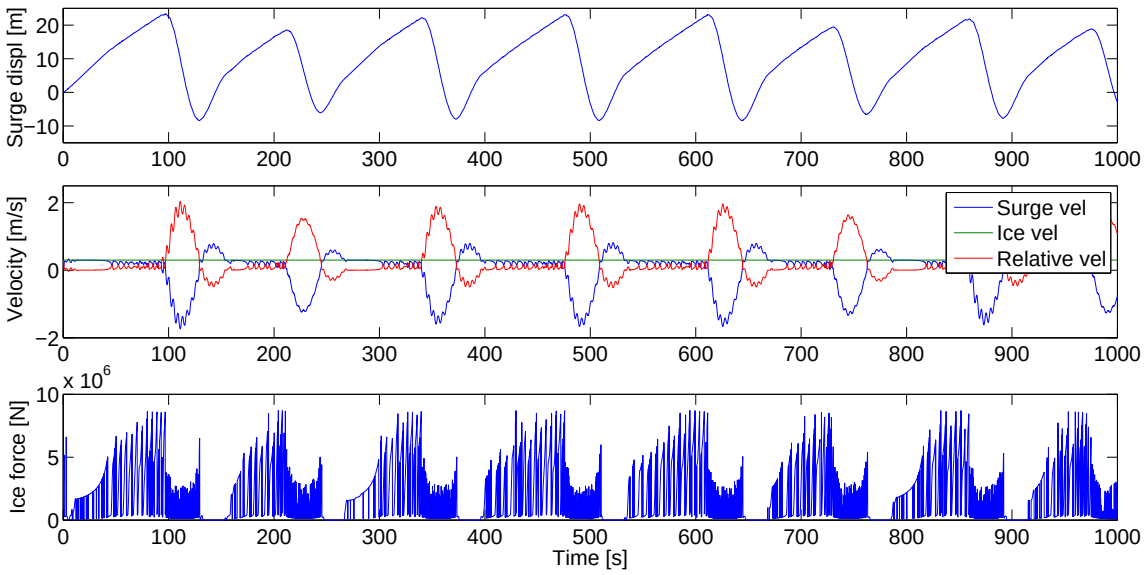


**Figure K-1:** Motions, velocities and ice load for brittle crushing action $v_{ice} = 0.3m/s$, $h_{ice} = 0.2m$

Comparing the outcomes in figure K-1 with the ductile crushing outcomes of figure 5-10 in chapter 5, significant differences are observed. The structure in ductile crushing action reaches a steady state offset around which it will oscillate as a result of ice loading. In the brittle

crushing outcomes no such stable position is reached, instead the structure will oscillate from positive to negative surge displacements and back.

This unstable behaviour is linked to the failure strength definition applied, where for crushing for ice velocities above transitional velocity failure strength decreases for increasing relative velocity. As a result, when the structure's velocity in positive surge direction decreases as a result of increasing restoring stiffness force, relative velocity shifts from ductile to brittle crushing resulting in a decrease in ice force. Following the decrease in ice force, the structure starts to move back in negative surge direction, further increasing relative velocity, resulting in decreasing ice load. As a result the structure will pass back through it's initial position until the mooring stiffness results in a restoring force in opposite direction again and the structure moves towards its initial position again and the cycle is repeated.

This cycle is intrinsically unstable and results in considerable platform oscillations.

In figure K-2 and K-3, the maximum tendon force resulting from the ductile crushing action presented in chapter 5 is compared to the simulation outcomes of brittle crushing action.

It can be observed that especially for the ice velocities near the transitional velocity of $0.1m/s$ the brittle crushing failure results in higher maximum tendon forces compared to the ductile failure. For the $0.3m/s$ and $0.4m/s$ ice velocities this difference is found to be smaller, and for the $0.4m/s$ load cases of large ice thickness, the ductile failure crushing even yields higher maximum tendon forces. These findings can be related to the fact that maximum crushing strength occurs at the ice's transitional velocity ($0.5m/s$ in ductile and $0.1m/s$ in the brittle case respectively).

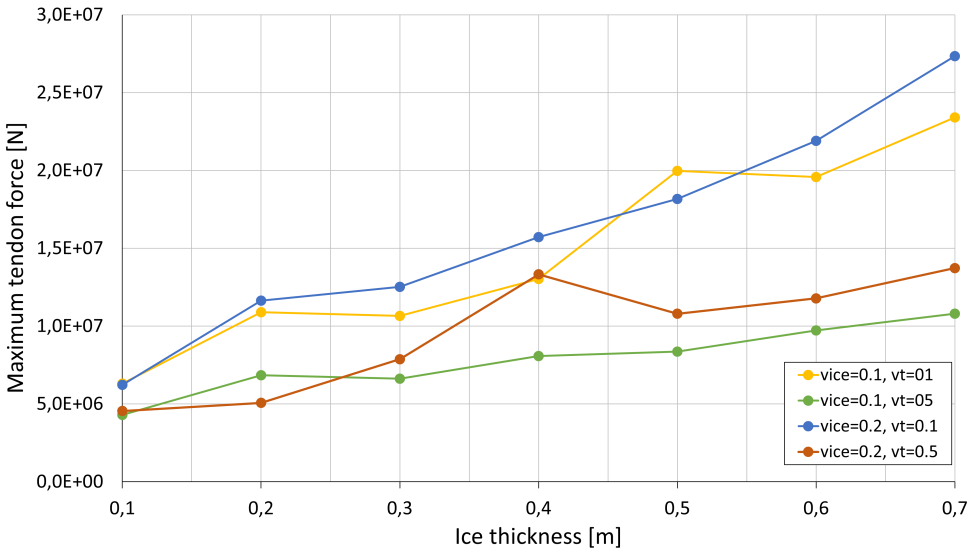


**Figure K-2:** Comparison of maximum tendon force brittle and ductile crushing $v_{ice} = 0.1m/s$ & $v_{ice} = 0.2m/s$

Besides the maximum tendon force in the figures presented above, the tendon force tendon deviation has been studied as well. In figures K-4 and K-5 below, the outcomes of the tendon

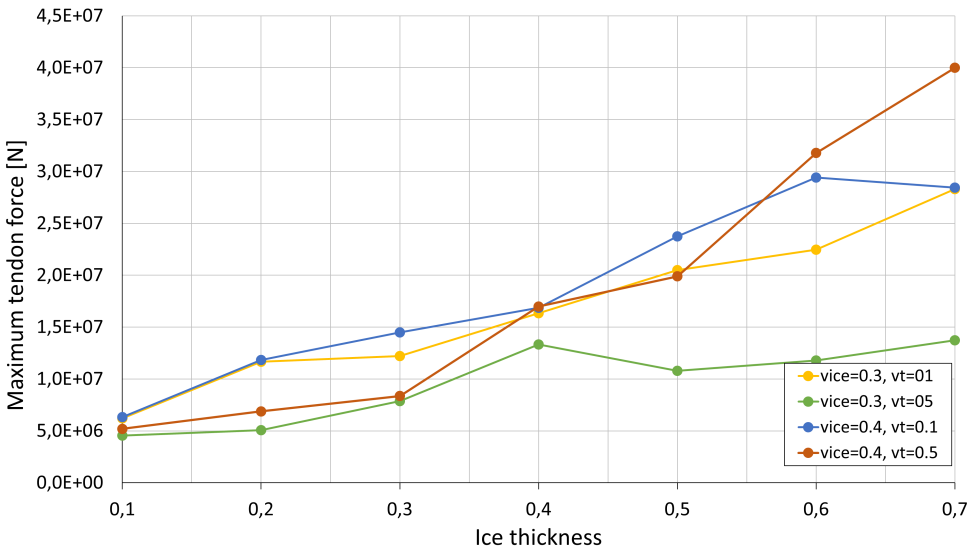


**Figure K-3:** Comparison of maximum tendon force brittle and ductile crushing $v_{ice} = 0.3m/s$ & $v_{ice} = 0.4m/s$

force analysis are presented. Here it can be observed that for loading in the brittle region of the ice crushing curve, tendon force standard deviation has a far more linear relation to ice thickness. This is a result of the unstable character of this type of loading, compared to ductile load cases. Whereas in the ductile load cases without dynamic amplifications a steady state surge offset was reached, in the brittle load cases this is not the case and force standard deviation is in direct relation to maximum tendon force.

Overall, it can be concluded that brittle crushing load cases do not yield the typical 'stable' steady state solution that results from ductile load cases. Furthermore, as to be expected from the crushing strength definitions, ice velocities near the transitional velocity characteristic of the ice yield the higher tendon forces (and motions offsets).

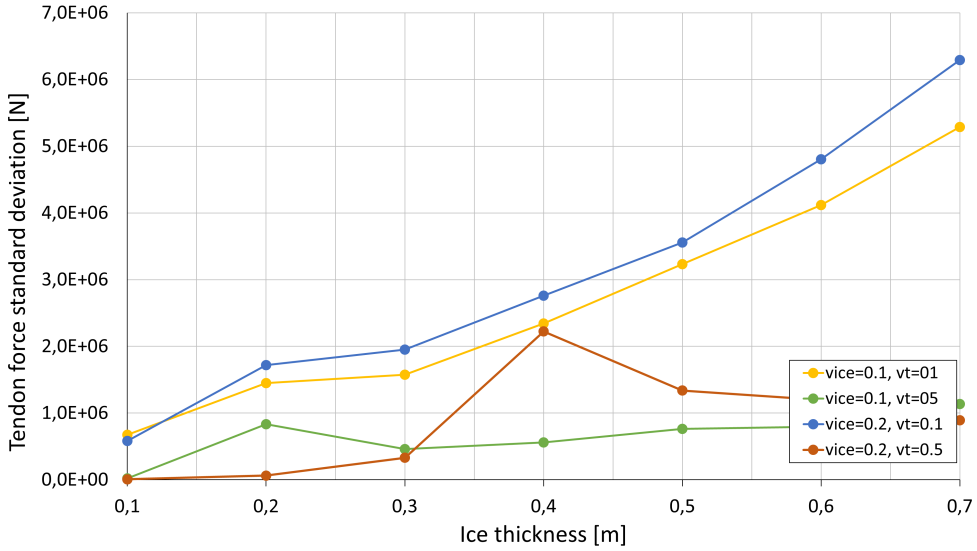


**Figure K-4:** Comparison of tendon force standard deviation brittle and ductile crushing $v_{ice} = 0.1m/s$ & $v_{ice} = 0.2m/s$

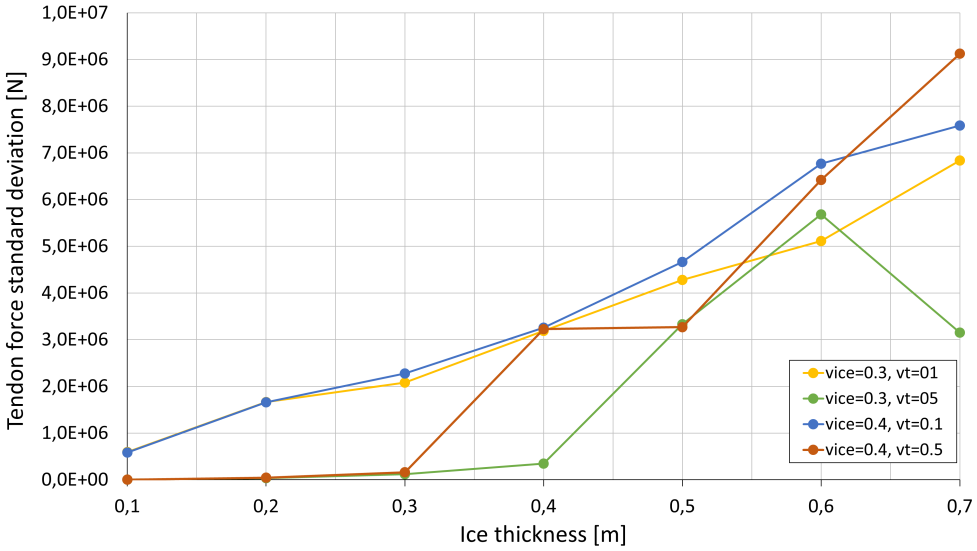


**Figure K-5:** Comparison of tendon force standard deviation brittle and ductile crushing $v_{ice} = 0.3m/s$ & $v_{ice} = 0.4m/s$

# Appendix L

# Load cases

In this Appendix, an overview of the considered load cases is provided, in the form of three tables covering the distinct open water, ice bending and ice crushing load cases. This numbering of load cases can be used to better understand the simulation outcomes presented in Appendix M.

## L-1 Open water load cases

For the open water load cases the variation along the load cases is both in hub height wind velocity and in sea state (combination of $H_s$ and $T_p$). The load case numbering definition can be found in table L-1 below.

**Table L-1:** Open water load case definitions

| | **Hs/Tp** | | | | | | |
|---|---|---|---|---|---|---|---|
| **Uwind** | 2/7 | 4/10 | 6/12.5 | 8/14 | 10/15.75 | 12/17.25 | 14/18.75 |
| 8 | OLC 1.1 | OLC 1.2 | OLC 1.3 | OLC 1.4 | OLC 1.5 | OLC 1.6 | OLC 1.7 |
| 11 | OLC 2.1 | OLC 2.2 | OLC 2.3 | OLC 2.4 | OLC 2.5 | OLC 2.6 | OLC 2.7 |
| 20 | OLC 3.1 | OLC 3.2 | OLC 3.3 | OLC 3.4 | OLC 3.5 | OLC 3.6 | OLC 3.7 |

The addition of current to the load case, as discussed in chapter 3 in the results will be indicated by the addition of a WC (with current) to the load-case abbreviation (OWLCWC, instead of OWLC). Note that the effects of current have only been studied for the $11m/s$ wind velocity cases.

## L-2 Ice crushing load cases

The ice main distinction between the ice crushing load cases is the combination of travelling ice velocity ($v_{ice}$) and ice thickness ($h_{ice}$). As discussed, the considered ranges are 0.1 to 0.4 and 0.1 to 0.7 respectively. The load case numbering definition can be found in table L-2 below.

**Table L-2:** Ice crushing load case definitions

| | **H ice** | | | | | | |
|---|---|---|---|---|---|---|---|
| **V ice** | 0.1 | 0.2 | 0.3 | 0.4 | 0.5 | 0.6 | 0.7 |
| 0.1 | ICLC 1.1 | ICLC 1.2 | ICLC 1.3 | ICLC 1.4 | ICLC 1.5 | ICLC 1.6 | ICLC 1.7 |
| 0.2 | ICLC 2.1 | ICLC 2.2 | ICLC 2.3 | ICLC 2.4 | ICLC 2.5 | ICLC 2.6 | ICLC 2.7 |
| 0.3 | ICLC 3.1 | ICLC 3.2 | ICLC 3.3 | ICLC 3.4 | ICLC 3.5 | ICLC 3.6 | ICLC 3.7 |
| 0.4 | ICLC 4.1 | ICLC 4.2 | ICLC 4.3 | ICLC 4.4 | ICLC 4.5 | ICLC 4.6 | ICLC 4.7 |

Besides this general numbering of ice crushing load cases, the addition of wind load and current loads is indicated in the numbering of cases in the presented outcomes as well. The abbreviation for ice crushing load cases is defined by ICWLC, which is provided for all ice thickness and velocity combinations, for a $11m/s$ wind velocity. Indicating the presence of current loads besides wind and ice loading, an additional C is added to the abbreviation (ICWCLC), which is done only for the $0.2m/s$ ice velocity and includes a $0.5m/s$ current.

## L-3 Ice bending load cases

The ice bending load cases are defined by ice thickness and velocity combination as well. Here, however the considered ranges are different from the crushing load cases (given the difference in failure mechanism points of interest differ). The ranges of thickness and velocity are 0.25 to 1.5 and 0.1 to 0.3 respectively.The load case numbering definition can be found in table L-3 below.

**Table L-3:** Ice bending load case definitions

| | **H ice** | | | | | |
|---|---|---|---|---|---|---|
| **V ice** | 0.25 | 0.5 | 0.75 | 1 | 1.25 | 1.5 |
| 0.1 | IBLC 1.1 | IBLC 1.2 | IBLC 1.3 | IBLC 1.4 | IBLC 1.5 | IBLC 1.6 |
| 0.2 | IBLC 2.1 | IBLC 2.2 | IBLC 2.3 | IBLC 2.4 | IBLC 2.5 | IBLC 2.6 |
| 0.3 | IBLC 3.1 | IBLC 3.2 | IBLC 3.3 | IBLC 3.4 | IBLC 3.5 | IBLC 3.6 |

For the ice bending load case an additional distinction is made between the breaking force contributions only and the overall ice bending load including residual loads to cover additional loading separate from breaking of the ice sheet. The overall loads are indicated by the abbreviation IBLCT.

Like for the crushing load cases, the addition of current and wind loads is indicated by alternative abbreviations. IBLCW and and IBLCWC respectively for wind and current.

# Appendix M

# Outcomes load cases

## M-1 Open water load cases

**Table M-1:** Open water load case simulation outcomes for $u_{mean} = 8m/s$

| | Motions | | | | Tendon Forces | | | | Wind & Waves | | | |
|---|---|---|---|---|---|---|---|---|---|---|---|---|
| | | Mean | Min | Max | | Min | Max | Std | | Min | Max | Std |
| **OWLC11** | Surge | 2.44 | 0.46 | 5.79 | Tww | 3.2E+06 | 6.0E+06 | 3.6E+05 | Wave Elev | -1.74 | 1.64 | 0.50 |
| | Heave | 0.00 | 0.00 | 0.00 | Tlw | 2.0E+06 | 4.8E+06 | 3.4E+05 | Wind Vel | 4.72 | 11.85 | 0.95 |
| | Pitch | 0.13 | -0.18 | 0.43 | | | | | | | | |
| | Motions | | | | Tendon Forces | | | | Wind & Waves | | | |
| | | Mean | Min | Max | | Min | Max | Std | | Min | Max | Std |
| **OWLC12** | Surge | 2.60 | -0.19 | 5.81 | Tww | 3.1E+06 | 6.7E+06 | 4.9E+05 | Eta | -3.61 | 3.19 | 1.00 |
| | Heave | 0.00 | -0.01 | 0.01 | Tlw | 1.4E+06 | 4.9E+06 | 4.8E+05 | Wind Vel | 5.00 | 11.64 | 0.95 |
| | Pitch | 0.14 | -0.20 | 0.57 | | | | | | | | |
| | Motions | | | | Tendon Forces | | | | Wind & Waves | | | |
| | | Mean | Min | Max | | Min | Max | Std | | Min | Max | Std |
| **OWLC13** | Surge | 2.48 | -2.44 | 10.61 | Tww | 2.0E+06 | 6.8E+06 | 5.3E+05 | Eta | -6.56 | 9.10 | 1.50 |
| | Heave | 0.00 | -0.05 | 0.05 | Tlw | 1.4E+06 | 6.1E+06 | 5.1E+05 | Wind Vel | 4.03 | 11.04 | 0.95 |
| | Pitch | 0.13 | -0.44 | 0.59 | | | | | | | | |
| | Motions | | | | Tendon Forces | | | | Wind & Waves | | | |
| | | Mean | Min | Max | | Min | Max | Std | | Min | Max | Std |
| **OWLC14** | Surge | 2.66 | -2.61 | 10.69 | Tww | 2.4E+06 | 7.0E+06 | 5.9E+05 | Eta | -7.57 | 7.68 | 2.00 |
| | Heave | 0.00 | -0.06 | 0.05 | Tlw | 1.4E+06 | 5.6E+06 | 5.6E+05 | Wind Vel | 4.51 | 11.12 | 0.95 |
| | Pitch | 0.13 | -0.35 | 0.57 | | | | | | | | |
| | Motions | | | | Tendon Forces | | | | Wind & Waves | | | |
| | | Mean | Min | Max | | Min | Max | Std | | Min | Max | Std |
| **OWLC15** | Surge | 2.66 | -3.75 | 11.13 | Tww | 1.9E+06 | 6.7E+06 | 6.1E+05 | Eta | -7.73 | 8.44 | 2.51 |
| | Heave | 0.00 | -0.08 | 0.08 | Tlw | 1.5E+06 | 6.1E+06 | 5.8E+05 | Wind Vel | 4.13 | 11.43 | 0.95 |
| | Pitch | 0.13 | -0.45 | 0.54 | | | | | | | | |
| | Motions | | | | Tendon Forces | | | | Wind & Waves | | | |
| | | Mean | Min | Max | | Min | Max | Std | | Min | Max | Std |
| **OWLC16** | Surge | 2.83 | -5.85 | 14.05 | Tww | 2.6E+06 | 7.2E+06 | 6.4E+05 | Eta | -11.78 | 10.68 | 3.01 |
| | Heave | 0.00 | -0.16 | 0.13 | Tlw | 1.2E+06 | 5.5E+06 | 6.0E+05 | Wind Vel | 4.13 | 12.03 | 0.95 |
| | Pitch | 0.14 | -0.30 | 0.60 | | | | | | | | |
| | Motions | | | | Tendon Forces | | | | Wind & Waves | | | |
| | | Mean | Min | Max | | Min | Max | Std | | Min | Max | Std |
| **OWLC17** | Surge | 2.83 | -6.44 | 17.07 | Tww | 1.9E+06 | 7.6E+06 | 6.5E+05 | Eta | -14.73 | 11.37 | 3.51 |
| | Heave | 0.00 | -0.15 | 0.14 | Tlw | 6.4E+05 | 6.2E+06 | 6.1E+05 | Wind Vel | 4.72 | 11.85 | 0.95 |
| | Pitch | 0.14 | -0.46 | 0.69 | | | | | | | | |

**Table M-2:** Open water load case simulation outcomes for $u_{mean} = 11m/s$

| | | Motions | | | | Tendon Forces | | | | Wind & Waves | | | |
|---|---|---|---|---|---|---|---|---|---|---|---|---|---|
| | | Mean | Min | Max | | Min | Max | Std | | Min | Max | Std |
| **OWLC21** | Surge | 4.11 | 0.23 | 7.37 | Tww | 3.3E+06 | 6.8E+06 | 4.3E+05 | Wave Elev | -1.84 | 1.87 | 0.50 |
| | Heave | 0.00 | 0.00 | 0.00 | Tlw | 1.5E+06 | 4.7E+06 | 4.0E+05 | Wind Vel | 4.21 | 15.97 | 1.31 |
| | Pitch | 0.22 | -0.14 | 0.56 | | | | | | | | |
| | | Motions | | | | Tendon Forces | | | | Wind & Waves | | | |
| | | Mean | Min | Max | | Min | Max | Std | | Min | Max | Std |
| **OWLC22** | Surge | 4.17 | -0.35 | 8.15 | Tww | 2.6E+06 | 6.9E+06 | 5.5E+05 | Eta | -3.86 | 3.90 | 1.00 |
| | Heave | 0.00 | -0.01 | 0.01 | Tlw | 1.3E+06 | 5.4E+06 | 5.1E+05 | Wind Vel | 5.75 | 16.73 | 1.31 |
| | Pitch | 0.22 | -0.31 | 0.60 | | | | | | | | |
| | | Motions | | | | Tendon Forces | | | | Wind & Waves | | | |
| | | Mean | Min | Max | | Min | Max | Std | | Min | Max | Std |
| **OWLC23** | Surge | 4.30 | -0.14 | 9.64 | Tww | 2.9E+06 | 7.2E+06 | 5.9E+05 | Eta | -5.70 | 5.89 | 1.50 |
| | Heave | 0.00 | -0.03 | 0.04 | Tlw | 1.1E+06 | 5.1E+06 | 5.5E+05 | Wind Vel | 6.13 | 15.38 | 1.31 |
| | Pitch | 0.23 | -0.24 | 0.65 | | | | | | | | |
| | | Motions | | | | Tendon Forces | | | | Wind & Waves | | | |
| | | Mean | Min | Max | | Min | Max | Std | | Min | Max | Std |
| **OWLC24** | Surge | 4.44 | -1.63 | 10.64 | Tww | 2.9E+06 | 7.3E+06 | 6.5E+05 | Eta | -7.03 | 7.45 | 2.00 |
| | Heave | 0.00 | -0.05 | 0.05 | Tlw | 1.1E+06 | 5.3E+06 | 6.0E+05 | Wind Vel | 6.27 | 16.31 | 1.31 |
| | Pitch | 0.23 | -0.25 | 0.65 | | | | | | | | |
| | | Motions | | | | Tendon Forces | | | | Wind & Waves | | | |
| | | Mean | Min | Max | | Min | Max | Std | | Min | Max | Std |
| **OWLC25** | Surge | 4.24 | -2.18 | 15.65 | Tww | 2.7E+06 | 7.4E+06 | 6.8E+05 | Eta | -8.40 | 8.51 | 2.51 |
| | Heave | 0.00 | -0.09 | 0.10 | Tlw | 7.3E+05 | 5.2E+06 | 6.3E+05 | Wind Vel | 5.52 | 14.85 | 1.31 |
| | Pitch | 0.22 | -0.27 | 0.70 | | | | | | | | |
| | | Motions | | | | Tendon Forces | | | | Wind & Waves | | | |
| | | Mean | Min | Max | | Min | Max | Std | | Min | Max | Std |
| **OWLC26** | Surge | 4.35 | -3.88 | 15.63 | Tww | 2.7E+06 | 7.8E+06 | 7.0E+05 | Eta | -9.61 | 9.43 | 3.01 |
| | Heave | 0.00 | -0.12 | 0.13 | Tlw | 8.5E+05 | 5.3E+06 | 6.4E+05 | Wind Vel | 6.46 | 15.72 | 1.31 |
| | Pitch | 0.22 | -0.29 | 0.74 | | | | | | | | |
| | | Motions | | | | Tendon Forces | | | | Wind & Waves | | | |
| | | Mean | Min | Max | | Min | Max | Std | | Min | Max | Std |
| **OWLC27** | Surge | 4.57 | -7.01 | 23.54 | Tww | 2.6E+06 | 9.4E+06 | 7.4E+05 | Eta | -14.25 | 14.99 | 3.52 |
| | Heave | 0.00 | -0.19 | 0.20 | Tlw | 9.7E+05 | 5.5E+06 | 6.6E+05 | Wind Vel | 6.52 | 15.74 | 1.31 |
| | Pitch | 0.23 | -0.31 | 0.67 | | | | | | | | |

**Table M-3:** Open water load case simulation outcomes for $u_{mean} = 20m/s$

| | Motions | | | | Tendon Forces | | | | Wind & Waves | | | |
|---|---|---|---|---|---|---|---|---|---|---|---|---|
| | | Mean | Min | Max | | Min | Max | Std | | Min | Max | Std |
| **OWLC31** | Surge | 2.35 | 0.17 | 4.91 | Tww | 3.1E+06 | 6.3E+06 | 4.0E+05 | Wave Elev | -1.87 | 2.08 | 0.50 |
| | Heave | 0.00 | 0.00 | 0.00 | Tlw | 1.8E+06 | 4.9E+06 | 3.9E+05 | Wind Vel | 10.18 | 28.03 | 2.37 |
| | Pitch | 0.12 | -0.19 | 0.48 | | | | | | | | |
| | Motions | | | | Tendon Forces | | | | Wind & Waves | | | |
| | | Mean | Min | Max | | Min | Max | Std | | Min | Max | Std |
| **OWLC32** | Surge | 2.49 | -0.09 | 6.27 | Tww | 2.6E+06 | 6.4E+06 | 5.2E+05 | Eta | -4.11 | 3.88 | 1.00 |
| | Heave | 0.00 | -0.01 | 0.01 | Tlw | 1.7E+06 | 5.4E+06 | 5.1E+05 | Wind Vel | 11.39 | 27.88 | 2.37 |
| | Pitch | 0.13 | -0.30 | 0.50 | | | | | | | | |
| | Motions | | | | Tendon Forces | | | | Wind & Waves | | | |
| | | Mean | Min | Max | | Min | Max | Std | | Min | Max | Std |
| **OWLC33** | Surge | 2.51 | -1.75 | 7.25 | Tww | 2.4E+06 | 6.6E+06 | 5.5E+05 | Eta | -5.10 | 5.94 | 1.50 |
| | Heave | 0.00 | -0.03 | 0.03 | Tlw | 1.4E+06 | 5.6E+06 | 5.3E+05 | Wind Vel | 10.01 | 29.22 | 2.37 |
| | Pitch | 0.13 | -0.35 | 0.56 | | | | | | | | |
| | Motions | | | | Tendon Forces | | | | Wind & Waves | | | |
| | | Mean | Min | Max | | Min | Max | Std | | Min | Max | Std |
| **OWLC34** | Surge | 2.63 | -2.14 | 9.59 | Tww | 2.5E+06 | 6.9E+06 | 5.9E+05 | Eta | -7.19 | 6.79 | 2.01 |
| | Heave | 0.00 | -0.06 | 0.06 | Tlw | 1.4E+06 | 5.5E+06 | 5.7E+05 | Wind Vel | 10.58 | 31.21 | 2.37 |
| | Pitch | 0.13 | -0.32 | 0.56 | | | | | | | | |
| | Motions | | | | Tendon Forces | | | | Wind & Waves | | | |
| | | Mean | Min | Max | | Min | Max | Std | | Min | Max | Std |
| **OWLC35** | Surge | 2.72 | -4.49 | 11.54 | Tww | 2.5E+06 | 6.7E+06 | 6.2E+05 | Eta | -7.81 | 7.88 | 2.51 |
| | Heave | 0.00 | -0.09 | 0.10 | Tlw | 1.3E+06 | 5.5E+06 | 5.9E+05 | Wind Vel | 12.11 | 29.16 | 2.37 |
| | Pitch | 0.13 | -0.32 | 0.57 | | | | | | | | |
| | Motions | | | | Tendon Forces | | | | Wind & Waves | | | |
| | | Mean | Min | Max | | Min | Max | Std | | Min | Max | Std |
| **OWLC36** | Surge | 2.77 | -6.78 | 16.97 | Tww | 2.6E+06 | 7.5E+06 | 6.4E+05 | Eta | -11.77 | 11.33 | 3.01 |
| | Heave | 0.00 | -0.14 | 0.14 | Tlw | 1.6E+06 | 5.6E+06 | 5.9E+05 | Wind Vel | 11.95 | 28.64 | 2.37 |
| | Pitch | 0.13 | -0.32 | 0.54 | | | | | | | | |
| | Motions | | | | Tendon Forces | | | | Wind & Waves | | | |
| | | Mean | Min | Max | | Min | Max | Std | | Min | Max | Std |
| **OWLC37** | Surge | 2.72 | -9.22 | 17.54 | Tww | 2.2E+06 | 7.4E+06 | 6.7E+05 | Eta | -12.43 | 13.36 | 3.51 |
| | Heave | 0.00 | -0.16 | 0.17 | Tlw | 1.2E+06 | 5.9E+06 | 6.2E+05 | Wind Vel | 9.80 | 27.68 | 2.37 |
| | Pitch | 0.13 | -0.40 | 0.60 | | | | | | | | |

**Table M-4:** Open water load case with current simulation outcomes for $u_{mean} = 11m/s$, $u_{current} = 0.5m/s$

**OWLCWC1**

| | Motions | | | | Tendon Forces | | | | Wind & Waves | | | |
|---|---|---|---|---|---|---|---|---|---|---|---|---|
| | Mean | Min | Max | | Min | Max | Std | | Min | Max | Std |
| Surge | 4,67 | 2,25 | 9,00 | Tww | 3,6E+06 | 7,0E+06 | 4,2E+05 | Wave Elev | -1,69 | 1,61 | 0,50 |
| Heave | 0,00 | 0,00 | 0,00 | Tlw | 1,3E+06 | 4,5E+06 | 3,9E+05 | Wind Vel | 6,48 | 16,26 | 1,31 |
| Pitch | 0,22 | -0,10 | 0,62 | | | | | | | | |

**OWLCWC2**

| | Motions | | | | Tendon Forces | | | | Wind & Waves | | | |
|---|---|---|---|---|---|---|---|---|---|---|---|---|
| | Mean | Min | Max | | Min | Max | Std | | Min | Max | Std |
| Surge | 5,04 | 1,48 | 9,01 | Tww | 3,4E+06 | 7,2E+06 | 5,4E+05 | Eta | -3,54 | 3,81 | 1,00 |
| Heave | 0,00 | -0,01 | 0,01 | Tlw | 1,1E+06 | 4,8E+06 | 5,0E+05 | Wind Vel | 6,65 | 16,61 | 1,31 |
| Pitch | 0,24 | -0,16 | 0,64 | | | | | | | | |

**OWLCWC3**

| | Motions | | | | Tendon Forces | | | | Wind & Waves | | | |
|---|---|---|---|---|---|---|---|---|---|---|---|---|
| | Mean | Min | Max | | Min | Max | Std | | Min | Max | Std |
| Surge | 4,83 | 0,72 | 9,56 | Tww | 2,9E+06 | 7,2E+06 | 5,8E+05 | Eta | -5,56 | 4,80 | 1,50 |
| Heave | 0,00 | -0,04 | 0,04 | Tlw | 1,1E+06 | 5,3E+06 | 5,3E+05 | Wind Vel | 5,87 | 16,81 | 1,31 |
| Pitch | 0,22 | -0,26 | 0,65 | | | | | | | | |

**OWLCWC4**

| | Motions | | | | Tendon Forces | | | | Wind & Waves | | | |
|---|---|---|---|---|---|---|---|---|---|---|---|---|
| | Mean | Min | Max | | Min | Max | Std | | Min | Max | Std |
| Surge | 5,18 | -0,04 | 11,71 | Tww | 3,1E+06 | 7,8E+06 | 6,5E+05 | Eta | -6,67 | 6,05 | 2,00 |
| Heave | 0,00 | -0,06 | 0,06 | Tlw | 5,3E+05 | 5,1E+06 | 5,9E+05 | Wind Vel | 6,78 | 16,00 | 1,31 |
| Pitch | 0,24 | -0,20 | 0,79 | | | | | | | | |

**OWLCWC5**

| | Motions | | | | Tendon Forces | | | | Wind & Waves | | | |
|---|---|---|---|---|---|---|---|---|---|---|---|---|
| | Mean | Min | Max | | Min | Max | Std | | Min | Max | Std |
| Surge | 5,03 | -1,93 | 19,98 | Tww | 1,9E+06 | 8,7E+06 | 6,6E+05 | Eta | -10,89 | 11,93 | 2,51 |
| Heave | 0,00 | -0,11 | 0,11 | Tlw | 4,5E+05 | 6,4E+06 | 6,0E+05 | Wind Vel | 5,54 | 15,28 | 1,31 |
| Pitch | 0,22 | -0,48 | 0,80 | | | | | | | | |

**OWLCWC6**

| | Motions | | | | Tendon Forces | | | | Wind & Waves | | | |
|---|---|---|---|---|---|---|---|---|---|---|---|---|
| | Mean | Min | Max | | Min | Max | Std | | Min | Max | Std |
| Surge | 5,31 | -2,13 | 16,35 | Tww | 2,4E+06 | 8,2E+06 | 7,1E+05 | Eta | -11,61 | 9,94 | 3,01 |
| Heave | 0,00 | -0,12 | 0,11 | Tlw | 7,5E+05 | 5,7E+06 | 6,3E+05 | Wind Vel | 6,25 | 15,30 | 1,31 |
| Pitch | 0,23 | -0,35 | 0,73 | | | | | | | | |

**OWLCWC7**

| | Motions | | | | Tendon Forces | | | | Wind & Waves | | | |
|---|---|---|---|---|---|---|---|---|---|---|---|---|
| | Mean | Min | Max | | Min | Max | Std | | Min | Max | Std |
| Surge | 5,36 | -3,12 | 20,45 | Tww | 2,2E+06 | 8,3E+06 | 7,4E+05 | Eta | -11,25 | 10,82 | 3,52 |
| Heave | 0,00 | -0,16 | 0,16 | Tlw | 4,4E+05 | 5,9E+06 | 6,4E+05 | Wind Vel | 5,63 | 15,87 | 1,31 |
| Pitch | 0,23 | -0,41 | 0,78 | | | | | | | | |

# M-2 Ice crushing load cases

**Table M-5:** Ice crushing load case simulation outcomes for $v_{ice} = 0.1m/s$

| | | Displacements | | | | Velocities | | | Tendon Forces | | |
|---|---|---|---|---|---|---|---|---|---|---|---|
| | | Mean | Min | Max | | Min | Max | | Min | Max | Std |
| **ICLC11** | Surge | 2.59 | 2.56 | 2.60 | Surge | -0.02 | 0.00 | Tww | 4.2E+06 | 4.3E+06 | 2.2E+04 |
| | Heave | -2.6E-09 | -1.0E-04 | 1.0E-04 | Heave | -2.8E-04 | 2.8E-04 | Tlw | 3.7E+06 | 3.8E+06 | 2.2E+04 |
| | Pitch | 0.05 | 0.04 | 0.06 | Pitch | -0.03 | 0.03 | | | | |
| | | Displacements | | | | Velocities | | | Tendon Forces | | |
| | | Mean | Min | Max | | Min | Max | | Min | Max | Std |
| **ICLC12** | Surge | 5.54 | 3.60 | 7.83 | Surge | -0.25 | 0.00 | Tww | 3.0E+06 | 6.8E+06 | 8.4E+05 |
| | Heave | 5.1E-08 | -9.0E-04 | 9.3E-04 | Heave | -2.5E-03 | 2.5E-03 | Tlw | 1.8E+06 | 5.6E+06 | 8.1E+05 |
| | Pitch | 0.10 | -0.28 | 0.55 | Pitch | -0.61 | 0.55 | | | | |
| | | Displacements | | | | Velocities | | | Tendon Forces | | |
| | | Mean | Min | Max | | Min | Max | | Min | Max | Std |
| **ICLC13** | Surge | 6.19 | 5.73 | 10.68 | Surge | -0.27 | 0.00 | Tww | 3.6E+06 | 6.6E+06 | 4.6E+05 |
| | Heave | 3.9E-09 | -4.0E-04 | 3.9E-04 | Heave | -1.1E-03 | 1.1E-03 | Tlw | 2.3E+06 | 5.0E+06 | 4.5E+05 |
| | Pitch | 0.12 | -0.15 | 0.45 | Pitch | -0.44 | 0.38 | | | | |
| | | Displacements | | | | Velocities | | | Tendon Forces | | |
| | | Mean | Min | Max | | Min | Max | | Min | Max | Std |
| **ICLC14** | Surge | 8.25 | 7.55 | 14.19 | Surge | -0.33 | 0.00 | Tww | 3.7E+06 | 8.1E+06 | 5.6E+05 |
| | Heave | 2.2E-09 | -1.9E-04 | 2.0E-04 | Heave | -5.2E-04 | 5.2E-04 | Tlw | 1.7E+06 | 5.8E+06 | 5.2E+05 |
| | Pitch | 0.15 | -0.19 | 0.68 | Pitch | -0.55 | 0.57 | | | | |
| | | Displacements | | | | Velocities | | | Tendon Forces | | |
| | | Mean | Min | Max | | Min | Max | | Min | Max | Std |
| **ICLC15** | Surge | 10.57 | 9.33 | 17.74 | Surge | -0.29 | 0.00 | Tww | 3.8E+06 | 8.4E+06 | 7.6E+05 |
| | Heave | -8.5E-09 | -2.9E-04 | 2.8E-04 | Heave | -7.5E-04 | 7.7E-04 | Tlw | 1.8E+06 | 5.7E+06 | 7.1E+05 |
| | Pitch | 0.20 | -0.17 | 0.62 | Pitch | -0.48 | 0.52 | | | | |
| | | Displacements | | | | Velocities | | | Tendon Forces | | |
| | | Mean | Min | Max | | Min | Max | | Min | Max | Std |
| **ICLC16** | Surge | 12.02 | 9.91 | 21.29 | Surge | -0.39 | 0.00 | Tww | 4.1E+06 | 9.7E+06 | 8.0E+05 |
| | Heave | 1.5E-10 | -3.0E-04 | 2.9E-04 | Heave | -7.4E-04 | 7.8E-04 | Tlw | 1.5E+06 | 6.6E+06 | 6.2E+05 |
| | Pitch | 0.22 | -0.20 | 0.89 | Pitch | -0.69 | 0.73 | | | | |
| | | Displacements | | | | Velocities | | | Tendon Forces | | |
| | | Mean | Min | Max | | Min | Max | | Min | Max | Std |
| **ICLC17** | Surge | 15.76 | 9.91 | 24.84 | Surge | -0.43 | 0.00 | Tww | 4.4E+06 | 1.1E+07 | 1.1E+06 |
| | Heave | -4.4E-08 | -4.7E-04 | 4.7E-04 | Heave | -1.2E-03 | 1.2E-03 | Tlw | 1.5E+06 | 6.7E+06 | 1.0E+06 |
| | Pitch | 0.29 | -0.17 | 0.90 | Pitch | -0.64 | 0.69 | | | | |

**Table M-6:** Ice crushing load case simulation outcomes for $v_{ice} = 0.2m/s$

| | | Displacements | | | | Velocities | | | Tendon Forces | | |
|---|---|---|---|---|---|---|---|---|---|---|---|
| | | Mean | Min | Max | | Min | Max | | Min | Max | Std |
| **ICLC21** | Surge | 4.87 | 4.84 | 4.89 | Surge | -0.01 | 0.00 | Tww | 4.5E+06 | 4.5E+06 | 7.0E+03 |
| | Heave | 0.00 | 0.00 | 0.00 | Heave | 0.00 | 0.00 | Tlw | 3.7E+06 | 3.7E+06 | 6.8E+03 |
| | Pitch | 0.09 | 0.09 | 0.09 | Pitch | -0.01 | 0.02 | | | | |
| | | Displacements | | | | Velocities | | | Tendon Forces | | |
| | | Mean | Min | Max | | Min | Max | | Min | Max | Std |
| **ICLC22** | Surge | 7.84 | 7.62 | 7.87 | Surge | -0.05 | 0.00 | Tww | 4.8E+06 | 5.1E+06 | 6.2E+04 |
| | Heave | 0.00 | 0.00 | 0.00 | Heave | 0.00 | 0.00 | Tlw | 3.5E+06 | 3.7E+06 | 6.0E+04 |
| | Pitch | 0.15 | 0.12 | 0.17 | Pitch | -0.06 | 0.07 | | | | |
| | | Displacements | | | | Velocities | | | Tendon Forces | | |
| | | Mean | Min | Max | | Min | Max | | Min | Max | Std |
| **ICLC23** | Surge | 9.06 | 8.85 | 12.50 | Surge | -0.23 | 0.00 | Tww | 3.5E+06 | 7.9E+06 | 3.3E+05 |
| | Heave | 0.00 | 0.00 | 0.00 | Heave | 0.00 | 0.00 | Tlw | 1.6E+06 | 5.9E+06 | 3.1E+05 |
| | Pitch | 0.17 | -0.26 | 0.68 | Pitch | -0.67 | 0.62 | | | | |
| | | Displacements | | | | Velocities | | | Tendon Forces | | |
| | | Mean | Min | Max | | Min | Max | | Min | Max | Std |
| **ICLC24** | Surge | 19.36 | 13.68 | 24.86 | Surge | -0.48 | 0.01 | Tww | 4.0E+06 | 1.3E+07 | 2.2E+06 |
| | Heave | 0.00 | 0.00 | 0.00 | Heave | -0.01 | 0.01 | Tlw | 9.8E+05 | 9.2E+06 | 2.0E+06 |
| | Pitch | 0.36 | -0.46 | 1.33 | Pitch | -1.31 | 1.17 | | | | |
| | | Displacements | | | | Velocities | | | Tendon Forces | | |
| | | Mean | Min | Max | | Min | Max | | Min | Max | Std |
| **ICLC25** | Surge | 17.95 | 17.32 | 20.97 | Surge | -0.36 | 0.00 | Tww | 4.8E+06 | 1.1E+07 | 1.3E+06 |
| | Heave | 0.00 | 0.00 | 0.00 | Heave | 0.00 | 0.00 | Tlw | 1.4E+06 | 7.3E+06 | 1.3E+06 |
| | Pitch | 0.34 | -0.25 | 1.01 | Pitch | -0.80 | 0.79 | | | | |
| | | Displacements | | | | Velocities | | | Tendon Forces | | |
| | | Mean | Min | Max | | Min | Max | | Min | Max | Std |
| **ICLC26** | Surge | 21.29 | 19.80 | 25.07 | Surge | -0.37 | 0.01 | Tww | 5.4E+06 | 1.2E+07 | 1.2E+06 |
| | Heave | 0.00 | 0.00 | 0.00 | Heave | -0.01 | 0.01 | Tlw | 1.5E+06 | 7.8E+06 | 1.2E+06 |
| | Pitch | 0.40 | -0.19 | 1.07 | Pitch | -0.85 | 0.91 | | | | |
| | | Displacements | | | | Velocities | | | Tendon Forces | | |
| | | Mean | Min | Max | | Min | Max | | Min | Max | Std |
| **ICLC27** | Surge | 23.90 | 19.81 | 29.24 | Surge | -0.43 | 0.00 | Tww | 7.2E+06 | 1.4E+07 | 8.9E+05 |
| | Heave | 0.00 | 0.00 | 0.00 | Heave | 0.00 | 0.00 | Tlw | 2.1E+06 | 8.8E+06 | 8.1E+05 |
| | Pitch | 0.45 | -0.17 | 1.25 | Pitch | -0.88 | 0.95 | | | | |

**Table M-7:** Ice crushing load case simulation outcomes for $v_{ice} = 0.3m/s$

| | | Displacements | | | | Velocities | | | Tendon Forces | | |
|---|---|---|---|---|---|---|---|---|---|---|---|
| | | Mean | Min | Max | | Min | Max | | Min | Max | Std |
| **ICLC31** | Surge | 6.96 | 6.94 | 6.97 | Surge | -0.01 | 0.00 | Tww | 4.8E+06 | 4.8E+06 | 3.8E+03 |
| | Heave | 0.00 | 0.00 | 0.00 | Heave | 0.00 | 0.00 | Tlw | 3.6E+06 | 3.6E+06 | 3.7E+03 |
| | Pitch | 0.13 | 0.13 | 0.13 | Pitch | -0.01 | 0.01 | | | | |
| | | Displacements | | | | Velocities | | | Tendon Forces | | |
| | | Mean | Min | Max | | Min | Max | | Min | Max | Std |
| **ICLC32** | Surge | 12.28 | 11.24 | 12.32 | Surge | -0.04 | 0.00 | Tww | 5.6E+06 | 5.9E+06 | 3.8E+04 |
| | Heave | 0.00 | 0.00 | 0.00 | Heave | 0.00 | 0.00 | Tlw | 3.6E+06 | 3.7E+06 | 2.9E+04 |
| | Pitch | 0.23 | 0.20 | 0.24 | Pitch | -0.04 | 0.06 | | | | |
| | | Displacements | | | | Velocities | | | Tendon Forces | | |
| | | Mean | Min | Max | | Min | Max | | Min | Max | Std |
| **ICLC33** | Surge | 14.88 | 13.26 | 14.98 | Surge | -0.08 | 0.00 | Tww | 5.9E+06 | 6.6E+06 | 1.2E+05 |
| | Heave | 0.00 | 0.00 | 0.00 | Heave | 0.00 | 0.00 | Tlw | 3.6E+06 | 4.0E+06 | 1.1E+05 |
| | Pitch | 0.28 | 0.21 | 0.31 | Pitch | -0.10 | 0.13 | | | | |
| | | Displacements | | | | Velocities | | | Tendon Forces | | |
| | | Mean | Min | Max | | Min | Max | | Min | Max | Std |
| **ICLC34** | Surge | 17.54 | 17.39 | 19.40 | Surge | -0.23 | 0.00 | Tww | 4.6E+06 | 9.9E+06 | 3.5E+05 |
| | Heave | 0.00 | 0.00 | 0.00 | Heave | 0.00 | 0.00 | Tlw | 1.4E+06 | 6.9E+06 | 3.2E+05 |
| | Pitch | 0.33 | -0.24 | 0.91 | Pitch | -0.82 | 0.70 | | | | |
| | | Displacements | | | | Velocities | | | Tendon Forces | | |
| | | Mean | Min | Max | | Min | Max | | Min | Max | Std |
| **ICLC35** | Surge | 23.86 | -12.71 | 37.51 | Surge | -2.66 | 0.01 | Tww | 1.1E+06 | 1.9E+07 | 3.3E+06 |
| | Heave | 0.00 | 0.00 | 0.00 | Heave | -0.01 | 0.01 | Tlw | 1.4E+06 | 1.3E+07 | 2.4E+06 |
| | Pitch | 0.44 | -0.79 | 1.77 | Pitch | -1.62 | 1.45 | | | | |
| | | Displacements | | | | Velocities | | | Tendon Forces | | |
| | | Mean | Min | Max | | Min | Max | | Min | Max | Std |
| **ICLC36** | Surge | 34.09 | -14.78 | 50.87 | Surge | -3.40 | 0.00 | Tww | 1.1E+06 | 2.8E+07 | 5.7E+06 |
| | Heave | 0.00 | 0.00 | 0.00 | Heave | 0.00 | 0.00 | Tlw | 9.8E+05 | 1.9E+07 | 4.1E+06 |
| | Pitch | 0.63 | -0.85 | 2.24 | Pitch | -1.97 | 1.79 | | | | |
| | | Displacements | | | | Velocities | | | Tendon Forces | | |
| | | Mean | Min | Max | | Min | Max | | Min | Max | Std |
| **ICLC37** | Surge | 39.69 | 29.63 | 42.98 | Surge | -0.47 | 0.00 | Tww | 8.9E+06 | 2.2E+07 | 3.2E+06 |
| | Heave | 0.00 | 0.00 | 0.00 | Heave | 0.00 | 0.00 | Tlw | 3.0E+06 | 1.5E+07 | 3.0E+06 |
| | Pitch | 0.74 | -0.30 | 1.90 | Pitch | -1.33 | 1.54 | | | | |

**Table M-8:** Ice crushing load case simulation outcomes for $v_{ice} = 0.4m/s$

| | | Displacements | | | | Velocities | | | Tendon Forces | | |
|---|---|---|---|---|---|---|---|---|---|---|---|
| | | Mean | Min | Max | | Min | Max | | Min | Max | Std |
| **ICLC41** | Surge | 8.98 | 8.96 | 9.00 | Surge | -0.01 | 0.00 | Tww | 5.2E+06 | 5.2E+06 | 3.4E+03 |
| | Heave | 0.00 | 0.00 | 0.00 | Heave | 0.00 | 0.00 | Tlw | 3.6E+06 | 3.6E+06 | 3.1E+03 |
| | Pitch | 0.17 | 0.17 | 0.17 | Pitch | -0.01 | 0.01 | | | | |
| | | Displacements | | | | Velocities | | | Tendon Forces | | |
| | | Mean | Min | Max | | Min | Max | | Min | Max | Std |
| **ICLC42** | Surge | 16.58 | 15.02 | 16.66 | Surge | -0.03 | 0.00 | Tww | 6.4E+06 | 6.9E+06 | 4.6E+04 |
| | Heave | 0.00 | 0.00 | 0.00 | Heave | 0.00 | 0.00 | Tlw | 3.8E+06 | 4.0E+06 | 2.1E+04 |
| | Pitch | 0.31 | 0.27 | 0.32 | Pitch | -0.03 | 0.05 | | | | |
| | | Displacements | | | | Velocities | | | Tendon Forces | | |
| | | Mean | Min | Max | | Min | Max | | Min | Max | Std |
| **ICLC43** | Surge | 21.50 | 17.76 | 21.68 | Surge | -0.07 | 0.00 | Tww | 7.0E+06 | 8.4E+06 | 1.6E+05 |
| | Heave | 0.00 | 0.00 | 0.00 | Heave | 0.00 | 0.00 | Tlw | 4.0E+06 | 4.6E+06 | 8.5E+04 |
| | Pitch | 0.40 | 0.31 | 0.42 | Pitch | -0.08 | 0.12 | | | | |
| | | Displacements | | | | Velocities | | | Tendon Forces | | |
| | | Mean | Min | Max | | Min | Max | | Min | Max | Std |
| **ICLC44** | Surge | 24.16 | -12.81 | 34.33 | Surge | -2.48 | 0.02 | Tww | 1.6E+06 | 1.7E+07 | 3.2E+06 |
| | Heave | 0.00 | -0.01 | 0.01 | Heave | -0.02 | 0.02 | Tlw | 1.2E+06 | 1.2E+07 | 2.2E+06 |
| | Pitch | 0.45 | -0.67 | 1.50 | Pitch | -1.35 | 1.33 | | | | |
| | | Displacements | | | | Velocities | | | Tendon Forces | | |
| | | Mean | Min | Max | | Min | Max | | Min | Max | Std |
| **ICLC45** | Surge | 25.72 | -13.31 | 38.64 | Surge | -2.76 | 0.01 | Tww | 7.0E+05 | 2.0E+07 | 3.3E+06 |
| | Heave | 0.00 | 0.00 | 0.00 | Heave | -0.01 | 0.01 | Tlw | 6.0E+05 | 1.4E+07 | 2.1E+06 |
| | Pitch | 0.48 | -0.88 | 1.77 | Pitch | -1.82 | 1.70 | | | | |
| | | Displacements | | | | Velocities | | | Tendon Forces | | |
| | | Mean | Min | Max | | Min | Max | | Min | Max | Std |
| **ICLC46** | Surge | 29.90 | -15.44 | 52.26 | Surge | -3.64 | 0.01 | Tww | -5.7E+05 | 3.2E+07 | 6.4E+06 |
| | Heave | 0.00 | 0.00 | 0.00 | Heave | -0.01 | 0.01 | Tlw | -1.3E+06 | 2.4E+07 | 4.2E+06 |
| | Pitch | 0.55 | -1.50 | 3.06 | Pitch | -3.23 | 3.10 | | | | |
| | | Displacements | | | | Velocities | | | Tendon Forces | | |
| | | Mean | Min | Max | | Min | Max | | Min | Max | Std |
| **ICLC47** | Surge | 41.45 | -16.55 | 65.83 | Surge | -4.20 | 0.01 | Tww | 4.4E+05 | 4.0E+07 | 9.1E+06 |
| | Heave | 0.00 | 0.00 | 0.00 | Heave | -0.01 | 0.01 | Tlw | 8.1E+05 | 3.0E+07 | 6.4E+06 |
| | Pitch | 0.77 | -1.02 | 2.75 | Pitch | -2.54 | 2.44 | | | | |

**Table M-9:** Ice crushing & wind load case simulation outcomes for $v_{ice} = 0.1m/s$, $u_{mean} = 11m/s$

| | | Displacements | | | | Velocities | | | Tendon Forces | | |
|---|---|---|---|---|---|---|---|---|---|---|---|
| | | Mean | Min | Max | | Min | Max | | Min | Max | Std |
| **ICWLC11** | Surge | 6.62 | 5.45 | 8.17 | Surge | -0.09 | 0.00 | Tww | 4.7E+06 | 6.5E+06 | 2.6E+05 |
| | Heave | -2.4E-08 | -4.7E-04 | 4.7E-04 | Heave | -1.3E-03 | 1.3E-03 | Tlw | 2.1E+06 | 3.7E+06 | 2.3E+05 |
| | Pitch | 0.26 | 0.10 | 0.46 | Pitch | -0.25 | 0.21 | | | | |
| | | Displacements | | | | Velocities | | | Tendon Forces | | |
| | | Mean | Min | Max | | Min | Max | | Min | Max | Std |
| **ICWLC12** | Surge | 8.39 | 6.12 | 9.90 | Surge | -0.16 | 0.00 | Tww | 4.3E+06 | 7.2E+06 | 4.6E+05 |
| | Heave | -8.6E-09 | -3.4E-04 | 3.5E-04 | Heave | -9.4E-04 | 9.3E-04 | Tlw | 1.7E+06 | 4.5E+06 | 4.3E+05 |
| | Pitch | 0.29 | -0.02 | 0.59 | Pitch | -0.37 | 0.37 | | | | |
| | | Displacements | | | | Velocities | | | Tendon Forces | | |
| | | Mean | Min | Max | | Min | Max | | Min | Max | Std |
| **ICWLC13** | Surge | 10.22 | 9.23 | 12.18 | Surge | -0.18 | 0.00 | Tww | 4.6E+06 | 7.5E+06 | 4.6E+05 |
| | Heave | 3.0E-08 | -2.5E-04 | 2.5E-04 | Heave | -6.9E-04 | 6.8E-04 | Tlw | 1.7E+06 | 4.4E+06 | 4.4E+05 |
| | Pitch | 0.33 | 0.02 | 0.61 | Pitch | -0.33 | 0.34 | | | | |
| | | Displacements | | | | Velocities | | | Tendon Forces | | |
| | | Mean | Min | Max | | Min | Max | | Min | Max | Std |
| **ICWLC14** | Surge | 12.15 | 10.77 | 16.53 | Surge | -0.22 | 0.00 | Tww | 4.8E+06 | 8.4E+06 | 5.1E+05 |
| | Heave | -3.7E-08 | -4.2E-04 | 4.2E-04 | Heave | -1.2E-03 | 1.2E-03 | Tlw | 1.5E+06 | 4.7E+06 | 4.7E+05 |
| | Pitch | 0.37 | 0.02 | 0.70 | Pitch | -0.42 | 0.39 | | | | |
| | | Displacements | | | | Velocities | | | Tendon Forces | | |
| | | Mean | Min | Max | | Min | Max | | Min | Max | Std |
| **ICWLC15** | Surge | 14.24 | 12.98 | 17.01 | Surge | -0.26 | 0.00 | Tww | 5.2E+06 | 8.8E+06 | 5.9E+05 |
| | Heave | 9.4E-08 | -4.8E-04 | 4.8E-04 | Heave | -1.3E-03 | 1.3E-03 | Tlw | 1.6E+06 | 4.8E+06 | 5.8E+05 |
| | Pitch | 0.41 | 0.04 | 0.75 | Pitch | -0.43 | 0.44 | | | | |
| | | Displacements | | | | Velocities | | | Tendon Forces | | |
| | | Mean | Min | Max | | Min | Max | | Min | Max | Std |
| **ICWLC16** | Surge | 16.77 | 13.63 | 22.76 | Surge | -0.34 | 0.00 | Tww | 5.8E+06 | 1.0E+07 | 7.1E+05 |
| | Heave | 5.9E-08 | -7.0E-04 | 7.0E-04 | Heave | -1.9E-03 | 1.9E-03 | Tlw | 1.4E+06 | 5.3E+06 | 6.5E+05 |
| | Pitch | 0.46 | 0.10 | 0.88 | Pitch | -0.46 | 0.47 | | | | |
| | | Displacements | | | | Velocities | | | Tendon Forces | | |
| | | Mean | Min | Max | | Min | Max | | Min | Max | Std |
| **ICWLC17** | Surge | 19.60 | 12.80 | 25.53 | Surge | -0.41 | 0.00 | Tww | 6.1E+06 | 1.2E+07 | 8.5E+05 |
| | Heave | 4.7E-08 | -4.0E-04 | 4.1E-04 | Heave | -1.1E-03 | 1.1E-03 | Tlw | 1.5E+06 | 6.5E+06 | 7.5E+05 |
| | Pitch | 0.52 | 0.07 | 1.10 | Pitch | -0.62 | 0.66 | | | | |

**Table M-10:** Ice crushing & wind load case simulation outcomes for $v_{ice} = 0.2m/s$, $u_{mean} = 11m/s$

| | | Displacements | | | | Velocities | | | Tendon Forces | | |
|---|---|---|---|---|---|---|---|---|---|---|---|
| | | Mean | Min | Max | | Min | Max | | Min | Max | Std |
| **ICWLC21** | Surge | 8.73 | 7.53 | 10.34 | Surge | -0.10 | 0.00 | Tww | 4.9E+06 | 6.9E+06 | 2.6E+05 |
| | Heave | 1.2E-08 | -1.8E-04 | 1.8E-04 | Heave | -4.9E-04 | 4.8E-04 | Tlw | 2.0E+06 | 3.7E+06 | 2.2E+05 |
| | Pitch | 0.30 | 0.14 | 0.51 | Pitch | -0.25 | 0.25 | | | | |
| | | Displacements | | | | Velocities | | | Tendon Forces | | |
| | | Mean | Min | Max | | Min | Max | | Min | Max | Std |
| **ICWLC22** | Surge | 11.69 | 10.92 | 13.04 | Surge | -0.11 | 0.00 | Tww | 5.6E+06 | 7.4E+06 | 2.6E+05 |
| | Heave | 5.3E-09 | -7.1E-04 | 7.0E-04 | Heave | -1.9E-03 | 1.9E-03 | Tlw | 2.1E+06 | 3.7E+06 | 2.2E+05 |
| | Pitch | 0.35 | 0.20 | 0.56 | Pitch | -0.27 | 0.28 | | | | |
| | | Displacements | | | | Velocities | | | Tendon Forces | | |
| | | Mean | Min | Max | | Min | Max | | Min | Max | Std |
| **ICWLC23** | Surge | 14.65 | 12.81 | 18.06 | Surge | -0.25 | 0.00 | Tww | 4.9E+06 | 9.7E+06 | 6.1E+05 |
| | Heave | -9.0E-08 | -7.8E-04 | 7.8E-04 | Heave | -2.1E-03 | 2.1E-03 | Tlw | 1.3E+06 | 5.6E+06 | 5.5E+05 |
| | Pitch | 0.42 | -0.02 | 0.89 | Pitch | -0.66 | 0.63 | | | | |
| | | Displacements | | | | Velocities | | | Tendon Forces | | |
| | | Mean | Min | Max | | Min | Max | | Min | Max | Std |
| **ICWLC24** | Surge | 20.46 | 14.64 | 24.43 | Surge | -0.34 | 0.00 | Tww | 5.6E+06 | 1.2E+07 | 1.3E+06 |
| | Heave | -2.6E-07 | -1.4E-03 | 1.4E-03 | Heave | -3.8E-03 | 3.8E-03 | Tlw | 1.2E+06 | 7.3E+06 | 1.2E+06 |
| | Pitch | 0.52 | -0.08 | 1.18 | Pitch | -0.80 | 0.86 | | | | |
| | | Displacements | | | | Velocities | | | Tendon Forces | | |
| | | Mean | Min | Max | | Min | Max | | Min | Max | Std |
| **ICWLC25** | Surge | 22.48 | 17.56 | 23.48 | Surge | -0.29 | 0.00 | Tww | 6.6E+06 | 1.2E+07 | 1.3E+06 |
| | Heave | -5.5E-08 | -5.5E-04 | 5.4E-04 | Heave | -1.5E-03 | 1.5E-03 | Tlw | 1.4E+06 | 6.9E+06 | 1.3E+06 |
| | Pitch | 0.57 | -0.03 | 1.14 | Pitch | -0.71 | 0.68 | | | | |
| | | Displacements | | | | Velocities | | | Tendon Forces | | |
| | | Mean | Min | Max | | Min | Max | | Min | Max | Std |
| **ICWLC26** | Surge | 24.87 | 21.06 | 27.06 | Surge | -0.34 | 0.00 | Tww | 7.5E+06 | 1.3E+07 | 9.7E+05 |
| | Heave | 2.2E-07 | -1.3E-03 | 1.3E-03 | Heave | -3.6E-03 | 3.6E-03 | Tlw | 2.0E+06 | 7.1E+06 | 9.8E+05 |
| | Pitch | 0.60 | 0.07 | 1.16 | Pitch | -0.68 | 0.78 | | | | |
| | | Displacements | | | | Velocities | | | Tendon Forces | | |
| | | Mean | Min | Max | | Min | Max | | Min | Max | Std |
| **ICWLC27** | Surge | 29.31 | 21.27 | 33.11 | Surge | -0.40 | 0.00 | Tww | 8.6E+06 | 1.6E+07 | 1.1E+06 |
| | Heave | 6.0E-08 | -6.8E-04 | 6.8E-04 | Heave | -1.8E-03 | 1.9E-03 | Tlw | 2.4E+06 | 8.8E+06 | 1.0E+06 |
| | Pitch | 0.68 | 0.10 | 1.39 | Pitch | -0.80 | 0.88 | | | | |

**Table M-11:** Ice crushing & wind load case simulation outcomes for $v_{ice} = 0.3m/s$, $u_{mean} = 11m/s$

| | | Displacements | | | | Velocities | | | Tendon Forces | | |
|---|---|---|---|---|---|---|---|---|---|---|---|
| | | Mean | Min | Max | | Min | Max | | Min | Max | Std |
| **ICWLC31** | Surge | 10.91 | 9.80 | 13.02 | Surge | -0.09 | 0.00 | Tww | 5.4E+06 | 7.5E+06 | 2.7E+05 |
| | Heave | 1.0E-08 | -1.7E-04 | 1.6E-04 | Heave | -4.5E-04 | 4.5E-04 | Tlw | 2.2E+06 | 3.7E+06 | 2.2E+05 |
| | Pitch | 0.34 | 0.19 | 0.57 | Pitch | -0.19 | 0.17 | | | | |
| | | Displacements | | | | Velocities | | | Tendon Forces | | |
| | | Mean | Min | Max | | Min | Max | | Min | Max | Std |
| **ICWLC32** | Surge | 16.19 | 15.03 | 17.17 | Surge | -0.08 | 0.00 | Tww | 6.6E+06 | 8.2E+06 | 2.6E+05 |
| | Heave | 7.0E-09 | -1.9E-04 | 2.0E-04 | Heave | -5.4E-04 | 5.5E-04 | Tlw | 2.5E+06 | 4.0E+06 | 2.1E+05 |
| | Pitch | 0.44 | 0.30 | 0.62 | Pitch | -0.23 | 0.23 | | | | |
| | | Displacements | | | | Velocities | | | Tendon Forces | | |
| | | Mean | Min | Max | | Min | Max | | Min | Max | Std |
| **ICWLC33** | Surge | 19.33 | 17.98 | 20.26 | Surge | -0.13 | 0.00 | Tww | 7.2E+06 | 9.4E+06 | 3.0E+05 |
| | Heave | -6.6E-08 | -8.5E-04 | 8.4E-04 | Heave | -2.3E-03 | 2.3E-03 | Tlw | 2.4E+06 | 4.4E+06 | 2.5E+05 |
| | Pitch | 0.51 | 0.30 | 0.73 | Pitch | -0.38 | 0.28 | | | | |
| | | Displacements | | | | Velocities | | | Tendon Forces | | |
| | | Mean | Min | Max | | Min | Max | | Min | Max | Std |
| **ICWLC34** | Surge | 22.59 | 21.22 | 30.98 | Surge | -0.30 | 0.00 | Tww | 7.3E+06 | 1.5E+07 | 7.7E+05 |
| | Heave | 8.7E-08 | -1.5E-03 | 1.5E-03 | Heave | -4.0E-03 | 4.0E-03 | Tlw | 1.7E+06 | 8.9E+06 | 5.8E+05 |
| | Pitch | 0.56 | -0.05 | 1.43 | Pitch | -1.01 | 0.99 | | | | |
| | | Displacements | | | | Velocities | | | Tendon Forces | | |
| | | Mean | Min | Max | | Min | Max | | Min | Max | Std |
| **ICWLC35** | Surge | 32.83 | -6.92 | 43.69 | Surge | -2.53 | 0.00 | Tww | 3.6E+06 | 2.2E+07 | 3.1E+06 |
| | Heave | 1.5E-07 | -1.5E-03 | 1.5E-03 | Heave | -4.0E-03 | 4.0E-03 | Tlw | 1.9E+06 | 1.3E+07 | 2.2E+06 |
| | Pitch | 0.76 | -0.13 | 1.79 | Pitch | -1.22 | 1.25 | | | | |
| | | Displacements | | | | Velocities | | | Tendon Forces | | |
| | | Mean | Min | Max | | Min | Max | | Min | Max | Std |
| **ICWLC36** | Surge | 38.19 | -9.82 | 55.59 | Surge | -3.12 | 0.00 | Tww | 2.8E+06 | 3.0E+07 | 5.9E+06 |
| | Heave | 3.6E-07 | -1.8E-03 | 1.8E-03 | Heave | -4.8E-03 | 4.8E-03 | Tlw | 1.7E+06 | 2.0E+07 | 4.1E+06 |
| | Pitch | 0.86 | -0.35 | 2.16 | Pitch | -1.43 | 1.47 | | | | |
| | | Displacements | | | | Velocities | | | Tendon Forces | | |
| | | Mean | Min | Max | | Min | Max | | Min | Max | Std |
| **ICWLC37** | Surge | 45.79 | 29.68 | 50.57 | Surge | -0.42 | 0.00 | Tww | 1.1E+07 | 2.7E+07 | 3.5E+06 |
| | Heave | 6.2E-08 | -1.2E-03 | 1.2E-03 | Heave | -3.3E-03 | 3.3E-03 | Tlw | 3.8E+06 | 1.7E+07 | 3.1E+06 |
| | Pitch | 1.00 | -0.06 | 2.09 | Pitch | -1.28 | 1.49 | | | | |

**Table M-12:** Ice crushing & wind load case simulation outcomes for $v_{ice} = 0.4m/s$, $u_{mean} = 11m/s$

| | | Displacements | | | | Velocities | | | Tendon Forces | | |
|---|---|---|---|---|---|---|---|---|---|---|---|
| | | Mean | Min | Max | | Min | Max | | Min | Max | Std |
| **ICWLC41** | Surge | 12.99 | 11.51 | 14.44 | Surge | -0.09 | 0.00 | Tww | 5.8E+06 | 7.7E+06 | 2.9E+05 |
| | Heave | 2.8E-08 | -1.6E-04 | 1.7E-04 | Heave | -4.5E-04 | 4.5E-04 | Tlw | 2.3E+06 | 3.9E+06 | 2.2E+05 |
| | Pitch | 0.38 | 0.21 | 0.58 | Pitch | -0.21 | 0.20 | | | | |
| | | Displacements | | | | Velocities | | | Tendon Forces | | |
| | | Mean | Min | Max | | Min | Max | | Min | Max | Std |
| **ICWLC42** | Surge | 20.86 | 19.18 | 22.14 | Surge | -0.09 | 0.00 | Tww | 7.7E+06 | 1.0E+07 | 3.0E+05 |
| | Heave | -2.0E-08 | -1.4E-04 | 1.4E-04 | Heave | -4.0E-04 | 3.9E-04 | Tlw | 2.9E+06 | 4.6E+06 | 2.1E+05 |
| | Pitch | 0.54 | 0.37 | 0.75 | Pitch | -0.22 | 0.20 | | | | |
| | | Displacements | | | | Velocities | | | Tendon Forces | | |
| | | Mean | Min | Max | | Min | Max | | Min | Max | Std |
| **ICWLC43** | Surge | 25.41 | 22.00 | 26.62 | Surge | -0.10 | 0.00 | Tww | 8.9E+06 | 1.1E+07 | 3.1E+05 |
| | Heave | 5.1E-09 | -4.0E-04 | 3.9E-04 | Heave | -1.1E-03 | 1.1E-03 | Tlw | 3.5E+06 | 5.1E+06 | 2.2E+05 |
| | Pitch | 0.61 | 0.46 | 0.80 | Pitch | -0.18 | 0.23 | | | | |
| | | Displacements | | | | Velocities | | | Tendon Forces | | |
| | | Mean | Min | Max | | Min | Max | | Min | Max | Std |
| **ICWLC44** | Surge | 28.87 | 25.38 | 29.89 | Surge | -0.18 | 0.00 | Tww | 1.0E+07 | 1.3E+07 | 4.0E+05 |
| | Heave | 1.5E-07 | -1.4E-03 | 1.4E-03 | Heave | -4.0E-03 | 4.0E-03 | Tlw | 3.9E+06 | 6.0E+06 | 3.2E+05 |
| | Pitch | 0.69 | 0.49 | 0.97 | Pitch | -0.38 | 0.39 | | | | |
| | | Displacements | | | | Velocities | | | Tendon Forces | | |
| | | Mean | Min | Max | | Min | Max | | Min | Max | Std |
| **ICWLC45** | Surge | 27.84 | -9.56 | 43.98 | Surge | -2.60 | 0.00 | Tww | 3.3E+06 | 2.2E+07 | 4.2E+06 |
| | Heave | -1.4E-07 | -1.8E-03 | 1.7E-03 | Heave | -4.7E-03 | 4.8E-03 | Tlw | 1.9E+06 | 1.3E+07 | 2.4E+06 |
| | Pitch | 0.65 | -0.23 | 1.77 | Pitch | -1.17 | 1.22 | | | | |
| | | Displacements | | | | Velocities | | | Tendon Forces | | |
| | | Mean | Min | Max | | Min | Max | | Min | Max | Std |
| **ICWLC46** | Surge | 34.12 | -10.60 | 57.90 | Surge | -3.25 | 0.00 | Tww | 2.5E+06 | 3.1E+07 | 7.0E+06 |
| | Heave | 2.6E-07 | -1.8E-03 | 1.8E-03 | Heave | -4.8E-03 | 4.9E-03 | Tlw | 2.0E+06 | 2.1E+07 | 4.5E+06 |
| | Pitch | 0.77 | -0.40 | 2.20 | Pitch | -1.44 | 1.46 | | | | |
| | | Displacements | | | | Velocities | | | Tendon Forces | | |
| | | Mean | Min | Max | | Min | Max | | Min | Max | Std |
| **ICWLC47** | Surge | 46.71 | -11.12 | 72.24 | Surge | -3.88 | 0.00 | Tww | 2.6E+06 | 4.4E+07 | 9.9E+06 |
| | Heave | 2.2E-08 | -1.4E-03 | 1.3E-03 | Heave | -3.5E-03 | 3.6E-03 | Tlw | 1.7E+06 | 3.0E+07 | 7.0E+06 |
| | Pitch | 1.02 | -0.42 | 2.65 | Pitch | -1.72 | 1.69 | | | | |

**Table M-13:** Ice crushing, wind & current load case simulation outcomes for $v_{ice} = 0.2m/s$, $u_{mean} = 11m/s$ and $u_{current=0.5m/s}$

| | | Displacements | | | | Velocities | | | Tendon Forces | | | |
|---|---|---|---|---|---|---|---|---|---|---|---|---|
| **ICWCLC1** | | Mean | Min | Max | | Min | Max | | Mean | Min | Max | Std |
| | Surge | 9,43 | 8,34 | 11,17 | Surge | -0,09 | 0,35 | Tww | 5,9E+06 | 5,0E+06 | 7,0E+06 | 2,7E+05 |
| | Heave | 1,9E-08 | -1,9E-04 | 1,9E-04 | Heave | -5,1E-04 | 5,2E-04 | Tlw | 3,0E+06 | 2,1E+06 | 3,8E+06 | 2,3E+05 |
| | Pitch | 0,31 | 0,12 | 0,52 | Pitch | 0,00 | 0,00 | | | | | |
| | | Displacements | | | | Velocities | | | Tendon Forces | | | |
| **ICWCLC2** | | Mean | Min | Max | | Min | Max | | Mean | Min | Max | Std |
| | Surge | 12,38 | 11,48 | 13,38 | Surge | -0,10 | 0,43 | Tww | 6,5E+06 | 5,7E+06 | 7,5E+06 | 2,6E+05 |
| | Heave | -8,4E-08 | -9,3E-04 | 9,4E-04 | Heave | -2,6E-03 | 2,6E-03 | Tlw | 3,1E+06 | 2,2E+06 | 3,8E+06 | 2,3E+05 |
| | Pitch | 0,37 | 0,21 | 0,56 | Pitch | -0,01 | 0,01 | | | | | |
| | | Displacements | | | | Velocities | | | Tendon Forces | | | |
| **ICWCLC3** | | Mean | Min | Max | | Min | Max | | Mean | Min | Max | Std |
| | Surge | 15,18 | 13,52 | 21,08 | Surge | -0,26 | 0,43 | Tww | 7,1E+06 | 4,8E+06 | 1,1E+07 | 7,0E+05 |
| | Heave | 1,0E-07 | -1,5E-03 | 1,5E-03 | Heave | -4,1E-03 | 4,1E-03 | Tlw | 3,2E+06 | 1,1E+06 | 6,4E+06 | 6,0E+05 |
| | Pitch | 0,42 | -0,14 | 1,11 | Pitch | -0,01 | 0,01 | | | | | |
| | | Displacements | | | | Velocities | | | Tendon Forces | | | |
| **ICWCLC4** | | Mean | Min | Max | | Min | Max | | Mean | Min | Max | Std |
| | Surge | 22,71 | 18,17 | 30,45 | Surge | -0,41 | 0,41 | Tww | 9,1E+06 | 5,9E+06 | 1,5E+07 | 1,7E+06 |
| | Heave | -2,1E-07 | -1,5E-03 | 1,6E-03 | Heave | -4,2E-03 | 4,2E-03 | Tlw | 4,0E+06 | 1,3E+06 | 8,9E+06 | 1,5E+06 |
| | Pitch | 0,56 | -0,13 | 1,35 | Pitch | -0,02 | 0,02 | | | | | |
| | | Displacements | | | | Velocities | | | Tendon Forces | | | |
| **ICWCLC5** | | Mean | Min | Max | | Min | Max | | Mean | Min | Max | Std |
| | Surge | 23,13 | 20,02 | 24,04 | Surge | -0,32 | 0,45 | Tww | 9,2E+06 | 6,7E+06 | 1,2E+07 | 1,2E+06 |
| | Heave | -8,3E-09 | -3,1E-04 | 3,0E-04 | Heave | -8,2E-04 | 7,7E-04 | Tlw | 4,1E+06 | 1,6E+06 | 7,0E+06 | 1,3E+06 |
| | Pitch | 0,56 | -0,03 | 1,11 | Pitch | -0,01 | 0,01 | | | | | |
| | | Displacements | | | | Velocities | | | Tendon Forces | | | |
| **ICWCLC6** | | Mean | Min | Max | | Min | Max | | Mean | Min | Max | Std |
| | Surge | 25,53 | 21,05 | 26,89 | Surge | -0,32 | 0,40 | Tww | 1,0E+07 | 8,0E+06 | 1,2E+07 | 8,8E+05 |
| | Heave | 5,0E-08 | -6,5E-04 | 6,4E-04 | Heave | -1,8E-03 | 1,8E-03 | Tlw | 4,4E+06 | 2,4E+06 | 6,7E+06 | 8,9E+05 |
| | Pitch | 0,61 | 0,14 | 1,07 | Pitch | -0,01 | 0,01 | | | | | |
| | | Displacements | | | | Velocities | | | Tendon Forces | | | |
| **ICWCLC7** | | Mean | Min | Max | | Min | Max | | Mean | Min | Max | Std |
| | Surge | 29,19 | 21,26 | 31,52 | Surge | -0,34 | 0,42 | Tww | 1,1E+07 | 8,7E+06 | 1,5E+07 | 7,7E+05 |
| | Heave | -2,1E-07 | -1,4E-03 | 1,4E-03 | Heave | -3,9E-03 | 3,9E-03 | Tlw | 5,1E+06 | 2,6E+06 | 7,7E+06 | 7,5E+05 |
| | Pitch | 0,68 | 0,21 | 1,29 | Pitch | -0,01 | 0,01 | | | | | |

# M-3 Ice bending load cases

**Table M-14:** Ice bending - breaking force only simulation outcomes $v_{ice} = 0.1$

| | | Displacements | | | | Velocities | | | Tendon Forces | | | |
|---|---|---|---|---|---|---|---|---|---|---|---|---|
| | | Mean | Min | Max | | Min | Max | | Mean | Min | Max | Std |
| **IBLC11** | Surge | 0,01 | -0,01 | 0,02 | Surge | -2,17E-03 | 2,57E-03 | Tww | 4,0E+06 | 4,0E+06 | 4,0E+06 | 2,1E+03 |
| | Heave | -1,0E-05 | -1,0E-03 | 1,0E-03 | Heave | -2,86E-03 | 2,86E-03 | Tlw | 4,0E+06 | 4,0E+06 | 4,0E+06 | 2,1E+03 |
| | Pitch | 0,00 | 0,00 | 0,00 | Pitch | -2,58E-05 | 2,70E-05 | | | | | |
| | | Displacements | | | | Velocities | | | Tendon Forces | | | |
| | | Mean | Min | Max | | Min | Max | | Mean | Min | Max | Std |
| **IBLC12** | Surge | 0,01 | -0,22 | 0,23 | Surge | -2,26E-02 | 2,15E-02 | Tww | 4,0E+06 | 4,0E+06 | 4,0E+06 | 1,1E+04 |
| | Heave | -2,6E-05 | -9,7E-03 | 9,5E-03 | Heave | -2,63E-02 | 2,63E-02 | Tlw | 4,0E+06 | 3,9E+06 | 4,0E+06 | 1,2E+04 |
| | Pitch | 0,00 | 0,00 | 0,01 | Pitch | -9,71E-05 | 1,02E-04 | | | | | |
| | | Displacements | | | | Velocities | | | Tendon Forces | | | |
| | | Mean | Min | Max | | Min | Max | | Mean | Min | Max | Std |
| **IBLC13** | Surge | 0,02 | -0,19 | 0,19 | Surge | -2,06E-02 | 2,22E-02 | Tww | 4,0E+06 | 3,9E+06 | 4,0E+06 | 1,4E+04 |
| | Heave | -3,5E-05 | -1,3E-02 | 1,1E-02 | Heave | -3,27E-02 | 3,16E-02 | Tlw | 4,0E+06 | 3,9E+06 | 4,0E+06 | 1,4E+04 |
| | Pitch | 0,00 | -0,01 | 0,01 | Pitch | -1,98E-04 | 2,06E-04 | | | | | |
| | | Displacements | | | | Velocities | | | Tendon Forces | | | |
| | | Mean | Min | Max | | Min | Max | | Mean | Min | Max | Std |
| **IBLC14** | Surge | 0,04 | -1,64 | 1,77 | Surge | -1,70E-01 | 1,70E-01 | Tww | 4,0E+06 | 3,8E+06 | 4,2E+06 | 4,5E+04 |
| | Heave | -7,8E-05 | -4,1E-02 | 3,7E-02 | Heave | -1,05E-01 | 1,02E-01 | Tlw | 4,0E+06 | 3,8E+06 | 4,1E+06 | 4,4E+04 |
| | Pitch | 0,00 | -0,03 | 0,03 | Pitch | -3,09E-04 | 3,01E-04 | | | | | |
| | | Displacements | | | | Velocities | | | Tendon Forces | | | |
| | | Mean | Min | Max | | Min | Max | | Mean | Min | Max | Std |
| **IBLC15** | Surge | 0,03 | -0,68 | 0,71 | Surge | -7,17E-02 | 7,32E-02 | Tww | 4,0E+06 | 3,9E+06 | 4,1E+06 | 3,3E+04 |
| | Heave | -7,0E-05 | -3,4E-02 | 2,9E-02 | Heave | -8,56E-02 | 8,15E-02 | Tlw | 4,0E+06 | 3,9E+06 | 4,1E+06 | 3,3E+04 |
| | Pitch | 0,00 | -0,01 | 0,02 | Pitch | -4,00E-04 | 4,07E-04 | | | | | |
| | | Displacements | | | | Velocities | | | Tendon Forces | | | |
| | | Mean | Min | Max | | Min | Max | | Mean | Min | Max | Std |
| **IBLC16** | Surge | 0,06 | -1,84 | 2,00 | Surge | -1,92E-01 | 1,77E-01 | Tww | 4,0E+06 | 3,8E+06 | 4,2E+06 | 6,1E+04 |
| | Heave | -1,1E-04 | -5,9E-02 | 5,7E-02 | Heave | -1,58E-01 | 1,58E-01 | Tlw | 4,0E+06 | 3,8E+06 | 4,2E+06 | 6,0E+04 |
| | Pitch | 0,00 | -0,03 | 0,04 | Pitch | -5,26E-04 | 5,16E-04 | | | | | |

**Table M-15:** Ice bending - breaking force only simulation outcomes $v_{ice} = 0.2$

| | | Displacements | | | | Velocities | | | Tendon Forces | | | |
|---|---|---|---|---|---|---|---|---|---|---|---|---|
| | | Mean | Min | Max | | Min | Max | | Mean | Min | Max | Std |
| **IBLC21** | Surge | 0,01 | 0,00 | 0,01 | Surge | -1,19E-03 | 1,33E-03 | Tww | 4,0E+06 | 4,0E+06 | 4,0E+06 | 1,3E+03 |
| | Heave | -1,1E-05 | -9,5E-04 | 9,5E-04 | Heave | -2,61E-03 | 2,61E-03 | Tlw | 4,0E+06 | 4,0E+06 | 4,0E+06 | 1,2E+03 |
| | Pitch | 0,00 | 0,00 | 0,00 | Pitch | -1,37E-05 | 1,43E-05 | | | | | |
| | | Displacements | | | | Velocities | | | Tendon Forces | | | |
| | | Mean | Min | Max | | Min | Max | | Mean | Min | Max | Std |
| **IBLC22** | Surge | 0,01 | -0,02 | 0,04 | Surge | -4,47E-03 | 5,43E-03 | Tww | 4,0E+06 | 4,0E+06 | 4,0E+06 | 6,7E+03 |
| | Heave | -2,5E-05 | -2,8E-03 | 2,7E-03 | Heave | -7,57E-03 | 7,57E-03 | Tlw | 4,0E+06 | 4,0E+06 | 4,0E+06 | 6,7E+03 |
| | Pitch | 0,00 | 0,00 | 0,00 | Pitch | -7,25E-05 | 7,51E-05 | | | | | |
| | | Displacements | | | | Velocities | | | Tendon Forces | | | |
| | | Mean | Min | Max | | Min | Max | | Mean | Min | Max | Std |
| **IBLC23** | Surge | 0,02 | -0,12 | 0,14 | Surge | -1,42E-02 | 1,52E-02 | Tww | 4,0E+06 | 4,0E+06 | 4,0E+06 | 1,3E+04 |
| | Heave | -3,8E-05 | -1,5E-02 | 1,5E-02 | Heave | -4,26E-02 | 4,26E-02 | Tlw | 4,0E+06 | 3,9E+06 | 4,0E+06 | 1,3E+04 |
| | Pitch | 0,00 | -0,01 | 0,00 | Pitch | -1,22E-04 | 1,27E-04 | | | | | |
| | | Displacements | | | | Velocities | | | Tendon Forces | | | |
| | | Mean | Min | Max | | Min | Max | | Mean | Min | Max | Std |
| **IBLC24** | Surge | 0,03 | -0,85 | 0,90 | Surge | -8,87E-02 | 9,59E-02 | Tww | 4,0E+06 | 3,9E+06 | 4,1E+06 | 3,6E+04 |
| | Heave | -6,2E-05 | -8,1E-03 | 6,6E-03 | Heave | -1,81E-02 | 1,81E-02 | Tlw | 4,0E+06 | 3,9E+06 | 4,1E+06 | 3,5E+04 |
| | Pitch | 0,00 | -0,02 | 0,02 | Pitch | -2,92E-04 | 3,38E-04 | | | | | |
| | | Displacements | | | | Velocities | | | Tendon Forces | | | |
| | | Mean | Min | Max | | Min | Max | | Mean | Min | Max | Std |
| **IBLC25** | Surge | 0,03 | -0,48 | 0,50 | Surge | -5,11E-02 | 4,69E-02 | Tww | 4,0E+06 | 3,9E+06 | 4,1E+06 | 4,0E+04 |
| | Heave | -6,7E-05 | -4,3E-02 | 4,3E-02 | Heave | -1,19E-01 | 1,19E-01 | Tlw | 4,0E+06 | 3,9E+06 | 4,1E+06 | 4,0E+04 |
| | Pitch | 0,00 | -0,01 | 0,02 | Pitch | -3,56E-04 | 3,70E-04 | | | | | |
| | | Displacements | | | | Velocities | | | Tendon Forces | | | |
| | | Mean | Min | Max | | Min | Max | | Mean | Min | Max | Std |
| **IBLC26** | Surge | 0,04 | -0,37 | 0,36 | Surge | -4,02E-02 | 4,59E-02 | Tww | 4,0E+06 | 3,9E+06 | 4,1E+06 | 3,6E+04 |
| | Heave | -8,7E-05 | -2,9E-02 | 2,9E-02 | Heave | -8,06E-02 | 8,06E-02 | Tlw | 4,0E+06 | 3,9E+06 | 4,1E+06 | 3,6E+04 |
| | Pitch | 0,00 | -0,02 | 0,02 | Pitch | -4,73E-04 | 4,92E-04 | | | | | |

**Table M-16:** Ice bending - breaking force only simulation outcomes $v_{ice} = 0.3$

| | | Displacements | | | | Velocities | | | Tendon Forces | | | |
|---|---|---|---|---|---|---|---|---|---|---|---|---|
| | | Mean | Min | Max | | Min | Max | | Mean | Min | Max | Std |
| **IBLC31** | Surge | 0,01 | 0,00 | 0,01 | Surge | -9,62E-04 | 1,15E-03 | Tww | 4,0E+06 | 4,0E+06 | 4,0E+06 | 2,0E+03 |
| | Heave | -1,1E-05 | -8,8E-04 | 8,8E-04 | Heave | -2,43E-03 | 2,43E-03 | Tlw | 4,0E+06 | 4,0E+06 | 4,0E+06 | 2,1E+03 |
| | Pitch | 0,00 | 0,00 | 0,00 | Pitch | -2,00E-05 | 2,00E-05 | | | | | |
| | | Displacements | | | | Velocities | | | Tendon Forces | | | |
| | | Mean | Min | Max | | Min | Max | | Mean | Min | Max | Std |
| **IBLC32** | Surge | 0,01 | -0,01 | 0,03 | Surge | -2,94E-03 | 3,90E-03 | Tww | 4,0E+06 | 4,0E+06 | 4,0E+06 | 3,2E+03 |
| | Heave | -2,6E-05 | -2,4E-03 | 2,4E-03 | Heave | -6,70E-03 | 6,70E-03 | Tlw | 4,0E+06 | 4,0E+06 | 4,0E+06 | 3,2E+03 |
| | Pitch | 0,00 | 0,00 | 0,00 | Pitch | -4,04E-05 | 4,22E-05 | | | | | |
| | | Displacements | | | | Velocities | | | Tendon Forces | | | |
| | | Mean | Min | Max | | Min | Max | | Mean | Min | Max | Std |
| **IBLC33** | Surge | 0,02 | -0,03 | 0,06 | Surge | -6,47E-03 | 7,93E-03 | Tww | 4,0E+06 | 4,0E+06 | 4,0E+06 | 8,4E+03 |
| | Heave | -3,8E-05 | -4,1E-03 | 4,1E-03 | Heave | -1,12E-02 | 1,12E-02 | Tlw | 4,0E+06 | 4,0E+06 | 4,0E+06 | 8,3E+03 |
| | Pitch | 0,00 | 0,00 | 0,00 | Pitch | -9,16E-05 | 9,42E-05 | | | | | |
| | | Displacements | | | | Velocities | | | Tendon Forces | | | |
| | | Mean | Min | Max | | Min | Max | | Mean | Min | Max | Std |
| **IBLC34** | Surge | 0,03 | -0,08 | 0,11 | Surge | -1,12E-02 | 1,37E-02 | Tww | 4,0E+06 | 4,0E+06 | 4,0E+06 | 1,1E+04 |
| | Heave | -5,4E-05 | -7,8E-03 | 7,8E-03 | Heave | -2,16E-02 | 2,16E-02 | Tlw | 4,0E+06 | 4,0E+06 | 4,0E+06 | 1,1E+04 |
| | Pitch | 0,00 | -0,01 | 0,01 | Pitch | -1,41E-04 | 1,48E-04 | | | | | |
| | | Displacements | | | | Velocities | | | Tendon Forces | | | |
| | | Mean | Min | Max | | Min | Max | | Mean | Min | Max | Std |
| **IBLC35** | Surge | 0,03 | -0,17 | 0,22 | Surge | -2,28E-02 | 2,59E-02 | Tww | 4,0E+06 | 3,9E+06 | 4,1E+06 | 2,1E+04 |
| | Heave | -6,7E-05 | -2,1E-02 | 2,1E-02 | Heave | -5,74E-02 | 5,74E-02 | Tlw | 4,0E+06 | 3,9E+06 | 4,0E+06 | 2,1E+04 |
| | Pitch | 0,00 | -0,01 | 0,01 | Pitch | -2,59E-04 | 2,76E-04 | | | | | |
| | | Displacements | | | | Velocities | | | Tendon Forces | | | |
| | | Mean | Min | Max | | Min | Max | | Mean | Min | Max | Std |
| **IBLC36** | Surge | 0,04 | -0,61 | 0,64 | Surge | -6,46E-02 | 7,07E-02 | Tww | 4,0E+06 | 3,6E+06 | 4,3E+06 | 1,0E+05 |
| | Heave | -9,5E-05 | -2,3E-01 | 2,3E-01 | Heave | -6,45E-01 | 6,45E-01 | Tlw | 4,0E+06 | 3,7E+06 | 4,3E+06 | 1,1E+05 |
| | Pitch | 0,00 | -0,02 | 0,02 | Pitch | -3,85E-04 | 4,23E-04 | | | | | |

**Table M-17:** Ice bending - total force simulation outcomes $v_{ice} = 0.1$

| | | Displacements | | | | Velocities | | | Tendon Forces | | | |
|---|---|---|---|---|---|---|---|---|---|---|---|---|
| | | Mean | Min | Max | | Min | Max | | Mean | Min | Max | Std |
| **IBLCT11** | Surge | 1,76 | 1,08 | 2,47 | Surge | -0,07 | 0,03 | Tww | 4,2E+06 | 4,1E+06 | 4,2E+06 | 2,5E+04 |
| | Heave | -2,1E-05 | -1,1E-02 | 1,1E-02 | Heave | -3,1E-02 | 3,1E-02 | Tlw | 3,9E+06 | 3,8E+06 | 3,9E+06 | 1,5E+04 |
| | Pitch | 0,03 | 0,02 | 0,04 | Pitch | 0,00 | 0,00 | | | | | |
| | | Displacements | | | | Velocities | | | Tendon Forces | | | |
| | | Mean | Min | Max | | Min | Max | | Mean | Min | Max | Std |
| **IBLCT12** | Surge | 4,13 | 2,84 | 5,44 | Surge | -0,13 | 0,03 | Tww | 4,4E+06 | 4,3E+06 | 4,6E+06 | 6,0E+04 |
| | Heave | -4,0E-05 | -1,0E-02 | 1,0E-02 | Heave | -2,8E-02 | 2,8E-02 | Tlw | 3,7E+06 | 3,7E+06 | 3,8E+06 | 1,4E+04 |
| | Pitch | 0,08 | 0,06 | 0,10 | Pitch | -0,01 | 0,01 | | | | | |
| | | Displacements | | | | Velocities | | | Tendon Forces | | | |
| | | Mean | Min | Max | | Min | Max | | Mean | Min | Max | Std |
| **IBLCT13** | Surge | 6,80 | 5,39 | 8,25 | Surge | -0,14 | 0,02 | Tww | 4,8E+06 | 4,6E+06 | 5,0E+06 | 8,0E+04 |
| | Heave | -5,6E-05 | -1,1E-02 | 8,0E-03 | Heave | -2,5E-02 | 2,2E-02 | Tlw | 3,6E+06 | 3,6E+06 | 3,7E+06 | 1,3E+04 |
| | Pitch | 0,13 | 0,10 | 0,15 | Pitch | -0,01 | 0,01 | | | | | |
| | | Displacements | | | | Velocities | | | Tendon Forces | | | |
| | | Mean | Min | Max | | Min | Max | | Mean | Min | Max | Std |
| **IBLCT14** | Surge | 9,88 | 8,06 | 11,74 | Surge | -0,19 | 0,03 | Tww | 5,3E+06 | 5,0E+06 | 5,7E+06 | 1,2E+05 |
| | Heave | -9,8E-05 | -1,3E-02 | 1,1E-02 | Heave | -3,1E-02 | 2,9E-02 | Tlw | 3,6E+06 | 3,5E+06 | 3,8E+06 | 3,3E+04 |
| | Pitch | 0,18 | 0,15 | 0,22 | Pitch | -0,02 | 0,02 | | | | | |
| | | Displacements | | | | Velocities | | | Tendon Forces | | | |
| | | Mean | Min | Max | | Min | Max | | Mean | Min | Max | Std |
| **IBLCT15** | Surge | 13,01 | 10,29 | 15,81 | Surge | -0,28 | 0,12 | Tww | 6,0E+06 | 5,4E+06 | 6,6E+06 | 2,0E+05 |
| | Heave | -1,9E-04 | -4,9E-02 | 4,3E-02 | Heave | -1,2E-01 | 1,2E-01 | Tlw | 3,7E+06 | 3,5E+06 | 4,0E+06 | 8,1E+04 |
| | Pitch | 0,24 | 0,20 | 0,29 | Pitch | -0,03 | 0,03 | | | | | |
| | | Displacements | | | | Velocities | | | Tendon Forces | | | |
| | | Mean | Min | Max | | Min | Max | | Mean | Min | Max | Std |
| **IBLCT16** | Surge | 16,26 | 14,18 | 18,41 | Surge | -0,21 | 0,05 | Tww | 6,8E+06 | 6,3E+06 | 7,3E+06 | 1,9E+05 |
| | Heave | -9,8E-05 | -2,5E-02 | 2,0E-02 | Heave | -5,9E-02 | 5,4E-02 | Tlw | 3,9E+06 | 3,7E+06 | 4,2E+06 | 9,0E+04 |
| | Pitch | 0,30 | 0,26 | 0,35 | Pitch | -0,03 | 0,04 | | | | | |

**Table M-18:** Ice bending - total force simulation outcomes $v_{ice} = 0.2$

| | | Displacements | | | | Velocities | | | Tendon Forces | | | |
|---|---|---|---|---|---|---|---|---|---|---|---|---|
| | | Mean | Min | Max | | Min | Max | | Mean | Min | Max | Std |
| **IBLCT21** | Surge | 1,78 | 1,05 | 2,54 | Surge | -0,07 | 0,03 | Tww | 4,2E+06 | 4,1E+06 | 4,2E+06 | 2,5E+04 |
| | Heave | -1,9E-05 | -9,1E-03 | 9,1E-03 | Heave | -2,5E-02 | 2,5E-02 | Tlw | 3,9E+06 | 3,8E+06 | 3,9E+06 | 1,5E+04 |
| | Pitch | 0,03 | 0,02 | 0,04 | Pitch | 0,00 | 0,00 | | | | | |
| | | Displacements | | | | Velocities | | | Tendon Forces | | | |
| | | Mean | Min | Max | | Min | Max | | Mean | Min | Max | Std |
| **IBLCT22** | Surge | 4,16 | 3,05 | 5,31 | Surge | -0,11 | 0,02 | Tww | 4,4E+06 | 4,3E+06 | 4,6E+06 | 4,7E+04 |
| | Heave | -2,6E-05 | -8,1E-03 | 7,8E-03 | Heave | -2,1E-02 | 2,1E-02 | Tlw | 3,7E+06 | 3,7E+06 | 3,8E+06 | 1,2E+04 |
| | Pitch | 0,08 | 0,06 | 0,10 | Pitch | -0,01 | 0,01 | | | | | |
| | | Displacements | | | | Velocities | | | Tendon Forces | | | |
| | | Mean | Min | Max | | Min | Max | | Mean | Min | Max | Std |
| **IBLCT23** | Surge | 6,82 | 5,45 | 8,27 | Surge | -0,14 | 0,08 | Tww | 4,8E+06 | 4,6E+06 | 5,0E+06 | 7,0E+04 |
| | Heave | -4,8E-05 | -3,0E-02 | 3,0E-02 | Heave | -8,4E-02 | 8,4E-02 | Tlw | 3,6E+06 | 3,6E+06 | 3,7E+06 | 2,3E+04 |
| | Pitch | 0,13 | 0,11 | 0,15 | Pitch | -0,01 | 0,02 | | | | | |
| | | Displacements | | | | Velocities | | | Tendon Forces | | | |
| | | Mean | Min | Max | | Min | Max | | Mean | Min | Max | Std |
| **IBLCT24** | Surge | 9,99 | 7,05 | 13,20 | Surge | -0,31 | 0,04 | Tww | 5,4E+06 | 4,9E+06 | 6,0E+06 | 1,5E+05 |
| | Heave | -1,1E-04 | -1,4E-02 | 1,4E-02 | Heave | -3,7E-02 | 3,7E-02 | Tlw | 3,6E+06 | 3,5E+06 | 3,9E+06 | 4,3E+04 |
| | Pitch | 0,19 | 0,14 | 0,24 | Pitch | -0,02 | 0,02 | | | | | |
| | | Displacements | | | | Velocities | | | Tendon Forces | | | |
| | | Mean | Min | Max | | Min | Max | | Mean | Min | Max | Std |
| **IBLCT25** | Surge | 13,02 | 11,60 | 14,56 | Surge | -0,15 | 0,11 | Tww | 6,0E+06 | 5,7E+06 | 6,3E+06 | 1,2E+05 |
| | Heave | -7,3E-05 | -3,9E-02 | 3,8E-02 | Heave | -1,1E-01 | 1,1E-01 | Tlw | 3,7E+06 | 3,6E+06 | 3,9E+06 | 5,3E+04 |
| | Pitch | 0,24 | 0,22 | 0,28 | Pitch | -0,02 | 0,03 | | | | | |
| | | Displacements | | | | Velocities | | | Tendon Forces | | | |
| | | Mean | Min | Max | | Min | Max | | Mean | Min | Max | Std |
| **IBLCT26** | Surge | 16,12 | 14,51 | 17,94 | Surge | -0,18 | 0,16 | Tww | 6,7E+06 | 6,3E+06 | 7,2E+06 | 1,5E+05 |
| | Heave | -7,0E-05 | -6,2E-02 | 6,0E-02 | Heave | -1,6E-01 | 1,6E-01 | Tlw | 3,9E+06 | 3,7E+06 | 4,2E+06 | 8,0E+04 |
| | Pitch | 0,30 | 0,27 | 0,33 | Pitch | -0,03 | 0,04 | | | | | |

**Table M-19:** Ice bending - total force simulation outcomes $v_{ice} = 0.3$

| | | Displacements | | | | Velocities | | | Tendon Forces | | | |
|---|---|---|---|---|---|---|---|---|---|---|---|---|
| | | Mean | Min | Max | | Min | Max | | Mean | Min | Max | Std |
| **IBLCT31** | Surge | 1,83 | 1,09 | 2,58 | Surge | -0,07 | 0,02 | Tww | 4,2E+06 | 4,1E+06 | 4,2E+06 | 2,5E+04 |
| | Heave | -1,5E-05 | -8,6E-03 | 8,6E-03 | Heave | -2,4E-02 | 2,4E-02 | Tlw | 3,8E+06 | 3,8E+06 | 3,9E+06 | 1,4E+04 |
| | Pitch | 0,03 | 0,02 | 0,04 | Pitch | 0,00 | 0,00 | | | | | |
| | | Displacements | | | | Velocities | | | Tendon Forces | | | |
| | | Mean | Min | Max | | Min | Max | | Mean | Min | Max | Std |
| **IBLCT32** | Surge | 4,22 | 3,04 | 5,45 | Surge | -0,12 | 0,05 | Tww | 4,4E+06 | 4,3E+06 | 4,6E+06 | 5,0E+04 |
| | Heave | -2,5E-05 | -1,7E-02 | 1,7E-02 | Heave | -4,8E-02 | 4,8E-02 | Tlw | 3,7E+06 | 3,7E+06 | 3,8E+06 | 1,5E+04 |
| | Pitch | 0,08 | 0,06 | 0,10 | Pitch | -0,01 | 0,01 | | | | | |
| | | Displacements | | | | Velocities | | | Tendon Forces | | | |
| | | Mean | Min | Max | | Min | Max | | Mean | Min | Max | Std |
| **IBLCT33** | Surge | 6,93 | 5,44 | 8,50 | Surge | -0,15 | 0,09 | Tww | 4,8E+06 | 4,6E+06 | 5,1E+06 | 7,7E+04 |
| | Heave | -5,1E-05 | -3,3E-02 | 3,2E-02 | Heave | -8,8E-02 | 8,8E-02 | Tlw | 3,6E+06 | 3,6E+06 | 3,7E+06 | 2,3E+04 |
| | Pitch | 0,13 | 0,11 | 0,16 | Pitch | -0,01 | 0,02 | | | | | |
| | | Displacements | | | | Velocities | | | Tendon Forces | | | |
| | | Mean | Min | Max | | Min | Max | | Mean | Min | Max | Std |
| **IBLCT34** | Surge | 9,95 | 8,42 | 11,54 | Surge | -0,15 | 0,06 | Tww | 5,4E+06 | 5,1E+06 | 5,6E+06 | 9,7E+04 |
| | Heave | -5,3E-05 | -2,1E-02 | 2,1E-02 | Heave | -5,7E-02 | 5,7E-02 | Tlw | 3,6E+06 | 3,5E+06 | 3,7E+06 | 3,1E+04 |
| | Pitch | 0,19 | 0,16 | 0,21 | Pitch | -0,01 | 0,02 | | | | | |
| | | Displacements | | | | Velocities | | | Tendon Forces | | | |
| | | Mean | Min | Max | | Min | Max | | Mean | Min | Max | Std |
| **IBLCT35** | Surge | 12,94 | 11,30 | 14,69 | Surge | -0,17 | 0,14 | Tww | 6,0E+06 | 5,6E+06 | 6,4E+06 | 1,2E+05 |
| | Heave | -5,3E-05 | -5,2E-02 | 5,1E-02 | Heave | -1,4E-01 | 1,4E-01 | Tlw | 3,7E+06 | 3,6E+06 | 3,9E+06 | 5,5E+04 |
| | Pitch | 0,24 | 0,21 | 0,27 | Pitch | -0,02 | 0,02 | | | | | |
| | | Displacements | | | | Velocities | | | Tendon Forces | | | |
| | | Mean | Min | Max | | Min | Max | | Mean | Min | Max | Std |
| **IBLCT36** | Surge | 16,38 | 13,88 | 19,01 | Surge | -0,26 | 0,15 | Tww | 6,8E+06 | 6,2E+06 | 7,5E+06 | 1,9E+05 |
| | Heave | -7,0E-05 | -5,4E-02 | 5,4E-02 | Heave | -1,5E-01 | 1,5E-01 | Tlw | 3,9E+06 | 3,6E+06 | 4,3E+06 | 9,4E+04 |
| | Pitch | 0,31 | 0,26 | 0,35 | Pitch | -0,03 | 0,03 | | | | | |

**Table M-20:** Ice bending load combinations with wind - simulation outcomes $v_{ice} = 0.2$, $u_{mean} = 11m/s$

| | | Displacements | | | | Velocities | | | Tendon Forces | | | |
|---|---|---|---|---|---|---|---|---|---|---|---|---|
| | | Mean | Min | Max | | Min | Max | | Mean | Min | Max | Std |
| **IBLCW1** | Surge | 5,82 | 0,90 | 9,71 | Surge | -0,36 | 0,02 | Tww | 5,3E+06 | 4,5E+06 | 6,5E+06 | 3,4E+05 |
| | Heave | -1,4E-05 | -7,8E-03 | 7,8E-03 | Heave | -2,2E-02 | 2,2E-02 | Tlw | 3,0E+06 | 2,2E+06 | 3,8E+06 | 2,6E+05 |
| | Pitch | 0,25 | 0,07 | 0,45 | Pitch | -0,22 | 0,20 | | | | | |
| | | Displacements | | | | Velocities | | | Tendon Forces | | | |
| | | Mean | Min | Max | | Min | Max | | Mean | Min | Max | Std |
| **IBLCW2** | Surge | 8,59 | 3,98 | 12,51 | Surge | -0,41 | 0,03 | Tww | 5,8E+06 | 4,7E+06 | 7,2E+06 | 3,9E+05 |
| | Heave | -3,4E-05 | -1,2E-02 | 1,2E-02 | Heave | -3,2E-02 | 3,2E-02 | Tlw | 2,9E+06 | 2,1E+06 | 3,9E+06 | 2,7E+05 |
| | Pitch | 0,31 | 0,12 | 0,54 | Pitch | -0,20 | 0,21 | | | | | |
| | | Displacements | | | | Velocities | | | Tendon Forces | | | |
| | | Mean | Min | Max | | Min | Max | | Mean | Min | Max | Std |
| **IBLCW3** | Surge | 10,92 | 7,18 | 15,43 | Surge | -0,40 | 0,10 | Tww | 6,2E+06 | 5,1E+06 | 7,8E+06 | 4,2E+05 |
| | Heave | -4,5E-05 | -3,5E-02 | 3,5E-02 | Heave | -9,6E-02 | 9,6E-02 | Tlw | 3,0E+06 | 2,1E+06 | 3,8E+06 | 2,6E+05 |
| | Pitch | 0,34 | 0,15 | 0,60 | Pitch | -0,23 | 0,23 | | | | | |
| | | Displacements | | | | Velocities | | | Tendon Forces | | | |
| | | Mean | Min | Max | | Min | Max | | Mean | Min | Max | Std |
| **IBLCW4** | Surge | 13,76 | 10,02 | 17,16 | Surge | -0,38 | 0,09 | Tww | 6,8E+06 | 5,4E+06 | 8,0E+06 | 4,4E+05 |
| | Heave | -6,3E-05 | -3,6E-02 | 3,3E-02 | Heave | -9,1E-02 | 9,1E-02 | Tlw | 3,1E+06 | 2,2E+06 | 4,1E+06 | 2,7E+05 |
| | Pitch | 0,40 | 0,18 | 0,61 | Pitch | -0,21 | 0,21 | | | | | |
| | | Displacements | | | | Velocities | | | Tendon Forces | | | |
| | | Mean | Min | Max | | Min | Max | | Mean | Min | Max | Std |
| **IBLCW5** | Surge | 17,29 | 12,53 | 22,09 | Surge | -0,42 | 0,13 | Tww | 7,7E+06 | 6,2E+06 | 9,6E+06 | 5,3E+05 |
| | Heave | -7,0E-05 | -4,7E-02 | 4,7E-02 | Heave | -1,3E-01 | 1,3E-01 | Tlw | 3,4E+06 | 2,3E+06 | 4,5E+06 | 3,1E+05 |
| | Pitch | 0,47 | 0,28 | 0,73 | Pitch | -0,20 | 0,20 | | | | | |
| | | Displacements | | | | Velocities | | | Tendon Forces | | | |
| | | Mean | Min | Max | | Min | Max | | Mean | Min | Max | Std |
| **IBLCW6** | Surge | 20,41 | 16,36 | 24,09 | Surge | -0,34 | 0,10 | Tww | 8,6E+06 | 7,1E+06 | 1,0E+07 | 5,4E+05 |
| | Heave | -6,6E-05 | -3,6E-02 | 3,5E-02 | Heave | -9,7E-02 | 9,7E-02 | Tlw | 3,7E+06 | 2,8E+06 | 4,6E+06 | 3,2E+05 |
| | Pitch | 0,53 | 0,31 | 0,75 | Pitch | -0,22 | 0,22 | | | | | |

# Appendix N

# Matlab code

In this appendix the Matlab code used in this thesis can be found, categorised in the different loads acting on the structure.

## N-1 Main files

### N-1-1 Excel input

```
%% Importing data from excel
f_ij = xlsread('Output.xlsx','Added Mass','A3:A52'); %Frequency range
A_input = xlsread('Output.xlsx','Added Mass','B3:J52'); %Added mass
for i = 1:length(A_input(:,1));
    A_ij(:,:,i) =[A_input(i,1) A_input(i,2) A_input(i,3); A_input(i,4)
        A_input(i,5) A_input(i,6); A_input(i,7) A_input(i,8) A_input(i,9)
        ];
end

B_input = xlsread('Output.xlsx','Added Damping','B3:J52'); %Added damping
for i = 1:length(B_input(:,1))
    B_ij(:,:,i) =[B_input(i,1) B_input(i,2) B_input(i,3); B_input(i,4)
        B_input(i,5) B_input(i,6); B_input(i,7) B_input(i,8) B_input(i,9)
        ];
end


%Read forcing vectors + interpolate to adjust freq step to fit T_sim
X_j = xlsread('Output_Filtered.xlsx','Forcing vectors','B2:G51');
freq_waves = [0.01:(1/T_sim):(max(f_ij))]';

X_i1 = spline(f_ij,X_j(:,1),freq_waves);
X_i2 = spline(f_ij,X_j(:,2),freq_waves);
X_i3 = spline(f_ij,X_j(:,3),freq_waves);
X_i4 = spline(f_ij,X_j(:,4),freq_waves);
X_i5 = spline(f_ij,X_j(:,5),freq_waves);
X_i6 = spline(f_ij,X_j(:,6),freq_waves);
X_i = [X_i1 X_i2 X_i3 X_i4 X_i5 X_i6];
```

```
25 clear freq_waves; clear X_j;
26
27 m_ij = xlsread('Excel input files\Output.xlsx','Matrices','B3:D5');
28
29 %% Transformation to time domain
30 Aij = A_ij(:,:,length(A_ij));
31 omega = f_ij*2*pi; d_omega = omega(2)-omega(1);
32
33 %Index determination by max simulation length and timestep.
34 for i = 1:25/delta_t
35 t_kernel(i) = 0+delta_t*i;
36
37 %With if loop, cut off signal after t=0.5/df to prevent mirroring signal
38     if delta_t*(i-1)<= 0.5/(d_omega/(2*pi))
39 %Set up vector cos(omega*t)*d_omega
40     cos_omega = cos(omega.*(delta_t*(i-1)))*d_omega;
41     else
42     cos_omega = zeros(length(omega),1);
43     end
44
45 m_cos_omega = repmat([cos_omega]',3,1,3); %Create matrix of 3x3xvector
46 M_cos_omega = permute(m_cos_omega,[1 3 2]); %Re-arrange matrix to fit
       B_ij
47
48 Kij_omega = B_ij.*M_cos_omega; %Multiplication before integration
49 K_ij(:,:,i) = sum(Kij_omega,3)*2/pi; %Intergration step (simple summation
       )
50 end
```

### N-1-2 Open water main file

```
1  close all; clear all; clc;
2
3  %% Run parameters
4  T_sim = 3600;   %Simulation time [s]
5  delta_t = 0.2;  %Timestep [s]
6
7  u_mean = 11;    %Mean wind speed [m/s]
8  Hs = 14;        %Significant wave height [Hs]
9  Tp = 18.75;     %Peak wave period [s]
10 u_current = 0;  %Curren velocity [m/s]
11 hw = 200;       %Water depth
12
13 %% Excel import and spectrum definitions
14 Excel_Input;
15 [A_kaimal,freq_wind,S_f,phi,a_induction] = WindSpectrum(u_mean,T_sim,
       delta_t);
16 [a,k,theta,freq_waves] = WaveSpectrum(T_sim,delta_t,Hs,Tp,hw);
17
18 %% Time loop
19
20 % First time step
21 for j = 1
```

```
22      t = -delta_t+j*delta_t;
23      Fradiation=[0;0;0];
24      q = [0  0  0  0  0  0];
25      [t,q] = ode45(@(t,q)EM(t,q,Aij,m_ij,X_i,freq_waves,a,hw,k,theta,
            A_kaimal,freq_wind,S_f,phi,Fradiation,a_induction,u_current,u_mean
            ),[t t+delta_t],q);
26      [qd,Fwaves,U_waves,eta,Fwind,u_ref,Fdrag,F,T_ww,T_lw] = EM(t(length(t
            )),q(length(q),:)',Aij,m_ij,X_i,freq_waves,a,hw,k,theta,A_kaimal,
            freq_wind,S_f,phi,Fradiation,a_induction,u_current,u_mean);
27      t_plot(j,:) = -delta_t+j*delta_t;
28      fwaves(j,:) = Fwaves';
29      fwind(j,:) = Fwind';
30      fdrag(j,:) = Fdrag;
31      f(j,:)=F';
32      Q(j,:) = q(length(q),:);
33      u_wind(j,:) = u_ref;
34      u_waves(j,:)=U_waves;
35  end
36
37  h = waitbar(0,'Please wait...');
38
39  % Remainder of the simulation
40  for j = 2:(T_sim/delta_t)
41      h = waitbar(j/(T_sim/delta_t));
42
43      t = -delta_t+j*delta_t;
44      % Radiation force definition for constant time-step
45      [Fradiation] = Radiation(t,K_ij,Q,delta_t);
46      [t,q] = ode45(@(t,q)EM(t,q,Aij,m_ij,X_i,freq_waves,a,hw,k,theta,
            A_kaimal,freq_wind,S_f,phi,Fradiation,a_induction,u_current,u_mean
            ),[t t+delta_t],q(length(q),:));
47      [qd,Fwaves,U_waves,eta,Fwind,u_ref,Fdrag,F,T_ww,T_lw] = EM(t(length(t
            )),q(length(q),:)',Aij,m_ij,X_i,freq_waves,a,hw,k,theta,A_kaimal,
            freq_wind,S_f,phi,Fradiation,a_induction,u_current,u_mean);
48      t_plot(j,:) = -delta_t+j*delta_t;
49      fwaves(j,:) = Fwaves';
50      fwind(j,:) = Fwind';
51      fdrag(j,:)=Fdrag';
52      T_windward(j,:)= T_ww;
53      T_leeward(j,:)= T_lw;
54
55      f(j,:)=F';
56      Q(j,:) = q(length(q),:);
57      eta_plot(j,:) = eta;
58      u_wind(j,:) = u_ref;
59      u_waves(j,:)=U_waves;
60  end
61
62  close(h);
63
64  % Plotting motion results
65  figure
```

```
66 subplot(3,1,1); plot(t_plot,Q(:,1)); legend('X1');subplot(3,1,2); plot(
       t_plot,Q(:,3)); legend('X2');subplot(3,1,3); plot(t_plot,Q(:,5));
       legend('X3');
```

### N-1-3 Ice crushing main file

```
1  close all; clear all; clc;
2
3  %% Run parameters
4  T_sim = 2000;    %Simulation time [s]
5  delta_t = 0.1;   %Timestep [s]
6
7  v_ice = 0.4;     %Incoming ice velocity [m/s]
8  h_ice = 0.4;     %Ice thickness [m]
9  u_mean = 11;     %Mean wind speed [m/s]
10 u_current = 0;   %Curren velocity [m/s]
11 hw = 200;        %Water depth
12
13 %% Excel import and spectrum definitions
14 Excel_Input;
15 [A_kaimal,freq_wind,S_f,phi,ThrustDef] = WindSpectrum(u_mean,T_sim,
       delta_t);
16
17 %% Time loop
18 for j = 1
19     t = -delta_t+j*delta_t;
20     Fradiation=[0;0;0];
21     q = [0 0 0 0 0 0];
22     [t,q] = ode45(@(t,q)EM_ice(t,q,Aij,m_ij,hw,A_kaimal,freq_wind,S_f,phi
           ,Fradiation,ThrustDef,u_current,u_mean,v_ice,h_ice),[t t+delta_t],
           q);
23     [qd,Fice,Fwind,u_ref,Fcurrent,F,T_ww,T_lw,d,df,Ff,sigf] = EM_ice(t(
           length(t)),q(length(q),:)',Aij,m_ij,hw,A_kaimal,freq_wind,S_f,phi,
           Fradiation,ThrustDef,u_current,u_mean,v_ice,h_ice);
24     t_plot(j,:) = -delta_t+j*delta_t;
25     fice(j,:) = Fice';
26     fwind(j,:) = Fwind';
27     fcurrent(j,:) = Fcurrent;
28     f(j,:)=F';
29     Q(j,:) = q(length(q),:);
30     u_wind(j,:) = u_ref;
31 end
32
33 h = waitbar(0,'Please wait...');
34
35 for j = 2:(T_sim/delta_t)
36     h = waitbar(j/(T_sim/delta_t));
37     t = -delta_t+j*delta_t;
38     [Fradiation] = Radiation(t,K_ij,Q,delta_t);
39     [t,q] = ode45(@(t,q)EM_ice(t,q,Aij,m_ij,hw,A_kaimal,freq_wind,S_f,phi
           ,Fradiation,ThrustDef,u_current,u_mean,v_ice,h_ice),[t t+delta_t],
           q(length(q),:));
```

```
40      [qd,Fice,Fwind,u_ref,Fcurrent,F,T_ww,T_lw,d,df,Ff,sigf] = EM_ice(t(
            length(t)),q(length(q),:)',Aij,m_ij,hw,A_kaimal,freq_wind,S_f,phi,
            Fradiation,ThrustDef,u_current,u_mean,v_ice,h_ice);
41      t_plot(j,:) = -delta_t+j*delta_t;
42      F_radiation(j,:)=Fradiation;
43      fice(j,:) = Fice';
44      fwind(j,:) = Fwind';
45      fcurrent(j,:)=Fcurrent';
46      T_windward(j,:)= T_ww;
47      T_leeward(j,:)= T_lw;
48      d_ice(j,:) = d;
49      f(j,:)=F';
50      Q(j,:) = q(length(q),:);
51      u_wind(j,:) = u_ref;
52      F_failure_ice(j,:)=Ff;
53      sig_ice(j,:)=sigf;
54  end
55
56  close(h);
57
58  %% Plot motion and ice-load results
59  figure
60  subplot(3,1,1); plot(t_plot,Q(:,1)); legend('X1');subplot(3,1,2); plot(
        t_plot,Q(:,3)); legend('X2');subplot(3,1,3); plot(t_plot,Q(:,5));
        legend('X3');
61  figure
62  subplot(5,1,1);plot(t_plot,v_ice*t_plot);legend('ice travelled distance')
        ;subplot(5,1,2);plot(t_plot,Q(:,1));legend('position floater');subplot
        (5,1,3);plot(t_plot,Q(:,2));legend('velocity floater');subplot(5,1,4);
        plot(t_plot,d_ice);legend('tooth displ');subplot(5,1,5);plot(t_plot,
        fice);legend('Ice force');
```

### N-1-4 Ice bending main file

```
1   clear all; clc;
2
3   %% Simulation parameters
4   h_ice = 2;          %Ice thickness
5   v_ice = 0.4;        %Ice velocity
6   u_mean = 11;        %Mean wind speed [m/s]
7   u_current = 0;      %Curren velocity [m/s]
8   hw = 200;           %Water depth
9
10  T_sim = 2000;       %Simulation duration
11  delta_t = 0.02;     %Time step
12
13  %% Loading external data
14  Excel_Input;
15  [A_kaimal,freq_wind,S_f,phi,ThrustDef] = WindSpectrum(u_mean,T_sim,
        delta_t);
16
17  %% Time loop
18  q = [0 0 0 0 0 0];
```

```
Q = [0 0 0 0 0 0];
i=0;
t=0;

X_br = 0;
x0 = 0;
X=0;

while t < T_sim
    i=i+1;
    dt = delta_t;

    % Calculate time and location
    if i-1~=0
        t_plot(i) = t_plot(i-1)+dt;
    else
        t_plot(i) = 0;
    end
    t = t_plot(i)

    if t ==0
        Fradiation=[0;0;0];
        [X_br,u,Fice,x] = IceBending(v_ice,Q,t,h_ice,X_br,x0,i);
        F_ice = Fice;
        [t,q] = ode45(@(t,q)EM_ice_bending(t,q,Aij,m_ij,hw,A_kaimal,
            freq_wind,S_f,phi,Fradiation,ThrustDef,u_current,u_mean,F_ice)
            ,[t t+dt],q);
        [qd,Fwind,u_ref,Fcurrent,F,T_ww,T_lw] = EM_ice_bending(t(length(t
            ),:),q(length(q),:)',Aij,m_ij,hw,A_kaimal,freq_wind,S_f,phi,
            Fradiation,ThrustDef,u_current,u_mean,F_ice);
    else
        [Fradiation] = Radiation(t,K_ij,Q,delta_t);
        [X_br,u,Fice,x] = IceBending(v_ice,Q,t,h_ice,X_br,x0,i-1);
        F_ice = Fice;
        [t,q] = ode45(@(t,q)EM_ice_bending(t,q,Aij,m_ij,hw,A_kaimal,
            freq_wind,S_f,phi,Fradiation,ThrustDef,u_current,u_mean,F_ice)
            ,[t t+dt],q(length(q),:));
        [qd,Fwind,u_ref,Fcurrent,F,T_ww,T_lw] = EM_ice_bending(t(length(t
            ),:),q(length(q),:)',Aij,m_ij,hw,A_kaimal,freq_wind,S_f,phi,
            Fradiation,ThrustDef,u_current,u_mean,F_ice);
    end

    Fice_plot(:,i) = F_ice;
    Q(i,:) = q(length(q),:);
    u_wind(i,:) = u_ref;
    T_windward(i,:)= T_ww;
    T_leeward(i,:)= T_lw;

end
```

# N-2 Equation of motions function

## N-2-1 E.M. open water

```
function [qd,Fwaves,U_waves,eta,Fwind,u_ref,Fdrag,F,T_ww,T_lw] = EM(t,q,
    Aij,m_ij,X_i,freq_waves,a,hw,k,theta,A_kaimal,freq_wind,S_f,phi,
    Fradiation,a_induction,u_current,u_mean)

    C = [0 0 0;0 0 0;0 0 0];
    m = [m_ij(1,1) m_ij(1,2) m_ij(1,3); m_ij(2,1) m_ij(2,2) m_ij(2,3);
        m_ij(3,1) m_ij(3,2) m_ij(3,3)];
    M = m+Aij;
    [K,T_ww,T_lw] = MooringStiffness(q,m_ij,hw);
    [Fwaves,eta,U_waves,U_waves_heave] = WaveLoads(t,q,X_i,a,hw,k,theta,
        freq_waves);
    [Fdrag] = DragLoads(q,u_current,U_waves,U_waves_heave);
    [Fwind,u_ref] = WindLoads(t,q,A_kaimal,freq_wind,S_f,phi,a_induction,
        u_mean);

    %% Free decay settings
    %Fwind = [0;0;0];
    %u_ref = 0;
    %Fwaves = [0;0;0];
    %U_waves =0;
    %U_waves_heave = 0;
    %eta = 0;

    %% Equation of motion
    F = [-1*Fradiation(1)+Fwaves(1)+Fwind(1)+Fdrag(1);-1*Fradiation(2)+
        Fwaves(2)+Fwind(2)+Fdrag(2);-1*Fradiation(3)+Fwaves(3)+Fwind(3)+
        Fdrag(3)];
    xdd = (inv(M))*(-C*q(2:2:6)-K*q(1:2:6)+F);

 qd = zeros(6,1);
 qd(1:2:6)=q(2:2:6);
 qd(2:2:6)=xdd;
 xd = q(2:2:6);
```

## N-2-2 E.M. ice crushing

```
function [qd,Fice,Fwind,u_ref,Fcurrent,F,T_ww,T_lw,d,df,Ff,sigf] = EM_ice
    (t,q,Aij,m_ij,hw,A_kaimal,freq_wind,S_f,phi,Fradiation,ThrustDef,
    u_current,u_mean,v_ice,h_ice)

    C = [0 0 0;0 0 0;0 0 0];
    m = [m_ij(1,1) m_ij(1,2) m_ij(1,3); m_ij(2,1) m_ij(2,2) m_ij(2,3);
        m_ij(3,1) m_ij(3,2) m_ij(3,3)];
    M = m+Aij;
    [K,T_ww,T_lw] = MooringStiffness(q,m_ij,hw);
    Fcurrent = CurrentLoads(q,u_current);
    [Fice,d,df,Ff,sigf] = IceLoading(v_ice,q,t,h_ice);
    [Fwind,u_ref] = WindLoads(t,q,A_kaimal,freq_wind,S_f,phi,ThrustDef,
        u_mean);
```

```
    %Fwind = [0;0;0];
    %u_ref = 0;
    F = [-1*Fradiation(1)+Fice(1)+Fwind(1)+Fcurrent(1);-1*Fradiation(2)+
        Fice(2)+Fwind(2)+Fcurrent(2);-1*Fradiation(3)+Fice(3)+Fwind(3)+
        Fcurrent(3)];

    xdd = (inv(M))*(-C*q(2:2:6)-K*q(1:2:6)+F);

 qd = zeros(6,1);
 qd(1:2:6)=q(2:2:6);
 qd(2:2:6)=xdd;
 xd = q(2:2:6);
```

### N-2-3 E.M. ice bending

```
function [qd,Fwind,u_ref,Fcurrent,F,T_ww,T_lw] = EM_ice_bending(t,q,Aij,
    m_ij,hw,A_kaimal,freq_wind,S_f,phi,Fradiation,ThrustDef,u_current,
    u_mean,F_ice)

       C = [0 0 0;0 0 0;0 0 0];
    m = [m_ij(1,1) m_ij(1,2) m_ij(1,3); m_ij(2,1) m_ij(2,2) m_ij(2,3);
        m_ij(3,1) m_ij(3,2) m_ij(3,3)];
    M = m+Aij;
    [K,T_ww,T_lw] = MooringStiffness(q,m_ij,hw);
    Fcurrent = CurrentLoads(q,u_current);
    [Fwind,u_ref] = WindLoads(t,q,A_kaimal,freq_wind,S_f,phi,ThrustDef,
        u_mean);
    %Fwind = [0;0;0];
    %u_ref = 0;
    F = [-1*Fradiation(1)+F_ice(1)+Fwind(1)+Fcurrent(1);-1*Fradiation(2)+
        F_ice(2)+Fwind(2)+Fcurrent(2);-1*Fradiation(3)+F_ice(3)+Fwind(3)+
        Fcurrent(3)];

    xdd = (inv(M))*(-C*q(2:2:6)-K*q(1:2:6)+F);

 qd = zeros(6,1);
 qd(1:2:6)=q(2:2:6);
 qd(2:2:6)=xdd;
 xd = q(2:2:6);
```

## N-3 System characteristics

### N-3-1 Stiffness definitions

```
function [K,T_ww,T_lw] = MooringStiffness(q,m_ij,hw)

rho_w = 1025;                %Water density
g = 9.81;

%% Platform dimensions
D = 18;                      %Floater diameter
draft = 47.89;               %Floater draft
```

```
Num_T = 8;                  %Number of tethers
X_T = 27;                   %Distance to tendon connection
E = 2.84205e11;             %Extensional stiffness
EA = 1.5e9;
EIy = Num_T/2*X_T^2*EA;

%% Structural properties
I_WL = (pi*D^4)/64;         %Waterplane moment of inertia
A_WL = 0.25*pi*D^2;         %Waterplane area
m = m_ij(1,1);              %Stystem mass, from Excel
L = hw-draft;               %Length of tethers

%% Force determination
U = A_WL*draft*rho_w*g;     %Buoyancy
Q = m*g;                    %Weight
Z_B = -draft/2;             %Z-Coordinate of CoB
Z_G = -32.5;                %Z-Coordinate of CoG
Z_T = -draft;               %Z-Coordinate tendon connection
T = U-Q;                    %Total mooring tension
T_n = T/Num_T;              %Tension per tendon
Lz = sqrt(L^2-q(1)^2);      %Effective vertical length
set_down = L-Lz;            %Set-down

%% Nonlinear Stiffness
    K11 = T/Lz + rho_w*g*A_WL*(set_down/Lz);
    K22 = rho_w*g*A_WL + (EA*Num_T)/L;
    K33 = (rho_w*g*I_WL)/cos(q(5))^3+U*(Z_B-Z_T)-Q*(Z_G-Z_T)+ rho_w*g*
        A_WL*(Z_B-Z_T)*set_down+(Num_T/2)*(EA/L)*X_T^2*cos(q(5))^2;
    K21 = (set_down/(2*L))*K22;

    K = [K11 0 Z_T*K11; K21 K22 Z_T*K21; Z_T*K11 0 K33+(Z_T)^2*K11];

%% Tension force determination

    T_ww = T_n + (q(3)+set_down)*(EA/L)/Num_T+ ((set_down*rho_w*g*A_WL)/
        Num_T) + sin(q(5))*X_T*(EA/L);
    T_lw = T_n + (q(3)+set_down)*(EA/L)/Num_T+ ((set_down*rho_w*g*A_WL)/
        Num_T) - sin(q(5))*X_T*(EA/L);

%% Linear Stiffness
%K11 = T/L;
%K22 = rho_w*g*A_WL + (EA*Num_T)/L;
%K33 = (rho_w*g*I_WL)+U*(Z_B-Z_T)-Q*(Z_G-Z_T)+(Num_T/2)*(EA/L)*X_T^2;
%K = [K11 0 Z_T*K11; 0 K22 0; Z_T*K11 0 K33+(-Z_T)^2*K11];
```

## N-3-2 Radiation

```
function [Fradiation] = Radiation(t,K_ij,Q,t_step)

%% Create velocity vector that fits K_ij

if t<=25

```

```
q_v_surge = [flip(Q(:,2));zeros(length(K_ij(1,1,:))-length(Q(:,2)),1)];
q_v_heave = [flip(Q(:,4));zeros(length(K_ij(1,1,:))-length(Q(:,4)),1)];
q_v_pitch = [flip(Q(:,6));zeros(length(K_ij(1,1,:))-length(Q(:,6)),1)];

else

q_v_surge = [flip(Q((length(Q(:,2))-25/t_step)+1:length(Q(:,2)),2))];
q_v_heave = [flip(Q((length(Q(:,2))-25/t_step)+1:length(Q(:,2)),4))];
q_v_pitch = [flip(Q((length(Q(:,2))-25/t_step)+1:length(Q(:,2)),6))];
end

%% Creata velocity matrix

q_h = [q_v_surge q_v_heave q_v_pitch];
q_m=repmat(q_h,1,1,3);
q_matrix = permute(q_m,[3,2,1]);

%% Force definition
F_i = q_matrix.*K_ij*t_step;
F_isum = sum(F_i,3);
Fradiation = sum(F_isum,1);
end
```

## N-4 Loading function files

### N-4-1 Wind loads

#### Spectrum definition

```
function [A_kaimal,freq_wind,S_f,phi,a_induction] = WindSpectrum(u_mean,
    T_sim,delta_t)
ThrustDef = xlsread('ThrustDef.xlsx','Thrust','B5:HN6');

%% Input parameters
    FB = 5;          % Floater freeboard
    z_hub = 90;      % Hubheight wrt tower bottom
    z0 = 0.025;      % Wind profile reference height

%% Vector definitions
    delta_f = 1/T_sim;
    f_max = (1/delta_t)/2;
    freq_wind = 0:delta_f:f_max;

%% Kaimal spectrum
L1((z_hub+FB)<=30)=5*(z_hub+FB);     % Turbulence length scale
L1((z_hub+FB)>30)=150;               % Turbulence length scale
sigma = u_mean/log((z_hub+FB)/z0);   % Turbulence standard deviation

% Spectral density
S_f = sigma^2*(((4*L1)/u_mean)./((1+6.*freq_wind.*L1./u_mean).^(5/3)));
A_kaimal = sqrt(2.*S_f.*(delta_f)); % Amplitude
phi = pi-(2*pi*rand(size(S_f)));    % Random phase angle
```

```
23
24 %% Determination of induction factor
25 rho_a = 1.225;                          % Air density
26 D_rotor = 126;                          % Rotor diameter
27 Ad = 0.25*pi*D_rotor^2;                 % Swept area
28
29 Fthrust(u_mean <= 3) = 0;
30 Fthrust((3<u_mean)&&(u_mean<25)) = 1000*ThrustDef(2,(round(ThrustDef(1,:)
       *10)/10 ==(round(10*u_mean)/10)));
31 Fthrust(u_mean >= 25) = 0;
32
33 % Define a from thrustcurve
34 qq = @(a) Ad*0.5*rho_a*u_mean^2*4*a*(1-a) - Fthrust;
35 a_induction = fzero(qq,0);
```

### Load definition

```
1  function [Fwind,u_ref] = WindLoads(t,q,A_kaimal,freq_wind,S_f,phi,
       a_induction,u_mean)
2
3  %% Input parameters
4      FB = 5;                          %Platform freeboard
5      D_platform = 18;                 %Platform diameter
6      z_hub = 90;                      %Turbine hubheight wrt tower bottom
7      D_rotor = 126;                   %Rotor diameter
8      Ad = 0.25*pi*D_rotor^2;          %Swept area
9
10 %Tower
11     delta_z = 5;                     % Stepsize along the height of the tower
12     z = [0:delta_z:(z_hub+FB)];      % Height vector
13     z_tower = [0:delta_z:z_hub];
14     D_bottom = 6;                    % Tower diameter at the bottom
15     D_top = 3.87;                    % Tower diameter at the top
16     FB_z = FB/delta_z;
17     Dz = [D_platform*ones(1,(FB_z)) (6-((6-3.87)/(z_hub)).*z_tower)];
18     Cd = 0.6;                        % Drag coefficient
19
20 % Wind parameters
21     z0 = 0.025;                      % Offshore surface roughness
22     alpha = 0.14;                    % Wind shear coefficient
23     rho_a = 1.225;                   % Air density
24
25 %% Frequency definition
26 omega = freq_wind.*(2*pi);           % Radial frequency range
27
28 %% Spectrum to time series conversion
29 u_ref = u_mean + sum(A_kaimal.*cos(omega.*t+phi)); % Reference wind vel
30 u_hub = u_ref - q(2)- q(6)*(z_hub+FB);             % Hubheight rel vel
31
32 %% Top load
33 Ftop = Ad*0.5*rho_a*u_hub^2*4*a_induction*(1-a_induction);
34
35 %% Distributed load on tower
```

```
uz = u_ref.*(z./(z_hub+FB)).^alpha;
Q_aero = sum((((Cd*0.5*rho_a)*(uz-q(2)-sin(q(6)).*z).^2).*Dz)*delta_z,2);
Q_z_aero = sum((((Cd*0.5*rho_a)*(uz-q(2)-sin(q(6)).*z).^2).*z.*Dz)*
    delta_z,2);

F1 = Ftop + Q_aero;
F3 = Ftop*(z_hub+FB) + Q_z_aero;

Fwind = [F1;0;F3];
```

## N-4-2 Wave loads

### Spectrum definition

```
function [a,k,theta,freq_waves] = WaveSpectrum(T_sim,delta_t,Hs,Tp,hw)
%% System parameters definition
df = 1/T_sim;                       %Frequency step size, based on Tsim
fmin = 0.01;                        %Lower frequency limit
fmax = 0.5;                         %Higher cut off frequency

freq_waves = fmin:df:fmax;          %Frequency vector definition
omega = freq_waves.*(2*pi);         %Radial frequency
d_omega = df*2*pi;                  %Radial frequency step size

%% Jonswap spectrum
omega_p = (2*pi)/Tp;                %Radial peak frequency
gamma_p = Tp/sqrt(Hs);              %Gamma factor

gamma(gamma_p<=3.6)= 5;
gamma(3.6<gamma_p<5) = exp(5.75-1.15*(Tp/sqrt(Hs)));
gamma(gamma_p>5) = 1;

sigma(omega<= omega_p) = 0.07;
sigma(omega> omega_p) = 0.09;

S_1sided = 1/(2*pi)*(5/16)*Hs^2*Tp.*((omega.*Tp)./(2*pi)).^-5.*exp(-(5/4)
    *((omega.*Tp)./(2*pi)).^-4).*(1-0.287*log(gamma)).*gamma.^exp
    (-0.5.*(((omega.*Tp)/(2*pi)-1)./sigma).^2);

%% Wave number definition using dispersion function (Newton Raphson
    method)
for i = 1:length(omega)
    [Lr(i),k(i),sigma(i)]=disper(hw,(2*pi)/omega(i));
end

a = sqrt(2*d_omega*S_1sided);           %Amplitude
theta = 2*pi*rand(1,length(omega));     %Random phase angle
```

### Load definition

```
function [Fwaves,eta,U_waves,U_waves_heave] = WaveLoads(t,q,X_i,a,hw,k,
    theta,freq_waves)
```

```
Draft = 48;
%% Spectrum range definition
omega = freq_waves.*(2*pi);
d_omega = (freq_waves(2)-freq_waves(1))*(2*pi);

%% Wave elevation
x = q(1);
v_eta = a.*cos(omega.*t-k*x+theta);
eta = sum(v_eta);

delta_z = 3;
z = -1*[0:delta_z:Draft];

 [mz,momega]=meshgrid(z,omega);
 [mz,ma]=meshgrid(z,a);
 [mz,mk]=meshgrid(z,k);
 [mz,mtheta]=meshgrid(z,theta);

 u_w1= momega.*ma.*(cosh(mk.*(mz+hw))./sinh(mk*hw)).*cos(momega*t-mk*x+
     mtheta);
 u_w2= -1*omega.*a.*(sinh(k.*(-48+hw))./sinh(k*hw)).*sin(omega*t-k*x+
     theta);
 U_waves = sum(u_w1,1);
 U_waves_heave = sum(u_w2);

%% Wave forces from AQWA
X_1 = X_i(:,1)';
X_1_phase = X_i(:,2)';
X_2 = X_i(:,3)';
X_2_phase = X_i(:,4)';
X_3 = X_i(:,5)';
X_3_phase = X_i(:,6)';

%Surge force (including phase shift)
v_F_surge = a.*cos(omega.*t-k.*x+theta+(X_1_phase.*((2*pi)/360))).*X_1;
%Heave force (including phase shift)
v_F_heave = a.*cos(omega.*t-k.*x+theta+(X_2_phase.*((2*pi)/360))).*X_2;
%Pitch moment (including phase shift)
v_F_pitch = a.*cos(omega.*t-k.*x+theta+(X_3_phase.*((2*pi)/360))).*X_3;
Fwaves = [sum(v_F_surge); sum(v_F_heave); sum(v_F_pitch)];
end
```

### N-4-3 Drag loads

```
function [Fdrag] = DragLoads(q,u_current,U_waves,U_waves_heave)
D_platform = 18;          %Platform diameter
Draft = 48;               %Platform draft
Cd = 1;                   %Drag coefficient horizontal flow
Cdz = 2;                  %Drag coefficient vertical flow
rho_water = 1000;         %Water density

delta_z = 3;              %Vertical stepsize
z = -1*[0:delta_z:Draft];
```

```
10
11 u_res = U_waves+u_current-q(2)+q(6)*abs(z); %Residual horizontal flow
12 u_res_heave = U_waves_heave-q(4);           %Residual vertical flow
13
14 %% Load defintions
15 F_drag_heave = (pi/8)*D_platform^2*rho_water*Cdz*u_res_heave*abs(
       u_res_heave);
16 F_drag = (0.5*Cd*rho_water*D_platform*delta_z).*abs(u_res).*u_res;
17 M_drag = F_drag.*z;
18
19 %% Force vector definition
20 F1 = sum(F_drag);
21 F2 = F_drag_heave;
22 F3 = sum(M_drag);
23
24 Fdrag = [F1;F2;F3];
```

### N-4-4 Ice crushing loads

```
1  function [ Fice,d,df,Ff,sigf] = IceLoading(v_ice,q,t,h_ice)
2
3  D = 18;   %Platform diameter
4
5  %% Velocity definitions
6  vr = v_ice-q(2);        %Relative velocity (ice vel-structure vel)
7  x0 = 0;                 %Initial displacement platform
8  F.vt = 0.5;             %Transitional velocity of ice [m/s]
9
10 %% Failure strength definition
11  sfm = 1.8e6;            % [Pa] Max failure strength ductile region
12  sfd = sfm*0.1;          % [Pa] Failure strength ductile region
13  sfb = sfm*0.1;          % [Pa] Failure strength brittle region
14  a   = 0.5;              % coefficient ductile
15  b   = -2;               % coefficient brittle
16
17  % Crushing strength definition
18  if vr<= F.vt
19      sigf = sfm*((1-(sfd/sfm))*(vr/F.vt)^a + (sfd/sfm));
20  else vr>F.vt
21      sigf = sfm*((1-(sfb/sfm))*(vr/F.vt)^b + (sfb/sfm));
22  end
23
24 %% Korzhavind force determination
25 I=2.5;                      %Indentation factor
26 K=0.6;                      %Contact factor
27 m=0.9;                      %Shape factor
28 Ff = sigf*I*K*m*D*h_ice;    %Ice failure force
29 Ffm = sfm*I*K*m*D*h_ice;    %Failure force at transitional velocity
30 F.FeFactor = 0.05;          %Residual force factor
31 Fe = F.FeFactor * Ff;       %Residual ice force after crushing
32 k = 2e7;                    %Ice stiffness
33
34 %% Failure length determination
```

```
35 df = (Ff-Fe)/k;                      % Failure deflection
36 p=(Ffm*(1-F.FeFactor))/k;            % Failure length
37 n = floor((v_ice*t-q(1))/p);         % Number of tooth in contact
38
39 d = x0 + v_ice*t - q(1) - p*(n);     % Tooth deflection
40
41 %% Force determination
42 if v_ice==0
43     Fice = 0;
44 else
45     if 0<=d && d<df && q(2)<=v_ice;
46         Fice = k*d +Fe;
47     elseif df<=d && d<p && q(2)<=v_ice;
48         Fice = Fe;
49     elseif q(2)>v_ice;
50         Fice=0;
51     elseif d<=0
52         Fice = 0;
53     end
54 end
55 Fice = [Fice;0;0];
56 end
```

### N-4-5 Ice bending loads

```
1  function [X_br,u,Fice,x] = IceBending(v_ice,Q,t,h_ice,X_br,x0,i)
2
3  %% Ice parameters
4  E = 2e9;                 %Flexural stiffness
5  B = 18;                  %Platform width
6  I = 1/12*B*h_ice^3;      %Ice moment of inertia
7  sigma_f = 700e3;         %Flexural strength
8  mu = 0.1;                %Kinetic roughness
9
10 %% External parameters
11 angle_str = 45;          %Structure slope angle
12 rho_w = 1000;            %Water density
13 g = 9.81;                %Gravitational accelleration
14
15 %% Simulation parameters
16 x = [0:1:10,10.01:.01:20,21:1:100];     %X-vector definition
17 pitch = Q(i,5);                         %Pitch angle
18 angle = (angle_str*2*pi)/360-pitch;     %Residual angle structure vs SWL
19
20 X = t*v_ice - X_br - x0;                %Position ice front
21
22 %% Determine beam tip ride up against structure
23 if X > Q(i,1)
24
25 Z_tip = (X-Q(i,1))*tan(angle);
26 interacting = 1;
27 else
28 Z_tip =0;
```

```
29 end
30
31
32     %% Beam model AKSNES MODEL NTNU
33     if Z_tip~=0
34
35     psi = (sin(angle)+mu*cos(angle))/(cos(angle)-mu*sin(angle));
36
37     lambda2 = sqrt((rho_w*g*B)/(4*E*I));
38     delta = psi/(4*E*I);
39
40     qq = @(F) (2*F)/(E*I)*(sqrt(lambda2-delta*F)*sqrt(lambda2+delta*F))
           /(2*sqrt(lambda2-delta*F)^3*sqrt(lambda2+delta*F)^2+sqrt(lambda2-
           delta*F)*sqrt(lambda2+delta*F)^4+sqrt(lambda2-delta*F)^5)-Z_tip;
41     F = fzero(qq,0);
42
43     P = F;
44     N = psi*F;
45
46     alpha = sqrt(lambda2-delta*F);
47     beta = sqrt(lambda2+delta*F);
48
49     C1 = (2*F)/(E*I)*(alpha*beta)/(2*alpha^3*beta^2+alpha*beta^4+alpha^5)
           ;
50     C2 = (F)/(E*I)*(beta^2-alpha^2)/(2*alpha^3*beta^2+alpha*beta^4+alpha
           ^5);
51
52     u = exp(-beta*x).*(C1*cos(alpha*x)+C2*sin(alpha*x));
53
54     sigma_M = (E*I*exp(-beta*x).*((C1*beta^2-2*C2*alpha*beta-C1*alpha^2)*
           cos(alpha*x)+(C2*beta^2+2*C1*alpha*beta-C2*alpha^2)*sin(alpha*x)))
           ./(B*h_ice^2/6);
55     sigma_Max = max(abs(sigma_M));
56
57     else
58     N = 0;
59     P = 0;
60     u = zeros(length(x),1);
61     sigma_M = zeros(length(x),1);
62     sigma_Max = 0;
63     end
64
65     if sigma_Max > sigma_f
66         X_br = X_br + x(sigma_M==sigma_Max);
67     else
68         X_br = X_br;
69     end
70
71     dz = Z_tip;
72     dx = B - dz/tan(angle);
73
74     Fice = [N;P;dz*N-P*dx];
75 end
```